BULLETIN OF RUSSIAN STATE MEDICAL UNIVERSITY

BIOMEDICAL JOURNAL OF PIROGOV RUSSIAN NATIONAL RESEARCH MEDICAL UNIVERSITY

SUBMISSION

SUBMISSION http://vestnik.rsmu.press/login?lang=en
CORRESPONDENCE editor@rsmu.press
COLLABORATION manager@rsmu.press
ADDRESS ul. Ostrovityanova, d. 1, Moscow, Russia, 117997

Indexed in Scopus. CiteScore 2024: 0.7

Indexed in WoS. JIF 2024: 0.4

Five-year h-index is 11

SCImago Journal & Country Rank 2024: 0.166

Indexed in DOAJ

Open access to archive

Issue DOI: 10.24075/brsmu.2026-04
Mass media registration certificate No. 012769, issued on July 29, 1994.
ISSN (Print): 2500-1094, ISSN (Online): 2542-1204.
Founder and publisher: Pirogov Russian National Research Medical University (Moscow, Russia).
The journal is indexed in the following scientific databases: Scopus, Web of Science, Google Scholar, SJR, DOAJ, Scilit, CyberLeninka, Embase, EZB, Lens.org, MIT Libraries, OpenAlex, Research4Life, Scholia, Wikidata, and ZDB.

Approved for print 31.08.2026
Circulation: 100 copies. Printed by Print.Formula
www.print-formula.ru

ВЕСТНИК РОССИЙСКОГО ГОСУДАРСТВЕННОГО МЕДИЦИНСКОГО УНИВЕРСИТЕТА

НАУЧНЫЙ МЕДИЦИНСКИЙ ЖУРНАЛ РНИМУ ИМ. Н. И. ПИРОГОВА

ПОДАЧА РУКОПИСЕЙ

ПОДАЧА РУКОПИСЕЙ https://vestnik.rsmu.press/login?lang=ru
ПЕРЕПИСКА С РЕДАКЦИЕЙ editor@rsmu.press
СОТРУДНИЧЕСТВО manager@rsmu.press
АДРЕС РЕДАКЦИИ ул. Островитянова, д. 1, г. Москва, 117997

Журнал включен в Scopus. CiteScore 2024: 0,7 — Журнал включен в WoS. JIF 2024: 0,4 — Индекс Хирша (h^5) журнала по оценке Google Scholar: 11

SJR SCImago Journal & Country Rank 2024: 0,166 — Журнал включен в DOAJ — Здесь находится открытый архив журнала

DOI выпуска: 10.24075/vrgmu.2026-04
Свидетельство о регистрации средства массовой информации № 012769 от 29 июля 1994 г.
ISSN (Print): 2500-1094, ISSN (Online): 2542-1204.
Учредитель и издатель — Российский национальный исследовательский медицинский университет имени Н. И. Пирогова (Москва, Россия).
Журнал индексируется в научных базах Scopus, Web of Science, Google Scholar, SJR, DOAJ, Scilit, CyberLeninka, Embase, EZB, Lens.org, MITLibaries, OpenAlex, Research4Life, Scholia, Wikidata, ZDB.

Подписано в печать 31.08.2026
Тираж 100 экз. Отпечатано в типографии Print.Formula
www.print-formula.ru

BULLETIN OF RSMU **4, 2026**
ВЕСТНИК РГМУ

Contents
Содержание

ORIGINAL RESEARCH 4

Effects of standard and photoactivated platelet-rich plasma on human meniscus fibrochondrocytes in IL-1β-induced inflammation
Kerimov KB, Ivanov AS, Tananakina TP, Kashchenko SA, Pogorelova IA

Влияние стандартной и фотоактивированной обогащенной тромбоцитами плазмы на фиброхондроциты мениска человека при IL1β-индуцированном воспалении
К. Б. Керимов, А. С. Иванов, Т. П. Тананакина, С. А. Кащенко, И. А. Погорелова

ORIGINAL RESEARCH 13

Platelet receptor gene polymorphisms and altered platelet aggregation in patients with COVID-19 and type 2 diabetes mellitus
Osikov MV, Antonov VN, Zotov SO

Полиморфизмы генов тромбоцитарных рецепторов и изменение агрегации тромбоцитов у больных COVID-19 и сахарным диабетом 2-го типа
М. В. Осиков, В. Н. Антонов, С. О. Зотов

ORIGINAL RESEARCH 21

Integrated reference panel of Macaca mulatta haplotypes for genotype imputation in populations of mixed origin
Sharko FS, Prokopenko AV, Izotova AO, Toshchakov SV

Интегрированная референсная панель гаплотипов *Macaca mulatta* для импутации генотипов в популяциях смешанного происхождения
Ф. С. Шарко, А. В. Прокопенко, А. О. Изотова, С. В. Тощаков

ORIGINAL RESEARCH 29

Molecular genetic aspects of predicting early pregnancy loss
Yusef OV, Ibragimov BR, Klimenko MP, Gerasimova AA, Aimetdinova AB, Marnat EG, Abramov DD, Klimenko PA, Kurtser MA

Молекулярно-генетические аспекты прогнозирования ранних репродуктивных потерь
О. В. Юсеф, Б. Р. Ибрагимов, М. П. Клименко, А. А. Герасимова, А. Б. Айметдинова, Е. Г. Марнат, Д. Д. Абрамов, П. А. Клименко, М. А. Курцер

ORIGINAL RESEARCH 36

Can autochthonous endometrial microbiota be detected by transcervical sampling?
Zornikov DL, Simarzina VM, Islamidi DK, Belykh NS, Kornilov DO, Abakumova EI, Khayutin LV, Plotko EE, Voroshilina ES

Можно ли обнаружить аутохтонную микробиоту эндометрия при трансцервикальном взятии проб?
Д. Л. Зорников, В. М. Симарзина, Д. К. Исламиди, Н. С. Белых, Д. О. Корнилов, Е. И. Абакумова, Л. В. Хаютин, Е. Э. Плотко, Е. С. Ворошилина

ORIGINAL RESEARCH 46

Construction and characterization of the attenuated recombinant influenza virus strains expressing human interleukin 1β
Romanovskaya-Romanko EA, Ozhereleva OO, Plotnikova MA, Altuhov AS, Stukova MA

Конструирование и характеристика аттенуированных рекомбинантных штаммов вируса гриппа, экспрессирующих интерлейкин-1β человека
Е. А. Романовская-Романько, О. О. Ожерельева, М. А. Плотникова, А. С. Алтухов, М. А. Стукова

ORIGINAL RESEARCH 54

FTIR signatures of protein conformational changes in gingival crevicular fluid in children with caries and gingivitis
Seredin PV, Ippolitov YuA, Ippolitov IYu, Goloshchapov DL, Litvinova TA

FTIR-признаки перестройки белков десневой жидкости у детей при кариесе и гингивите
П. В. Середин, Ю. А. Ипполитов, И. Ю. Ипполитов, Д. Л. Голощапов, Т. А. Литвинова

ORIGINAL RESEARCH 61

Chronic fatigue in siblings of pediatric cancer survivors: children's self-reports and parents' proxy-reports
Likhomanova EN, Shevaldova OV, Kovaleva AV

Хроническое утомление у сиблингов детей с онкологическими заболеваниями: самоотчеты детей и наблюдения родителей
Е. Н. Лихоманова, О. В. Шевалдова, А. В. Ковалева

ORIGINAL RESEARCH 70

Integrative pharmacognostical profiling & *in vitro* antibacterial activity assessment of *Murraya koenigii* (L.) Spreng
Ashwaq T. Kareem

Комплексный фармакогностический анализ и оценка антибактериальной активности *Murraya koenigii* (L.) Spreng *in vitro*
Ашвак Т. Карим

EFFECTS OF STANDARD AND PHOTOACTIVATED PLATELET-RICH PLASMA ON HUMAN MENISCUS FIBROCHONDROCYTES IN IL-1β-INDUCED INFLAMMATION

Kerimov KB[1], Ivanov AS[1,2,3] ✉, Tananakina TP[3], Kashchenko SA[3], Pogorelova IA[3]

[1] MEDSI Clinic, Clinical Hospital No. 1, Moscow, Russia
[2] Scientific and Diagnostic Center "Polyclinic on Smolenskaya", Moscow, Russia
[3] St. Luke Lugansk State Medical University, Russia

The meniscus degeneration pathogenesis is important for understanding and developing new treatment methods; it includes biochemical, structural, and microcirculatory alterations affecting all joint structures. The study aimed to perform *in vitro* assessment of the effects of standard and photoactivated platelet-rich plasma (PRP) on the IL6, IL17A concentrations, expression of COL2A1 and CD95 apoptosis marker in human meniscus fibrochondrocytes in the IL1β-induced inflammation. The human knee meniscus cartilage tissue was collected from 12 somatically healthy donors aged 18 to 35 years for the experiment. Cells were divided into four groups: the first was intact (control), the second, third, and fourth ones were exposed to IL1β to induce degenerative alterations; the second one was supplemented with 0.9% NaCl, the third one with donor PRP, and the fourth one with photoactivated PRP. Parameters were determined after 48 h. Statistical analysis was performed in GraphPad Prism 9. The rm-ANOVA was used for related groups. Data were presented as mean ± SD, at $p < 0.05$. IL6 (79.6 ± 4.3 pg/mL vs. 28.4 ± 2.1 pg/mL), IL17A (42.8 ± 2.5 pg/mL vs. 14.2 ± 1.0 pg/mL), CD95 (28.5 ± 2.2% vs. 6.8 ± 0.7%) levels increased in group II compared to group I; COL2A1 levels decreased from 1.00 ± 0.08 to 0.42 ± 0.5. IL6 levels decreased to 55.1 ± 3.4 pg/mL, IL17A — to 29.4 ± 2.1 pg/mL, CD95 — to 17.2 ± 1.5%, and COL2A1 levels increased to 0.71 ± 0.06 in group III compared to group II. IL6 levels decreased to 38.2 ± 2.6 pg/mL, IL17A — to 18.6 ± 1.7 pg/mL, CD95 — to 9.4 ± 0.8%, and COL2A1 levels increased to 0.94 ± 0.07 ($p < 0.05$) in group IV compared to group III. Standard PRP has a positive effect on meniscus tissue *in vitro* after 48 h. The effect is enhanced after the PRP exposure to red light.

Keywords: meniscus, fibrochondrocytes, platelet-rich plasma, PRP, photoactivation, red light, interleukin, COL2A1, CD95

Author contribution: Kerimov KB — study design, experimental procedure, calculations; Ivanov AS — study design, experimental design; Tananakina TP — study design, experimental design, scientific supervision; Kashchenko SA — scientific editing, scientific supervision, part in preparing the experiment; Pogorelova IA — technical proofreading, part in preparing the experiment.

Compliance with ethical standards: the study approved by the Ethics Committee of the St. Luke Lugansk State Medical University (protocol No. 2 dated May 26, 2026) was fully compliant with the Eurasian Economic Commission (EEC) Board "Guidelines for the Use of Laboratory (Experimental) Animals in Preclinical (Non-Clinical) Studies" dated November 14, 2023, No. 33, principles of the European Convention for the Protection of Vertebrate Animals used for Experimental and Other Scientific Purposes, as well as the Directive of the European Parliament and of the Council of the European Union on the Protection of Animals Used for Scientific Purposes. All the patients submitted the written informed consent for the material collected to be used for experimental purposes.

✉ **Correspondence should be addressed:** Aleksey S. Ivanov
A. Dikogo 16A, 73, 111396, Moscow, Russia, sashatravmatolog1985@mail.ru

Received: 27.06.2026 **Accepted:** 20.08.2026 **Published online:** 26.08.2026

DOI: 10.24075/brsmu.2026.046

ВЛИЯНИЕ СТАНДАРТНОЙ И ФОТОАКТИВИРОВАННОЙ ОБОГАЩЕННОЙ ТРОМБОЦИТАМИ ПЛАЗМЫ НА ФИБРОХОНДРОЦИТЫ МЕНИСКА ЧЕЛОВЕКА ПРИ IL1β-ИНДУЦИРОВАННОМ ВОСПАЛЕНИИ

К. Б. Керимов[1], А. С. Иванов[1,2,3] ✉, Т. П. Тананакина[3], С. А. Кащенко[3], И. А. Погорелова[3]

[1] Клиника «МЕДСИ», Клиническая больница № 1, Москва, Россия
[2] Научно-диагностический центр «Поликлиника на Смоленской», Москва, Россия
[3] ФГБОУ ВО ЛГМУ имени Святителя Луки Минздрава России, Россия

Патогенез дегенеративных изменений мениска важен для понимания и разработки новых методик лечения и включает в себя биохимические, структурные и микроциркуляторные изменения, затрагивающие все структуры сустава. Цель исследования — изучить влияние стандартной и фотоактивированной обогащенной тромбоцитами плазмы (PRP) *in vitro* на концентрацию IL6, IL17A, экспрессию COL2A1 и маркера апоптоза CD95 фиброхондроцитов мениска человека при IL1β-индуцированном воспалении. Для эксперимента отобрали хрящевую ткань мениска коленного сустава человека у 12 соматически здоровых доноров от 18 до 35 лет. Клетки разделены на четыре группы: первая — интактная (контроль), вторая, третья и четвертая подвергались воздействию IL1β для индукции дегенеративных изменений, во вторую вносили 0,9% NaCl, в третью — PRP доноров, в четвертую — PRP с фотоактивацией. Показатели определяли через 48 ч. Статистические расчеты проводили в GraphPad Prism 9. Для связанных групп применяли rm-ANOVA. Данные представлены как mean ± SD, при $p < 0,05$. Во II группе в сравнении с I возрастали IL6 (79,6 ± 4,3 пг/мл против 28,4 ± 2,1 пг/мл), IL17A (42,8 ± 2,5 пг/мл против 14,2 ± 1,0 пг/мл), CD95 (28,5 ± 2,2% против 6,8 ± 0,7%) соответственно; снизился COL2A1 (с 1,00 ± 0,08 до 0,42 ± 0,05); в III группе по сравнению со II снижались IL6 до 55,1 ± 3,4 пг/мл, IL17A — до 29,4 ± 2,1 пг/мл, CD95 до 17,2 ± 1,5%, COL2A1 повысился до 0,71 ± 0,06; IV группе по сравнению с III снижались IL6 до 38,2 ± 2,6 пг/мл, IL17A — до 18,6 ± 1,7 пг/мл, CD95 — до 9,4 ± 0,8%; повысился COL2A1 до 0,94 ± 0,07 ($p < 0,05$). Стандартная PRP оказывает положительное влияние на ткани мениска *in vitro* через 48 ч. Эффект усиливается после воздействия красного света на PRP.

Ключевые слова: мениск, фиброхондроциты, обогащенная тромбоцитами плазма, PRP, фотоактивация, красный свет, интерлейкин, COL2A1, CD95

Вклад авторов: К. Б. Керимов — дизайн исследования, экспериментальная часть работы, расчеты; А. С. Иванов — дизайн исследования, экспериментальная часть работы; Т. П. Тананакина — дизайн исследования, экспериментальная часть работы, научное сопровождение; С. А. Кащенко — научное редактирование, научное сопровождение, подготовка эксперимента; Погорелова И. А. — техническое редактирование, подготовка эксперимента.

Соблюдение этических стандартов: исследование одобрено этическим комитетом ФГБОУ ВО ЛГМУ имени Святителя Луки, МЗ РФ (протокол № 2 от 26 мая 2026 г.), полностью соответствует рекомендации Коллегии ЕЭК «Руководство по работе с лабораторными (экспериментальными) животными при проведении доклинических (неклинических) исследований от 14.11.2023 № 33», принципам Европейской конвенции о защите позвоночных животных, используемых для экспериментов или в иных научных целях, а также в соответствии с директивой Европейского парламента и совета Европейского союза по охране животных, в научных целях. Все пациенты подписали письменное согласие на использование полученного материала для экспериментальных целей.

✉ **Для корреспонденции:** Алексей Сергеевич Иванов
ул. А. Дикого, д. 16А, кв. 73, 111396, г. Москва, Россия, sashatravmatolog1985@mail.ru

Статья получена: 27.06.2026 **Статья принята к печати:** 20.08.2026 **Опубликована онлайн:** 26.08.2026

DOI: 10.24075/vrgmu.2026.046

Musculoskeletal disorders with the human knee meniscus degenerative-dystrophic alterations affect a broad segment of the population, primarily people of working age, and often become the cause of disability, which determines the medical, social and economic burden for each patient and society as a whole [1]. The meniscus tissue degeneration pathogenesis includes biochemical, structural, and microcirculatory alterations affecting all joint structures, and understanding the pathogenesis is important for the development of new treatment methods [2]. The cartilage degeneration results from the combined effects of biological and mechanical factors leading to violation of the joint homeostasis, subsequent development of persistent inflammation with the increase in pro-inflammatory cytokine concentrations, initiation of apoptotic processes, downregulation of the genes encoding the extracellular matrix components, and, finally, to the cartilage tissue volume reduction and the joint biomechanics alteration [3].

Pro-inflammatory cytokines (IL1β, IL6, IL8, IL17A, and tumor necrosis factor) play a significant role in the development of progression of the meniscus tissue degeneration. IL1β causes inhibition of the new collagen and proteoglycan synthesis in chondrocytes, including due to activation of metalloproteinase enzymes. The tumor necrosis factor induces local synovial membrane inflammation and chondrocyte apoptosis in the joint. IL8 causes the recruitment of immune cells (neutrophils and macrophages) into the joint cavity, thereby increasing damage [4]. IL6 is known not only as an inflammation development and progression factor; its physiological effects are of great importance. It is produced by T and B cells, granulocytes, smooth muscle cells, eosinophils, mast cells, glial cells, keratocytes; it is involved in the endocrine, hematopoietic, nervous system functioning [5]. In previous *in vitro* studies, the IL6 capability of inducing inhibitors of matrix metalloproteinases was determined [6]. The increase in the synovial fluid cytokine concentrations leads to increased pain and loss of cartilage tissue volume, especially in end-stage osteoarthritis [1, 7]. It has been shown that in patients with the combination of obesity and osteoarthritis, blood levels of IL6 are elevated and correlation with the progression of these disorders [8].

IL17A plays an important role in the pathogenesis of the knee meniscus tissue degeneration. The cytokine is produced by macrophages, as well as by the γδ–T cells that are found in mucous membranes and involved in antimicrobial immunity. It is assumed that these cells contribute to bone tissue regeneration. In individuals with the knee meniscus tissue degeneration, γδ–T cells can cause the increased interleukin production on a par with NK cells, the synovial membrane counts of which are increased in osteoarthritis [9]. NK cells accumulate in inflamed tissues, where these are stimulated by other pro-inflammatory cytokines (IL12, IL15, and IL18) secreted by monocytes. Suppression of anabolic factors (for example, downregulation of the COL2A1 gene) in chondrocytes with subsequent degenerative changes occurs under the exposure to IL17A. Thus, it has been found that the concentration of pro-inflammatory cytokines is significantly decreased in patients post total knee replacement [10–13].

Collagen, ensuring the connective tissue strength, elasticity, regulation, and regeneration, is the main structural component of extracellular matrix. Collagen type II is a component of cartilage tissue, being the main component of the alpha chain; it is encoded by the *COL2A1* gene [14, 15]. The *COL2A1* expression tissue-specific nature is a fundamental factor in determining the clinical features of associated diseases, divided into two groups depending on the affected tissue type. The first group includes developmental disorders of the musculoskeletal system (for example, dwarfism, kyphoscoliosis, limb shortening, joint abnormalities, hard palate malformations) and its functional competence in adulthood (for example, osteoarthritis affecting joints of various localizations). The second group includes extraskeletal abnormalities (hearing loss, eye disorder, such as myopia, retinal detachment, etc.) [16, 17].

Apoptosis, oxidative stress, age, nutrition, and hereditary factors are elements of the meniscus tissue degeneration process [18]. Apoptosis is triggered by activation of the CD95 receptor located on the cell membrane that is a member of the tumor necrosis factor α (TNF α) group [19]. The CD95 receptor triggering results in the emergence of a multi-protein complex, the interaction of which with the adapter molecules results in not only cell death, but also cell proliferation. Apoptosis most often occurs via the mitochondrial pathway, in which mitochondrial contents enter the cytoplasm due to activation of the p53 protein, activation of enzymes, DNA fragmentation, production of proapoptotic bodies and subsequent cell phagocytosis [20].

Nonsteroidal anti-inflammatory drugs (NSAIDs) are conventionally used for treatment of chondropathy of various origins, including osteoarthritis affecting joints. However, platelet-rich plasma (PRP) has become increasingly widely used in recent years. Various studies have shown that PRP can reduce inflammation and chondrocyte degeneration [21–24]. Photoactivated PRP enhances bioactivity and regeneration capacity of platelets through active release of growth factors contained in alpha granules, specifically the transforming growth factor β1 (TGF-β1), fibroblast growth factor, and platelet-derived growth factor [25]. The effectiveness of the treatment method used was demonstrated in large cohorts of patients, along with NSAIDs and glucocorticoids, but the mechanism underlying alteration of the secretory, phenotypic, and matrix profiles of chondrocytes in the meniscus tissue with degenerative alterations is poorly understood, it is of great interest in terms of determining biological targets when using PRP.

The study aimed to assess the effects of standard and photoactivated PRP on pro-inflammatory cytokine (IL6, IL17A) concentration, collagen type II (*COL2A1*) gene expression, and the CD95 apoptosis and meniscus degeneration marker in human meniscus fibrochondrocytes in the IL1β-induced inflammation *in vitro*.

METHODS

Chondrocytes isolated from the patients' knee joint menisci were used for the study; fragments of menisci were collected by arthroscopic resection during reconstruction of the anterior cruciate ligament. Experiments were conducted at the St. Luke Lugansk State Medical University.

The meniscus cartilage tissue samples were collected from 12 somatically healthy patients aged 18–35 years. Exclusion criteria: patients having systemic inflammatory disorders of immune and infectious origin; septic arthritis; treatment with intra-articular glucocorticoid injections throughout a month before the intervention. Inclusion criteria: degeneration of the knee meniscus verified based on the knee magnetic resonance imaging data and confirmed during arthroscopy; possibility of collecting sufficient quantities of tissue samples (4–8 mm^3 in total) to be later used in the experiment.

The collected meniscus tissue samples of all 12 donors were washed in phosphate buffered saline supplemented with penicillin (100 U/mL) and streptomycin (100 μg/mL), then crushed to 1–2 mm^3, and further treated with the 0.2% collagenase type II enzyme (Thermo Fisher Scientific, USA; catalog number 17101015, specific activity ≥ 125 U/mg (Mandl

units)). This enzyme was selected due to optimal ratio of the associated proteases, clostripain, and lipases essential for the hydrolysis of rigid collagen type II fibers. Cartilage disaggregation was conducted throughout 12 h at a temperature of 37 °C in the 5% CO_2 atmosphere with constant rocking. The resulting cell suspension was filtered through the nylon filter with the pore diameter of 70 μm and then centrifuged at 1500 rpm for 5 min. The isolated chondrocytes were cultured in the DMEM/F12 medium (Dulbecco's Modified Eagle Medium/Nutrient Mixture F-12) supplemented with the 10% fetal bovine serum and 1% penicillin and streptomycin solution at 37 °C, 5% CO_2. Cells from 2–3 passages were used for the experiment. Meniscus tissue samples from each donor were divided into four groups [26]: the first group remained unexposed, in all other samples degenerative damage was modeled by adding IL1β, standard PRP was added to cells of the third group, photoactivated PRP was added to cells of the fourth one.

Degenerative changes in the cells were induced by exposing the conjugated chondrocyte cultures (80–90%) to recombinant human IL1β (R&D Systems (Bio-Techne, USA; catalog number: 201-LB-005 per 5 μg) at a concentration of 10 ng/mL throughout 48 h. Such experimental approach was selected based on the earlier validated models of ostheoarthrosis and degenerative damage to meniscus tissue showing the IL1β-mediated activation of catabolic signaling pathways, degradation of the extracellular matrix, production of pro-inflammatory cytokines, and activation of apoptosis [27].

PRP was produced from the peripheral venous blood of the meniscus tissue donors after the admission and before the drug and surgical treatment in order to minimize the effects of medications used for anesthesia and further treatment. To strictly control the method reproducibility, avoid the cell composition contamination, and ensure dosage standardization, the Ycellbio test tubes (Ycellbio Medical Co., Ltd., Korea) and the two-step centrifugation protocol were used. Whole blood was collected straight in the test tubes containing 3.8% sodium citrate solution as an anticoagulant in a standard ratio. Sodium citrate was used strictly as an inhibitor of premature platelet activation during blood sampling and fractionation. The platelet concentrate isolation was performed using a specialized PLC-02 laboratory centrifuge (Ycellbio Medical Co., Ltd., Korea) equipped with the 45° fixed angle rotor with the maximum radius of rotation R_{max} = 13.5 cm. The first centrifugation was carried out at 1500 rpm (relative centrifugal force about 300 × g) for 10 min; after a few seconds, a second centrifugation was performed at 3500 rpm (relative centrifugal force about 1650× g) for 10 min. The resulting PRP produced in accordance with the manufacturer's instructions contained 1.0–1.2 × 10^6 platelets/μL, which corresponded to the 4–5-fold increase in platelet concentration compared to the baseline peripheral blood level. According to PAW (Platelet, Activation, White blood cells) classification: class P3-A (high platelet concentration, no previous exogenous activation, leukocyte-erythrocyte fraction) [28].

Photoactivation of experimental PRP samples without cartilage cells was performed by exposure to red light using a LED photoactivation system (Juventix LED Activator, USA) with the following settings: wavelength — 650 ± 10 nm, power density — 80 mW/cm^2, radiation spectrum full width at half maximum (FWHM) — 20 nm, beam divergence angle — 120°, exposure time — 7 min, distance from the light source — 10 cm, ambient temperature — 22–24 °C. The output power density (80 mW/cm^2) stability was ensured by a precision current power supply with the integrated power feedback, certified by the equipment manufacturer. Such parameters were selected to ensure the release of growth factors from alpha-granules of platelets due to more intense energy effect. Such PRP activation parameters were also selected considering the plasma optical density (possibility of light absorption by proteins). Immediately after photoactivation PRP added to the culture medium containing chondrocytes at the final concentration of 10% [29].

Biological samples obtained from each donor were evenly distributed across all experimental groups. Samples from each donor (n = 12 biological units (donors)) were coded with numbers, and laboratory tests were carried out in a blind manner. Cells from each donor were divided into four experimental groups, for each of which three technical replicates were performed: group 1 (control) — intact chondrocytes, no experimental exposure to interleukin; group 2 — chondrocytes exposed to IL1β supplemented with saline (0.9% sodium chloride solution); group 3 — cells altered under exposure to IL1β added PRP without photoactivation; group 4 — cells altered under exposure to IL1β added photoactivated PRP only. Equivalent volumes of saline (0.9% sodium chloride solution) and PRP were added. IL6, IL17A, CD95, *COL2A1* levels were assessed 48 h after the start of cell incubation with the addition of normal and photoactivated PRP.

The IL6, IL17A concentrations were determined using the R&D Systems kits (by Bio-Techne), series Quantikine ELISA (USA), in accordance with the manufacturer's protocol. The CD95 apoptosis marker was assessed using flow cytometry, the *COL2A1* expression was determined using the real-time polymerase chain reaction (RT-qPCR).

The *COL2A1* (collagen type II) expression levels were determined by the real-time quantitative polymerase chain reaction (RT-qPCR) in strict compliance with the MIQE international standard [30].

The total RNA extraction from the cartilage tissue samples was performed using the RNeasy Mini Kit (Qiagen, Germany) in accordance with the manufacturer's protocol. The extracted RNA concentration and purity were assessed by spectrophotometry using NanoDrop 2000 (Thermo Scientific, USA) based on the A260/A280 optical density ratio (within the range of 1.8–2.0). The RNA integrity was confirmed by the 1% agarose gel electrophoresis. The complementary DNA (cDNA) was synthesized from 1 μg of the total RNA using the RevertAid RT Reverse Transcription Kit (Thermo Scientific, USA) and the mixture of oligo (dT) and random primers.

To avoid errors associated with the use of only one unvalidated reference, the data were normalized to the geometric mean of two stable human genes: GAPDH (glyceraldehyde-3-phosphate dehydrogenase) and ACTB (β-actin). Human-specific oligonucleotide primers (NCBI Primer-BLAST) were selected at the boundaries of exon-exon junctions (intron-spanning) to avoid amplification of the genomic DNA. Amplification was accomplished in the CFX96 Touch system (Bio-Rad, USA) with the SYBR Green intercalating dye using the PowerUp SYBR Green Master Mix (Applied Biosystems, USA). The protocol included denaturation (95 °C, 2 min) and 40 cycles: denaturation (95 °C, 15 c), annealing/elongation (60 °C, 30 c). To verify product specificity after each launch, melting curves were analyzed with the range of 65–95 °C; in all reactions, a single melting peak without primer dimers was recorded. Each biological sample was tested in technological triplicates with the mandatory use of controls with no template (NTC) and no reverse transcriptase (NRT).

The amplification efficiency (E) was determined based on calibration curves of 5-fold serial dilutions of the cDNA pool. The straight line slope was between –3.31 and –3.34 (R_2 > 0.99), which showed high and comparable efficacy of reactions:

(E = 99.1%) for *COL2A1*, (E = 99.6%) for GAPDH, and (E = 98.9%) for ACTB. The *COL2A1* mRNA relative expression was calculated using the comparative 2-ΔΔ *Ct* method [31]. The Δ*Ct* value was determined as the difference between the threshold cycle of the target gene and the geometric mean of threshold cycles of reference genes (*CtCOL2A1* — geometric mean *Ct*ref). The final value of the fold change of expression was expressed relative to the control group (intact/healthy untreated cells).

Determination of the CD95 membrane receptor expression by flow cytometry

The CD95-positive cell counts and the receptor expression density on the membrane were assessed using a monoclonal mouse antibody against human CD95 (Mouse Anti-Human CD95, BioLegend, USA). The phycoerythrin (PE) fluorochrome was used for conjugation of antibodies (BioLegend, Inc., USA).

The chondrocyte suspension in the amount of 1×10^6 cells per test was precipitated by centrifugation at 300× g for 5 min. The cell sediment was resuspended in 100 µL of phosphate-buffered saline (PBS) containing 0.5% bovine serum albumin (BSA) and 2 mM EDTA (cytometry buffer). In order to minimize nonspecific binding via Fc receptors the samples were pre-incubated with the reagent for Fc receptor blockage (Human TruStain FcX (BioLegend), USA), 10 min at +4 °C. The Anti-CD95 monoclonal antibody was added (BioLegend, Inc., USA), 5 µL per test, and incubation was performed for 30 min in a dark place at a temperature of +4 °C. After the end of incubation the cells were twice washed with 1 mL of excess cold cytometry buffer by centrifugation (300× g, 5 min). The resulting sediment was resuspended in 300 µL of buffer. A vital dye, propidium iodide (PI) (Sigma-Aldrich (Merck), USA), at a concentration of 1 µg/mL was added to samples 5 min before the analysis in order to avoid artifacts.

Gating was performed in the BD FACSCanto II flow cytometer (BD Biosciences, USA), it involved recording of at least 50,000 target events for each sample. Data analysis was conducted using the FlowJo software (FlowJo, LLC (subsidiary of Becton, Dickinson and Company/BD Biosciences), USA). The live cell gating was performed by constructing the vital dye PI/7-AAD (Sigma-Aldrich, USA; BD Biosciences, USA) fluorescence distribution histogram. In further analyses, only the negative fraction dye was used ($PI^-/7\text{-}AAD^-$) to completely exclude dead cells from the CD95 expression analysis. Final gating was performed based on the fluorescence histogram in the PE detection channel through determination of the boundary (gate) separating $CD95^-$and $CD95^+$events. The boundary positioning was carried out strictly according to the upper fluorescence boundary of the isotype/FMO control (no more than 0.1–0.5% false positives were allows in the control). Quantity was assessed as a percentage of CD95-positive cells and the mean fluorescence intensity (MFI) reflecting the density of Fas receptors on the cell.

Data analysis was conducted in GraphPad Prism 9.4.1 (GraphPad Software, LLC (USA) and G*Power 3.1.9.7 (Heinrich Heine University Düsseldorf, Germany). A priori power calculation for the rm-ANOVA model (intragroup factor, four groups, $\alpha = 0.05$, power $1\text{-}\beta = 0.80$, expected large effect size f = 0.45 based on pilot data) defined the minimum sample size of n = 10. A total of 12 individual chondrocyte donors were included in the study. The distribution was tested for normality using the Shapiro–Wilk test and Q–Q plots [31], testing for homogeneity of variance was performed using the Levene's test [32], and that for sphericity was performed using the Mauchly's sphericity test. The rm-ANOVA (with the Greenhouse–Geisser correction for violation of sphericity) with the specified F-statistics F (f_{effect}, df_{error}) was used for related groups. Considering the simultaneous analysis of four indicators (IL6, IL17A, CD95, COL2A1), the critical significance level for rm-ANOVA was Bonferroni adjusted to $p_{crit} = 0.0125$). The pairwise post-hoc comparison was performed using the Tukey's test (p <0.05) based on the within-subject residual variance of the error (MS_{error}). The data are presented as mean ± SD and box-and-whisker plots with individual points. The 95% CI for the difference between means, partial eta-squared (η^2p) for the group factor, and the Cohen's d (d_z) for pairwise comparison were calculated.

RESULTS

Under the exposure of human meniscus chondrocytes to IL1β in vitro, the development of stable immune-inflammatory alterations, associated with the considerable increase in the levels of the studied pro-inflammatory cytokines, was reported within 48 h at the molecular level. The IL6 level increased 2.8-fold; $p < 0.05$; 95% CI for the difference between means: [48.2; 54.2]; $\eta^2 = 0.984$. Similar changes were reported for the IL17A concentration that increased 3-fold, $p < 0.05$; 95% CI for the difference between means: [26.8; 30.4]; $\eta^2 = 0.984$. In the cell cultures of donors included in group 2, the percentage of CD95-positive chondrocytes increased 4.2-fold, $p < 0.05$; 95% CI for the difference between means: [20.1; 23.3]; $\eta^2 = 0.980$), which suggests the fibrochondrocyte apoptosis initiation at the phenotype level. At the same time the expression of the main matrix protein COL2A1 was depressed 2.4-fold, $p < 0.05$; 95% CI for the difference between means: [–0.62; –0.54]; $\eta^2 = 0.954$, which may indicate the collagen synthesis suppression and its degradation under the exposure to IL1β (Table 1).

Adding standard PRP to the meniscus cell samples resulted in partial mitigation of induced inflammatory and degenerative processes in all the studied cultures. This clearly manifested itself in the 1.4-fold decrease in the IL6 concentration; $p < 0.05$; 95% CI for the difference between means: [–27.1; –21.9]; $\eta^2 = 0.911$, 1.5 decrease in the IL17A concentration; $p < 0.05$; 95% CI for the difference between means: [–15.4; –11.4]; $\eta^2 = 0.879$. At the cell phenotype level, the percentage of CD95-positive cells decreased 1.66-fold; $p < 0.05$; 95% CI for the difference between means: [–12.8; –9.8]; $\eta^2 = 0.919$. The *COL2A1* gene expression increased 1.7-fold, $p < 0.05$; 95% CI for the difference between means: [0.24; 0.34]; $\eta^2 = 0.896$ (Table 2).

After adding photoactivated PRP, a significant regression of inflammatory chondrocyte alteration was reported in all the studied groups. The IL6 levels decreased 1.4-fold; $p < 0.05$; 95% CI for the difference between means: [–19.1; –14.7]; $\eta^2 = 0.970$ compared to the values obtained after adding standard PRP. The IL17A concentration decreased 1.6-fold; $p < 0.05$; 95% CI for the difference between means: [–12.1; –9.5]; $\eta^2 = 0.972$. At the phenotype level, the 1.8-fold decrease in the percentage of CD95-positive cells was observed after adding photoactivated PRP; $p < 0.05$; 95% CI for the difference between means: [–8.4; –7.2]; $\eta^2 = 0.975$ compared to the groups of cells treated with standard PRP. The *COL2A1* gene expression increased 1.3-fold, $p < 0.05$; 95% CI for the difference between means: [0.18; 0.28]; $\eta^2 = 0.931$, which was almost compared with the values of the intact group (Table 3).

The dynamic changes in the studied indicators for all groups of *in vitro* cultures of the human meniscus cartilage are presented in Fig.

Table 1. Effects of interleukin-1β on the secretory, phenotypic and matrix profiled of human meniscus chondrocytes *in vitro* after the 48-h incubation (M ± SD [95% CI], *n* = 12)

Indicator	Control	*p*	IL1β + 0,9% NaCl	*p*
IL6 (pg/mL)	28.4 ± 2.1 [27.1; 29.7]	0.01	79.6 ± 4.3* [76.9; 82.3]	0.04
IL17A (pg/mL)	14.2 ± 1.0 [13.6; 14.8]	0.05	42.8 ± 2.5* [41.2; 44.4]	0.05
CD95 (%)	6.8 ± 0.7 [6.4; 7.2]	0.04	28.5 ± 2.2* [27.1; 29.9]	0.05
COL2A1 (2-ΔΔ *Ct*)	1.00 ± 0.08 [0.95; 1.05]	0.001	0.42 ± 0.05* [0.39; 0.45]	0.001

Note: * — $p < 0.05$ compared to control.

The IL6 concentration in group 2 increased by 180.3% (2.8-folda), IL17A concentration increased by 201.4% (3-fold), CD95 level increased by 319.1% (4.2-fold), and *COL2A1* level decreased by 58.0% (2.4-fold) compared to the control group (Fig.). The use of standard PRP resulted in the IL6 decrease by 30.8%, IL17A decrease by 31.3%, CD95 decrease by 39.6%; *COL2A1* increased by 69.0% compared to group 2. The use of photoactivated PRP resulted in the decrease in the levels of pro-inflammatory cytokines: IL6 by 52.01% (2.08-fold), IL17A by 5654% (2.30-fold), CD95 apoptosis marker by 67.02% (3.03-fold); *COL2A1* increased by 123.81% (2.24-fold) compared to group 2. When compared to the indicators of group 3, the effect of photoactivated PRP was superior to that of standard PRP: for IL6 — by 30.67% (1.44-fold), for IL17A — by 36.73% (1.58-fold), for CD95 — by 45.35% (1.83-fold); the *COL2A1* growth by 32.39% (1.32-fold) was reported, confirmed by the paired post-hoc Tukey's test.

DISCUSSION

The meniscus tissue degeneration is accompanied by low-grade inflammation due to the increase in the levels of pro-inflammatory cytokines, as well as by the cartilage tissue volume reduction [1, 5, 7]. In our study, the exposure to IL1β resulted in triggering the immune inflammation and the meniscus tissue degeneration *in vitro* as early, as 48 h after incubation. This is supported by the considerable increase in IL6 and IL17A levels compared to the control group, the increase in apoptosis marker levels, and the decrease in the *COL2A1* gene expression. This fact suggests that the more prolonged exposure to IL1β may result in more pronounced alterations, being one of the key cytokines of the degenerative damage to the meniscus tissue [8].

The *COL2A1* was selected as one of the molecular indicators of the meniscus fibrocartilaginous tissue due to its high pathogenetic significance for modeling osteoarthritis. The meniscus tissue is heterogeneous due to predominance of collagen type I ensuring elasticity in the vascular zone; the structure of the avascular zone that was collected for the study was close to that of the hyaline cartilage due to chondrocyte-like cells and the expression of collagen type II [33]. In the osteoarthritis- and obesity-associated inflammation, a phenotypic shift occurs in the meniscus cells, resulting in apoptosis and the decreased collagen type II synthesis (COL2A1). This gene is a marker of the meniscus avascular zone extracellular matrix degeneration and loss of shock-

Table 2. Effects of platelet-rich plasma on the inflammatory, phenotypic, and matrix profiles of human meniscus chondrocytes *in vitro* in the context of interleukin-1β-induced inflammation (M ± SD [95% CI], *n* = 12).

Indicator	IL1β + 0,9% NaCl	*p*	IL1β + PRP	*p*
IL6 (pg/mL)	79.6 ± 4.3 [76.9; 82.3]	0.04	55.1 ± 3.4# [52.9; 57.3]	0.001
IL17A (pg/mL)	42.8 ± 2.5 [41.2; 44.4]	0.05	29.4 ± 2.1# [28.1; 30.7]	0.05
CD95 (%)	28.5 ± 2.2 [27.1; 29.9]	0.05	17.2 ± 1.5# [16.2; 18.2]	0.01
COL2A1 (2-ΔΔ *Ct*)	0.42 ± 0.05 [0.39; 0.45]	0.001	0.71 ± 0.06# [0.67; 0.75]	0.04

Note: # — $p < 0.05$ compared to the group of IL1β.

Table 3. Comparative analysis of the effects of standard and photoactivated platelet-rich plasma on the inflammatory, phenotypic, and matrix profiles of human meniscus chondrocytes *in vitro* in the context of interleukin-1β-induced inflammation (M ± SD [95% CI], *n* = 12).

Indicator	IL1β + PRP	*p*	IL1β + photoactivated PRP	*p*
IL6 (pg/mL)	55.1 ± 3.4 [52.9; 57.3]	0.001	38.2 ± 2.6† [36.5; 39.9]	0.01
IL17A (pg/mL)	29.4 ± 2.1 [28.1; 30.7]	0.05	18.6 ± 1.7† [17.5; 19.7]	0.001
CD95 (%)	17.2 ± 1.5 [16.2; 18.2]	0.01	9.4 ± 0.8† [8.9; 9.9]	0.003
COL2A1 (2-ΔΔ *Ct*)	0.71 ± 0.06 [0.67; 0.75]	0.04	0.94 ± 0.07† [0.90; 0.98]	0.04

Note: † — $p < 0.05$ compared to the group of standard PRP.

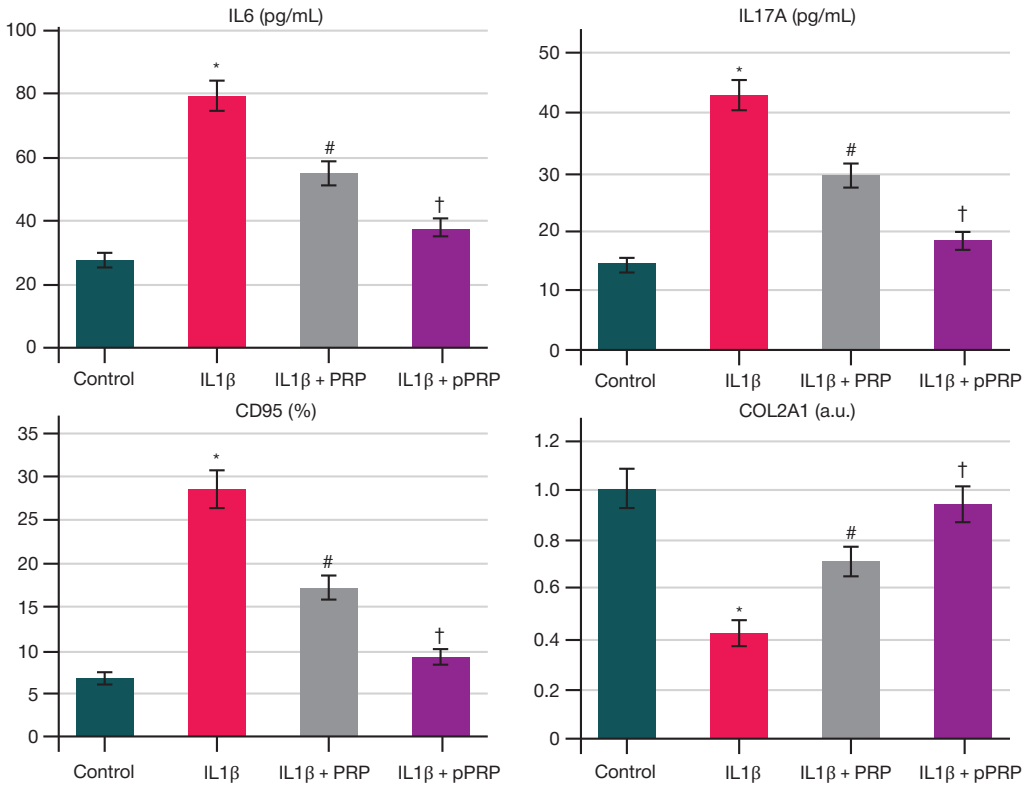

Fig. 1. Inflammatory (IL6, IL17A), phenotypic (CD95), and matrix (COL2A1) profiles of human meniscus chondrocytes *in vitro* I the IL1β-induced inflammation adjusted with standard and photoactivated PRP. Control — intact control group not exposed to IL1β; IL1β + 0,9% NaCl — group 2, IL1β + PRP — group 3; IL1β + p PRP — group 4. Each individual point on the graph corresponds to the average value of technical replicates for one biological donor out of 12. # — $p < 0.05$ compared to the "IL1β" group; † — $p < 0.05$ compared to the "IL1β + PRP" group (post-hoc Tukey's test for repeated measurements)

absorbing properties, up to the emergence of perforations [34]. Assessment of this indicator makes it possible to verify the therapy capability of preserving the chondrocyte-like phenotype of the meniscus cells and blocking the catabolic cascade, which cannot be assessed by analyzing distinct fibrous tissue substitution markers only (of collagen type I) [35].

Adjustment with platelet-rich plasma that can reduce the degenerative alteration manifestations in chondrocytes leads to the reduction of inflammation, which is similar to the effects of nonsteroidal anti-inflammatory drugs or glucocorticoids [2, 21–24]. Furthermore, PRP contains no additional chemical components. It contains only platelets that, in addition to their regenerative properties, can reduce manifestations of inflammation. The decrease in the IL6, IL17A, and CD95 marker concentrations was determined, along with the increase in the COL2A1 expression due to the PRP biological activity. Some in vitro and ex vivo studies suggest that PRP can cause chondrocyte proliferation. This process can come at the expense of mature cells, which, under similar conditions, exhibit the properties of fibroblasts, reducing the *COL2A1* expression, and synthesize the fibrous collagen type I (*COL2A1*) [36]; this was not confirmed in our study.

As determined in our experiment, the use of photoactivated plasms leads to further enhancement of the platelet biological activity and regenerative capacity. This can be due to the active release of the platelet-derived growth factors deposited in alpha granules and the inflammatory signaling pathway modulation. The key role in the fibrocartilaginous tissue regeneration and reduction of damage is played by the transforming growth factor β-1 (TGF-β1), fibroblast growth factor (bFGF/FGF2), and platelet-derived growth factor (PDGF) [24, 25]. The reported molecular genetic and cellular effects were especially significant in group 4: the IL6, IL17A, and CD95 levels decreased and the *COL2A1* gene expression increased almost to the values of intact chondrocytes in group 1. The pro-inflammatory cytokine levels decreased due to inhibition of the key transcription factor NF-κB (nuclear factor kappa B). Phosphorylation and degradation of the IκB inhibitory protein are blocked under the exposure to PRP, which later leads to the knockout of the genes encoding pro-inflammatory cytokines. Photoactivation leads to the enhancement of such effect through activation of the mitochondrial cytochrome C oxidase activation, adenosine triphosphoric acid (ATP) stimulation, and the short-term release of reactive oxygen species activating endogenous pro-inflammatory factors. The phosphorylation cascade activation leads to inhibition of proapoptotic proteins of the Bcl-2 family (Bax and Bad), FoxO transcription factor blockage, resulting in the CD95 receptor deactivation and further triggering of effector caspases [37].

The *COL2A1* gene expression increase following adding photoactivated PRP results from activation of the Smad2/3 signaling pathway under the exposure to TGF-β1 binding to the TGFBR1/TGFBR2 receptors. As a result, the Smad2 and Smad3 protein phosphorylation occurs. The resulting complex translocates to the nuclear region and binds to the SOX9 gene promoter responsible for chondrogenesis. When activated, the gene ensures triggering of the *COL2A1* mRNA expression cascade, resulting in the increased synthesis of collagen type II and the increased density of the meniscus extracellular matrix [38]. The use od standard PRP has less potential for *COL2A1* compared to the photoactivated form, since the degranulation kinetics are lower. Sharp and excessive proliferative stimulation of chondrocytes with standard PRP can cause their transient differentiation, leading to the suppression of the synthesis of key structural markers [39]. When the irradiation protocol is violated, photoactivated plasma may have restructured degranulation kinetics, providing a prolonged release of growth factors (PDGF, bFGF). The excess of the latter leads to continuous division of

chondrocytes, causing the shutdown of anabolic synthesis of the cellular matrix *COL2A1* and ACAN [25].

The experimental data obtained suggest the possibility of using platelet-rich plasma by the standard method and with photoactivation for the cartilage tissue regeneration, as well as using it for reconstructive surgery of the meniscus and chondroplasty.

Limitations of the study

The exceptionally high effect size (η^2 = 0.879–0.984) and low inter-donor variability (CV ≈ 5–8%) reported for human material result from the strict biological standardization (use of early passage cells, synchronization of the cell cycle) and mathematical specificity of the rm-ANOVA model. Such a design isolates the donors' individual variability from the error variance, thereby naturally inflating the share of variance (η^2p) explained by the group factor and possibly limiting the direct extrapolation of the data *in vivo*.

CONCLUSIONS

During the study it has been found that the exposure of the culture of human meniscus tissue chondrocytes to IL1β *in vitro* leads to the increase in the concentrations of pro-inflammatory cytokines IL6, IL17 and the $CD95^+$ cell apoptosis marker, as well as to the decrease in the *COL2A1* gene expression in the culture. Such alterations demonstrate an immune inflammatory pattern with triggering the chondrocyte apoptosis and the extracellular matrix degradation in the cartilage under the exposure to IL1β. The use of PRP possessing biological activity and having a regeneration potential due to high platelet counts can reduce the severity of inflammation and apoptosis in the cartilage tissue, it positively affects regeneration and the collagen type II synthesis, i.e. effectively affects on the secretory (IL6, IL17A), matrix (*COL2A1*), and phenotypic (*CD95*) profiles of human meniscus fibrochondrocytes in the IL1β-induced inflammation *in vitro*. The study has shown that photoactivated PRP can have a more pronounced biological effect on all the studied parameters due to more active release of growth factors by platelets accompanied by normalization of the secretory, phenotypic, and matrix profiles. Further exploration of the effects of standard and photoactivated PRP in clinical practice with the development of optimal terms and frequency of intra-articular administration will make it possible to assess the chondrocyte regeneration mechanism when selecting a cell-based therapy method in patients with the meniscus cartilage tissue degeneration, including osteoarthritis.

References

1. Gladkova EV, Ivanov AN. Vzaimosvyaz' strukturnyh narushenij sustavnogo gialinovogo hryashcha i parametrov sistemnyh proyavlenij vospalitel'noj reakcii v patogeneze rannih stadij pervichnogo osteoartroza. Saratovskij nauchno-medicinskij zhurnal. 2018; 14 (3): 518–23. Dostupno po ssylke: https://cyberleninka.ru/article/n/vzaimosvyaz-strukturnyh-narusheniy-sustavnogo-gialinovogo-hryascha-i-parametrov-sistemnyh-proyavleniy-vospalitelnoy-reaktsii-v (data obrashcheniya: 27.06.2026). Russian.
2. Ivanov AS, Tananakina TP, Kashchenko SA, Pogorelova IA. Expression of microRNA miR146a in the blood plasma of rats with obesity and knee arthrosis after administration of dexamethasone. Bulletin of RSMU. 2025; 6: 209–15. DOI: 10.24075/brsmu.2025.056.
3. Plekhova NG, Kabalyk MA, Prosekova EV, Shumatov VB. Provospalitel'nye citokiny, hemokin CXSL17 i belki teplovogo shoka pri osteoartrite kolennogo sustava. Rossijskij immunologicheskij zhurnal. 2025; 28 (1): 129–34. DOI: 10.46235/1028-7221-16975-PCC. Russian.
4. Chow YY, Chin KY. The Role of Inflammation in the Pathogenesis of Osteoarthritis. Mediators Inflamm. 2020; 2020: 8293921. DOI: 10.1155/2020/8293921.
5. McGregor NE, Murat M, Elango J, Poulton IJ, Walker EC, et al. IL6 exhibits both cis- and trans-signaling in osteocytes and osteoblasts, but only trans-signaling promotes bone formation and osteoclastogenesis. J Biol Chem. 2019; 294 (19): 7850–63. DOI: 10.1074/jbc.RA119.008074.
6. Vadalà G, Di Giacomo G, Ambrosio L, Cannata F, Cicione C, Papalia R, Denaro V. Irisin Recovers Osteoarthritic Chondrocytes In Vitro. Cells. 2020; 9 (6): 1478. DOI: 10.3390/cells9061478.
7. Li L, Li Z, Li Y, Hu X, Zhang Y, et al. Profiling of inflammatory mediators in the synovial fluid related to pain in knee osteoarthritis. BMC Musculoskelet Disord. 2020; 21 (1): 99. DOI: 10.1186/s12891-020-3120-0.
8. Fedulichev NP. Provospalitel'nye citokiny v patogeneze osteoartrita. Universitetskaya klinika. 2024; 4 (53): 70–81. Dostupno po ssylke: https://cyberleninka.ru/article/n/provospalitelnye-tsitokiny-v-patogeneze-osteoartrita (data obrashcheniya: 27.06.2026). Russian.
9. Jaime P, García-Guerrero N, Estella R, Pardo J, GarcíaÁlvarez F, et al. CD56+/CD16- Natural Killer cells expressing the inflammatory protease granzyme are enriched in synovial fluid from patients with osteoarthritis. Osteoarthritis Cartilage. 2017; 25 (10): 1708–18. DOI: 10.1016/j.joca.2017.06.007.
10. Mimpen JY, Carr AJ, Dakin SG, Snelling SJ. Inhibition of interleukin-17-induced effects in osteoarthritis — An in vitro study. Osteoarthritis Cartilage. 2018; 26: S118. DOI: 10.1016/j.joca.2018.02.258.
11. Babaei M, Javadian Y, Narimani H, Ranaei M, Heidari B, et al. Correlation between systemic markers of inflammation and local synovitis in knee osteoarthritis. Caspian J Intern Med. 2019; 10 (4): 383–7. DOI: 10.22088/ cjim.10.4.383.
12. Snelling SJ, Bas S, Puskas GJ, Dakin SG, Suva D, et al. Presence of IL17 in synovial fluid identifies a potential inflammatory osteoarthritic phenotype. PLoS One. 2017; 12 (4): e0175109. DOI: 10.1371/journal.pone.0175109.
13. Lee YH, Song GG. Association between IL17 gene polymorphisms and circulating IL17 levels in osteoarthritis: a meta-analysis. Z Rheumatol. 2020; 79 (5): 482–90. DOI: 10.1007/s00393-019-00720-2.
14. Dydykina IS, Kovalenko PS, Kovalenko AA, Aboleshina AV. Znachenie nedenaturirovannogo kollagena dlya normalizacii funkcii hryashchevoj tkani sustavov. Medicinskij sovet. 2022; 16 (14): 145–53. DOI: 10.21518/2079- 701X-2022-16-14-145-153. Russian.
15. Zhang B, Zhang Y, Wu N, Li J, Liu H, Wang J. Integrated analysis of COL2A1 variant data and classification of type II collagenopathies. Clin Genet. 2020; 97: 383–95. DOI: 10.1111/cge.13680.
16. Mortier GR, Cohn DH, Cormier-Daire V, Hall C, Krakow D, Mundlos S, et al. Nosology and classification of genetic skeletal disorders: 2019 revision. Am J Med Genet A. 2019; 179 (12): 2393–419. DOI: 10.1002/ajmg.a.61366.
17. Viakhireva I, Bychkov I, Markova T, Shatokhina O, Karandasheva K, Udalova V, Bekhtereva Y, Ryzhkova O, Skoblov M. The molecular complexity of COL2A1 splicing variants and their significance in phenotype severity. Bone. 2024; 181: 117013. DOI: 10.1016/j.bone.2024.117013.
18. Huan Yu, Sai Yao, Chengchong Zhou, Fangda Fu, Huan Luo, Weibin Du, et al. Morroniside attenuates apoptosis and pyroptosis of chondrocytes and ameliorates osteoarthritic development by inhibiting NF-κB signaling. Journal of Ethnopharmacology. 2021; 266: 113447. DOI: 10.1016/j.jep.2020.113447.
19. Hussain A, Tarahomi T, Singh L, Bollampally M, Heydari-Kamjani M, Kesselman MM. Cardiovascular Risk Associated with TNF Alpha Inhibitor Use in Patients with Rheumatoid Arthritis. Cureus. 2021;

13 (9): e17938. DOI: 10.7759/cureus.17938.
20. Abramova TYa, Blinova EA, Pashkina EA, Grishina LV, Ilina NA, Chumasova O. A., i dr. Issledovanie effektornyh molekul avtonomnogo i neavtonomnogo vliyaniya apoptoza T-limfocitov v usloviyah «kletochnogo sosedstva» v kul'ture u zdorovyh lyudej i pacientov s RA. Medicinskaya immunologiya. 2022; 24 (6): 1119–38. DOI: 10.15789/1563-0625-SOE-2527. Russian.
21. Bagmut IYu, Ivanov OS, Sheremet MI, Smirnov SM, Kolisnyk IL, Ivanova JV, et al. Isolation of megakaryocytes using magnetic cell separation and adverse effects induced by diclofenac toxicity in an experiment. J Med Life. 2022; 15 (1): 65–70. DOI: 10.25122/jml-2020-0129.
22. Ivanov O, Haidash O, Voloshin V, Kondratov S, Smirnov A. Influence of the acting substance sodium diclofenac on bone marrow cells. Georgian Medical News. 2020; 306: 137–42. PMID: 33130661.
23. Ivanova YuV, Gramatiuk SM, Kryvoruchko IA, Prasol VO, Pulyaeva IS, Miasoiedov KV, et al. The Effect of pulsed photobiomodulation on proliferation and migration of human mesenchymal stem cells in vitro. Clinical and preventive medicine. 2024; (5): 87–92. DOI: 10.31612/2616-4868.5.2024.11.
24. Medvedev VL, Opolskij AM, Kogan MI. Perspektivy razvitiya regenerativnyh tekhnologij. Sovremennye znaniya ob autoplazme, obogashchennoi trombocitami i vozmozhnosti ee primeneniya v lechenii urologicheskih zabolevanii. Kubanskij nauchnyj medicinskij vestnik. 2018; 25 (3): 155–61. DOI: 10.25207/1608-6228-2018-25-3-155-161.
25. Irmak G, Gümüşderelioğlu M. Photo-activated platelet-rich plasma (PRP)-based patient-specific bio-ink for cartilage tissue engineering. Biomed Mater. 2020; 15 (6): 065010. DOI: 10.1088/1748-605X/ab9e46.
26. Gramatiuk S, Kryvoruchko I, Ivanova Y, Emily Hubbard, Maria Noebauer-Babenko, Karine Sargsyan. Artificial Intelligence-Based Quality Control of Cell Lines. Biopreserv Biobank. 2025; DOI: 10.1177/19475535251367317.
27. Li Y, Wang F, Ji B, Amati A, Cao L. FHL2 deteriorates IL-1β induced inflammation, apoptosis, and extracellular matrix degradation in chondrocyte-like ATDC5 cells by mTOR and NF-κB pathways. BMC Musculoskelet Disord. 2025; 26 (1): 331. DOI: 10.1186/s12891-025-08536-9.
28. Collins T, Alexander D, Barkatali B. Platelet-rich plasma: a narrative review. EFORT Open Rev. 2021; 6 (4): 225–35. DOI: 10.1302/2058-5241.6.200017.
29. Mishra Kanchan, Desai Pooja, Khanna Manish, Malhotra Sayesha. Photoactivated platelet-rich plasma (PA-PRP): A safe and effective treatment for musculoskeletal disorders. IP International Journal of Orthopaedic Rheumatology. 2025; 11: 71–75. DOI: 10.18231/j.ijor.25218.1765359797.
30. Bustin SA, Ruijter JM, van den Hoff MJB, Kubista M, Pfaffl MW, Shipley GL, et al. MIQE 2.0: Revision of the Minimum Information for Publication of Quantitative Real-Time PCR Experiments Guidelines. Clin Chem. 2025; 71 (6): 634–51. DOI: 10.1093/clinchem/hvaf043.
31. Videla-Jiménez P, Ruz F, López-Martín M. Research on box plot knowledge in statistical education: a systematic review of the literature. Eur J Psychol Educ. 2025; 40: 141. DOI: 10.1007/s10212-025-01048-z.
32. Livak KJ, Schmittgen TD. Analysis of relative gene expression data using real-time quantitative PCR and the 2(-Delta Delta C(T)) Method. Methods. 2001; 25 (4): 402–8. DOI: 10.1006/meth.2001.1262.
33. Raut RD, Chakraborty AK, Neogi T, Michael Albro, Brian Snyder, Thomas P. Schaer, et al. A multi-tissue human knee single-cell atlas identifies that osteoarthritis reduces regenerative tissue stem cells while increasing inflammatory pain macrophages. Commun Biol. 2025; 8: 1146. DOI: 10.1038/s42003-025-08586-8.
34. Mocanu V, Timofte DV, Zară-Dănceanu C-M, Labusca L, Obesity. Metabolic Syndrome, and Osteoarthritis Require Integrative Understanding and Management. Biomedicines. 2024; 12: 1262. DOI: 10.3390/biomedicines12061262.
35. Galicia-Canales BE, del Rocío Aguilar-Gaytán M, Álvarez-Pérez MA, Jarquín-Yáñez K, et al. Effect of peniocerol on human meniscal fibrochondrocyte inflammation induced by IL-1β and TNF-α through the NF-κB signaling pathway. Cellular and Molecular Biology. 2026; 72 (3): 36–44. DOI: 10.14715/cmb/2025.72.3.5.
36. Rikkers M, Dijkstra K, Terhaard BF, Admiraal J, Levato R, Malda J, et al. Platelet-Rich Plasma Does Not Inhibit Inflammation or Promote Regeneration in Human Osteoarthritic Chondrocytes In Vitro Despite Increased Proliferation. Cartilage. 2021; 13 (2_suppl): 991S–1003S. DOI: 10.1177/1947603520961162.
37. Zhao H, Zhu W, Mao W, Shen C. Platelet-rich plasma inhibits Adriamycin-induced inflammation via blocking the NF-κB pathway in articular chondrocytes. Mol Med. 2021; 27 (1): 66. DOI: 10.1186/s10020-021-00314-2.
38. O'Donnell C, Migliore E, Grandi FC, et al. Platelet-Rich Plasma (PRP) From Older Males With Knee Osteoarthritis Depresses Chondrocyte Metabolism and Upregulates Inflammation. J Orthop Res. 2019; 37: 1760–70. DOI: 10.1002/jor.24322.
39. Li M, Jing C, Liu Q, Zhang Y, Li K. Platelet-rich plasma in cartilage repair: biological mechanisms and clinical perspectives. Front Sports Act Living. 2026; 8: 1785754. DOI: 10.3389/fspor.2026.1785754.

Литература

1. Гладкова Е. В., Иванов А. Н. Взаимосвязь структурных нарушений суставного гиалинового хряща и параметров системных проявлений воспалительной реакции в патогенезе ранних стадий первичного остеоартроза. Саратовский научно-медицинский журнал. 2018; 14 (3): 518–23. Доступно по ссылке: https://cyberleninka.ru/article/n/vzaimosvyaz-strukturnyh-narusheniy-sustavnogo-gialinovogo-hryascha-i-parametrov-sistemnyh-proyavleniy-vospalitelnoy-reaktsii-v (дата обращения: 27.06.2026).
2. Иванов А. С., Тананакина Т. П., Кащенко С. А., Погорелова И. А. Экспрессия микроРНК miR146a в плазме крови крыс с ожирением и артрозом коленного сустава на фоне введения дексаметазона. Вестник РГМУ. 2025; 6: 223–9. DOI: 10.24075/vrgmu.2025.056.
3. Плехова Н. Г., Кабалык М. А., Просекова Е. В., Шуматов В. Б. Провоспалительные цитокины, хемокин CXCL17 и белки теплового шока при остеоартрите коленного сустава. Российский иммунологический журнал. 2025; 28 (1): 129–34. DOI: 10.46235/1028-7221-16975-PCC.
4. Chow YY, Chin KY. The Role of Inflammation in the Pathogenesis of Osteoarthritis. Mediators Inflamm. 2020; 2020: 8293921. DOI: 10.1155/2020/8293921.
5. McGregor NE, Murat M, Elango J, Poulton IJ, Walker EC, et al. IL6 exhibits both cis- and trans-signaling in osteocytes and osteoblasts, but only trans-signaling promotes bone formation and osteoclastogenesis. J Biol Chem. 2019; 294 (19): 7850–63. DOI: 10.1074/jbc.RA119.008074.
6. Vadalà G, Di Giacomo G, Ambrosio L, Cannata F, Cicione C, Papalia R, Denaro V. Irisin Recovers Osteoarthritic Chondrocytes In Vitro. Cells. 2020; 9 (6): 1478. DOI: 10.3390/cells9061478.
7. Li L, Li Z, Li Y, Hu X, Zhang Y, et al. Profiling of inflammatory mediators in the synovial fluid related to pain in knee osteoarthritis. BMC Musculoskelet Disord. 2020; 21 (1): 99. DOI: 10.1186/s12891-020-3120-0.
8. Федуличев Н. П. Провоспалительные цитокины в патогенезе остеоартрита. Университетская клиника. 2024; 4 (53): 70–81. Доступно по ссылке: https://cyberleninka.ru/article/n/provospalitelnye-tsitokiny-v-patogeneze-osteoartrita (дата обращения: 27.06.2026).
9. Jaime P, García-Guerrero N, Estella R, Pardo J, GarcíaÁlvarez F, et al. CD56+/CD16- Natural Killer cells expressing the inflammatory protease granzyme are enriched in synovial fluid from patients with osteoarthritis. Osteoarthritis Cartilage. 2017; 25 (10): 1708–18. DOI: 10.1016/j.joca.2017.06.007.
10. Mimpen JY, Carr AJ, Dakin SG, Snelling SJ. Inhibition of interleukin-17-induced effects in osteoarthritis — An in vitro study. Osteoarthritis

Cartilage. 2018; 26: S118. DOI: 10.1016/j.joca.2018.02.258.
11. Babaei M, Javadian Y, Narimani H, Ranaei M, Heidari B, et al. Correlation between systemic markers of inflammation and local synovitis in knee osteoarthritis. Caspian J Intern Med. 2019; 10 (4): 383–7. DOI: 10.22088/ cjim.10.4.383.
12. Snelling SJ, Bas S, Puskas GJ, Dakin SG, Suva D, et al. Presence of IL17 in synovial fluid identifies a potential inflammatory osteoarthritic phenotype. PLoS One. 2017; 12 (4): e0175109. DOI: 10.1371/journal.pone.0175109.
13. Lee YH, Song GG. Association between IL17 gene polymorphisms and circulating IL17 levels in osteoarthritis: a meta-analysis. Z Rheumatol. 2020; 79 (5): 482–90. DOI: 10.1007/s00393-019-00720-2.
14. Дыдыкина И. С., Коваленко П. С., Коваленко А. А., Аболешина А. В. Значение неденатурированного коллагена для нормализации функции хрящевой ткани суставов. Медицинский совет. 2022; 16 (14): 145–53. DOI: 10.21518/2079- 701X-2022-16-14-145-153.
15. Zhang B, Zhang Y, Wu N, Li J, Liu H, Wang J. Integrated analysis of COL2A1 variant data and classification of type II collagenopathies. Clin Genet. 2020; 97: 383–95. DOI: 10.1111/cge.13680.
16. Mortier GR, Cohn DH, Cormier-Daire V, Hall C, Krakow D, Mundlos S, et al. Nosology and classification of genetic skeletal disorders: 2019 revision. Am J Med Genet A. 2019; 179 (12): 2393–419. DOI: 10.1002/ajmg.a.61366.
17. Viakhireva I, Bychkov I, Markova T, Shatokhina O, Karandasheva K, Udalova V, Bekhtereva Y, Ryzhkova O, Skoblov M. The molecular complexity of COL2A1 splicing variants and their significance in phenotype severity. Bone. 2024; 181: 117013. DOI: 10.1016/j.bone.2024.117013.
18. Huan Yu, Sai Yao, Chengchong Zhou, Fangda Fu, Huan Luo, Weibin Du, et al. Morroniside attenuates apoptosis and pyroptosis of chondrocytes and ameliorates osteoarthritic development by inhibiting NF-κB signaling. Journal of Ethnopharmacology. 2021; 266: 113447. DOI: 10.1016/j.jep.2020.113447.
19. Hussain A, Tarahomi T, Singh L, Bollampally M, Heydari-Kamjani M, Kesselman MM. Cardiovascular Risk Associated with TNF Alpha Inhibitor Use in Patients with Rheumatoid Arthritis. Cureus. 2021; 13 (9): e17938. DOI: 10.7759/cureus.17938.
20. Абрамова Т. Я., Блинова Е. А., Пашкина Е. А., Гришина Л. В., Ильина Н. А., Чумасова О. А., Сизиков А. Э., Козлов В. А. Исследование эффекторных молекул автономного и неавтономного влияния апоптоза Т-лимфоцитов в условиях «клеточного соседства» в культуре у здоровых людей и пациентов с РА. Медицинская иммунология. 2022; 24 (6): 1119–38. DOI: 10.15789/1563-0625-SOE-2527.
21. Bagmut IYu, Ivanov OS, Sheremet MI, Smirnov SM, Kolisnyk IL, Ivanova JV, et al. Isolation of megakaryocytes using magnetic cell separation and adverse effects induced by diclofenac toxicity in an experiment. J Med Life. 2022; 15 (1): 65–70. DOI: 10.25122/jml-2020-0129.
22. Ivanov O, Haidash O, Voloshin V, Kondratov S, Smirnov A. Influence of the acting substance sodium diclofenac on bone marrow cells. Georgian Medical News. 2020; 306: 137–42. PMID: 33130661.
23. Ivanova YuV, Gramatiuk SM, Kryvoruchko IA, Prasol VO, Pulyaeva IS, Miasoiedov KV, et al. The Effect of pulsed photobiomodulation on proliferation and migration of human mesenchymal stem cells in vitro. Clinical and preventive medicine. 2024; (5): 87–92. DOI: 10.31612/2616-4868.5.2024.11.
24. Медведев В. Л., Опольский А. М., Коган М. И. Перспективы развития регенеративных технологий. Современные знания об аутоплазме, обогащеннои тромбоцитами и возможности ее применения в лечении урологических заболеваний. Кубанский научный медицинский вестник. 2018; 25 (3): 155–61. DOI: 10.25207/1608-6228-2018-25-3-155-161.
25. Irmak G, Gümüşderelioğlu M. Photo-activated platelet-rich plasma (PRP)-based patient-specific bio-ink for cartilage tissue engineering. Biomed Mater. 2020; 15 (6): 065010. DOI: 10.1088/1748-605X/ab9e46.
26. Gramatiuk S, Kryvoruchko I, Ivanova Y, Emily Hubbard, Maria Noebauer-Babenko, Karine Sargsyan. Artificial Intelligence-Based Quality Control of Cell Lines. Biopreserv Biobank. 2025; DOI: 10.1177/19475535251367317.
27. Li Y, Wang F, Ji B, Amati A, Cao L. FHL2 deteriorates IL-1β induced inflammation, apoptosis, and extracellular matrix degradation in chondrocyte-like ATDC5 cells by mTOR and NF-κB pathways. BMC Musculoskelet Disord. 2025; 26 (1): 331. DOI: 10.1186/s12891-025-08536-9.
28. Collins T, Alexander D, Barkatali B. Platelet-rich plasma: a narrative review. EFORT Open Rev. 2021; 6 (4): 225–35. DOI: 10.1302/2058-5241.6.200017.
29. Mishra Kanchan, Desai Pooja, Khanna Manish, Malhotra Sayesha. Photoactivated platelet-rich plasma (PA-PRP): A safe and effective treatment for musculoskeletal disorders. IP International Journal of Orthopaedic Rheumatology. 2025; 11: 71–75. DOI: 10.18231/j.ijor.25218.1765359797.
30. Bustin SA, Ruijter JM, van den Hoff MJB, Kubista M, Pfaffl MW, Shipley GL, et al. MIQE 2.0: Revision of the Minimum Information for Publication of Quantitative Real-Time PCR Experiments Guidelines. Clin Chem. 2025; 71 (6): 634–51. DOI: 10.1093/clinchem/hvaf043.
31. Videla-Jiménez P, Ruz F, López-Martín M. Research on box plot knowledge in statistical education: a systematic review of the literature. Eur J Psychol Educ. 2025; 40: 141. DOI: 10.1007/s10212-025-01048-z.
32. Livak KJ, Schmittgen TD. Analysis of relative gene expression data using real-time quantitative PCR and the 2(-Delta Delta C(T)) Method. Methods. 2001; 25 (4): 402–8. DOI: 10.1006/meth.2001.1262.
33. Raut RD, Chakraborty AK, Neogi T, Michael Albro, Brian Snyder, Thomas P. Schaer, et al. A multi-tissue human knee single-cell atlas identifies that osteoarthritis reduces regenerative tissue stem cells while increasing inflammatory pain macrophages. Commun Biol. 2025; 8: 1146. DOI: 10.1038/s42003-025-08586-8.
34. Mocanu V, Timofte DV, Zară-Dănceanu C-M, Labusca L, Obesity. Metabolic Syndrome, and Osteoarthritis Require Integrative Understanding and Management. Biomedicines. 2024; 12: 1262. DOI: 10.3390/biomedicines12061262.
35. Galicia-Canales BE, del Rocío Aguilar-Gaytán M, Álvarez-Pérez MA, Jarquín-Yáñez K, et al. Effect of peniocerol on human meniscal fibrochondrocyte inflammation induced by IL-1β and TNF-α through the NF-κB signaling pathway. Cellular and Molecular Biology. 2026; 72 (3): 36–44. DOI: 10.14715/cmb/2025.72.3.5.
36. Rikkers M, Dijkstra K, Terhaard BF, Admiraal J, Levato R, Malda J, et al. Platelet-Rich Plasma Does Not Inhibit Inflammation or Promote Regeneration in Human Osteoarthritic Chondrocytes In Vitro Despite Increased Proliferation. Cartilage. 2021; 13 (2_suppl): 991S–1003S. DOI: 10.1177/1947603520961162.
37. Zhao H, Zhu W, Mao W, Shen C. Platelet-rich plasma inhibits Adriamycin-induced inflammation via blocking the NF-κB pathway in articular chondrocytes. Mol Med. 2021; 27 (1): 66. DOI: 10.1186/s10020-021-00314-2.
38. O'Donnell C, Migliore E, Grandi FC, et al. Platelet-Rich Plasma (PRP) From Older Males With Knee Osteoarthritis Depresses Chondrocyte Metabolism and Upregulates Inflammation. J Orthop Res. 2019; 37: 1760–70. DOI: 10.1002/jor.24322.
39. Li M, Jing C, Liu Q, Zhang Y, Li K. Platelet-rich plasma in cartilage repair: biological mechanisms and clinical perspectives. Front Sports Act Living. 2026; 8: 1785754. DOI: 10.3389/fspor.2026.1785754.

PLATELET RECEPTOR GENE POLYMORPHISMS AND ALTERED PLATELET AGGREGATION IN PATIENTS WITH COVID-19 AND TYPE 2 DIABETES MELLITUS

Osikov MV[1,2], Antonov VN[2,3], Zotov SO[1,3]✉

[1] South Ural State Medical University, Chelyabinsk, Russia

[2] Chelyabinsk Regional Clinical Hospital, Chelyabinsk, Russia

[3] Regional Clinical Hospital No. 3, Chelyabinsk, Russia

COVID-19 is characterized by diffuse alveolar damage (COVID-19-DAD). The COVID-19-associated hemostatic alterations manifested by venous and arterial thrombosis deserve special attention. The issue is especially urgent for patients with diabetes mellitus. An observational study aimed to assess the role of polymorphisms of the genes *ITGB3*, *ITGA2*, and *GP1BA* in aggregation alteration in patients having COVID-19-DAD combined with type 2 diabetes mellitus (T2D). The control group included healthy volunteers (group 1; $n = 22$). Patients with COVID-19-DAD were divided into two groups based on the fact of having or not having T2D: group 2 with no T2D ($n = 52$) and group 3 with T2D ($n = 56$). Platelet aggregation was assessed with the ALAT-2 laser platelet aggregation analyzer; adenosine diphosphate (ADP) at a concentration of 2.5 μg/mL, collagen 2.0 μg/mL, adrenaline 5 μg/mL, and ristomycin 7.5 mg/mL were used as aggregation inducers. In patients with COVID-19-DAD and T2D, the rate of aggregate formation with the ADP induction was higher in carriers of the T/C and C/C variants compared to carriers of the T/T variant — by 14 and 23% based on the median ($p < 0.05$). Polymorphisms were determined by polymerase chain reaction in buccal epithelial scrapings. In the group of patients with COVID-19-DAD having no T2D, depending on the *ITGA2* gene rs1126643 polymorphism the collagen-induced platelet aggregation is accelerated with the C/T and T/T variants compared to the C/C variant — by 55 and 49%, respectively ($p < 0.05$); among individuals with COVID-19-DAD and T2D, carriers of the T/T variant show the rate of the collagen-induced platelet aggregation 30% higher compared to carriers of the C/C variant ($p < 0.05$). Conclusion: in patients with COVID-19-DAD and T2D, the presence of the mutant allele T of the *ITGA2* gene rs1126643 polymorphism and allele C of the *ITGB3* gene rs5918 polymorphism increases the rate of the collagen- and ADP-induced platelet aggregation.

Keywords: COVID-19, platelets, aggregation, polymorphisms, genotype, alleles

Author contribution: Osikov MV, Antonov VN — study planning; Zotov SO — literature review, data acquisition, analysis, and interpretation.

Compliance with ethical standards: the study was approved by the Ethics Committee of the South Ural State Medical University (protocol No. 4 dated May 24, 2021, protocol No. 2 dated March 5, 2026). All patients submitted the informed consent.

✉ **Correspondence should be addressed:** Semen O. Zotov
Vorovsky, 64, Chelyabinsk, 454092, Russia; semenz2007@yandex.ru

Received: 18.05.2026 **Accepted:** 17.07.2026 **Published online:** 28.07.2026

DOI: 10.24075/brsmu.2026.041

ПОЛИМОРФИЗМЫ ГЕНОВ ТРОМБОЦИТАРНЫХ РЕЦЕПТОРОВ И ИЗМЕНЕНИЕ АГРЕГАЦИИ ТРОМБОЦИТОВ У БОЛЬНЫХ COVID-19 И САХАРНЫМ ДИАБЕТОМ 2-ГО ТИПА

М. В. Осиков[1,2], В. Н. Антонов[2,3], С. О. Зотов[1,3]✉

[1] Южно-Уральский государственный медицинский университет, Челябинск, Россия

[2] Челябинская областная клиническая больница, Челябинск, Россия

[3] Областная клиническая больница № 3, Челябинск, Россия

COVID-19 характеризуется диффузным альвеолярным повреждением легких (COVID-19-АПЛ). Особого внимания заслуживают изменения гемостаза при COVID-19, проявлениями которых выступают венозные и артериальные тромбозы. Проблема особенно актуальна у больных с сахарным диабетом. Цель наблюдательного исследования — оценить роль полиморфизмов генов *ITGB3*, *ITGA2* и *GP1BA* в изменении агрегации тромбоцитов у больных с COVID-19-АПЛ в сочетании с сахарным диабетом второго типа (СД 2). В контрольную группу вошли клинически здоровые добровольцы (группа 1; $n = 22$). В зависимости от наличия СД 2 больные с COVID-19-АПЛ поделены на группы: группа 2 без СД 2 ($n = 52$) и группа 3 с СД 2 ($n = 56$). Агрегацию тромбоцитов оценивали на лазерном анализаторе агрегации тромбоцитов «АЛАТ-2», в качестве индукторов агрегации использовали аденозиндифосфат (АДФ) в концентрации 2,5 мкг/мл, коллаген 2,0 мкг/мл, адреналин 5 мкг/мл и ристомицин 7,5 мг/мл. Скорость формирования агрегатов при индукции АДФ у больных с COVID-19-АПЛ и СД 2 выше у носителей T/C- и C/C-вариантов по сравнению с T/T-вариантом на 14 и 23% по медиане ($p < 0,05$). Полиморфизмы определяли методом полимеразной цепной реакции в буккальном соскобе эпителия. В группе больных COVID-19-АПЛ без СД 2 в зависимости от полиморфизма rs1126643 гена *ITGA2* при вариантах C/T и T/T по сравнению с C/C ускоряется коллаген-индуцированная агрегация тромбоцитов — на 55 и 49% соответственно ($p < 0,05$); при COVID-19-АПЛ с СД 2 у носителей T/T-варианта скорость коллаген-индуцированной агрегации выше на 30% по сравнению с носителями C/C-варианта ($p < 0,05$). Вывод: у больных COVID-19-АПЛ и СД 2 наличие мутантного аллеля T полиморфизма rs1126643 гена *ITGA2* и аллеля C полиморфизма rs5918 гена *ITGB3* увеличивает скорость коллаген- и АДФ-индуцированной агрегации тромбоцитов.

Ключевые слова: COVID-19, тромбоциты, агрегация, полиморфизмы, генотип, аллели

Вклад авторов: М. В. Осиков, В. Н. Антонов — планирование исследования; С. О. Зотов — анализ литературы, сбор, анализ и интерпретация данных.

Соблюдение этических стандартов: исследование одобрено этическим комитетом ФГБОУ ВО ЮУГМУ Минздрава России (протокол № 4 от 24 мая 2021 г., протокол № 2 от 05 марта 2026 г.). Все пациенты подписали добровольное информированное согласие.

✉ **Для корреспонденции:** Семён Олегович Зотов
ул. Воровского, д. 64, г. Челябинск, 454092, Россия; semenz2007@yandex.ru

Статья получена: 18.05.2026 **Статья принята к печати:** 15.07.2026 **Опубликована онлайн:** 28.07.2026

DOI: 10.24075/vrgmu.2026.041

The COVID-19-DAD manifestation severity is determined inter alia by the genetic diversity of patients. The active search for markers of genetic determination of the COVID-19 course severity and outcomes is currently in progress. Most studies are focused on polymporphisms of the genes encoding angiotensin-converting enzymes and the membrane-anchored serine protease (*TMPRSS2*). There are data on the influence of polymorphisms of the genes encoding endothelial cell adhesion molecules, vitamin K epoxide reductase complex, interferon system components, cytokines and transcription factors, oxidative stress, metabolic molecules, and some other factors on the COVID-19 course [1–4].

At the same time, COVID-19-DAD can occur with the hemostasis system-associated complications and without any complications; some patients are sensitive to anticoagulant therapy and some are not. To determine the platelet function, it is feasible to explore its molecular genetic basis and the contribution to complications associated with thrombosis in COVID-19. High prevalence of thrombotic complications in individuals with severe COVID-19-DAD forms is associated with platelet hyperreactivity in the context of alteration of such genes, as *GP1BA* (glycoprotein Ib-alpha), *ITGB3* (integrin beta 3), and *ITGA2* (integrin alpha 2) [5].

A number of earlier studies revealed no differences in the effect on platelets in polymorbid individuals with *ITGA2* and *ITGB3* polymorphisms; conflicting information about the contribution of the genes *F2*, *NLRP3*, *TLR4*, *CX3CR*, *IL1RN*, and *IL1B* to the course of COVID-19 was obtained [6]. Polymorphisms of the genes regulating the homeostasis system can help identify the differences in susceptibility and severity in different patients. However, specific genetic factors and the extent, to which these can explain the susceptibility and COVID-19-DAD severity variation, are still unclear.

In patients with type 2 diabetes mellitus (T2D), hyperglycemia and insulin resistance cause the increased platelet production and activation, qualitative and quantitative changes in coagulation and fibrinolysis factors, thereby aggravating the hemostatic dysfunction [7]. However, alterations in hemostasis are observed in patients with COVID-19-DAD and T2D, along with the considerable functional variability of distinct hemostasis components, which can be associated inter alia with polymorphisms of factor genes.

The clinical and pathogenetic aspects of hemostasis in COVID-19, especially combined with T2D, are poorly understood, but it is well known that genetic factors have an effect on changes in the function of hemostatic links. The COVID-19 thrombohemorrhagic complications represent a pressing medical and social issue, despite the fact that the pandemic is over, due to their significant effect on the patients' quality of life, development of complications, and delayed mortality. To understand the mechanisms underlying the severe course and the emergence of thrombohemorrhagic complications in COVID-19 with T2D, clinical and laboratory, instrumental, and mathematical methods should be used to explore the role of genetic factors in alteration of hemostatic indicators.

The study aimed to assess the role of *ITGB3*, *ITGA2*, and GP1BA polymorphisms in platelet aggregation alteration in patients with COVID-19-associated pulmonary lesions combined with T2D.

METHODS

A total of 108 patients with COVID-19 admitted to the Regional Clinical Hospital No. 3 in Chelyabinsk (50 females and 58 males aged 45–74 years) took part in the study; they used no anticoagulants or other pharmaceuticals affecting hemostasis. The chest multispiral computed tomography performed using the Siemens SOMATOM Definition AS 64 scanner (Siemens AG, Germany) revealed bilateral diffuse lung tissue compaction (ground-glass opacity and consolidation) in combination with the reticular pattern (pulmonary involvement 11–64%) in all patients. The diagnosis of COVID-19 was confirmed by the detection of the SARS-CoV-2 viral RNA on the mucous membranes of the pharynx and nasal cavity by polymerase chain reaction (RealBest RNA SARS-CoV-2; Vector Best, Russia); the patients met the criteria of moderate-to-severe disease in accordance with the current version of the guidelines [8]. The control group consisted of 22 clinically healthy volunteers (group 1), who were matched for gender and age with COVID-19 patients. Patients with COVID-19-DAD were divided into two groups based on the fact of having or not having T2D: group 2 without T2D (n = 52) and group 3 with T2D (n = 56). Inclusion criteria for group 3: clinical diagnosis of T2D with the disease duration of 1–5 years (to rule out angiopathies, the T2D complications), achieved blood glucose and glycated hemoglobin targets. Exclusion criteria: cancer, autoimmune disorders, chronic diseases of the cardiovascular, respiratory, nervous systems, organs of the gastrointestinal tract and the kidney; extremely severe COVID-19-DAD course demanding the patient's admission to the ICU; development of the bacterial and/or other viral infection, fact of having stage 3 or more advanced stage arterial hypertension, body mass index (BMI) over 35 kg/m^2, anemia (hemoglobin levels below 119 g/L).

Blood sampling was performed on day 7 of hospital stay. The standard thromboprophylaxis provided to all subjects was the same. It consisted of the subcutaneous administration of low molecular weight heparin (enoxaparin sodium 4000 anti-Xa IU (40 mg) twice a day throughout the period of hospital stay). In addition to anticoagulant therapy, the patients received standard therapy with favibirin and glucocorticoids, antibacterial therapy.

To assess the inflammation severity in COVID-19-DAD, the serum C-reactive protein concentration was determined with the ChemWell 2910 EIA analyzer (Awareness Technology Inc., USA) using the test system manufactured by Vector-Best (Novosibirsk, Russia); blood lactate was assessed using the Medica Corp EasyLyte Plus acid-base state analyzer (Medica Corporation, USA). Blood platelet counts and morphological characteristics of platelets were determined using the Mindray BC 5800 analyzer (Mindray Co. Ltd., China). Plasma levels of fibrinogen (g/L), D-dimer (mg/L) were determined using the APG4-02P coagulometer (EMKO LLC, Russia) and test systems (Tehnologia-Standart, Russia).

Polymorphisms of the genes, the products of which are involved in platelet aggregation and plasma hemostasis, were studied. Testing of single polymorphisms was performed by real-time PCR (Roche LightCycler 96; Roche Molecular Systems, USA); buccal epithelial scrapes were used as biomaterial. The SNP-Express-Cardiogenetics reagent kits for identification of gene polymorphisms (Litech, Russia) were used. Polymorphisms rs6065 of the gene *GP1BA*, rs1126643 of the gene *ITGA2*, and rs5918 of the gene *ITGB3* were determined; mutant homozygous and heterozygous polymorphisms of these genes increase the risk of platelet aggregation and, therefore, the likelihood of thrombosis. Selection of polymorphisms was determined by their ability to take part in regulation of the function of appropriate key cellular hemostasis elements (in particular, components of major platelet receptors) and their clinical significance.

Table 1. Main clinical, laboratory, and instrumental indicators of the studied groups at admission

Indicator	Group 2 COVID-19-DAD, *n* = 52	Group 3 COVID-19-DAD + T2D, *n* = 56	p_{1-2}
Age, years [Me (Q_{25}; Q_{75})]	59.3 (55.8; 67.2)	61.1 (55.4; 68.6)	0.48
Male, *n* (%)	28 (53.8)	30 (53.6)	0.872
Female, *n* (%)	24 (46.2)	26 (46.4)	0.87
Number of patients with RD, *n* (%)	43 (82.7)	48 (85.7)	0.67
Grade I, *n* (%)	35 (67.3)	34 (60.7)	0.26
Grade II, *n* (%)	8 (15.4)	14 (25.0)	0.33
BMI, kg/m^2 [Me (Q_{25}; Q_{75})]	26.7 (21.5; 30.4)	31.2 (28.5; 33.4)	0.040 *
SpO_2, % [Me (Q_{25}; Q_{75})]	93.2 (89.4; 96.1)	91.0 (86.3; 93.6)	0.74
Lactate, mmol/L [Me (Q_{25}; Q_{75})]	1.86 (1.21; 2.26)	2.47 (2.01; 3.12)	0.003 *
CRP, mg/L [Me (Q_{25}; Q_{75})]	97.7 (71.2; 120.8)	123.4 (101.5; 162.5)	0.010 *
D-dimer, mg/L [Me (Q_{25}; Q_{75})]	1.39 (0.81; 2.11)	2.65 (1.87; 3.13)	0.040 *
Platelets, × 10^9/L	346.00 (245.00; 422.00)	275.00 (204.00; 316.50)	0.010 *
Fibrinogen, g/L	3.31 (2.88; 5.07)	5.84 (4.34; 7.19)	0.016 *

Note: * — significant ($p < 0.05$) differences from group 1.

Platelet aggregation was assessed with the ALAT-2 laser platelet aggregation analyzer (BIOLA, Russia). To obtain platelet-rich plasma (PRP), whole venous blood was centrifuged at 1500 rpm for 5 min. To obtain platelet-poor plasma (PPP), the residue was centrifuged for 15 min at 4500 rpm. The induced aggregation was assessed using the aggregation inducer kits by Tehnologia-Standart LLC (Russia): ADP at a final concentration of 2.5 μg/mL, collagen at a concentration of 2.0 μg/mL, adrenalin at a concentration of 5 μg/mL, and ristomycin at a concentration of 7.5 mg/mL. The intense two-wave (biphasic) aggregation with minimal disaggregation was observed with the ADP concentration of 2.5 μg/mL. Therefore, this ADP concentration was selected for the study.

Based on the light transmission curve the following were recorded by the Born method: aggregation amplitude or extent (%), aggregation time (min), aggregation rate (%/min); the extent of PRP aggregation was taken as 0 %, the extent of PPP aggregation was taken as 100 %. In addition, aggregation parameters were determined based on the average aggregate size curve [9]. After the system calibration the single platelet size was taken as 1 relative unit; the maximum aggregate size (hereinafter, aggregate size) was determined after adding the inducer. The rate of aggregate formation was determined as the maximum slope of the average curve and measured in relative units per minute (relative units/min).

Statistical processing was performed using IBM SPSS Statistics v. 23 (SPSS: An IBM Company; USA). Characteristics of samples are presented in the Me (Q_{25}; Q_{75}) format, where Me is the median, Q_{25}, Q_{75} are the lower and upper quartile values, respectively. The Hardy–Weinberg Carrier Frequency software tool (Focus Information Technology; USA) was used to test for the Hardy–Weinberg equilibrium. The Shapiro–Wilk test was used to assess the distribution of continuous variables. Testing statistical hypotheses in groups was performed using the nonparametric Mann–Whitney *U*-test with the calculation of the exact test *p*. The differences were considered significant at $p \leq 0.05$.

RESULTS

General characteristics of the surveyed patients are provided in Table 1. According to the data obtained, patients with COVID-19-DAD in combination with T2D show higher BMI, higher plasma levels of CRP, lactate, D-dimer, and fibrinogen, decreased platelet counts compared to patients having no T2D.

To determine the role of genetic factors in alteration of the platelet hemostatic link, the abundance of polymorphisms rs5918 of the gene *ITGB3*, rs1126643 of the gene *ITGA2*, and rs6065 of the gene *GP1BA* was assessed in patients with COVID-19-DAD and T2D. The above polymorphisms were selected due to their role in expression and realization of the function of platelet receptors involved in aggregation with ADP, collagen, and ristomycin. Considering the Shapiro–Wilk test results ($p \leq 0.05$) for the studied variables, further analysis was conducted using nonparametric methods for all comparisons. The distribution of *ITGB3*, *ITGA2*, *GP1BA* genotype frequencies was compliant with the expected equilibrium according to the Hardy–Weinberg exact test in the control group ($p = 0.77$; $p = 0.18$; $p = 0.31$, respectively), in the group of patients with COVID-19-DAD ($p = 0.50$; $p = 0.87$; $p = 0.82$, respectively), and in the group of patients with COVID-19-DAD and T2D ($p = 0.47$; $p = 0.82$; $p = 0.71$). A combination of two mutations was identified in five individuals (22.7%) in the control group; in 13 (25%) individuals with COVID-19-DAD without T2D; in six individuals (10.7%) with COVID-19-DAD and T2D. A combination of three mutations at once was identified in one patient (4.4%) in the control group; in four patients (7.7%) in the group of COVID-19-DAD without T2D; in three patients (5.4%) with COVID-19-DAD and T2D.

The *ITGB3* gene regulates the synthesis of the integrin β-3 membrane protein, the component of glycoprotein IIb/IIIa involved in the interplay between platelets. The rs5918 polymorphism of the gene *ITGB3* results from the nucleotide thymine (T) replacement with cytosine (C) in a certain DNA region, due to which the amino acid leucine (33rd in the protein chain) is replaced with proline, and the receptor 3D structure is disrupted [10]. The receptor structure disruption, in turn, results in the increased platelet reactivity and contributes to the platelet aggregation enhancement [11]. Individuals with the C/C variant of this polymorphism become more prone to platelet aggregation and, therefore, the risk of thrombosis increases [10]. In the group of patients with COVID-19-DAD having no T2D, there are no significant differences in the abundance of T/T, T/C, C/C genotypes in the gene *ITGB3* compared to controls ($p > 0.05$); the C allele of the *ITGB3* gene rs5918 polymorphism is more abundant ($p = 0.045$) (Table 2).

Table 2. Genotype abundance when analyzing polymorphisms of the genes *ITGB3*, *GP1BA* and *ITGA2* in individuals with COVID-19-DAD and T2D

Polymorphism	Genotypes/alleles		Genotype abundance, *n* (%)		
			Group 1 Healthy, *n* = 22	Group 2 COVID-19-DAD, *n* = 52	Group 3 COVID-19-DAD + T2D, *n* = 56
rs5918 of the gene *ITGB3*	Genotypes	0 (T/T)	17 (77.3)	34 (65.4)	29 (51.9) *
		I (T/C)	4 (18.2)	15 (28.8)	16 (29.6)
		II (C/C)	1 (4.5)	3 (5.8)	11 (18.5) * #
	Alleles	T	38 (86.4)	83 (79.8)	74 (64.8)
		C	6 (13.6)	21 (20.2) *	38 (35.2) * #
rs1126643 of the gene *ITGA2*	Genotypes	0 (C/C)	16 (72.7)	31 (59.6)	34 (60.7)
		I (C/T)	4 (18.2)	13 (25.0)	13 (23.2)
		II (T/T)	2 (9.1)	8 (15.4) *	9 (16.1)
	Alleles	C	36 (81.8)	75 (72.2)	81 (72.3)
		T	8 (18.2)	29 (27.8) *	31 (27.7) *
rs6065 of the gene *GP1BA*	Genotypes	0 (C/C)	19 (83.4)	42 (79.1)	46 (81.4)
		I (C/T)	3 (16.6)	9 (18.8)	10 (18.6)
		II (T/T)	0	1 (2.1)	0
	Alleles	C	40 (90.9)	93 (89.4)	102 (91.1)
		T	4 (9.1)	11 (10.6)	10 (8.9)

Note: * — significant ($p < 0.05$) differences from group 1; # — from group 2; 0 — wild type genotype; I — heterozygote; II — mutant homozygote.

In patients with COVID-19-DAD and T2D, the T/T genotype of the polymorphism considered is less abundant compared to controls, the T/C variant abundance is the same ($p > 0.05$), the C/C variant is more abundant ($p = 0.03$), and the C allele is 1.82 times more abundant ($p = 0.049$). In patients with COVID-19-DAD and T2D, the abundance of the T/T and T/C genotypes of the polymorphism considered is the same as in patients with COVID-19-DAD having no T2D, the C/C variant is 3.86 times more abundant ($p = 0.01$), and the C allele is 2.43 times more abundant ($p = 0.04$).

The *ITGA2* gene encodes the integrin alpha-2 protein, the membrane glycoprotein GPIa found on the membranes of various cells, including platelets. GPIa forms a complex with GPIIa being one of the collagen receptors on the platelet membrane. The *ITGA2* gene rs1126643 polymorphism results from the nucleotide cytosine (C) replacement with thymine (T) [12]. This mutation does not change the amino acid sequence, but determines the correlation between this polymorphism and the GPIa expression on the platelet membrane. When there is a T/T variant of the rs1126643 polymorphism, binding of platelets and collagen is faster; heterozygous individuals having the C/T variant demonstrate intermediate receptor expression levels [13].

In the group of patients with COVID-19-DAD having no T2D, there were no differences in the C/C, C/T, and T/T genotype abundance from controls ($p > 0.05$); the T allele of the *ITGA2* gene rs1126643 polymorphism was 1.82 times more abundant ($p = 0.007$). In patients with COVID-19-DAD and T2D, there were no differences in the C/C, C/T, T/T genotype abundance from controls ($p > 0.05$); the T allele of the *ITGA2* gene rs1126643 polymorphism was more abundant ($p = 0.03$). In patients with COVID-19-DAD and T2D, there were no differences in the C/C, C/T, T/T genotype and T allele abundance from patients with COVID-19-DAD having no T2D ($p > 0.05$).

The *GP1BA* gene encodes the α-subunit of the glycoprotein Ib involved in the GpIb/IX/V platelet receptor formation. vWF linking platelets to the damaged blood vessel site is the main receptor ligand [14]. The strength of the resulting link between the above depends largely on the receptor configuration,

Table 3. Characteristics of patients with COVID-19-DAD and T2D based on the abundance of *ITGB3*, *GP1BA*, and *ITGA2* polymorphisms

Polymorphism	Genotype/ alleles	COVID-19-DAD relative to control		COVID-19-DAD + T2D relative to control		COVID-19-DAD + T2D relative to COVID-19-DAD	
		χ^2 (*p*)	OR (95% CI)	χ^2 (*p*)	OR (95 % CI)	χ^2 (*p*)	ОШ (95 % CI)
rs5918 of the gene *ITGB3*	I (T/C)	0.99 (0.32)	1.86 (0.54–6.53)	1.85 (0.181)	2.34 (0.67–8.17)	1.19 (0.28)	1.25 (0.68–2.31)
	II (C/C)	0.12 (0.73)	1.50 (0.16–15.52)	1.53 (0.25)	1.80 (0.43–7.51)	6.55 (0.011) *	3.89 (1.07–14.12) *
	C	3.86 (0.045) *	1.61 (1.32–4.29)	7.60 (0.02) *	1.82 (1.15–2.86) *	9.35 (0.002) *	2.43 (1.54–3.83) *
rs6065 of the gene *GP1BA*	I (C/T)	1.465 (0.226)	1.36 (0.33–5.58)	1.77 (0.18)	0.65 (0.21–2.08)	0.04 (0.84)	1.02 (0.38–2.74)
	II (T/T)	–	–	–	–	–	–
	T	0.12 (0.73)	0.83 (0.47–3.90)	0.75 (0.39)	0.69 (0.37–1.28)	0.16 (0.69)	0.83 (0.44–1.58)
rs1126643 of the gene *ITGA2*	I (C/T)	0.1 (0.093)	0.96 (0.32–2.77)	0.16 (0.69)	1.15 (0.38–3.50)	0.08 (0.78)	0.91 (0.47–1.77)
	II (T/T)	3.68 (0.060)	2.11 (0.98–4.61)	0.40 (0.80)	1.07 (0.23–4.91)	0.12 (0.73)	1.08 (0.44–2.69)
	T	1.33 (0.04) *	1.71 (1.23–3.90) *	1.78 (0.013) *	1.84 (1.11–3.26) *	0.42 (0.52)	0.24 (0.11–0.52)

Note: * — significant ($p < 0.05$) differences; I — heterozygote; II — mutant homozygote.

Table 4. Induced platelet aggregation in individuals with COVID-19-DAD and T2D depending on the *ITGB3*, *ITGA2*, and *GP1BA* polymorphisms on day 7, Me(Q_{25}; Q_{75})

Polymorphism	Genotypes	Group 2 COVID-19-DAD, *n* = 52	Group 3 COVID-19-DAD + T2D, *n* = 56
rs1126643 of the gene *ITGB3*	Rate of ADP-induced aggregation, %/min		
	0 (T/T)	7.70 (5.07; 9.44)	8.53 (7.89; 12.35)
	I (T/C)	8.98 (5.78; 13.81)	11.44 (9.61; 15.24) *
	II (C/C)	8.28 (6.51; 9.57)	16.53 (7.89; 18.35) * #
	Rate of aggregate formation, ADP-induced aggregation, relative units/min		
	0 (T/T)	17.22 (12.38; 22.11)	20.19 (17.11; 23.17)
	I (T/C)	17.38 (11.26; 24.75)	23.19 (17.31; 25.72) *
	II (C/C)	18.04 (13.26; 21.82)	24.74 (16.91; 28.12) *
rs6065 of the gene *ITGA2*	Rate of collagen-induced aggregation, %/min		
	0 (C/C)	7.80 (6.97; 10.01)	9.39 (7.78; 11.55)
	I (C/T)	12.09 (10.37; 18.22) *	11.11 (9.51; 13.05)
	II (T/T)	11.59 (10.24; 13.39) *	12.24 (10.98; 14.45) *
	Rate of aggregate formation, collagen-induced aggregation, relative units/min		
	0 (C/C)	13.17 (7.31; 19.63)	17.17 (12.60; 24.11)
	I (C/T)	14.02 (8.67; 24.15)	18.24 (13.41; 22.58)
	II (T/T)	17.25 (9.42; 22.14) * #	16.22 (13.01; 19.28)
rs6065 of the gene *GP1BA*	Rate of ristomycin-induced aggregation, %/min		
	0 (C/C)	8.34 (5.02; 10.24)	9.34 (4.54; 12.06)
	I (C/T)	10.41 (8.67; 12.34)	10.32 (7.66; 14.43)
	II (T/T)	7.92	–
	Rate of aggregate formation, ristomycin-induced aggregation, relative units/min		
	0 (C/C)	12.72 (6.17; 19.03)	21.59 (11.24; 25.74)
	I (C/T)	13.06 (8.44; 17.28)	22.44 (12.78; 26.67)
	II (T/T)	13.68	–

Note: * — significant ($p < 0.05$) differences from the homozygous non-mutant variant within the group based on the Kruskal–Wallis test with the Dunn's test; # — from the heterozygous variant within the group; 0 — wild type genotype; I — heterozygote; II — mutant homozygote.

vWF structure, and blood flow rate. The *GP1BA* gene rs6065 polymorphism is associated with the cytosine (C) replacement with thymine (T) near the gene transcription start, resulting in the threonine replacement with methionine in the receptor fragment responsible for binding to vWF, so that carriers of the T/T genotype have a higher concentration of glycoprotein Ib on the platelet membrane compared to individuals with other genotype variants. With the mutant homozygous T/T form (frequency in the population about 1.5%), the risk of thrombosis is dramatically increased [15]. With the heterozygous C/T variant, the GpIb/IX/V receptor expression on platelets is less pronounced, but some studies have revealed the increased risk of thrombosis in carriers of this gene variant [16]. The study revealed no differences in the abundance of the studied genotypes of the *GP1BA* gene rs6065 polymorphism between patients with COVID-19-DAD and controls ($p > 0.05$); in patients with COVID-19-DAD and T2D, there were no differences in genotype frequency from both the control group and the group with COVID-19-DAD and no T2D.

Assessment of the abundance of polymorphisms considered based on the Pearson's test with calculation of the odds ratio (OR) was conducted (Table 3).

In patients with COVID-19-DAD, the T allele of the *ITGA2* gene rs1126643 polymorphism is 1.71 times more abundant compared to controls (95% CI: 1.23–3.90); in patients with COVID-19-DAD and T2D, mutant C and T alleles of the *ITGB3* gene rs5918 polymorphism and *ITGA2* gene rs1126643 polymorphism are 1.82 times (95% CI: 1.15–2.86) and 1.84 times (95% CI: 1.11–3.26) more abundant, respectively. In patients with COVID-19-DAD and T2D, the C/C variant and C allele of the *ITGB3* gene rs5918 polymorphism are 3.89 times (95% CI: 1.07–14.12) and 2.43 times (95% CI: 1.54–3.83) more abundant compared to patients having no T2D.

To determine the role of genetic factors in changes of indicators of the cellular hemostatic link in patients with COVID-19-DAD and T2D, the rate of the ADP-, collagen-, and ristomycin-induced platelet aggregation was assessed in individuals with variants of polymorphisms rs5918 of the gene *ITGB3*, rs1126643 of the gene *ITGA2*, and rs6065 of the gene *GP1BA* (Table 4, Fig.).

The analysis of platelet aggregation in patients with COVID-19-DAD having no T2D has shown that the *ITGB3* gene rs5918 polymorphism has no effect on the rate of the ADP-induced platelet aggregation; among patients with COVID-19-DAD and T2D, carriers of the T/C variants show the rate of the ADP-induced platelet aggregation 34% higher compared to carriers of the T/T variant; in carriers of C/C, it is 92% higher compared to T/T and 44% higher compared to T/C. In patients with COVID-19-DAD having no T2D, the rate of aggregate formation with the ADP induction does not change depending on the presence of the mutant allele; in patients with T2D, it is higher in carriers of T/C and C/C variants compared to carriers of the T/T variant — by 14 and 23 % based on the median, respectively.

To determine the role of *ITGB3* gene rs5918 polymorphism in changing the rate of the ADP-induced platelet aggregation in patients with COVID-19-DAD and T2D, the Kruskal–Wallis

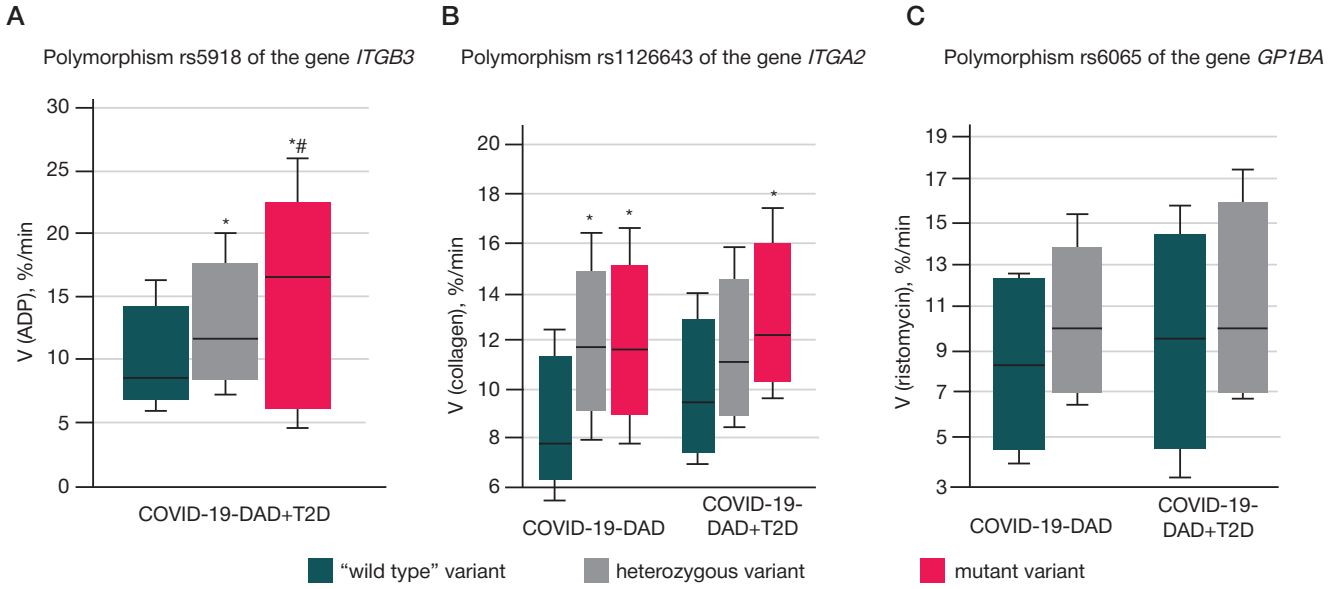

Fig. Hemostasis indicators in patients with COVID-19-DAD and T2D, carriers of the hemostasis factor gene mutant polymorphisms: rs5918 of the gene ITGB3 **(A)**; rs1126643 of the gene ITGA2 **(B)**; rs6065 of the gene GP1BA **(C)**. V (inducer) — rate of induced platelet aggregation; * — significant differences ($p < 0.05$) from carriers of the "wild type" genotype; # — from carriers of heterozygote

test with the Dunn's test was used; it was found that the presence of the mutant allele explained a large proportion of the overall variability of the ADP-induced platelet aggregation rate in patients with COVID-19-DAD having T2D ($p = 0.0045$). The increase in the average platelet volume in carriers of the increased amount of glycoprotein IIb/IIIa on the platelet membrane and, therefore, the increased platelet reactivity can be a possible explanation of the data obtained. However, the exact mechanisms causing platelet aggregation when there is a C/C variant of the rs5918 polymorphism are poorly understood and require further research.

When analyzing platelet aggregation in the group of patients with COVID-19-DAD having no T2D depending on the ITGA2 gene rs1126643 polymorphism, it was noted that the collagen-induced platelet aggregation is accelerated with the C/T and T/T variants compared to the C/C variant — by 55 and 49%, respectively ($p = 0.003$, $p = 0.005$); among individuals with COVID-19-DAD and T2D, carriers of the T/T variant show the collagen-induced platelet aggregation rate 30% higher compared to carriers of the C/C variant ($p = 0.014$).

DISCUSSION

Platelets of patients with T2D demonstrate a stronger response to agonists and the more apparent membrane expression of adhesion molecules, such as thrombospondin, P-selectin, GPIIb-IIIa, GPVI, and CD40L [17]. The T2D-associated hyperglycemia affects the expression of the key receptor and the activity of platelet enzymes: the expression of prostacyclin receptors is decreased in individuals with T2D, which enhances the platelet aggregation; the activity of the insulin-like growth factor 1 receptor (IGF1R) is increased, which makes platelets of such patients more sensitive to IGF1, being a regulator of the signal transmission and platelet responses, and causes platelet hyperactivity [18]. In T2D, the expression of integrin β3, the component of glycoprotein IIb/IIIa ensuring platelet aggregation, on platelets is increased, which results in the increased platelet activation and explains the platelet aggregation indicators obtained [19].

The findings of the study, i.e. the collagen-induced platelet aggregation acceleration, are consistent with the known information about the function of integrin alpha-2 and can indicate the role of the *ITGA2* gene rs1126643 polymorphism in the COVID-19 pathogenesis, despite the fact that the mechanism is poorly understood. The observed results demonstrate the polymorphism lower impact on the collagen-induced platelet aggregation rate in patients with T2D, which can be explained by predominance of other platelet activators in this group: oxidative stress or chronic inflammation.

The reported study has yielded no data suggesting the influence of the *GP1BA* gene rs6065 polymorphism on the acceleration of the ristomycin-induced platelet aggregation reflecting the vWF interaction with the GPIb receptor. The lack of the large number of the T/T homozygous mutant gene variant carriers in the population can be a possible explanation. Furthermore, there is a cooperativity effect in binding between vWF and platelet GpIb: glycoproteins IX and V, the structure of which can remain intact, are involved in the formation of a complex with collagen [20]. Moreover, the GpIb/IX/V receptor serves mostly for platelet adhesion; its role in aggregation is less pronounced [21]. Thus, the *GP1BA* gene rs6065 polymorphism is not the leading factor in acceleration of the ristomycin-induced platelet aggregation in patients with COVID-19-DAD; the finding can be explained by the predominant effect of other platelet activators: oxidative stress or hyperergic inflammation.

The data obtained suggest a possible role of genetic predisposition, particularly polymorphisms rs5918 of the gene *ITGB3* and rs1126643 of the gene *ITGA2*, in platelet hyperactivation in patients with COVID-19-DAD due to strengthening the binding of IIb/IIIa receptors to ADP and the GPIa/IIa collagen receptor expression increase [22].

The differences in hemostatic indicators in patients with COVID-19-DAD and that combined with T2D is a matter of scientific debate; one of the key issues is a controversial nature of the data on the contribution of genetic factors. On the one hand, modern research suggests that polymorphisms of the genes involved in hemostatic regulation can determine the individual's predisposition to thrombosis activated in the context of the T2D-associated metabolic disorder; on the other hand, there is credible evidence confirming that the inflammatory response and COVID-19 course severity are so dominant in the pathophysiological process that completely mask any genetic differences, making hemostatic

indicators merely a reflection of the acute systemic damage, and not the patient's constitutional characteristics [7, 17–19].

Despite the fact that the study was conducted in the context of using pharmaceuticals altering aggregation, is can be assumed that the effect of therapeutic doses of low molecular weight heparin and short courses of glucocorticoids on the aggregation indicators was minimal, which is in line with the earlier research results [23, 24].

Limitations of the study

The reported study limitations include the small sample size limiting the use of corrections for multiple comparisons, genetic models of inheritance, and other statistical methods, specifically the logistic regression method, and hampering the Hardy–Weinberg test interpretation. Furthermore, in addition to genetic factors, the platelet function in COVID-19-DAD is affected by the features of the patients' immune response and redox status, which should also be taken into account when interpreting the results.

CONCLUSIONS

Among individuals with COVID-19-DAD, the mutant allele T of the *ITGA2* gene rs1126643 polymorphism is 1.71 times more often found in patients having no T2D and 1.84 times more often in those having T2D, the rate of the collagen-induced platelet aggregation is increased in polymorphism carriers (by 30–55%, $p < 0.05$); in individuals with COVID-19-DAD and T2D, the *ITGB3* gene rs5918 polymorphism mutant variant C/C is 3.89 times more abundant and the C allele is 2.43 times more abundant, the ADP-induced platelet aggregation is increased in the carriers (by 14–23%, $p < 0.05$). The findings are a precondition for further research focused on exploring the pathogenesis of hemostasis alteration, developing personalized approaches to the diagnosis, treatment, and prevention of thrombotic complications of COVID-19-DAD in the context of T2D and other comorbidities, including the role of epigenetic factors and the studied polymorphisms' multicollinearity in shaping the platelet hyperreactivity as one of the key pathogenetic links.

References

1. Degenhardt F, Ellinghaus D, Juzenas J, et al. Detailed stratified GWAS analysis for severe COVID-19 in four European populations. Human Molecular Genetics. 2022; 31 (23): 3945–66.
2. Koyou HL, Salleh MN, Jelemie CS, et al. TMPRSS2: A Key Host Factor in SARS-CoV-2 Infection and Potential Therapeutic Target. Medical Management Journal. 2025; 26 (4): 101–9.
3. Janssen R, Walk J. Vitamin K epoxide reductase complex subunit 1 (VKORC1) gene polymorphism as determinant of differences in Covid-19-related disease severity. Medical Hypotheses. 2020; 144. Available from: https://www.sciencedirect.com/science/article/pii/ S0306987720324713?via%3Dihub (data obrashcheniya: 23.04.2026).
4. Ponti G, Pastorino L, Manfredini M, et al. COVID-19 spreading across world correlates with C677T allele of the methylenetetrahydrofolater eductase (MTHFR) gene prevalence. Journal of Clinical Laboratory Analysis. 2021; 35 (7). Available from: https://onlinelibrary.wiley.com/doi/10.1002/jcla.23798 (data obrashcheniya: 23.04.2026).
5. Ryu T, Adler BL, Jeong SJ, et al. Quantitative serum proteomic analysis for biomarker discovery in post-COVID-19 postural orthostatic tachycardia syndrome (PC-POTS) patients. Autonomic Neuroscience: Basic and Clinical. 2025; 258. Available from: https://www.autonomicneuroscience.com/article/S1566-0702(25)00009-8/fulltext (data obrashcheniya: 23.04.2026).
6. Feng S, Song F, Guo W, et al. Potential Genes Associated with COVID-19 and Comorbidity. International Journal of Molecular Sciences. 2022; 19 (2): 402–15.
7. Lima-Martínez MM, Carrera Boada C, Madera-Silva MD, et al. COVID-19 and diabetes: A bidirectional relations. Clínica e Investigación en Arteriosclerosis. 2021; 33 (3): 151–7.
8. Vremennye metodicheskie rekomendacii Ministerstva zdravoohraneniya Rossijskoj Federacii «Profilaktika, diagnostika i lechenie novoj koronavirusnoj infekcii (COVID-19)», versiya 18 (26.10.2023). KonturNormativ. Available from: https://normativ.kontur.ru/document?moduleId=1&documentId=458540&ysclid=mieheo3zin907543662 (data obrashcheniya: 22.04.2026). Russian.
9. Gabbasov ZA, Popov BG, Gavrilov IYu, i dr. Novyj vysokochuvstvitel'nyj metod analiza agregacii trombocitov. Laboratornoe delo. 1989; 10: 15–18. Russian.
10. Khatami M, Heidari MM, Soheilyfar S. Common rs5918 (PlA1/A2) polymorphism in the ITGB3 gene and risk of coronary artery disease. Archives of Medical Sciences. Atherosclerotic Diseases. 2016; 1 (1): e9–e15.
11. Alsulaim AY, Azam F, Sebastian T, et al. The association between two genetic polymorphisms in ITGB3 and increase risk of venous thromboembolism in cancer patients in Eastern Province of Saudi Arabia. Saudi Journal of Biological Sciences. 2022; 29 (1): 183–9.
12. Yuan J, Jiang Z, Li M, et al. Integrin α2 gene polymorphism is a risk factor of coronary artery lesions in Chinese children with Kawasaki disease. Pediatric Rheumatology Online Journal. 2021; 19 (1). Available from: https://link.springer.com/article/10.1186/s12969-021-00494-5 (data obrashcheniya: 23.04.2026).
13. Aloui C, Prigent A, Tariket S, et al. Levels of human platelet-derived soluble CD40 ligand depend on haplotypes of CD40LG-CD40-ITGA2. Scientific Reports. 2016; 6. Available from: https://www.nature.com/articles/srep24715 (data obrashcheniya: 23.04.2026).
14. Dib F, Quéméner A, Bayart S, et al. Biological, clinical features and modelling of heterozygous variants of glycoprotein Ib platelet subunit alpha (GP1BA) and glycoprotein Ib platelet subunit beta (GP1BB) genes responsible for constitutional thrombocytopenia. British Journal of Haematology. 2022; 199 (5): 744–53.
15. Ko EJ, Ahn EH, Park HW, et al. Genetic Associations of ITGB3, FGG, GP1BA, PECAM1, and PEAR1 Polymorphisms and the Platelet Activation Pathway with Recurrent Pregnancy Loss in the Korean Population. International Journal of Molecular Sciences. 2025; 26 (15). Available from: https://www.mdpi.com/1422-0067/26/15/7505 (дата обращения: 23.04.2026).
16. Castaman G, Federici AB. Type 2B von Willebrand Disease: A Matter of Plasma Plus Platelet Abnormality. Seminars in Thrombosis and Hemostasis. 2016; 42 (5): 478–82.
17. Fields AT, Andraska EA, Kaltenmeier C, et al. Effects of the circulating environment of COVID-19 on platelet and neutrophil behavior. Frontiers in Immunology. 2023; 14 Available from: https://www.frontiersin.org/journals/immunology/articles/10.3389/fimmu.2023.1130288/full (data obrashcheniya: 23.04.2026).
18. Henein MY, Vancheri S, Longo G, et al. The Role of Inflammation in Cardiovascular Disease. International Journal of Molecular Sciences. 2022; 23 (21). Available from: https://www.mdpi.com/1422-0067/23/21/12906 (data obrashcheniya: 23.04.2026).
19. Timóteo AT. Is There a Second Wind for Glycoprotein IIb/IIIa Inhibitors in Elderly Diabetic Females with ST-Elevation Myocardial Infarction, or are We on Thin Ice? Arquivos Brasileiros de Cardiologia. 2021; 116 (2): 236–37.
20. Seth R, McKinnon TAJ, Zhang XF. Contribution of the von Willebrand factor/ADAMTS13 imbalance to COVID-19 coagulopathy. American Journal of Physiology-Heart and Circulatory Physiology. 2022; 322 (1): H87–H93.
21. Li, R. Recent advances on GPIb-IX-V complex. Platelets. 2022;

33 (6): 809–10.
22. Osikov MV, Antonov VN, Zotov SO. Rol' polimorfizma genov ITGB3, GP1B1 i ITGA2 v patogeneze giperreaktivnosti trombocitov pri COVID-19-associirovannom porazhenii legkih srednej i tyazheloj stepeni tyazhesti. Acta Biomedica Scientifica. 2023; 8 (6): 14–22. Russian.
23. Buryachkovskaya L, Lomakin N, et al. Enoxaparin dose impacts blood cell phenotypes during mild SARS-CoV-2 infection: the observational single-center study. Reviews in Cardiovascular Medicine. 2021; 22 (4). Available from: https://www.imrpress.com/journal/RCM/22/4/10.31083/j.rcm2204176 (data obrashcheniya: 31.05.2026).
24. Adiguzel C, Iqbal O. Comparative anticoagulant and platelet modulatory effects of enoxaparin and sulodexide. Clinical and applied thrombosis/hemostasis: official journal of the International Academy of Clinical and Applied Thrombosis/Hemostasis. 2009; 15 (5): 501–11.

Литература

1. Degenhardt F, Ellinghaus D, Juzenas J, et al. Detailed stratified GWAS analysis for severe COVID-19 in four European populations. Human Molecular Genetics. 2022; 31 (23): 3945–66.
2. Koyou HL, Salleh MN, Jelemie CS, et al. TMPRSS2: A Key Host Factor in SARS-CoV-2 Infection and Potential Therapeutic Target. Medical Management Journal. 2025; 26 (4): 101–9.
3. Janssen R, Walk J. Vitamin K epoxide reductase complex subunit 1 (VKORC1) gene polymorphism as determinant of differences in Covid-19-related disease severity. Medical Hypotheses. 2020; 144. Available from: https://www.sciencedirect.com/science/article/pii/ S0306987720324713?via%3Dihub (дата обращения: 23.04.2026).
4. Ponti G, Pastorino L, Manfredini M, et al. COVID-19 spreading across world correlates with C677T allele of the methylenet etrahydrofolatereductase (MTHFR) gene prevalence. Journal of Clinical Laboratory Analysis. 2021; 35 (7). Available from: https://onlinelibrary.wiley.com/doi/10.1002/jcla.23798 (дата обращения: 23.04.2026).
5. Ryu T, Adler BL, Jeong SJ, et al. Quantitative serum proteomic analysis for biomarker discovery in post-COVID-19 postural orthostatic tachycardia syndrome (PC-POTS) patients. Autonomic Neuroscience: Basic and Clinical. 2025; 258. Available from: https://www.autonomicneuroscience.com/article/S1566-0702(25)00009-8/fulltext (дата обращения: 23.04.2026).
6. Feng S, Song F, Guo W, et al. Potential Genes Associated with COVID-19 and Comorbidity. International Journal of Molecular Sciences. 2022; 19 (2): 402–15.
7. Lima-Martínez MM, Carrera Boada C, Madera-Silva MD, et al. COVID-19 and diabetes: A bidirectional relations. Clínica e Investigación en Arteriosclerosis. 2021; 33 (3): 151–7.
8. Временные методические рекомендации Министерства здравоохранения Российской Федерации «Профилактика, диагностика и лечение новой коронавирусной инфекции (COVID-19)», версия 18 (26.10.2023). КонтурНорматив. Available from: https://normativ.kontur.ru/document?moduleId=1&documentId=458540&ysclid=mieheo3zin907543662 (дата обращения: 22.04.2026).
9. Габбасов З. А., Попов Б. Г., Гаврилов И. Ю., и др. Новый высокочувствительный метод анализа агрегации тромбоцитов. Лабораторное дело. 1989; 10: 15–18.
10. Khatami M, Heidari MM, Soheilyfar S. Common rs5918 (PlA1/A2) polymorphism in the ITGB3 gene and risk of coronary artery disease. Archives of Medical Sciences. Atherosclerotic Diseases. 2016; 1 (1): e9–e15.
11. Alsulaim AY, Azam F, Sebastian T, et al. The association between two genetic polymorphisms in ITGB3 and increase risk of venous thromboembolism in cancer patients in Eastern Province of Saudi Arabia. Saudi Journal of Biological Sciences. 2022; 29 (1): 183–9.
12. Yuan J, Jiang Z, Li M, et al. Integrin α2 gene polymorphism is a risk factor of coronary artery lesions in Chinese children with Kawasaki disease. Pediatric Rheumatology Online Journal. 2021; 19 (1). Available from: https://link.springer.com/article/10.1186/s12969-021-00494-5 (дата обращения: 23.04.2026).
13. Aloui C, Prigent A, Tariket S, et al. Levels of human platelet-derived soluble CD40 ligand depend on haplotypes of CD40LG-CD40-ITGA2. Scientific Reports. 2016; 6. Available from: https://www.nature.com/articles/srep24715 (дата обращения: 23.04.2026).
14. Dib F, Quéméner A, Bayart S, et al. Biological, clinical features and modelling of heterozygous variants of glycoprotein Ib platelet subunit alpha (GP1BA) and glycoprotein Ib platelet subunit beta (GP1BB) genes responsible for constitutional thrombocytopenia. British Journal of Haematology. 2022; 199 (5): 744–53.
15. Ko EJ, Ahn EH, Park HW, et al. Genetic Associations of ITGB3, FGG, GP1BA, PECAM1, and PEAR1 Polymorphisms and the Platelet Activation Pathway with Recurrent Pregnancy Loss in the Korean Population. International Journal of Molecular Sciences. 2025; 26 (15). Available from: https://www.mdpi.com/1422-0067/26/15/7505 (дата обращения: 23.04.2026).
16. Castaman G, Federici AB. Type 2B von Willebrand Disease: A Matter of Plasma Plus Platelet Abnormality. Seminars in Thrombosis and Hemostasis. 2016; 42 (5): 478–82.
17. Fields AT, Andraska EA, Kaltenmeier C, et al. Effects of the circulating environment of COVID-19 on platelet and neutrophil behavior. Frontiers in Immunology. 2023; 14 Available from: https://www.frontiersin.org/journals/immunology/articles/10.3389/fimmu.2023.1130288/full (дата обращения: 23.04.2026).
18. Henein MY, Vancheri S, Longo G, et al. The Role of Inflammation in Cardiovascular Disease. International Journal of Molecular Sciences. 2022; 23 (21). Available from: https://www.mdpi.com/1422-0067/23/21/12906 (дата обращения: 23.04.2026).
19. Timóteo AT. Is There a Second Wind for Glycoprotein IIb/IIIa Inhibitors in Elderly Diabetic Females with ST-Elevation Myocardial Infarction, or are We on Thin Ice? Arquivos Brasileiros de Cardiologia. 2021; 116 (2): 236–37.
20. Seth R, McKinnon TAJ, Zhang XF. Contribution of the von Willebrand factor/ADAMTS13 imbalance to COVID-19 coagulopathy. American Journal of Physiology-Heart and Circulatory Physiology. 2022; 322 (1): H87–H93.
21. Li, R. Recent advances on GPIb-IX-V complex. Platelets. 2022; 33 (6): 809–10.
22. Осиков М. В., Антонов В. Н., Зотов С. О. Роль полиморфизма генов ITGB3, GP1B1 и ITGA2 в патогенезе гиперреактивности тромбоцитов при COVID-19-ассоциированном поражении легких средней и тяжелой степени тяжести. Acta Biomedica Scientifica. 2023; 8 (6): 14–22.
23. Buryachkovskaya L, Lomakin N, et al. Enoxaparin dose impacts blood cell phenotypes during mild SARS-CoV-2 infection: the observational single-center study. Reviews in Cardiovascular Medicine. 2021; 22 (4). Available from: https://www.imrpress.com/journal/RCM/22/4/10.31083/j.rcm2204176 (дата обращения: 31.05.2026).
24. Adiguzel C, Iqbal O. Comparative anticoagulant and platelet modulatory effects of enoxaparin and sulodexide. Clinical and applied thrombosis/hemostasis: official journal of the International Academy of Clinical and Applied Thrombosis/Hemostasis. 2009; 15 (5): 501–11.

INTEGRATED REFERENCE PANEL OF MACACA *MULATTA HAPLOTYPES* FOR GENOTYPE IMPUTATION IN POPULATIONS OF MIXED ORIGIN

Sharko FS, Prokopenko AV, Izotova AO, Toshchakov SV ✉

National Research Centre "Kurchatov Institute", Moscow, Russia

Genotype imputation makes it possible to considerably reduce the cost of whole-genome data acquisition preserving the information value, but its accuracy depends directly on the availability of a high-quality phased reference panel of haplotypes. The existing panels for *Macaca mulatta* cover mostly the Indian species lineage and do not reflect the genetic structure of laboratory populations of mixed origin. This retrospective bioinformatics study aimed to produce and validate a phased reference panel based on the consolidation of publicly available whole-genome datasets from 618 *M. mulatta* individuals of both geographic lineages processed in accordance with the common standardized protocol. The resulting panel includes 33,457,491 SNP markers. Validation on samples of Indian and Chinese origin with ultra-low coverage (0.1x–0.9x) confirmed high imputation accuracy, which was highest for the Indian lineage dominant in the panel. Testing on 10 independent samples with the 0.6x coverage showed a high average imputation reliability score (INFO = 0.898). The created resource opens the prospects for cost-effective genotyping of large *M. mulatta* cohorts and provides the basis for whole-genome association and population genetic studies in domestic and foreign primate research centers.

Keywords: genotype imputation, reference panel, *Macaca mulatta*, whole-genome sequencing, GLIMPSE2, SHAPEIT5, bioinformatics

Funding: the study was supported by the Ministry of Science and Higher Education of the Russian Federation (Federal Scientific and Technical Program for the Development of Genetic Technologies for 2019–2030), agreement No. 075-15-2025-491 dated 30.05.2025.

Acknowledgements: the study was conducted using the equipment of the shared use center "Complex for Modeling and Processing Data from Mega-Class Research Facilities", National Research Centre "Kurchatov Institute", http://ckp.nrcki.ru/.

Author contribution: Toshchakov SV — research design, manuscript writing; Sharko FS — bioinformatics analysis, manuscript draft; Prokopenko AV, Izotova AO — manuscript editing.

Compliance with ethical standards: the studies were approved by the Ethics Committee of the National Research Centre "Kurchatov Institute" (protocol №2-2пр dated June 30, 2025).

✉ **Correspondence should be addressed:** Stepan V. Toshchakov
Academician Kurchatov pl, 1, Moscow, 123098, Russia; stepan.toshchakov@gmail.com

Received: 14.07.2026 **Accepted:** 14.08.2026 **Published online:** 21.08.2026

DOI: 10.24075/brsmu.2026.045

ИНТЕГРИРОВАННАЯ РЕФЕРЕНСНАЯ ПАНЕЛЬ ГАПЛОТИПОВ *MACACA MULATTA* ДЛЯ ИМПУТАЦИИ ГЕНОТИПОВ В ПОПУЛЯЦИЯХ СМЕШАННОГО ПРОИСХОЖДЕНИЯ

Ф. С. Шарко, А. В. Прокопенко, А. О. Изотова, С. В. Тощаков ✉

Национальный исследовательский центр «Курчатовский институт», Москва, Россия

Импутация генотипов позволяет значительно снизить затраты на получение полногеномных данных при сохранении информативности, однако ее точность напрямую зависит от наличия качественной фазированной референсной панели гаплотипов. Существующие панели для *Macaca mulatta* охватывают преимущественно индийскую линию вида и не отражают генетическую структуру лабораторных популяций смешанного происхождения. Целью ретроспективного биоинформатического исследования было создать и отвалидировать фазированную референсную панель на основе консолидации 618 общедоступных полногеномных данных *M. mulatta* обеих географических линий, обработанных по единому стандартизированному протоколу. Итоговая панель включает 33 457 491 SNP-маркер. Валидация на образцах индийского и китайского происхождения при сверхнизком покрытии (0,1×–0,9×) подтвердила высокую точность импутации, максимальную для доминирующей в панели индийской линии. Апробация на 10 независимых образцах при покрытии 0,6x показала высокий средний показатель достоверности импутации (INFO = 0,898). Созданный ресурс открывает возможности для экономически эффективного генотипирования больших когорт *M. mulatta* и служит основой для проведения полногеномных ассоциативных и популяционно-генетических исследований в отечественных и зарубежных приматологических центрах.

Ключевые слова: импутация генотипов, референсная панель, *Macaca mulatta*, полногеномное секвенирование, GLIMPSE2, SHAPEIT5, биоинформатика

Финансирование: работа выполнена при поддержке Министерства науки и высшего образования Российской Федерации (Федеральная научно-техническая программа развития генетических технологий на 2019–2030 г.), соглашение №075-15-2025-491 от 30.05.2025.

Благодарности: работа выполнена с использованием оборудования центра коллективного пользования «Комплекс моделирования и обработки данных исследовательских установок мега-класса» НИЦ «Курчатовский институт», http://ckp.nrcki.ru/.

Вклад авторов: С. В. Тощаков — дизайн работы, написание рукописи; Ф. С. Шарко — биоинформатический анализ, подготовка черновика; А. В. Прокопенко, А. О. Изотова — редактирование рукописи.

Соблюдение этических стандартов: исследования одобрены этическим комитетом НИЦ «Курчатовский институт» (протокол №2-2пр от 30 июня 2025 г.).

✉ **Для корреспонденции:** Степан Владимирович Тощаков
пл. Академика Курчатова, д. 1, г. Москва, 123098, Россия; stepan.toshchakov@gmail.com

Статья получена: 14.07.2026 **Статья принята к печати:** 14.08.2026 **Опубликована онлайн:** 21.08.2026

DOI: 10.24075/vrgmu.2026.045

The rhesus macaque (*Macaca mulatta*) is one of the model organisms most often used in biomedical research. In the area of infectious diseases this species is used as a model for studying human diseases of various etiologies, including HIV/AIDS, tuberculosis, hepatitis and influenza [1]. Furthermore, due to the high phylogenetic similarity of the macaque's and human nervous systems, macaques are widely used in neurobiology, specifically when modeling neurodegenerative processes and Alzheimer's disease [2], a number of rare congenital disorders [3], as well as for preclinical assessment of neuroactive medicinal products [4]. The wide use of this species in experimental biomedicine determines the great interest in studying the genetic basis of the *M. mulatta* phenotypic variation, particularly differences in the susceptibility to diseases and the response to therapy [5].

Genome-wide association studies (GWAS) are the key instrument for solving such problems, but such studies involving large cohorts are limited by the high cost of whole genome sequencing [6]. When the budget is limited, approaches that make it possible to reduce the cost of obtaining genomic data without the decrease in their information content are of particular importance. The low-coverage sequencing with subsequent genotype imputation is an effective alternative to deep sequencing. Such an approach makes it possible to reconstruct missing genotypes based on the known haplotypes from the standard (reference) panel, significantly reducing the cost of analysis compared to the standard coverage (from 20x) and allowing for the population studies on the sets of thousands of samples [7]. Availability of the reference panel that is representative, phased, and genetically close to the target sample is the key factor determining the imputation effectiveness [8].

A number of genomic resources focused on the cataloging and annotation of known genetic variants have been created for *M. mulatta*. Of those the largest one is mGAP representing a catalogue of the annotated variants obtained as a result of sequencing 2.5 thousand animals [5]. The RhesusBase database including 46.1 million polymorphic sites [9] and the MACSNVdb resource for interspecies comparisons within the genus *Macaca* (74.5 million SNV) [10] should be also noted. These resources solve the problems of cataloging, annotating, and searching for known variants, but do not provide a phased haplotype reference panel necessary for the reconstruction of whole-genome genotypes in new, previously unsequenced samples.

In current practice, phased reference panels for genotype imputation represent a basic instrument used in large genomic projects related with human studies and studies involving livestock [11, 12]. Extensive *Macaca mulatta* whole-genome sequencing data sets are available in international repositories. In 2025, the first specialized reference panel for this species was published, providing high genotype imputation accuracy even with the 0.5× coverage [13]. However, this resource is primarily confined to the Indian Macaca mulatta lineage. The genetic structure of artificially created closed populations, whose genesis is associated with the heterogeneous ancestry of the source stock, the fragmentary nature of archive data on introduction, and many years of panmixia, remains beyond the scope of this analysis [14, 15]. For populations of mixed origin, the optimal approach involves employing an integrated panel that incorporates the major geographic lineages of the species, thereby combining population specificity with versatility.

This study aimed to describe the development and validation of a phased reference panel for *M. mulatta* genotype imputation. The panel was generated using the results of whole-genome sequencing of 618 samples of Indian and Chinese origin obtained from open sources, processed in accordance with a single standardized protocol employing contemporary phasing and imputation algorithms. When assessing imputation accuracy using independent test samples from both lineages, high R^2 and concordance values were obtained within the coverage depth range of 0.1x–0.9x, with the expected advantage of the Indian lineage dominant in the panel. The resource developed provides the basis for genome-wide association and population genetic studies involving rhesus macaques in both domestic and international primatology centers, where the genetic structure of populations may be heterogeneous and apriori unknown [16, 17].

METHODS

Collection and systematization of publicly available whole-genome sequencing data

A systematic search for *M. mulatta* whole-genome sequencing data was conducted in the NCBI SRA [18], EA [19], and NGDC [20] international repositories. Data were selected based on the following criteria: confirmed fact of belonging to the species *M. mulatta*, sequencing depth of at least 20x, as well as availability of verified meta-data on the animal's geographic origin (India or China) and sex. A total of 1808 samples were identified during the primary search. After filtering based on coverage values and meta-data validation the number of candidates was 982. The animals defined in metadata as interspecies hybrids (*M. mulatta* × *M. fascicularis*) and samples of undefined geographic origin were excluded from further analysis.

In the final phase of sampling a stratification procedure was applied aimed at achieving the composition balanced based on sex within each population group and minimizing potential systematic distortions due to uneven presentation of data from different studies. The resulting data set included 618 unique animals from three projects: PRJNA251548 (BCM, $n = 21$), PRJNA382404 (OHSU, $n = 397$), and CRA014717 (KIZ, $n = 200$). Among all samples 418 were of Indian origin and 200 were of Chinese origin; there were 410 females and 208 males. Information about the geographic origin and sex of each sample is provided in the dataset-description.xlsx file in the Zenodo open repository: https://doi.org/10.5281/zenodo.21296424.

Bioinformatics processing and SNP identification

The common standardized bioinformatics processing pipeline that ensured data consistency at all stages was developed and used for all 618 samples. The raw reads were filtered by quality using fastp v0.23.2 [21] with the following parameters: -w 12 -z 7 -V -g --poly_g_min_len 5 -x --poly_x_min_len 10 -5 -3 -M 30 -n 1 -e 20 -l 50 --c. The filtered reads were mapped to the M. mulatta reference genome (assembly Mmul_10, GCF_003339765.1) using Bowtie2 v2.3.5.1 [22] with default settings. SNPs were identified using bcftools v1.15 [23] (mpileup and call commands) with the following key parameters: --redo-BAQ --min-BQ 30 --per-sample-mF --annotate DP,AD --multiallelic-caller --variants-only. In the next phase, insertions and deletions were deleted from the resulting VCF files using vcftools v0.1.16 (--remove-indels parameters) to leave only single nucleotide substitutions (SNPs) for further analysis. The resulting VCF file was subjected to further strict filtering using vcftools v0.1.16 [24] based on the following criteria: genotype quality (GQ) ≥ 30, read depth (DP) 15–180, percentage of missing genotypes per site ≤ 0.02, minimal minor allele frequency (MAF) ≥ 0.01.

Reference panel phasing

The SHAPEIT5 v5.1.0 software package [25] developed for large sets of WG data and characterized by high accuracy of haplotype phase reconstruction when dealing with large samples was used to reconstruct the chromosomal phases of haplotypes of the filtered data set. Stage-by-stage phasing with the genome division into independent blocks was applied to increase the computing efficiency and reduce the RAM requirements. At first, the SHAPEIT5_phase_common module was used for processing in the 20 cM-long chromosome blocks; independent phasing with subsequent quality assessment was performed for each block. To ensure the complete chromosome assembly integrity and eliminate artifacts arising at block boundaries, further phasing was performed in overlapping regions at the junctions (overlap of 2 cM) followed by merging the phases into a single chromosome sequence. As a result, fully phased panel was produced that contained two haplotypes (maternal and paternal) for each of 618 animals, which was essential for subsequent genotype imputation.

Genotype imputation and panel validation

To assess the accuracy of the reference panel produced, two samples of known geographic origin were excluded from the panel: M00016 (Indian population) and CRR1023808 (Chinese population). The source BAM files with high coverage for each such sample were subjected to downsampling to five coverage depth levels: 0.1x, 0.3x, 0.5x, 0.7x, and 0.9x, which made it possible to simulate the low-coverage sequencing conditions.

Genotype imputation for simulated data was performed using the GLIMPSE2 v2.0.0 pipeline [26]. The procedure included sequential steps: genome splitting into overlapping windows using the GLIMPSE2_chunk utility, creation of the reference panel in the GLIMPSE2 format by means of GLIMPSE2_split_reference, the imputation itself and phasing via GLIMPSE2_phase, as well as combining the results from all windows to restore full-chromosome files using GLIMPSE2_ligate.

The imputation accuracy was assessed by matching imputed genotypes with reference ones, for which the original high-confidence genotypes of the same samples before downsampling were used. The GLIMPSE2_concordance tool calculating two indicators was used for calculation: concordance (percentage of completely matched genotypes) and R^2 (square of the correlation coefficient between imputed and reference allele dosages). Such an approach allowed for quantitative characterization of the imputation accuracy as a function of the target sample coverage depth and the degree of its similarity to the reference panel. The reference panel is available from the Zenodo open repository: https://doi.org/10.5281/zenodo.21296424.

RESULTS

Characteristics of the created reference panel

As a result of consolidation and unified processing of 618 *M. mulatta* macaques the phased reference haplotype panel has been produced that includes 33,457,491 highly reliable SNP markers. The panel population structure is determined by the composition of projects included. Most samples are of Indian origin (418 animals; 67.6%), which is due to the PRJNA382404 project predominance in the sample (OHSU, $n = 397$). Samples of the project belong to the Indian population. The Chinese origin is reported for 200 animals (32.4%; project CRA014717, KIZ). Such ratio guarantees the representation of both major geographic lineages in the panel, thereby expanding its application area to laboratory populations of mixed or undefined origin. The sex composition of the sample is characterized by the predominance of females: 410 females (66.3%) and 208 males (33.7%), which reflects the structure of the source publicly available WGS data.

Imputation accuracy evaluation

The imputation accuracy was assessed based on two metrics: concordance (percentage of completely matched genotypes) and R^2 (square of the correlation coefficient between imputed and reference allele dosages). In contrast to concordance, R^2 is more sensitive to errors in cases of rare variants, since it reflects the correlation between the allele dosages. As expected, both indicators were directly dependent on the target sample coverage: the imputation accuracy consistently increased with greater sequencing depth. In addition, the imputation accuracy was assessed depending on the minor allele frequency (MAF) within the range of 1–45%.

As for the M00016 sample of Indian origin, the R^2 value increased from 0.56 to 0.96 when coverage increased from 0.1× to 0.9× (Fig. 1A). Stratification by MAF showed that the R^2 values for common variants (MAF ≥ 10%) reached 0.95–0.96 even with the coverage of 0.7×, while the R^2 values for rare variants (MAF < 1%) was 0.56 at 0.1x and 0.84 at 0.9x. At 0.9x, concordance for this sample varied between 0.61 (MAF 1%) and 0.96–0.97 (MAF ≥ 10%).

As for the CRR1023808 sample from the Chinese population, the R^2 value increased from 0.58 at 0.1x to 0.95 at 0.9x (Fig. 1B). The R^2 values for common variants (MAF ≥ 10%) reached 0.93–0.95 with the coverage of 0.7×, and that for rare variants (MAF 1%) reached 0.58 at 0.1x and 0.82 at 0.9×. At 0.9×, concordance for this sample varied between 0.63 (MAF 1%) and 0.95–0.97 (MAF ≥ 10%).

The R^2 and concordance values obtained suggest high efficiency of the produced reference panel for genotype imputation in rhesus macaques. The R^2 values for common and mid-frequency variants (MAF ≥ 10%) reach 0.93–0.96 even with the coverage of 0.7×, and concordance at 0.9× exceeds 0.95 for both test samples, confirming the genotype reconstruction reliability for this category of markers. The imputation accuracy for rare variants (MAF 1%) was predictably lower: R^2 was 0.82–0.84 at 0.9×, concordance was 0.86–0.88, which suggests the need for deeper coverage (at least 0.7×–0.9×) when conducting the studies focused on the analysis of rare genetic variants. Thus, the panel created ensures high imputation accuracy for a broad range of variants and can be used in population and association studies of rhesus macaques.

Population structure analysis

The principal component analysis (PCA) was conducted based on 33,457,491 SNP markers in order to assess the reference panel genetic structure. The first principal component (PC1, 68.5% of total variance) clearly divides samples of Indian and Chinese origin into two distinct clusters (Fig. 2), which is consistent with the earlier published data in the considerable genetic divergence among two major geographic lineages of *M. mulatta* [27]. The second principal component (PC2, 5.2% of dispersion) reveals an extra structure within each group: samples of Indian origin demonstrate a relatively compact distribution, while Chinese samples are characterized by the

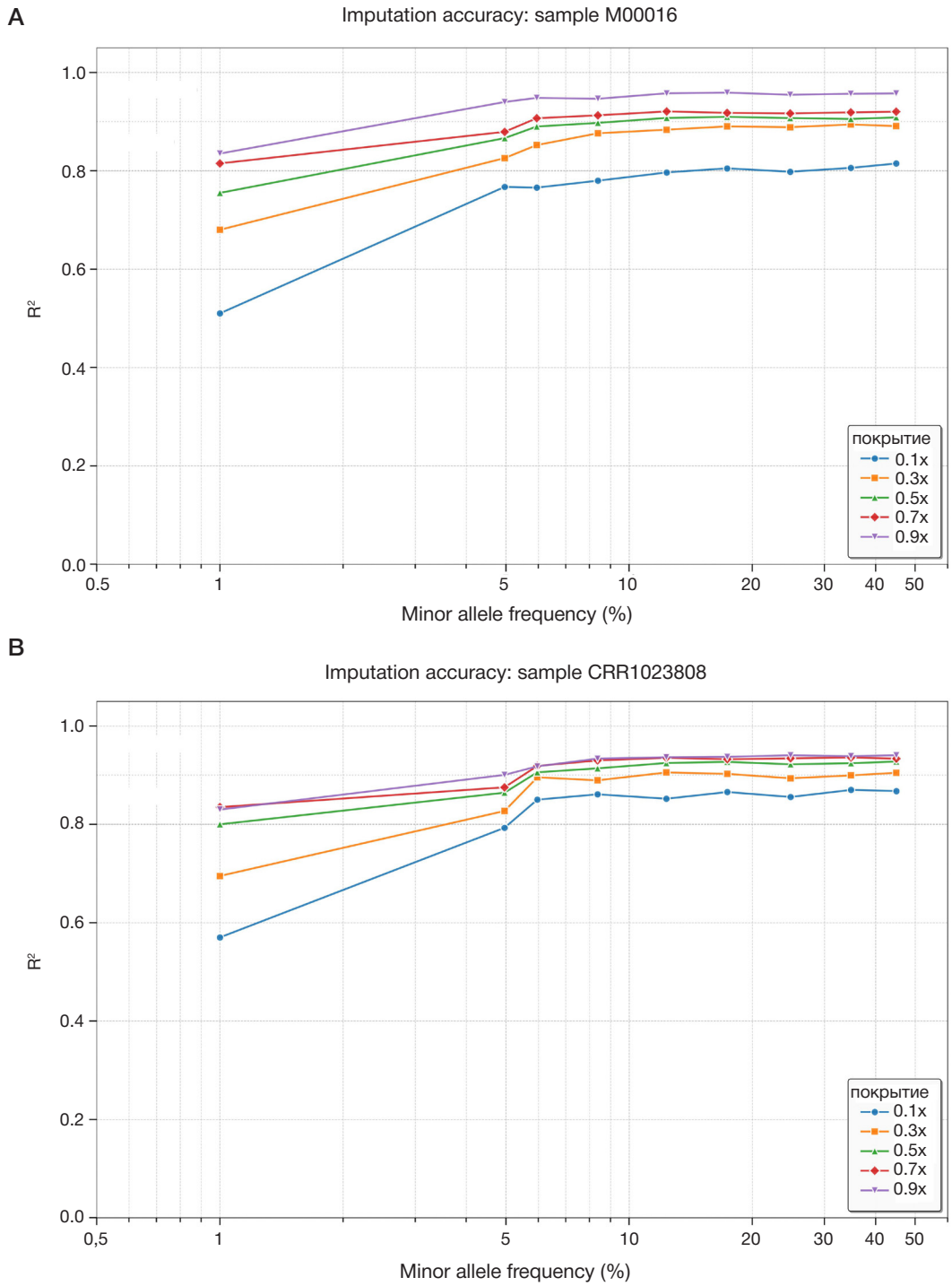

Fig. 1. Genotype imputation accuracy (R^2) depending on the coverage depth and minor allele frequency (MAF) for two test samples. The horizontal axis shows the minor allele frequency (%), the vertical axis shows the R^2 coefficient between imputed and reference allele dosages. Each curve corresponds to one of five coverage levels (0.1×; 0.3×; 0.5×; 0.7×; 0.9×). **A**. M00016 sample of Indian origin. **B**. CRR1023808 sample of Chinese origin

wider spread along the PC2, which corresponds to the higher genetic heterogeneity of the East Asian lineage resulting from its subspecies-level diversity [28].

Panel testing on independent samples

To test the panel using independent data, imputation of genotypes of 10 *M. mulatta* macaques from the collection of the Kurchatov Medical Primatology Complex, National Research Centre "Kurchatov Institute", not included in the reference panel, was performed. Sequencing was conducted with the average coverage of 0.6×, which was compliant with the experimental design ensuring the optimal balance between the cost and reliability when using low-coverage sequencing [7, 12]. Imputation was performed by applying the GLIMPSE2 algorithm to the reference panel created.

The imputation quality was assessed based on the INFO/RSQ indicator which reflects the confidence level for each imputed variant and ranges from 0 to 1. In the studied sample, the INFO/RSQ values varied between 0.862 and 0.934, and the average value was 0.898. All the variants identified were characterized by INFO values > 0.8, corresponding to the strict selection threshold for frequent and mid-frequency variants [29, 30].

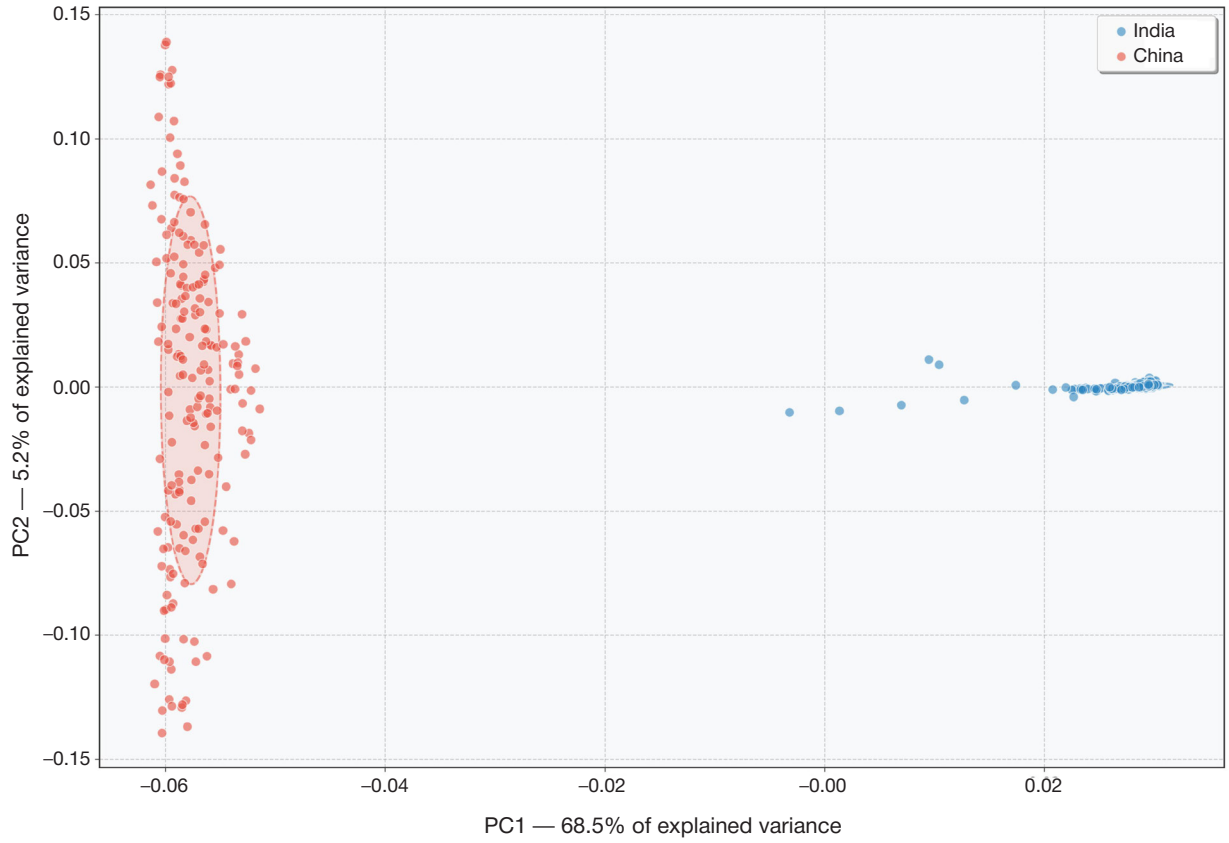

Fig. 2. *M. mulatta* reference haplotype panel principal component analysis (*n* = 618). *Blue* indicates samples of Indian origin (*n* = 418), *red* indicates samples of Chinese origin (*n* = 200)

DISCUSSION

In this study the phased reference haplotype panel for genotype imputation in *Macaca mulatta* that included 618 animals and 33.4 million SNP markers processed using the common standardized pipeline was produced and validated. Among available resources for imputation of genotypes of this species, the panel of 741 animals of the Indian lineage should be highlighted [13], as well as the large cohort of 919 Chinese macaques with phenotypic data representing the GWAS-oriented resource, but not a single phased imputation panel [31]. Neither resource covers both geographic lineages of the species within the framework of the common standardized processing pipeline. At the same time, many laboratory *M. mulatta* populations in the global research centers were formed over decades through the importation of animals from different regions and subsequent uncontrolled crossbreeding, which often led to the unknown or mixed origin of animals [14, 27, 32]. This determines the practical need in the integrated resource covering both lineages, developed in this study.

The imputation accuracy indicators obtained are fully in line with the published data. The highest accuracy was achieved for samples of Indian origin: R^2 0.95–0.96 for common variants even with the coverage of 0.7x, which is comparable with the results obtained based on the Indian panel [13]. Indicators for the Chinese lineage are slightly lower, which naturally reflects its lower representation. The panel developed is far beyond the earlier available resources in marker density, ensuring the coverage of over 33 million SNPs, which corresponds to the level of contemporary reference panels for livestock and opens the prospects for the high-resolution population and association analysis. The panel ensures the imputation quality comparable with that of commercially available SNP chips even with the coverage of 0.6x, which makes the approach cost-effective when used for genotyping of large cohorts.

The practical value of the resource created is determined by the broad range of biomedical tasks, for which *M. mulatta* is the main model: research focused on infectious diseases, research in the field of neurobiology, pharmacology, and toxicology. The imputation-based whole-genome sequencing enables the population screening of animals for carriage of variants orthologous to human pathogenic mutations [33], as well as for controlling the inter-individual pharmacokinetic variability due to polymorphic variants of drug metabolism enzymes [34]. This approach has proven its efficacy in other model and livestock species. A multi-breed panel was created for cattle, including 61.8 million SNP markers. When applying the GLIMPSE2 algorithm, which was also used in our study, the panel showed the concordance over 99% even with the coverage of 0.1× [35]. The SWIM panel (2259 animals of 44 breeds) [36] and the PHARP panel constructed based on the data of 1181 animals from 71 populations [37] were reported for swine. All these panels have been generated by combining the data of several publicly available projects focused on genotyping of various populations, which is consistent with the approach implemented in our study. The growing interest in this area has been also reported in domestic studies: the prospects of low-coverage sequencing for genomic selection of cattle are discussed in the review by Russian authors [38], and the imputed whole-genome data are already used for the association analysis of economically significant traits in Russian herds [39]. The successful experience of creating such resources for other species confirms that the bioinformatics pipeline developed in our study is reproducible and can be adapted for the development of similar panels for other primate species used in biomedical research.

The main directions of the resource development are the panel Chinese component expansion based on the publicly available data and the inclusion of samples from domestic primatology collection, which will make it possible to increase the imputation accuracy for populations of mixed origin. The reference panel created and the bioinformatics approach developed provide the basis for conducting large genome-wide association and population genetic studies involving rhesus macaques in domestic laboratories.

Limitations of the study

The main limitation of the study is uneven representation of geographic lineages in the panel: the number of samples of Indian origin (418) is more than double the number of Chinese ones (200). This has determined the higher imputation accuracy for the Indian one. Furthermore, the panel has been constructed based on the data from foreign repositories (BCM, OHSU, KIZ), so further inclusion of samples from domestic primatology collection is required to more accurately reflect local populations. Accuracy assessment by artificial downsampling was performed for two samples within the coverage range of 0.1–0.9x, while testing on real low-coverage data involved 10 independent samples with the average coverage of 0.6x. In this regard, further testing in the larger heterogeneous sample will make it possible to further confirm reproducibility of the results.

CONCLUSIONS

The phased reference haplotype panel for genotype imputation in *Macaca mulatta* including 618 animals and 33.4 million SNP markers of both major geographic lineages of the species processed using the common standardized pipeline has been created and validated. The panel ensuring high imputation accuracy with the ultralow coverage is ready for practical use in population genetic and association studies. The pipeline developed can serve as a template for the creation of similar resources for other primate species used in biomedical research.

References

1. Gardner MB, Luciw PA. Macaque models of human infectious disease. ILAR J. 2008; 49: 220–55. Available from: https://doi.org/10.1093/ilar.49.2.220.
2. Joho D, Sato K, Kumita W, Saido TC, Sasaki E, Sasaguri H. Advances in non-human primate models for Alzheimer's disease research. Neurosci Res. 2025; 221: 104984. Available from: https://doi.org/10.1016/j.neures.2025.104984.
3. Vallender EJ, Hotchkiss CE, Lewis AD, Rogers J, Stern JA, Peterson SM, et al. Nonhuman primate genetic models for the study of rare diseases. Orphanet J Rare Dis. 2023; 18: 20. Available from: https://doi.org/10.1186/s13023-023-02619-3.
4. Warren WC, Harris RA, Haukness M, Fiddes IT, Murali SC, Fernandes J, et al. Sequence diversity analyses of an improved rhesus macaque genome enhance its biomedical utility. Science, N.Y. 2020; 370: eabc6617. Available from: https://doi.org/10.1126/science.abc6617.
5. Bimber BN, Yan MY, Peterson SM, Ferguson B. mGAP: the macaque genotype and phenotype resource, a framework for accessing and interpreting macaque variant data, and identifying new models of human disease. BMC Genomics. 2019; 20: 176. Available from: https://doi.org/10.1186/s12864-019-5559-7.
6. Bimber BN, Raboin MJ, Letaw J, Nevonen KA, Spindel JE, McCouch SR, et al. Whole-genome characterization in pedigreed non-human primates using genotyping-by-sequencing (GBS) and imputation. BMC Genomics. 2016; 17: 676. Available from: https://doi.org/10.1186/s12864-016-2966-x.
7. Rubinacci S, Ribeiro DM, Hofmeister RJ, Delaneau O. Efficient phasing and imputation of low-coverage sequencing data using large reference panels. Nat Genet. 2021; 53: 120–6. Available from: https://doi.org/10.1038/s41588-020-00756-0.
8. Mitt M, Kals M, Pärn K, Gabriel SB, Lander ES, Palotie A, et al. Improved imputation accuracy of rare and low-frequency variants using population-specific high-coverage WGS-based imputation reference panel. Eur J Hum Genet. 2017; 25: 869–76. Available from: https://doi.org/10.1038/ejhg.2017.51.
9. Zhong X, Peng J, Shen QS, Chen J-Y, Gao H, Luan X, et al. RhesusBase PopGateway: Genome-Wide Population Genetics Atlas in Rhesus Macaque. Mol Biol Evol. 2016; 33: 1370–5. Available from: https://doi.org/10.1093/molbev/msw025.
10. Du L, Guo T, Liu Q, Li J, Zhang X, Xing J, et al. MACSNVdb: a high-quality SNV database for interspecies genetic divergence investigation among macaques. Database (Oxford). 2020; 2020: baaa027. Available from: https://doi.org/10.1093/database/baaa027.
11. Quick C, Anugu P, Musani S, Weiss ST, Burchard EG, White MJ, et al. Sequencing and imputation in GWAS: Cost-effective strategies to increase power and genomic coverage across diverse populations. Genet Epidemiol. 2020; 44: 537–49. Available from: https://doi.org/10.1002/gepi.22326.
12. Pasaniuc B, Rohland N, McLaren PJ, Garimella K, Zaitlen N, Li H, et al. Extremely low-coverage sequencing and imputation increases power for genome-wide association studies. Nat Genet. 2012; 44: 631–5. Available from: https://doi.org/10.1038/ng.2283.
13. Watowich MM, Chiou KL, Graves B, Montague MJ, Brent LJN, Higham JP, et al. Best practices for genotype imputation from low-coverage sequencing data in natural populations. Mol Ecol Resour. 2025; 25: e13854. Available from: https://doi.org/10.1111/1755-0998.13854.
14. Kanthaswamy S, Trask JS, Ross CT, Kou A, Houghton P, Smith DG, et al. A large-scale SNP-based genomic admixture analysis of the captive rhesus macaque colony at the California National Primate Research Center. Am J Primatol. 2012; 74: 747–57. Available from: https://doi.org/10.1002/ajp.22025.
15. Kanthaswamy S, Satkoski J, Kou A, Malladi V, Glenn Smith D. Detecting signatures of inter-regional and inter-specific hybridization among the Chinese rhesus macaque specific pathogen-free (SPF) population using single nucleotide polymorphic (SNP) markers. J Med Primatol. 2010; 39: 252–65. Available from: https://doi.org/10.1111/j.1600-0684.2010.00430.x.
16. Wang J, Wang M, Moshiri A, Harris RA, Raveendran M, Nguyen T, et al. Genetic diversity of 1,845 rhesus macaques improves genetic variation interpretation and identifies disease models. Nat Commun. 2024; 15: 5658. Available from: https://doi.org/10.1038/s41467-024-49922-6.
17. Rogers J. Genomic resources for rhesus macaques (Macaca mulatta). Mamm Genome. 2022; 33: 91–9. Available from: https://doi.org/10.1007/s00335-021-09922-z.
18. Katz K, Shutov O, Lapoint R, Kimelman M, Brister JR, O'Sullivan C. The Sequence Read Archive: a decade more of explosive growth. Nucleic Acids Res. 2022; 50: D387–90. Available from: https://doi.org/10.1093/nar/gkab1053.
19. David Y, Alisha A, Awais A, Rajkumar D, Dipayan G, Muhammad H, et al. The European Nucleotide Archive in 2025. Nucleic Acids Res. 2026; 54: D120–7. Available from: https://doi.org/10.1093/nar/gkaf1295.
20. CNCB-NGDC Members and Partners. Database Resources of the National Genomics Data Center, China National Center for Bioinformation in 2025. Nucleic Acids Res. 2025; 53: D30–44. Available from: https://doi.org/10.1093/nar/gkae978.
21. Chen S, Zhou Y, Chen Y, Gu J. fastp: an ultra-fast all-in-one FASTQ

preprocessor. Bioinformatics. 2018; 34: 1884–90. Available from: https://doi.org/10.1093/bioinformatics/bty560.
22. Langmead B, Salzberg SL. Fast gapped-read alignment with Bowtie 2. Nat Methods. 2012; 9: 357–9. Available from: https://doi.org/10.1038/nmeth.1923.
23. Danecek P, Bonfield JK, Liddle J, Marshall J, Ohan V, Pollard MO, et al. Twelve years of SAMtools and BCFtools. Gigascience. 2021; 10: giab008. Available from: https://doi.org/10.1093/gigascience/giab008.
24. Danecek P, Auton A, Abecasis G, Albers CA, Banks E, DePristo MA, et al. The variant call format and VCFtools. Bioinformatics. 2011; 27: 2156–8. Available from: https://doi.org/10.1093/bioinformatics/btr330.
25. Hofmeister RJ, Ribeiro DM, Rubinacci S, Delaneau O. Accurate rare variant phasing of whole-genome and whole-exome sequencing data in the UK Biobank. Nat Genet. Nature Publishing Group. 2023; 55: 1243–9. Available from: https://doi.org/10.1038/s41588-023-01415-w.
26. Rubinacci S, Hofmeister RJ, Sousa da Mota B, Delaneau O. Imputation of low-coverage sequencing data from 150,119 UK Biobank genomes. Nat Genet. 2023; 55: 1088–90. Available from: https://doi.org/10.1038/s41588-023-01438-3.
27. Smith DG. Genetic characterization of Indian-origin and Chinese-origin rhesus macaques (Macaca mulatta). Comp Med. 2005; 55: 227–30.
28. Liu Z, Tan X, Orozco-terWengel P, Zhou X, Zhang L, Tian S, et al. Population genomics of wild Chinese rhesus macaques reveals a dynamic demographic history and local adaptation, with implications for biomedical research. Gigascience. 2018; 7: giy106. Available from: https://doi.org/10.1093/gigascience/giy106.
29. Stahl K, Papiol S, Budde M, Heilbronner M, Oraki Kohshour M, Falkai P, et al. Aggregating single nucleotide polymorphisms improves filtering for false-positive associations postimputation. G3 (Bethesda). Bethesda, Md. 2025; 15: jkaf043. Available from: https://doi.org/10.1093/g3journal/jkaf043.
30. Fu J, Zhang Q, Wang J, Wang M, Zhang B, Zhu W, и др. Cross-ancestry genome-wide association studies of brain imaging phenotypes. Nat Genet. 2024; 56: 1110–20. Available from: https://doi.org/10.1038/s41588-024-01766-y.
31. Zhang B-L, Chen Y, Zhang Y, Qiao Y, Wu Y, Zhang Y, et al. Forward and reverse genomic screens enhance the understanding of phenotypic variation in a large Chinese rhesus macaque cohort. Nat Commun. Nature Publishing Group. 2025; 16: 8703. Available from: https://doi.org/10.1038/s41467-025-63747-x.
32. Lyke MM, Bagwell A, Newman D, Galindo S, Church T, Christensen C, et al. Mergers and migrations: drivers of population genetic structure in a captive rhesus macaque colony. BMC Genomics. 2026; Available from: https://doi.org/10.1186/s12864-026-13090-2.
33. Wang J, Wang M, Moshiri A, Harris RA, Raveendran M, Nguyen T, et al. Genetic diversity of 1,845 rhesus macaques improves genetic variation interpretation and identifies disease models. Nat Commun. 2024; 15: 5658. Available from: https://doi.org/10.1038/s41467-024-49922-6.
34. Uno Y, Uehara S, Yamazaki H. Genetic polymorphisms of drug-metabolizing cytochrome P450 enzymes in cynomolgus and rhesus monkeys and common marmosets in preclinical studies for humans. Biochem Pharmacol. 2018; 153: 184–95. Available from: https://doi.org/10.1016/j.bcp.2017.12.015.
35. Zhang Z, Wang A, Hu H, Wang L, Gong M, Yang Q, et al. The efficient phasing and imputation pipeline of low-coverage whole genome sequencing data using a high-quality and publicly available reference panel in cattle. Animal Research and One Health. 2023; 1: 4–16. Available from: https://doi.org/10.1002/aro2.8.
36. Ding R, Savegnago R, Liu J, Long N, Tan C, Cai G, et al. The SWine IMputation (SWIM) haplotype reference panel enables nucleotide resolution genetic mapping in pigs. Commun Biol. 2023; 6: 577. Available from: https://doi.org/10.1038/s42003-023-04933-9.
37. Wang Z, Zhang Z, Chen Z, Sun J, Cao C, Wu F, et al. PHARP: a pig haplotype reference panel for genotype imputation. Sci Rep. 2022; 12: 12645. Available from: https://doi.org/10.1038/s41598-022-15851-x.
38. Kostyunina O, Koldichev N, Nemkovskiy G, Traspov A, Ermilov A, Bakoev F, et al. Low-Coverage Whole-Genome Sequencing (lcWGS) in Cattle: Analysis of Potential and Prospects for Application. Animals (Basel). 2025; 15: 3538. Available from: https://doi.org/10.3390/ani15243538.
39. Genome-wide association study of carcass traits in an Angus beef cattle Russian herd using imputed Whole-Genome Sequence data. The Thirteenth International Multiconference. Institute of Cytology and Genetics, the Siberian Branch of the Russian Academy of Sciences; 2022 [дата обращения: 4 август 2026 г.]. Available from: https://doi.org/10.18699/SBB-2022-397.

Литература

1. Gardner MB, Luciw PA. Macaque models of human infectious disease. ILAR J. 2008; 49: 220–55. Available from: https://doi.org/10.1093/ilar.49.2.220.
2. Joho D, Sato K, Kumita W, Saido TC, Sasaki E, Sasaguri H. Advances in non-human primate models for Alzheimer's disease research. Neurosci Res. 2025; 221: 104984. Available from: https://doi.org/10.1016/j.neures.2025.104984.
3. Vallender EJ, Hotchkiss CE, Lewis AD, Rogers J, Stern JA, Peterson SM, et al. Nonhuman primate genetic models for the study of rare diseases. Orphanet J Rare Dis. 2023; 18: 20. Available from: https://doi.org/10.1186/s13023-023-02619-3.
4. Warren WC, Harris RA, Haukness M, Fiddes IT, Murali SC, Fernandes J, et al. Sequence diversity analyses of an improved rhesus macaque genome enhance its biomedical utility. Science, N.Y. 2020; 370: eabc6617. Available from: https://doi.org/10.1126/science.abc6617.
5. Bimber BN, Yan MY, Peterson SM, Ferguson B. mGAP: the macaque genotype and phenotype resource, a framework for accessing and interpreting macaque variant data, and identifying new models of human disease. BMC Genomics. 2019; 20: 176. Available from: https://doi.org/10.1186/s12864-019-5559-7.
6. Bimber BN, Raboin MJ, Letaw J, Nevonen KA, Spindel JE, McCouch SR, et al. Whole-genome characterization in pedigreed non-human primates using genotyping-by-sequencing (GBS) and imputation. BMC Genomics. 2016; 17: 676. Available from: https://doi.org/10.1186/s12864-016-2966-x.
7. Rubinacci S, Ribeiro DM, Hofmeister RJ, Delaneau O. Efficient phasing and imputation of low-coverage sequencing data using large reference panels. Nat Genet. 2021; 53: 120–6. Available from: https://doi.org/10.1038/s41588-020-00756-0.
8. Mitt M, Kals M, Pärn K, Gabriel SB, Lander ES, Palotie A, et al. Improved imputation accuracy of rare and low-frequency variants using population-specific high-coverage WGS-based imputation reference panel. Eur J Hum Genet. 2017; 25: 869–76. Available from: https://doi.org/10.1038/ejhg.2017.51.
9. Zhong X, Peng J, Shen QS, Chen J-Y, Gao H, Luan X, et al. RhesusBase PopGateway: Genome-Wide Population Genetics Atlas in Rhesus Macaque. Mol Biol Evol. 2016; 33: 1370–5. Available from: https://doi.org/10.1093/molbev/msw025.
10. Du L, Guo T, Liu Q, Li J, Zhang X, Xing J, et al. MACSNVdb: a high-quality SNV database for interspecies genetic divergence investigation among macaques. Database (Oxford). 2020; 2020: baaa027. Available from: https://doi.org/10.1093/database/baaa027.
11. Quick C, Anugu P, Musani S, Weiss ST, Burchard EG, White MJ, et al. Sequencing and imputation in GWAS: Cost-effective strategies to increase power and genomic coverage across diverse populations. Genet Epidemiol. 2020; 44: 537–49. Available from: https://doi.org/10.1002/gepi.22326.
12. Pasaniuc B, Rohland N, McLaren PJ, Garimella K, Zaitlen N, Li H, et al. Extremely low-coverage sequencing and imputation increases power for genome-wide association studies. Nat Genet. 2012; 44: 631–5. Available from: https://doi.org/10.1038/ng.2283.
13. Watowich MM, Chiou KL, Graves B, Montague MJ, Brent LJN, Higham JP, et al. Best practices for genotype imputation from low-coverage sequencing data in natural populations. Mol Ecol Resour. 2025; 25: e13854. Available from: https://doi.org/10.1111/1755-0998.13854.
14. Kanthaswamy S, Trask JS, Ross CT, Kou A, Houghton P, Smith DG,

et al. A large-scale SNP-based genomic admixture analysis of the captive rhesus macaque colony at the California National Primate Research Center. Am J Primatol. 2012; 74: 747–57. Available from: https://doi.org/10.1002/ajp.22025.
15. Kanthaswamy S, Satkoski J, Kou A, Malladi V, Glenn Smith D. Detecting signatures of inter-regional and inter-specific hybridization among the Chinese rhesus macaque specific pathogen-free (SPF) population using single nucleotide polymorphic (SNP) markers. J Med Primatol. 2010; 39: 252–65. Available from: https://doi.org/10.1111/j.1600-0684.2010.00430.x.
16. Wang J, Wang M, Moshiri A, Harris RA, Raveendran M, Nguyen T, et al. Genetic diversity of 1,845 rhesus macaques improves genetic variation interpretation and identifies disease models. Nat Commun. 2024; 15: 5658. Available from: https://doi.org/10.1038/s41467-024-49922-6.
17. Rogers J. Genomic resources for rhesus macaques (Macaca mulatta). Mamm Genome. 2022; 33: 91–9. Available from: https://doi.org/10.1007/s00335-021-09922-z.
18. Katz K, Shutov O, Lapoint R, Kimelman M, Brister JR, O'Sullivan C. The Sequence Read Archive: a decade more of explosive growth. Nucleic Acids Res. 2022; 50: D387–90. Available from: https://doi.org/10.1093/nar/gkab1053.
19. David Y, Alisha A, Awais A, Rajkumar D, Dipayan G, Muhammad H, et al. The European Nucleotide Archive in 2025. Nucleic Acids Res. 2026; 54: D120–7. Available from: https://doi.org/10.1093/nar/gkaf1295.
20. CNCB-NGDC Members and Partners. Database Resources of the National Genomics Data Center, China National Center for Bioinformation in 2025. Nucleic Acids Res. 2025; 53: D30–44. Available from: https://doi.org/10.1093/nar/gkae978.
21. Chen S, Zhou Y, Chen Y, Gu J. fastp: an ultra-fast all-in-one FASTQ preprocessor. Bioinformatics. 2018; 34: 1884–90. Available from: https://doi.org/10.1093/bioinformatics/bty560.
22. Langmead B, Salzberg SL. Fast gapped-read alignment with Bowtie 2. Nat Methods. 2012; 9: 357–9. Available from: https://doi.org/10.1038/nmeth.1923.
23. Danecek P, Bonfield JK, Liddle J, Marshall J, Ohan V, Pollard MO, et al. Twelve years of SAMtools and BCFtools. Gigascience. 2021; 10: giab008. Available from: https://doi.org/10.1093/gigascience/giab008.
24. Danecek P, Auton A, Abecasis G, Albers CA, Banks E, DePristo MA, et al. The variant call format and VCFtools. Bioinformatics. 2011; 27: 2156–8. Available from: https://doi.org/10.1093/bioinformatics/btr330.
25. Hofmeister RJ, Ribeiro DM, Rubinacci S, Delaneau O. Accurate rare variant phasing of whole-genome and whole-exome sequencing data in the UK Biobank. Nat Genet. Nature Publishing Group. 2023; 55: 1243–9. Available from: https://doi.org/10.1038/s41588-023-01415-w.
26. Rubinacci S, Hofmeister RJ, Sousa da Mota B, Delaneau O. Imputation of low-coverage sequencing data from 150,119 UK Biobank genomes. Nat Genet. 2023; 55: 1088–90. Available from: https://doi.org/10.1038/s41588-023-01438-3.
27. Smith DG. Genetic characterization of Indian-origin and Chinese-origin rhesus macaques (Macaca mulatta). Comp Med. 2005; 55: 227–30.
28. Liu Z, Tan X, Orozco-terWengel P, Zhou X, Zhang L, Tian S, et al. Population genomics of wild Chinese rhesus macaques reveals a dynamic demographic history and local adaptation, with implications for biomedical research. Gigascience. 2018; 7: giy106. Available from: https://doi.org/10.1093/gigascience/giy106.
29. Stahl K, Papiol S, Budde M, Heilbronner M, Oraki Kohshour M, Falkai P, et al. Aggregating single nucleotide polymorphisms improves filtering for false-positive associations postimputation. G3 (Bethesda). Bethesda, Md. 2025; 15: jkaf043. Available from: https://doi.org/10.1093/g3journal/jkaf043.
30. Fu J, Zhang Q, Wang J, Wang M, Zhang B, Zhu W, и др. Cross-ancestry genome-wide association studies of brain imaging phenotypes. Nat Genet. 2024; 56: 1110–20. Available from: https://doi.org/10.1038/s41588-024-01766-y.
31. Zhang B-L, Chen Y, Zhang Y, Qiao Y, Wu Y, Zhang Y, et al. Forward and reverse genomic screens enhance the understanding of phenotypic variation in a large Chinese rhesus macaque cohort. Nat Commun. Nature Publishing Group. 2025; 16: 8703. Available from: https://doi.org/10.1038/s41467-025-63747-x.
32. Lyke MM, Bagwell A, Newman D, Galindo S, Church T, Christensen C, et al. Mergers and migrations: drivers of population genetic structure in a captive rhesus macaque colony. BMC Genomics. 2026; Available from: https://doi.org/10.1186/s12864-026-13090-2.
33. Wang J, Wang M, Moshiri A, Harris RA, Raveendran M, Nguyen T, et al. Genetic diversity of 1,845 rhesus macaques improves genetic variation interpretation and identifies disease models. Nat Commun. 2024; 15: 5658. Available from: https://doi.org/10.1038/s41467-024-49922-6.
34. Uno Y, Uehara S, Yamazaki H. Genetic polymorphisms of drug-metabolizing cytochrome P450 enzymes in cynomolgus and rhesus monkeys and common marmosets in preclinical studies for humans. Biochem Pharmacol. 2018; 153: 184–95. Available from: https://doi.org/10.1016/j.bcp.2017.12.015.
35. Zhang Z, Wang A, Hu H, Wang L, Gong M, Yang Q, et al. The efficient phasing and imputation pipeline of low-coverage whole genome sequencing data using a high-quality and publicly available reference panel in cattle. Animal Research and One Health. 2023; 1: 4–16. Available from: https://doi.org/10.1002/aro2.8.
36. Ding R, Savegnago R, Liu J, Long N, Tan C, Cai G, et al. The SWine IMputation (SWIM) haplotype reference panel enables nucleotide resolution genetic mapping in pigs. Commun Biol. 2023; 6: 577. Available from: https://doi.org/10.1038/s42003-023-04933-9.
37. Wang Z, Zhang Z, Chen Z, Sun J, Cao C, Wu F, et al. PHARP: a pig haplotype reference panel for genotype imputation. Sci Rep. 2022; 12: 12645. Available from: https://doi.org/10.1038/s41598-022-15851-x.
38. Kostyunina O, Koldichev N, Nemkovskiy G, Traspov A, Ermilov A, Bakoev F, et al. Low-Coverage Whole-Genome Sequencing (lcWGS) in Cattle: Analysis of Potential and Prospects for Application. Animals (Basel). 2025; 15: 3538. Available from: https://doi.org/10.3390/ani15243538.
39. Genome-wide association study of carcass traits in an Angus beef cattle Russian herd using imputed Whole-Genome Sequence data. The Thirteenth International Multiconference. Institute of Cytology and Genetics, the Siberian Branch of the Russian Academy of Sciences; 2022 [дата обращения: 4 август 2026 г.]. Available from: https://doi.org/10.18699/SBB-2022-397.

MOLECULAR GENETIC ASPECTS OF PREDICTING EARLY PREGNANCY LOSS

Yusef OV[1], Ibragimov BR[2], Klimenko MP[1]✉, Gerasimova AA[3], Aimetdinova AB[1], Marnat EG[1], Abramov DD[4], Klimenko PA[1], Kurtser MA[1]

[1] Pirogov Russian National Research Medical University, Moscow, Russia
[2] Dagestan State Medical University, Makhachkala, Russia
[3] Patrice Lumumba Peoples' Friendship University of Russia, Moscow, Russia
[4] Institute of Immunology of the Federal Medical Biological Agency of Russia, Moscow, Russia

Missed abortion is one of the most prevalent forms of early pregnancy loss that remains a pressing issue of obstetrics and gynecology. Despite advances in reproductive medicine, the molecular mechanisms underlying the embryo development termination in early gestation are poorly understood. A comparative single-center study aimed to assess the expression of *TGF-β* and *MMP-9* genes in peripheral blood of women with physiological and missed abortion and assess their potential prognostic value for evaluation of the risk of early pregnancy loss. A total of 40 pregnant women were included in the study: 20 patients with the 9–11 week physiological pregnancy (control group) and 20 women diagnosed with missed abortion (index group). The *TGF-β* and *MMP-9* gene expression was determined by the real-time polymerase chain reaction method after the total RNA isolation from peripheral blood. The Mann–Whitney U-test and ROC analysis were used for statistical data processing. No significant differences in the *TGF-β* and *MMP-9* gene expression between the studied groups were revealed. At the same time, ROC analysis made it possible to determine the threshold values of the studied indicators having some diagnostic information content. As for *MMP-9*, the threshold value $Ct \leq 29$ ensuring the 80% sensitivity and 60% specificity turned out to be the most informative. As for *TGF-β*, the threshold value $Ct \leq 27.4$ was characterized by the 75% sensitivity and 70% specificity. The findings suggest the potential prognostic value of the studied genes for evaluation of the risk of missed abortion.

Keywords: expression of *TGF-β* and *MMP-9* genes, missed abortion, physiological pregnancy, prognosis of pregnancy course

Funding: the study was conducted as part of the Program for Basic Research in the Russian Federation for the Long Term (2021–2030) (No. 122030100170-5).

Author contribution: Yusef OV — clinical material collection, laboratory testing; Ibragimov BR — statistical processing, analysis of results; Klimenko MP — database creation; Gerasimova AA — ultrasound examination, clinical assessment of results; Aimetdinova AB — clinical and functional assessment of patients; Marnat EG — laboratory testing (PCR); Abramov DD — literature review, interpretation of results, manuscript writing; Klimenko PA — study design, clinical phase arrangement, interpretation of results; Kurtser MA — study concept and design, academic advising, manuscript approval.

Compliance with ethical standards: the study was approved by the Ethics Committee of the Pirogov Russian National Research Medical University (protocol No. 258 dated February 16, 2026). All the surveyed individuals submitted the informed consent to take part in the study.

✉ **Correspondence should be addressed:** Pyotr A. Klimenko
Sevastopolsky prospekt, 24a, Moscow, 117209; pa.klimenko@mail.ru

Received: 24.06.2026 **Accepted:** 05.08.2026 **Published online:** 18.08.2026

DOI: 10.24075/brsmu.2026.043

МОЛЕКУЛЯРНО-ГЕНЕТИЧЕСКИЕ АСПЕКТЫ ПРОГНОЗИРОВАНИЯ РАННИХ РЕПРОДУКТИВНЫХ ПОТЕРЬ

О. В. Юсеф[1], Б. Р. Ибрагимов[2], М. П. Клименко[1]✉, А. А. Герасимова[3], А. Б. Айметдинова[1], Е. Г. Марнат[1], Д. Д. Абрамов[4], П. А. Клименко[1], М. А. Курцер[1]

[1] Российский национальный исследовательский медицинский университет имени Н. И. Пирогова, Москва, Россия
[2] Дагестанский государственный медицинский университет, Махачкала, Россия
[3] Российский университет дружбы народов имени Патриса Лумумбы, Москва, Россия
[4] Институт иммунологии Федерального медико-биологического агентства России, Москва, Россия

Замершая беременность относится к числу наиболее распространенных форм ранних репродуктивных потерь и остается актуальной проблемой акушерства и гинекологии. Несмотря на достижения в области репродуктивной медицины, молекулярные механизмы, лежащие в основе прекращения развития эмбриона на ранних сроках гестации, изучены недостаточно. Целью сравнительного одноцентрового исследования было оценить уровень экспрессии генов *TGF-β* и *MMP-9* в периферической крови женщин с физиологической и замершей беременностью и определить их потенциальную прогностическую значимость при оценке риска ранних репродуктивных потерь. В исследование были включены 40 беременных женщин: 20 пациенток с физиологически протекающей беременностью сроком 9–11 недель (контрольная группа) и 20 женщин с диагнозом замершей беременности (основная группа). Уровень экспрессии генов *TGF-β* и *MMP-9* определяли методом полимеразной цепной реакции в режиме реального времени после выделения тотальной РНК из периферической крови. Для статистической обработки результатов использовали критерий Манна–Уитни и ROC-анализ. Статистически значимых различий между исследуемыми группами по уровням экспрессии генов *TGF-β* и *MMP-9* выявлено не было. Вместе с тем ROC-анализ позволил определить пороговые значения исследуемых показателей, обладающие определенной диагностической информативностью. Для *MMP-9* наиболее информативным оказалось значение $Ct \leq 29$, обеспечивающее чувствительность 80% и специфичность 60%. Для *TGF-β* пороговое значение $Ct \leq 27{,}4$ характеризовалось чувствительностью 75% и специфичностью 70%. Полученные результаты свидетельствуют о потенциальной прогностической значимости исследуемых генов при оценке риска замершей беременности.

Ключевые слова: экспрессия генов *TGF-β* и *MMP-9*, физиологическая и замершая беременность, прогнозирование течения беременности

Финансирование: работа выполнена в рамках Программы фундаментальных научных исследований в Российской Федерации на долгосрочный период (2021–2030 гг.) (№ 122030100170-5).

Вклад авторов: О. В. Юсеф — сбор клинического материала, проведение лабораторных исследований; Б. Р. Ибрагимов — статистическая обработка, анализ результатов; М. П. Клименко — формирование базы данных; А. А. Герасимова — ультразвуковое исследование, клиническая оценка результатов; А. Б. Айметдинова — клинико-функциональное обследование пациентов; Е. Г. Марнат — проведение лабораторных исследований (ПЦР); Д. Д. Абрамов — анализ литературы, интерпретация результатов, подготовка текста рукописи; П. А. Клименко — дизайн исследования, организация клинического этапа, интерпретация результатов; М. А. Курцер — концепция и дизайн исследования, научное руководство, утверждение рукописи.

Соблюдение этических стандартов: исследование одобрено этическим комитетом РНИМУ им. Н. И. Пирогова (протокол № 258 от 16 февраля 2026 г.). Все обследованные подписали добровольное информированное согласие на участие в исследовании.

✉ **Для корреспонденции:** Петр Афанасьевич Клименко
Севастопольский пр-т, д. 24а, г. Москва, 117209; pa.klimenko@mail.ru

Статья получена: 24.06.2026 **Статья принята к печати:** 05.08.2026 **Опубликована онлайн:** 18.08.2026

DOI: 10.24075/vrgmu.2026.043

Missed abortion is one of the most significant problems of modern reproductive medicine that occupies an important place in the structure of early pregnancy loss. Despite the improvement of the diagnosis and treatment methods, the prevalence of this disorder remains high. Abnormal embryo development in early gestation results from the combination of genetic, immune, endocrine, infectious, and vascular factors, the contribution of each of which can be different depending on the clinical situation.

The normal pregnancy course is ensured by the coherent interaction between the mother's body and the developing embryo. Successful implantation and subsequent formation of the placental complex require an adequate trophoblast invasion, extracellular matrix remodeling, vascular network formation, and immune tolerance maintenance. Violation of any of the above processes can result in pregnancy arrest.

The earlier studies revealed molecular features of the tissues collected from individuals with missed abortion. It has been found that early pregnancy loss is associated with changes in the ribosomal DNA content [1, 2], abnormal expression of a number of placenta-specific proteins of the PSG family [3, 4], as well as downregulation of the reticulon 4 (RTN4) protein involved in apoptosis and cell differentiation. The results obtained suggest that there are complex molecular abnormalities affecting various phases of embryo development and placenta formation [1–6]. At the same time, the immune regulation and tissue remodeling mechanisms in patients with miscarriage are poorly understood. In this regard, the transforming growth factor β (*TGF-β*) and matrix metalloproteinase 9 (*MMP-9*) genes play an important role in ensuring the immune tolerance, trophoblast invasion, and placental bed formation are of special interest.

MMP-9 is an enzyme involved in degradation of the extracellular matrix components. Its activity is important for the throphoblastic cell migration and invasion, endometrial tissue remodeling, and placental complex formation. The *MMP-9* regulation impairment can be associated with placentation defects and complicated pregnancy course [7–13].

Matrix metalloproteinase 9, also playing an important role in leukocyte migration, osteoclastic bone resorption, belongs to the M10A peptidase family; it functions as a growth factor regulating the cell differentiation, migration, and cell death, activates the signaling cascades via CD63 and ITGB1. According to the String data (Fig. 1), it is also involved in protein-protein interaction.

TGF-β belongs to the key regulators of cell proliferation, differentiation, and immune response. During pregnancy this cytokine is involved in developing the immune tolerance between the mother's body and the fetus, limiting the development of excess immune responses and contributing to continuation of pregnancy [14–25].

Despite a large number of studies focused on the role of TGF-β and MMP-9 in reproductive processes, the information about the specifics of their expression in patients with missed abortion is still limited and largely controversial. This determines the need for further study of these molecular markers.

According to the String data (Fig. 2), TGF-β is involved in protein-protein interaction in the following way.

The studied genes (proteomes) almost never interact with each other or together (Fig. 3).

The study aimed to assess the *TGF-β* and *MMP-9* gene expression in peripheral blood of women with physiological pregnancy and missed abortion, as well as to determine their

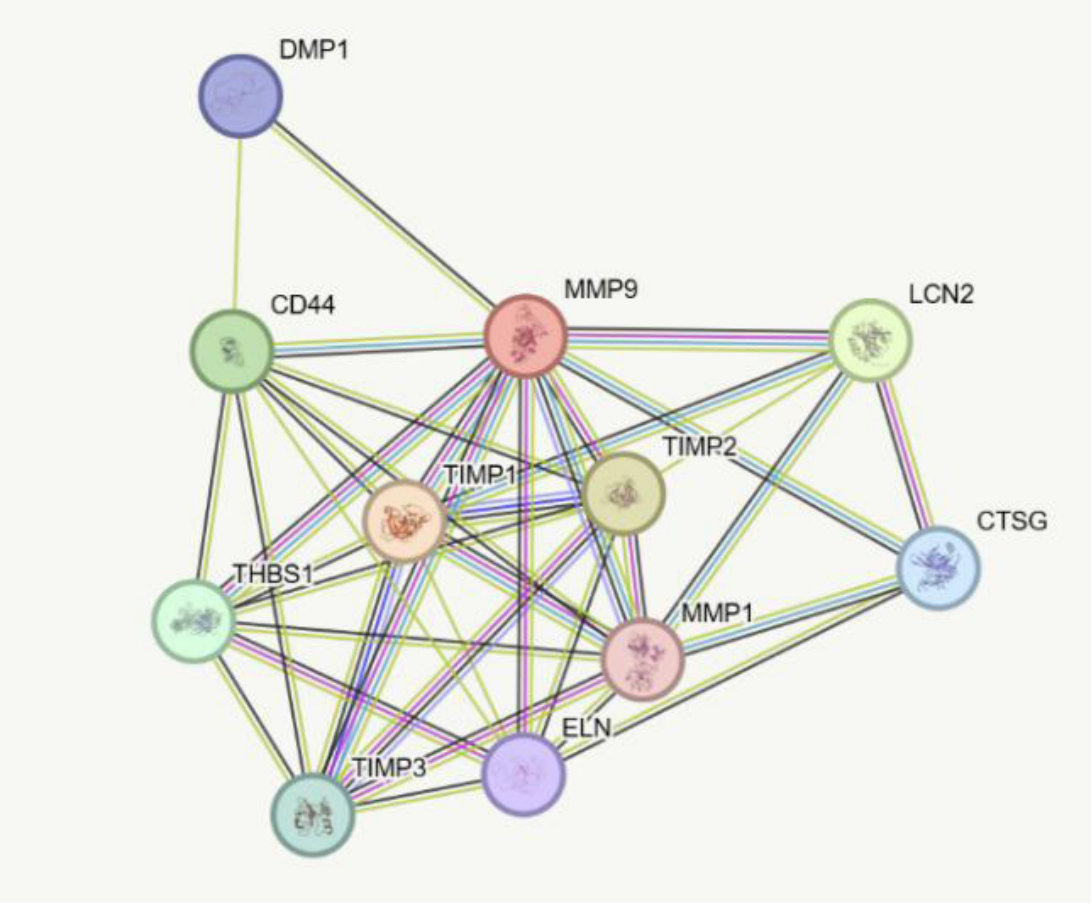

Fig. 1. Protein-protein interaction of MMP-9. Contribution of the MMP-9 biochemical interaction with other bioactive substances. The interaction network is constructed using the STRING resource (https://string-db.org)

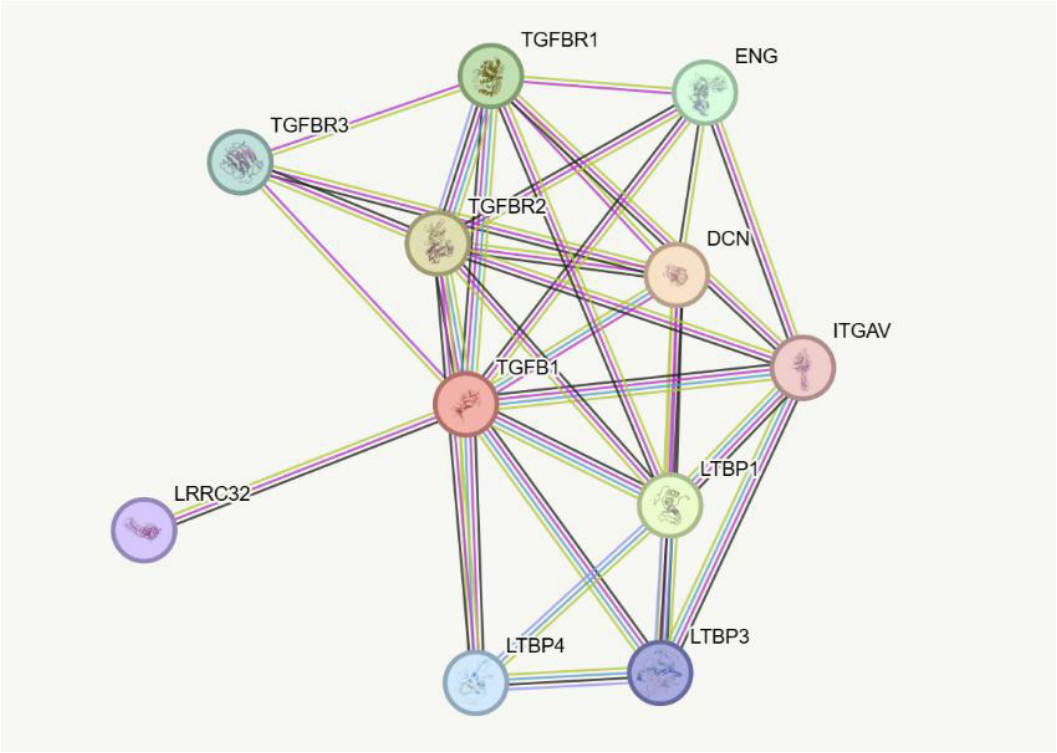

Fig. 2. Protein-protein interaction of TGF-β. Contribution of the TGF-β biochemical interaction with other bioactive substances. The interaction network is constructed using the STRING resource (https://string-db.org)

potential prognostic value for evaluation of the risk of early pregnancy loss.

METHODS

Research design. A comparative single-center study aimed at assessing the *TGF-β* and *MMP-9* gene expression in peripheral blood of women with physiological pregnancy and missed abortion was conducted.

Characteristics of surveyed patients

A total of 40 pregnant women were included in the study. The control group consisted of 20 patients with the 9–11-week physiological singleton pregnancy, who were through the first prenatal screening. The index group consisted of 20 women diagnosed with missed abortion. Missed abortion was detected during the scheduled visit and the ultrasound examination, and the pregnancy age was determined based on the medical history data and fetal ultrasound. In 13 patients, pregnancy arrest occurred at 6–9 weeks of gestation, and in 4 patients it occurred at 9–12 weeks. Furthermore, a mismatch between anthropometric measurements based on the ultrasound examination of dead embryos and the gestational age of 3–5 weeks. In 3 patients, pregnancy was terminated for medical reasons (teratogenic effects) after the genetic counseling and the consilium at 13–21 weeks. Fetal karyotypes were not determined in cases of developmental abnormalities. Inclusion criteria: age over 18 years; confirmed intrauterine pregnancy; signed informed consent to take part in the study. Exclusion criteria: multiple pregnancy.

Biomaterial collection

Peripheral venous blood collection from the cubital vein was performed in all patients prior to surgery and ultrasound examination. The main diagnosis was made after the embryo tissue assessment at the cytogenetic laboratory.

RNA isolation and cDNA synthesis

Whole venous blood was used to isolate total RNA. After lysis of cellular elements samples were centrifuged, and further RNA extraction was performed using the ExtractRNA kit (Evrogen, Russia) in accordance with the manufacturer's guidelines. The quality of the RNA obtained was controlled by electrophoresis. The nucleic acid concentration was determined by spectrophotometry using the Nano500 system (AllSheng, China). The BioMaster RNAscribe RT Plus kit (Biolabmix, Russia) was used to synthesize complementary DNA. A total of 1 μg of total RNA was added to the reverse transcription reaction. After the reaction was complete the resulting cDNA was diluted with nuclease-free water and used for further gene expression analysis.

Determination of gene expression

The expression of the *TGF-β* and *MMP-9* genes was determined by the real-time polymerase chain reaction method. Amplification was accomplished in the DT-96 cycler (DNA-Technology, Russia). All the samples were analyzed in two technical replicates. To increase the analysis specificity,

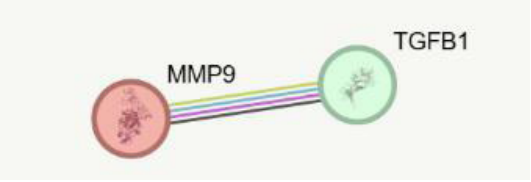

Fig. 3. Biological interaction of TGF-β and MMP9 between each other in the pregnant woman's body. The interaction network is constructed using the STRING resource (https://string-db.org)

Table. Comparative statistics of the *TGF-β* and *MMP-9* expression in blood of patients physiological pregnancy and missed abortion

Parameters	Group	Number of cases	Mean	Standard error (±)	Minimum	Maximum
Ct_TGFb	Missed abortion	20	27.15	0.3	24.7	30.8
Ct_TGFb	Control	20	28.205	0.33	26	32.7
Ct_MMP9	Missed abortion	20	27.805	0.42	25.4	32.1
Ct_MMP9	Control	20	29.31	0.37	26.2	32.4
Ct_B2M	Missed abortion	20	19.935	0.37	17.9	24.8
Ct_B2M	Control	20	20.5	0.28	18.4	23.7
Ct_GUSB	Missed abortion	20	28.265	0.37	25.9	33.4
Ct_GUSB	Control	20	29.47	0.37	26.2	33.1
Ctref	Missed abortion	20	24.1	0.36	22.3	29.1
Ctref	Control	20	24.985	0.31	23	28.4
ΔCt_TGFb	Missed abortion	20	3.05	0.21	1.2	4.9
ΔCt_TGFb	Control	20	3.22	0.2	2	6.1
ΔCt_MMP9	Missed abortion	20	3.705	0.23	2.35	6.15
ΔCt_MMP9	Control	20	4.325	0.26	2.8	8.3

Note: Ct_TGFb — *Ct* value of *TGF-β* gene amplification, Ct_MMP9 — *Ct* value of *MMP-9* gene amplification.

primer was placed on the exon–exon junction, which prevented amplification with the genomic DNA. *B2M* and *GUSB* were used as reference genes. Relative expression was calculated by the *ΔΔCt* method with subsequent mean reference gene normalization.

Statistical analysis

Statistical data processing was performed using the StatPlus 2007 software. The mean, standard error of the mean, median minimum and maximum values were calculated for quantitative indicators. Independent groups were compared using the nonparametric Mann–Whitney test. This method was selected due to small sample size and no need to assume the normal distribution of the studied traits. The differences were considered significant at $p < 0.05$. ROC analysis involving determination of optimal threshold values, sensitivity and specificity was used to assess the diagnostic informativity of the studied indicators. No adjustment for multiple comparisons was applied. The study was preliminary, since the cohort size was 20 individuals per group.

RESULTS

Comparative analysis of the *TGF-β* and *MMP-9* gene expression in peripheral blood of women with physiological

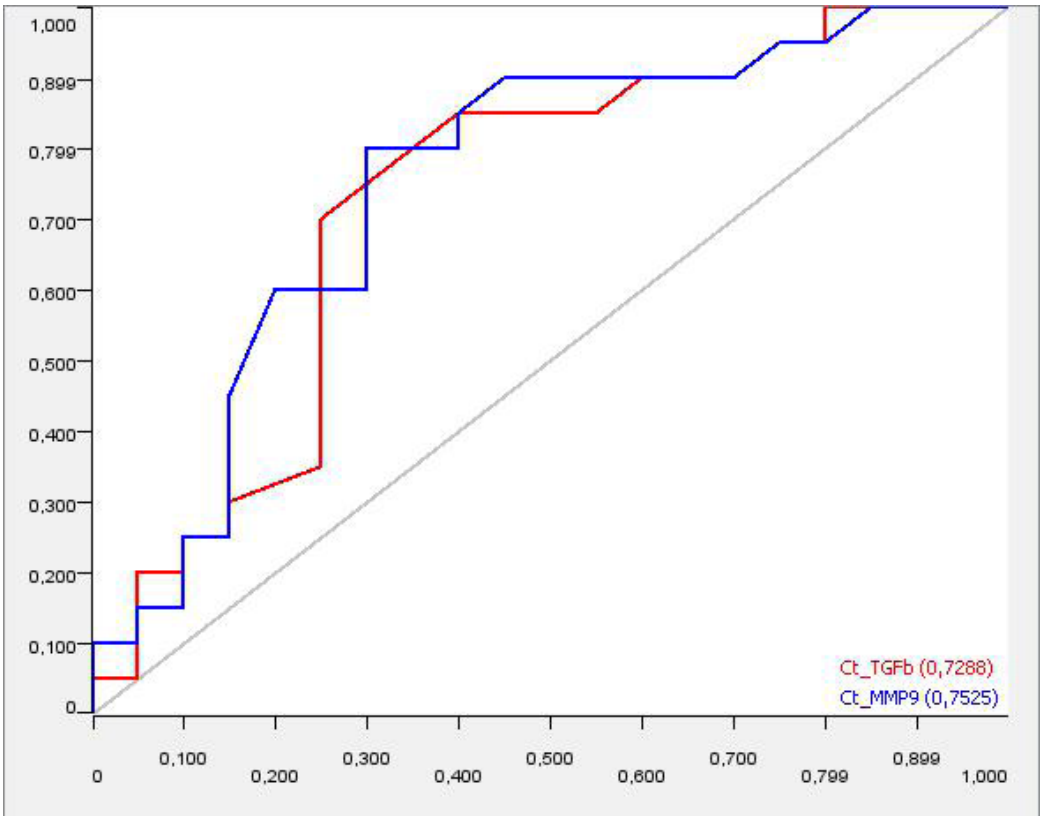

Fig. 4. ROC curves characterizing the Ct_TGFb and Ct_MMP9 expression sensitivity and specificity for the success of missed abortion prediction. X axis — False positive rate (specificity), Y axis — True positive rate (sensitivity)

pregnancy and missed abortion was conducted. The analysis of threshold amplification cycles revealed no significant intergroup differences (Table). The mean *Ct* value for *TGF-β* was 27.15 ± 0.30 in the group with missed abortion, while in the control group it was 28.21 ± 0.33. As for the *MMP-9* gene, the mean *Ct* values were 27.81 ± 0.42 and 29.31 ± 0.37, respectively.

Therefore, *TGFb* and *MMP-9* do not have a 100% diagnostic value for prediction of missed abortion, but in fact there are more data: for example, we accurately calculated the limits of intervals, based on which the subtle difference was found. Thus, the analysis of parameters for the risk of "missed abortion" (Fig. 4) showed the most significant differences for the Ct_TGFb and Ct_MMP9 parameters.

The value ≤ 29, at which sensitivity reaches 80% with the 60% specificity, is diagnostically important for Ct_MMP9 (Fig. 4). As for Ct_TGFb, such expression value is 27.4, at which sensitivity reaches 75% with the 70% specificity. Prediction of missed abortion based on the Ct_TGFb and Ct_MMP9 expression can yield the result of up to 80%/70%.

DISCUSSION

In this study the expression of the *TGF-β* and *MMP-9* genes in peripheral blood of women with physiological pregnancy and missed abortion was assessed. Despite the fact that there were no significant differences between the studied groups, the ROC analysis results showed that there were threshold values of the studied indicators having some prognostic informativity. The data obtained suggest that changes in the *TGF-β* and *MMP-9* expression cannot be considered as the only mechanism underlying the development of missed abortion. It is likely that the molecular alterations identified reflect only some links of a complex pathogenetic process including impaired placentation, immune adaptation, and cell-cell interactions at the maternal-fetal interface [14–25].

It is well known that successful implantation of the embryo and further pregnancy development require the adequate throphoblast invasion of the endometrium and development of the full-fledged maternal-placental blood flow. Matrix metalloproteinases ensuring the controlled extracellular matrix remodeling play an important role in these processes [7–13]. Among members of this family of special importance is MMP-9 involved in degradation of the basal membrane components, throphoblastic cell migration, and placental bed formation [7–13].

According to a number of studies, the MMP-9 activity is strongly associated with the throphoblast invasion and normal development of the placenta [7–13]. Abnormal metalloproteinase regulation can result in incomplete placentation at different fetus's gestational ages and the development of pregnancy complications [7–13]. The data on the MMP-9 potential prognostic value obtained in this study are in line with modern views of the role of this enzyme in early gestation.

An equally important component of the successful pregnancy is the formation of immunological tolerance between the mother's body and the fetus [15–25]. A central place in the regulation of this process is occupied by TGF-β having pronounced immunomodulatory properties [15–25]. This cytokine is involved in controlling the activity of T cells, natural killers, and other immunocompetent cells, it ensures maintenance of the immune balance essential for pregnancy continuation [14–25].

According to the literature, the decrease in activity of the TGF-β signaling pathways can be associated with violation of the maternal-fetal immune tolerance and the increased risk of miscarriage [15–25]. Our results revealed no significant intergroup differences due to insufficient number of measurements of the studied indicators at various embryogenesis and placentation terms. However, the fact that there is a diagnostically significant threshold value suggests the TGF-β involvement in the mechanisms associated with the risk of pregnancy arrest.

It should be taken into account that the missed abortion pathogenesis is multifactorial [7–25]. Genetic abnormalities in the embryo, endocrine disorders, infectious processes, hemostatic disorders, and immune alterations can be realized simultaneously to form various clinical variants of the disease. In this regard, the use of distinct molecular markers does not always ensure high diagnostic accuracy. Limitations of the study include the relatively small sample size and heterogeneity of pregnancy age in the group of patients with missed abortion. Furthermore, biomaterial was collected after making the diagnosis, which did not allow us to assess the dynamic changes in expression of the studied genes at various stages of the disease process.

Thus, the findings confirm that further investigation of *TGF-β* and *MMP-9* as the components of complex prognostic models for assessment of the risk of early pregnancy loss is promising [7–25]. To clarify clinical significance of the patterns identified, studies with the inclusion of a larger number of observations and the expanded range of molecular genetic indicators are necessary.

The study made it possible to assess the features of the *TGF-β* and *MMP-9* gene expression in peripheral blood of women with physiological pregnancy and missed abortion. No significant intergroup differences in expression of the studied genes were revealed. At the same time, the ROC analysis results showed that there were threshold values of the *TGF-β* and *MMP-9* indicators having some prognostic informativity when assessing the risk of missed abortion.

The data obtained suggest possible involvement of the studied genes in the molecular mechanisms ensuring the normal pregnancy course. However, the small sample size makes it impossible to consider the patterns revealed as the definitely proven ones. Further research should be focused on assessing the *TGF-β* and *MMP-9* expression in the larger and clinically homogeneous groups of patients, as well as on developing the complex prognostic models combining molecular genetic, laboratory, and clinical indicators.

CONCLUSIONS

There were no significant differences in the *TGF-β* and *MMP-9* gene expression in peripheral blood of women with physiological pregnancy and missed abortion. The threshold value *Ct* ≤ 29 enduring the 80% sensitivity and 60% specificity turned out to be of diagnostic value for the *MMP-9* gene. As for the *TGF-β* gene, the value *Ct* ≤ 27.4 with the 75% sensitivity and 70% specificity was the most informative. The findings suggest the potential prognostic value of these molecular markers and the need for further research aimed to confirm their clinical significance and ensure validation in the independent sample.

References

1. Malinovskaya EM, Ershova ES, Golimbet VE, Porokhovnik LN, Lyapunova NA, Kutsev SI, et al. Copy Number of Human Ribosomal Genes With Aging: Unchanged Mean, but Narrowed Range and Decreased Variance in Elderly Group. Front Genet. 2018; 9: 306. DOI: 10.3389/fgene.2018.00306. PMID: 30131826; PMCID: PMC6090032.
2. Lyapunova NA, Vejko NN. Ribosomnye geny v genome cheloveka: identifikaciya chetyrekh frakcij, ih lokalizaciya v yadryshke i metafaznyh hromosomah. Genetika. 2010; 46 (9): 1205–9. Russian.
3. Myao Z, Chen M, U H, Din H, Shi Z. Sravnitel'nyj proteomnyj profil' chelovecheskoj placenty v normal'nom i fetal'nom roste. Restrikcionnye sub"ekty. Cell Physiol Biochem. 2014; 34: 1701–10.
4. Tubaon R, Haddad P, Kirino Dzh. Strategii ochistki obrazcov dlya prilozhenij mass-spektrometrii ESI v voskhodyashchej proteomike: Tendencii s 2012 po 2016 god. Proteomika. 2017; 17: 1700011.
5. Horami Sarvestani S, Shodzhaeyan S, Vanaki N, Gresi-Fard B, Amini M, Dzhilani K, i dr. Proteomnoe profilirovanie chelovecheskoj placenty vyyavlyaet izmeneniya v belkovoj signature, zavisyashchie ot stadii razvitiya. Klinicheskaya proteomika. 2021; 18: 18.
6. Braunridzh P, Bejnon R. Vazhnost' dajdzhesta: proteoliz i absolyutnaya kolichestvennaya ocenka v proteomike. Metody. 2011; 54: 351–60.
7. Matthielsen L, Kalkunte S, Sharma S. Multiple pregnancy failures: an immunological paradigm. Am J Reprod Immunol. 2012; 67 (4): 334–40.
8. Staun-Ram E, Goldman S, Gabarin D, Shalev E. Expression and importance of matrix metalloproteinase 2 and 9 (MMP-2 and –9) in human trophoblast invasion. Reprod Biol Endocrinol. 2004; 2: 59.
9. Moore CS, Crocker SJ. An alternate perspective on the roles of TIMPs and MMPs in pathology. Am J Pathol. 2012; 180: 12–16.
10. Kizaki K, Ushizawa K, Takahashi T, Yamada O, Todoroki J, Sato T, et al. Gelatinase (MMP-2 and –9) expression profiles during gestation in the bovine endometrium. Reprod Biol Endocrinol. 2008; 6: 66.
11. Seval Y, Akkoyunlu G, Demir R, Asar M. Distribution pattern of matrix metalloproteinase MMP-2 and MMP-9 and their inhibitors (TIMP-1 and TIMP-2) in the human decidua during early pregnancy. Acta Histochem. 2004; 5: 353–62.
12. Diaz P, Solar P, Juica N, Orihuela P, Cardenas H, Christodoulides M, et al. Differential expression of extracellular matrix components in the Fallopian tubes throughout the menstrual cycle. Reprod Biol Endocrinol. 2012; 10: 56.
13. Zaga-Clavellina V, Garcia-Lopez G, Flores-Pliego A, Merchant-Larios H, Vadillo-Ortega F. In vitro secretion and activity profiles of matrix metalloproteinases MMP-9 and MMP-2 in human term extra-placental membranes after exposure to Escherichia coli. Reprod Biol Endocrinol. 2011; 9: 13–15.
14. Yusefzade J, Soltani-Zangbar MS, Hemmatzade M, Shomali N, Mahmudpur A, Heris DzhA, et al. Fetomaterinskaya immunnaya tolerantnost': vazhnejshie mekhanizmy tolerantnosti dlya uspeshnoj beremennosti u cheloveka. Immunolog. issledovaniya. 2022; 51: 1108–25.
15. Munos-Suano A, Gamilton AB, Betc AG. Dajte mne ubezhishche: immunnaya sistema vo vremya beremennosti. Immunologicheskij obzor. 2011; 241: 20–38.
16. Parhizkar F, Motavalli-Hiavi R, Agebati-Maleki L, Parhizkar Purakbari, Kafil HS, i dr. Vliyanie novyh immunologicheskih terapevticheskih strategij na recidiviruyushchie vykidyshi i recidiviruyushchie neudachi implantacii. Immunologiya. Pis'ma. 2021; 236: 20–30.
17. Parhizkar F, Kiani A, Darzi S, Motavalli R, Dolama FN, Yusefzade Yu, i dr. Ocenka ekspressii CD39, CD73 i HIF-1α, a takzhe rodstvennyh im mikroRNK v RVMS zhenshchin s privychnym nevynashivaniem beremennosti. Dzh Reprod Immunol. 2023; 156: 103820.
18. Nin F, Lyu H, Lash GE. Rol' decidual'nyh makrofagov vo vremya normal'noj i patologicheskoj beremennosti. Am J Reprod Immunol. 2016; 75: 298–309.
19. Yutel M, Akdis M, Budak F, Ebisher-Kasaulta K, Vzhishch M, Blazer K, i dr. IL-10 i TGF-beta vzaimodejstvuyut v otvete regulyatornyh T-kletok na slizistye allergeny pri normal'nom immunitete i specificheskoj immunoterapii. Eur J Immunol. 2003; 33: 1205–14.
20. Herder K, Zirer A, Kenig V, Roden M, Mejzinger K, Torand B. Transformiruyushchij faktor rosta β1 i vozniknovenie diabeta 2 tipa: rezul'taty kogortnogo issledovaniya MONICA/KORA, 1984–2002 gg. Diabetes Care. 2009; 32: 1921–23.
21. Chzhu Dzh, Song G, Chzhou S, Han T-L, Y S, Chen H, i dr. Narushenie regulyacii metabolizma adenozina CD39/CD73 uvelichivaet citotoksichnost' decidual'nyh estestvennyh kletok-killerov: posledstviya dlya neob"yasnimyh recidiviruyushchih samoproizvol'nyh abortov. Front Immunol. 2022; 13: 813218.
22. Allan DSDzh, Rybalov B, Avong G, Zuniga-Pflyuker DzhK, Kopkov HD, Karlajl DzhR, dr. TGF-β vliyaet na razvitie i differencirovku subpopulyacij estestvennyh kletok-killerov cheloveka. Eur J Immunol. 2010; 40: 2289–95.
23. Shalmin F, Mino G, Brushar M, Shevrio A, Vegran F, Ishami A, i dr. Transkripcionnye faktory Stat3 i Gfi-1 kontroliruyut immunosupressivnuyu aktivnost' Th17-kletok posredstvom regulyacii ekspressii ektonukleotidazy. Immunitet. 2012; 36: 362–73.
24. Shuler P Dzh, Shilling B, Harasimchuk M, Hoffmann TK, Dzhonson Dzh, Lang S, Uajtsajd TL. Fenotipicheskie i funkcional'nye harakteristiki subpopulyacij T-kletok CD4+ CD39+ FOXP3+ i CD4+ CD39+ FOXP3neg u onkologicheskih bol'nyh. Eur J Immunol. 2012; 42: 1876–85.
25. Eltcshig HK, Sitkovski MV, Robson SK. Purinergicheskaya signalizaciya vo vremya vospaleniya. N Engl J Med. 2012; 367: 2322–33.

Литература

1. Malinovskaya EM, Ershova ES, Golimbet VE, Porokhovnik LN, Lyapunova NA, Kutsev SI, et al. Copy Number of Human Ribosomal Genes With Aging: Unchanged Mean, but Narrowed Range and Decreased Variance in Elderly Group. Front Genet. 2018; 9: 306. DOI: 10.3389/fgene.2018.00306. PMID: 30131826; PMCID: PMC6090032.
2. Ляпунова Н. А., Вейко Н. Н. Рибосомные гены в геноме человека: идентификация четырех фракций, их локализация в ядрышке и метафазных хромосомах. Генетика. 2010; 46 (9): 1205–9.
3. Мяо З., Чэнь М., У Х., Дин Х., Ши З. Сравнительный протеомный профиль человеческой плаценты в нормальном и фетальном росте. Рестрикционные субъекты. Cell Physiol Biochem. 2014; 34: 1701–10.
4. Тубаон Р., Хаддад П., Кирино Дж. Стратегии очистки образцов для приложений масс-спектрометрии ESI в восходящей протеомике: Тенденции с 2012 по 2016 год. Протеомика. 2017; 17: 1700011.
5. Хорами Сарвестани С., Шоджаеян С., Ванаки Н., Греси-Фард Б., Амини М., Джилани К., и др. Протеомное профилирование человеческой плаценты выявляет изменения в белковой сигнатуре, зависящие от стадии развития. Клиническая протеомика. 2021; 18: 18.
6. Браунридж П., Бейнон Р. Важность дайджеста: протеолиз и абсолютная количественная оценка в протеомике. Методы. 2011; 54: 351–60.
7. Matthielsen L, Kalkunte S, Sharma S. Multiple pregnancy failures: an immunological paradigm. Am J Reprod Immunol. 2012; 67 (4): 334–40.
8. Staun-Ram E, Goldman S, Gabarin D, Shalev E. Expression and importance of matrix metalloproteinase 2 and 9 (MMP-2 and –9) in human trophoblast invasion. Reprod Biol Endocrinol. 2004; 2: 59.
9. Moore CS, Crocker SJ. An alternate perspective on the roles of TIMPs and MMPs in pathology. Am J Pathol. 2012; 180: 12–16.
10. Kizaki K, Ushizawa K, Takahashi T, Yamada O, Todoroki J, Sato T, et al. Gelatinase (MMP-2 and –9) expression profiles during gestation in the bovine endometrium. Reprod Biol Endocrinol. 2008; 6: 66.

11. Seval Y, Akkoyunlu G, Demir R, Asar M. Distribution pattern of matrix metalloproteinase MMP-2 and MMP-9 and their inhibitors (TIMP-1 and TIMP-2) in the human decidua during early pregnancy. Acta Histochem. 2004; 5: 353–62.
12. Diaz P, Solar P, Juica N, Orihuela P, Cardenas H, Christodoulides M, et al. Differential expression of extracellular matrix components in the Fallopian tubes throughout the menstrual cycle. Reprod Biol Endocrinol. 2012; 10: 56.
13. Zaga-Clavellina V, Garcia-Lopez G, Flores-Pliego A, Merchant-Larios H, Vadillo-Ortega F. In vitro secretion and activity profiles of matrix metalloproteinases MMP-9 and MMP-2 in human term extra-placental membranes after exposure to Esherichia coli. Reprod Biol Endocrinol. 2011; 9: 13–15.
14. Юсефзаде Й., Солтани-Зангбар М. С., Хемматзаде М., Шомали Н., Махмудпур А., Херис Дж. А., et al. Фетоматеринская иммунная толерантность: важнейшие механизмы толерантности для успешной беременности у человека. Иммунолог. исследования. 2022; 51: 1108–25.
15. Муньос-Суано А., Гамильтон А. Б., Бетц А. Г. Дайте мне убежище: иммунная система во время беременности. Иммунологический обзор. 2011; 241: 20–38.
16. Пархизкар Ф., Мотавалли-Хиави Р., Агебати-Малеки Л., Пархизкар Пуракбари, Кафил Х. С., и др. Влияние новых иммунологических терапевтических стратегий на рецидивирующие выкидыши и рецидивирующие неудачи имплантации. Иммунология. Письма. 2021; 236: 20–30.
17. Пархизкар Ф., Киани А., Дарзи С., Мотавалли Р., Долама Ф. Н., Юсефзаде Ю., и др. Оценка экспрессии CD39, CD73 и HIF-1α, а также родственных им микроРНК в PBMC женщин с привычным невынашиванием беременности. Дж Репрод Иммунол. 2023; 156: 103820.
18. Нин Ф., Лю Х., Лаш Г. Е. Роль децидуальных макрофагов во время нормальной и патологической беременности. Am J Reprod Immunol. 2016; 75: 298–309.
19. Ютель М., Акдис М., Будак Ф., Эбишер-Касаулта К., Вжищ М., Блазер К., и др. IL-10 и TGF-бета взаимодействуют в ответе регуляторных Т-клеток на слизистые аллергены при нормальном иммунитете и специфической иммунотерапии. Eur J Immunol. 2003; 33: 1205–14.
20. Хердер К., Зирер А., Кениг В., Роден М., Мейзингер К., Торанд Б. Трансформирующий фактор роста β1 и возникновение диабета 2 типа: результаты когортного исследования MONICA/KORA, 1984–2002 гг. Diabetes Care. 2009; 32: 1921–23.
21. Чжу Дж., Сонг Г., Чжоу С., Хан Т.-Л., Ю С., Чен Х., и др. Нарушение регуляции метаболизма аденозина CD39/CD73 увеличивает цитотоксичность децидуальных естественных клеток-киллеров: последствия для необъяснимых рецидивирующих самопроизвольных абортов. Front Immunol. 2022; 13: 813218.
22. Аллан Д. С. Дж., Рыбалов Б., Авонг Г., Зунига-Пфлюкер Дж. К., Копков Х. Д., Карлайл Дж. Р., др. TGF-β влияет на развитие и дифференцировку субпопуляций естественных клеток-киллеров человека. Eur J Immunol. 2010; 40: 2289–95.
23. Шалмин Ф., Миньо Г., Брушар М., Шеврио А., Вегран Ф., Ишами А., и др. Транскрипционные факторы Stat3 и Gfi-1 контролируют иммуносупрессивную активность Th17-клеток посредством регуляции экспрессии эктонуклеотидазы. Иммунитет. 2012; 36: 362–73.
24. Шулер П. Дж., Шиллинг Б., Харасимчук М., Хоффманн Т. К., Джонсон Дж., Ланг С., Уайтсайд Т. Л. Фенотипические и функциональные характеристики субпопуляций Т-клеток CD4+ CD39+ FOXP3+ и CD4+ CD39+ FOXP3neg у онкологических больных. Eur J Immunol. 2012; 42: 1876–85.
25. Эльтцшиг Х. К., Ситковски М. В., Робсон С. К. Пуринергическая сигнализация во время воспаления. N Engl J Med. 2012; 367: 2322–33.

CAN AUTOCHTHONOUS ENDOMETRIAL MICROBIOTA BE DETECTED BY TRANSCERVICAL SAMPLING?

Zornikov DL[1] ✉, Simarzina VM[1], Islamidi DK[1,2], Belykh NS[2], Kornilov DO[1], Abakumova EI[2], Khayutin LV[2], Plotko EE[2], Voroshilina ES[1,2]

[1] Ural State Medical University, Yekaterinburg, Russia

[2] Medical Center "Garmonia", Yekaterinburg, Russia

Transcervical endometrial sampling is widely used to study the uterine microbiota, but the risk of cervical contamination raises doubts about whether detected microorganisms genuinely originate from the endometrium. This study aimed to determine whether autochthonous endometrial microbiota can be detected in transcervically collected samples by quantitative PCR after accounting for cervical contamination. Paired cervical and endometrial samples were collected from 185 reproductive-age women using an Endobrush catheter for endometrial sampling. Microbiota composition was assessed by real-time PCR targeting 27 microbial groups. An endometrial signal was considered true if its quantity exceeded that in the paired cervical sample, adjusted for transfer thresholds of 30% (expected, based on prior *in vitro* data) and 100% (conservative). Before correction, microbial signals were detected in endometrial samples from 144 (77.8%) women. After correction, positive signals remained in 44.3% (30% threshold) and 37.3% (100% threshold) of women. Most *Lactobacillus* spp. positives fell into an uninterpretable gray zone (47.6% and 55.1% at the 30% and 100% thresholds, respectively). In contrast, opportunistic microorganisms largely remained true positives after correction. Autochthonous endometrial microbiota was detected in approximately 37% of women, typically comprising 1–3 predominantly non-lactobacillus taxa. Detection of opportunistic microorganisms in the endometrium therefore likely reflects their genuine presence, whereas *Lactobacillus* detection is, in most cases, indistinguishable from cervical contamination.

Keywords: endometrial microbiota, autochthonous microbiota, cervical contamination, transcervical sampling, quantitative PCR.

Acknowledgments: the authors thank V. N. Khayutin, General Director of the Harmony Medical Center (Yekaterinburg), for the opportunity to conduct the study at the center.

Author contribution: Zornikov DL — conceptualization, visualization, formal analysis, writing — manuscript preparation; Simarzina VM — laboratory investigations, interpretation of laboratory results, writing — review and editing; Islamidi DK — participant enrollment, formation of clinical groups, collection of biomaterial, anamnestic and clinical data, analysis and interpretation of clinical data, writing — review and editing; Belykh NS — participant enrollment, collection of biomaterial, anamnestic and clinical data; Kornilov DO — laboratory investigations, interpretation of laboratory results, writing — review and editing; Abakumova EI — participant enrollment, collection of anamnestic and clinical data; Khayutin LV — collection of anamnestic and clinical data, writing — review and editing; Plotko EE — project administration, writing — review and editing; Voroshilina ES — supervision, study design, data analysis and interpretation, writing — review and editing.

Compliance with ethical standards: the study was approved by the Ethics Committee of Ural State Medical University (Protocol No. 1 dated January 24, 2020; Protocol No. 4 dated May 26, 2023). Informed consent was obtained from all study participants.

✉ **Correspondence should be addressed:** Danila L. Zornikov
Klyuchevskaya, 17, Yekaterinburg, 620109, Russia; zornikovdl@gmail.com

Received: 28.05.2026 **Accepted:** 14.06.2026 **Published online:** 05.07.2026

DOI: 10.24075/brsmu.2026.039

МОЖНО ЛИ ОБНАРУЖИТЬ АУТОХТОННУЮ МИКРОБИОТУ ЭНДОМЕТРИЯ ПРИ ТРАНСЦЕРВИКАЛЬНОМ ВЗЯТИИ ПРОБ?

Д. Л. Зорников[1] ✉, В. М. Симарзина[1], Д. К. Исламиди[1,2], Н. С. Белых[1], Д. О. Корнилов[1], Е. И. Абакумова[2], Л. В. Хаютин[2], Е. Э. Плотко[2], Е. С. Ворошилина[1,2]

[1] Уральский государственный медицинский университет, Екатеринбург, Россия

[2] Медицинский центр «Гармония», Екатеринбург, Россия

Трансцервикальный сбор образцов эндометрия традиционно используют для изучения микробиоты полости матки, однако неизбежный риск контаминации цервикальной микробиотой ставит под сомнение происхождение обнаруживаемых микроорганизмов. Цель исследования — определить, можно ли обнаружить аутохтонную микробиоту эндометрия в трансцервикально собранных образцах методом количественной ПЦР с учетом цервикальной контаминации. В одномоментное методологическое исследование включены 185 женщин репродуктивного возраста, у которых проводили забор парных цервикальных и эндометриальных образцов (для эндометриальных образцов использовали зонд Endobrush, Пайпель С2). Микробиоту оценивали методом ПЦР в реальном времени на 27 групп микроорганизмов. Сигнал в эндометрии считали истинным, если его количество превышало таковое в цервикальном образце с учетом порогов переноса 30% (ожидаемый) и 100% (консервативный). Микробные сигналы в эндометрии до поправки обнаружены у 144 (77,8%) пациенток; после поправки положительные сигналы сохранялись у 44,3% (порог 30%) и 37,3% (порог 100%) женщин. Большинство положительных проб на *Lactobacillus* spp. попадали в неинтерпретируемую «серую зону» (47,6 и 55,1% от всех пациенток при порогах 30 и 100% соответственно). Напротив, условно-патогенные микроорганизмы в большинстве случаев оставались истинно положительными после поправок. Аутохтонная микробиота эндометрия обнаруживалась у 37,3% женщин и была представлена 1–3 таксонами, преимущественно не лактобациллами. Таким образом, обнаружение условно-патогенных микроорганизмов в эндометрии можно интерпретировать как маркер их реального присутствия, тогда как лактобациллы в большинстве случаев неотличимы от цервикальной контаминации.

Ключевые слова: микробиота эндометрия, аутохтонная микробиота, цервикальная контаминация, трансцервикальный забор, количественная ПЦР

Благодарности: авторы благодарят генерального директора Медицинского центра «Гармония» (г. Екатеринбург) В. Н. Хаютина за возможность выполнения исследования на базе центра.

Вклад авторов: Д. Л. Зорников — концепция, анализ, интерпретация и визуализация результатов, подготовка рукописи; В. М. Симарзина — проведение лабораторных исследований, интерпретация результатов, редактирование; Д. К. Исламиди — набор участников исследования, формирование клинических групп, сбор биоматериала, анамнестических и клинических данных, анализ и интерпретация данных, редактирование; Н. С. Белых — набор участников исследования, сбор биоматериала, анамнестических и клинических данных; Д. О. Корнилов — проведение лабораторных исследований, интерпретация результатов, редактирование; Е. И. Абакумова — набор участников исследования, сбор анамнестических и клинических данных; Л. В. Хаютин — сбор анамнестических и клинических данных, редактирование; Е. Э. Плотко — организация исследования, редактирование; Е. С. Ворошилина — научное руководство, дизайн исследования, анализ и интерпретация данных, редактирование.

Соблюдение этических стандартов: исследование одобрено этическим комитетом ФГБОУ ВО УГМУ Минздрава России (протокол № 1 от 24 января 2020 г.; протокол № 4 от 26 мая 2023 г.); информированное согласие на участие в исследовании пациенток получено.

✉ **Для корреспонденции:** Данила Леонидович Зорников
ул. Ключевская, д. 17, г. Екатеринбург, 620109, Россия; zornikovdl@yandex.ru

Статья получена: 28.05.2026 **Статья принята к печати:** 14.06.2026 **Опубликована онлайн:** 05.07.2026

DOI: 10.24075/vrgmu.2026.039

In 2015, culture-based methods and quantitative PCR (qPCR) revealed a distinct microbial community within the uterine cavity using tissue specimens obtained during hysterectomies [1]. By utilizing post-hysterectomy tissue, that study effectively eliminated the risk of vaginal and cervical contamination. A subsequent study, which also evaluated hysterectomy specimens alongside rigorous negative controls, provided a definitive answer to a foundational question: does the uterine cavity harbor a detectable microbiota when assessed by molecular methods? [2]. The resulting data prompted a paradigm shift away from the traditional assumption of a sterile uterine cavity. Today, it is generally accepted that the endometrium harbors its own low-biomass microbial community, making the study of the endometrial microbiota a priority within human microbiome research [3, 4].

Clinical studies, however, cannot rely on hysterectomy specimens. Consequently, nearly all published literature evaluating the endometrial microbiota and its association with reproductive outcomes relies on transcervical sampling—most commonly performed using devices such as Pipelle or Endobrush (Tao Brush) [5–13]. To collect a sample, these instruments must traverse the heavily colonized cervical canal.

Studies employing transcervical sampling have reported associations between the endometrial microbiota and early pregnancy loss [14], chronic endometritis [15], endometrial polyps [5, 16, 17], endometrial hyperplasia [12], and endometriosis [18]. Yet, a critical question remains unanswered: do these associations reflect genuine alterations within the endometrial cavity, or do they largely capture cervical microbiota carried upward during sampling? This uncertainty stems from an unavoidable technical limitation: any instrument traversing the cervical canal risks contaminating the endometrial specimen with cervical microorganisms. This concern is particularly acute given that the baseline bacterial load in the uterine cavity is often substantially lower than that of the cervix [19]. Consequently, even minor contamination could mask a true endometrial signal or, conversely, be misinterpreted as evidence of an indigenous uterine microbial community.

Most published studies attempt to mitigate this risk by pre-treating the vagina and cervix with saline or antiseptics, and by using vaginal or cervical samples as contamination controls [5–10, 12, 13, 15–17, 20, 21]. While these measures reduce contamination risks, they do not eliminate them, nor do they permit reliable quantification of the carryover.

In a recent *in vitro* study using a physical model of the cervical canal, we quantified the extent of microbial carryover associated with Pipelle and Endobrush devices [22]. We demonstrated that both instruments transfer a substantial amount of microbiota from cervical mucus into model endometrial samples, yielding a median carryover of 81.6% for Pipelle and 29.8% for Endobrush. These findings cast serious doubt on the true origin of the microbiota detected in clinical, transcervically collected specimens. However, because *in vitro* models cannot fully replicate the physiological complexity of a clinical setting, the actual extent of contamination in patient samples remains unknown.

Therefore, the objective of the present study was to determine whether a true, autochthonous endometrial microbial signal — previously demonstrated in hysterectomy specimens [1, 2] — can be detected behind the inevitable “curtain” of cervical contamination introduced during routine clinical sampling. In this study, we classify an endometrial signal as autochthonous (true endometrial) only if the concentration of bacterial DNA in the endometrial sample exceeds the level that could be explained by cervical carryover alone.

Aim: To determine whether an autochthonous endometrial microbiota can be detected in transcervically collected samples by quantitative PCR after adjusting for cervical contamination.

METHODS

Patients

The study included 185 reproductive-age women (median 32.9, Q_1–Q_3 [29.9–37] years). All patients were examined at the Garmonia Medical Center (Yekaterinburg, Russia) between January 2020 and August 2023 for either a history of reproductive dysfunction or suspected endometrial pathology.

Inclusion criteria were: reproductive age (18–45 years), non-pregnant status, preserved menstrual cycle, clinical or ultrasound signs of endometrial pathology or infertility, feasibility of simultaneous collection of paired clinical samples (cervical and endometrial), and written informed consent.

Exclusion criteria at enrollment were: use of hormonal or intrauterine contraception at the time of examination or within the preceding six months, malignancy of any site, acute inflammatory diseases of the lower reproductive tract or pelvic organs at the time of examination, antibiotic therapy within four weeks prior to enrollment, and refusal to participate.

Post-enrollment exclusion criterion was: detection of sexually transmitted infections caused by obligate pathogens — *Neisseria gonorrhoeae*, *Chlamydia trachomatis*, *Mycoplasmoides genitalium* (formerly *Mycoplasma genitalium*), *Trichomonas vaginalis* — as determined by the Androflor assay (DNA-Technology, Russia).

Microbiota composition in cervical and endometrial samples was assessed by real-time PCR targeting 27 microbial groups.

Sample Collection

All procedures were performed on days 8–12 of the menstrual cycle. To minimize contamination risk, samples were collected in ascending order (vagina → cervical canal → uterine cavity).

Vaginal sample

A vaginal sample was collected from the posterior-lateral fornix before antiseptic treatment using a sterile standard urogenital swab. The biomaterial was transferred to a tube containing sterile saline (0.9% NaCl). Vaginal samples were not analyzed in the present study.

Vaginal preparation

Following vaginal sampling, the vagina was irrigated with 150–200 mL of 0.05% chlorhexidine bigluconate using a low-frequency ultrasonic cavitation device (AUZKh-100; Fotek, Russia) according to the manufacturer’s protocol [23]: exposure time, 1–2 min; power setting, 6–8 units. This procedure served as prophylaxis against infectious-inflammatory complications prior to intrauterine sampling [24].

Cervical sample

After vaginal preparation, a cervical mucus sample was collected using a new sterile standard urogenital swab inserted into the cervical canal to a depth of 1–1.5 cm. The biomaterial was transferred to a tube containing sterile saline.

Endometrial sample

Endometrial sampling was performed using the Endobrush Standard for Endometrial Cytology device (Laboratoire C.C.D., France). The device is equipped with a protective sheath that shields the internal brush from contact with the cervical mucosa: the brush is deployed only after the device enters the uterine cavity and is retracted into the sheath before withdrawal. The cervix was visualized with a speculum and recleaned with a swab soaked in 0.05% chlorhexidine. The device was then introduced into the uterine cavity transcervically, avoiding contact with the vaginal walls. Once inside the uterine cavity, the protective sheath was retracted to expose the brush, and 3–5 rotational movements were performed to collect the sample. The brush was then retracted into the sheath and the device was withdrawn. The outer surface of the sheath was thoroughly wiped with a sterile swab soaked in 96% ethanol to remove residual cervical mucus and prevent sample contamination. Finally, the brush was extended and the biomaterial was transferred to a tube containing sterile saline.

DNA Extraction

DNA was extracted using the Proba-NK-PLUS kit (DNA-Technology, Russia) according to the manufacturer's instructions. Endometrial samples underwent a preliminary deproteinization step: sample tubes were centrifuged at 13,000 rpm for 10 min on a MiniSpin centrifuge (Eppendorf, Germany), the supernatant was discarded, and the pellet was resuspended in 100 µL of lysis solution from the Proba-NK-PLUS kit and vortexed to homogeneity. A 50 µL aliquot of the resulting homogenate was transferred to a clean tube containing a mixture of 25 µL lysis solution, 5 µL proteinase K (20 mg/mL; VWR Life Science, USA), and 120 µL sterile saline. After mixing, samples were incubated at 60 °C for 30 min, then at 95 °C for 10 min. Following incubation, tubes were centrifuged at 13,000 rpm for 60 s. A 100 µL volume of the supernatant was used for DNA extraction according to the Proba-NK-PLUS kit protocol. The deproteinization step for endometrial samples was necessitated by their high viscosity due to abundant protein and mucus, which could reduce DNA extraction efficiency. Cervical samples did not require this step owing to their different consistency. Negative controls (sterile saline) were included in each DNA extraction and PCR run to rule out reagent contamination.

Microbiota Analysis

Each sample was analyzed by real-time PCR for 27 microbial groups: *Lactobacillus* spp., *Lactobacillus crispatus*, *Lactobacillus acidophilus*, *Lactobacillus iners*, *Lactobacillus jensenii*, *Lactobacillus gasseri*, *Lactobacillus johnsonii*, *Lactobacillus vaginalis*, *Staphylococcus* spp., *Streptococcus* spp., *Corynebacterium* spp., *Gardnerella vaginalis*, *Megasphaera* spp. / *Veillonella* spp. / *Dialister* spp. (MVD group), *Sneathia* spp. / *Leptotrichia* spp. / *Fusobacterium* spp. (SLF group), *Atopobium cluster*, *Bacteroides* spp. / *Porphyromonas* spp. / *Prevotella* spp. (BPP group), *Anaerococcus* spp., *Peptostreptococcus* spp. / *Parvimonas* spp. (PP group), *Eubacterium* spp., *Haemophilus* spp., *Pseudomonas aeruginosa* / *Ralstonia* spp. / *Burkholderia* spp. (PRB group), *Enterobacteriaceae* / *Enterococcus* spp., *Ureaplasma urealyticum*, *Ureaplasma parvum*, *Metamycoplasma hominis*, and *Candida* spp.

PCR was performed using the Androflor kit and a kit for species-level identification of vaginal lactobacilli (both manufactured by DNA-Technology, Russia) on DT-Prime and DT-96 thermal cyclers with the accompanying software and amplification protocols (DNA-Technology, Russia). According to the kit instructions, samples were considered positive for *Ureaplasma urealyticum*, *Ureaplasma parvum*, and *Metamycoplasma hominis* at any non-zero quantity. For all other microbial groups, the detection threshold was 10^3 genome equivalents per sample (GE/sample).

Statistical Analysis

Data processing and visualization were performed in R version 4.6.0 (R Foundation for Statistical Computing; Vienna, Austria). Central tendency is reported as median with first and third quartiles (Q_1 and Q_3). Differences in detection frequencies were assessed using two-tailed Fisher's exact test; differences in quantitative variables were assessed using the Mann–Whitney U test. All differences were considered statistically significant at $p < 0.05$.

RESULTS

Clinical Characteristics of the Patients

At the time of examination, patients presented with menstrual cycle abnormalities, ultrasound signs of endometrial pathology, or were undergoing evaluation for infertility. These conditions served as the indications for the workup, which included intrauterine sampling for microbiota analysis. The majority of patients had a history of obstetric-gynecological pathology, while 17 (9.2%) women had an uneventful history (Table 1).

Comparison of the Microbiota in Cervical and Endometrial Samples

Microbial signals were detected in endometrial samples from 144 (77.8%) patients. For most microbial groups, the detection frequency in cervical samples was 1.3-3 times higher than in endometrial samples (Fig. 1). The groups detected significantly more frequently in cervical samples included *Lactobacillus* spp. (88.6% vs. 68.1%), *L. crispatus* (39.5% vs. 15.7%), *L. iners* (41.6% vs. 28.1%), *L. jensenii* (31.9% vs. 10.8%), *L. gasseri* (16.8% vs. 8.1%), *L. johnsonii* (3.2% vs. 0%), *L. vaginalis* (23.8% vs. 2.7%), *Anaerococcus* spp. (10.8% vs. 2.2%), *Eubacterium* spp. (31.9% vs. 20%), *Enterobacteriaceae/Enterococcus* spp. (13% vs. 5.9%), *U. parvum* (6.5% vs. 0%).

Statistically significant differences in microbial quantity between cervical and endometrial samples were found for 13 microbial groups: *Lactobacillus* spp., *L. crispatus*, *L. iners*, *L. jensenii*, *L. gasseri*, *L. johnsonii*, *L. vaginalis*, *G. vaginalis*, *Anaerococcus* spp., PP group, *Eubacterium* spp., *Enterobacteriaceae/Enterococcus* spp., *U. parvum* (Fig. 1). *Lactobacillus* spp. exhibited the highest quantities at both anatomical sites, with $10^{4.9}$ ($10^{3.8}$–$10^{6.1}$) GE/sample in cervical samples versus $10^{3.5}$ (0–$10^{4.2}$) GE/sample in endometrial samples ($p < 0.001$). Median quantities for all other microbial groups were zero at both sites; the significant differences were driven entirely by higher concentrations in the upper quartiles of the cervical sample distributions.

Endometrial Signals After Correction for Potential Contamination

For each positive signal in an endometrial sample, we calculated the ratio of the microorganism's quantity in the endometrium to

Table 1. Clinical characteristics of the patients

Parameter	Value
Age, years	32.9 (29.9–37.0)
Body mass index, kg/m²	22.1 (20.2–24.4)
Obstetric and gynecological history	
Age at menarche, years	13 (12–14)
Menstrual cycle length, days	29 (28–30)
Duration of menses, days	5 (5–7)
Total pregnancies	1 (0–2)
Parity (deliveries)	78 (42.4%)
History of abortion	44 (23.8%)
History of pregnancy loss	40 (21.6%)
Gynecological pathology*	
Infertility	77 (41.6%)
Endometriosis	32 (17.3%)
Uterine fibroids	17 (9.2%)
Endometrial hyperplasia	13 (7.0%)
Pelvic inflammatory disease	10 (5.4%)
HPV carrier	7 (3.8%)
Hyperprolactinemia	7 (3.8%)
Recurrent pregnancy loss	6 (3.2%)
Heavy menstrual bleeding	6 (3.2%)
Chronic cervicitis	6 (3.2%)
Cervical dysplasia	4 (2.2%)
Endometrial polyp	4 (2.2%)
Polycystic ovary syndrome	2 (1.1%)
Teratoma	1 (0.5%)
Chronic endometritis	1 (0,5%)
No gynecological pathology	17 (9.2%)

Note: * — the sum of obstetric-gynecologic diagnoses exceeds 100% because several patients had more than one diagnosis.

its quantity in the paired cervical sample from the same patient. A signal was considered truly endometrial if this ratio exceeded the established cervical carryover threshold. Two carryover thresholds were applied: 30% (the expected threshold, based on our prior *in vitro* experiment [22]) and 100% (a conservative threshold, requiring the microbial load in the endometrium to exceed that in the cervix). When the target microorganism was absent from the cervical sample, any positive endometrial signal was considered to exceed the carryover threshold, as it could not be explained by cervical contamination.

After applying these thresholds, microorganisms were detected in 82 (44.3%) samples at the 30% threshold and 69 (37.3%) samples at the 100% threshold (Fig. 2). The majority of positive samples contained no more than three microbial groups. Specifically, at the 30% threshold, one, two, and three groups were detected in 31 (16.8%), 13 (7%), 15 (8.1%) cases, respectively; at the 100% threshold, these counts were 28 (15.1%), 12 (6.5%), 12 (6.5%) cases. In a few exceptional samples, up to 11 microbial groups were present at the 30% threshold and up to 10 groups at the 100% threshold.

We next evaluated the detection frequency of each microbial group in endometrial samples after correcting for potential cervical contamination. Based on the results, each sample was assigned to one of three categories: negative (no signal detected), “gray zone” (signal detected but not exceeding the established carryover threshold), or true endometrial signal (exceeding the threshold, thereby ruling out cervical contamination as the sole source) (Fig. 3):

$$x = \frac{\text{Quantity of target microorganism}_{(\text{endometrium})}}{\text{Quantity of target microorganism}_{(\text{cervix})} \times \text{Carryover threshold}}$$

where $x > 1$ — indicates a true signal and $x \leq 1$ indicates the gray zone. Carryover thresholds were set at 0.3 (30% carryover) and 1.0 (100% carryover).

At the 30% carryover threshold, *Lactobacillus* spp. fell into the gray zone in 88 (47.6% of all patients), as did *L. crispatus* in 18 (9.7%), *L. iners* in 38 (20.5%), *L. jensenii* in 12 (6.5%), and *L. vaginalis* in 1 (0.5%). Among opportunistic microorganisms (OMs), the highest proportions of gray-zone results were observed for *G. vaginalis* and *Eubacterium* spp.—16 (8.6%) and 7 (3.8%), respectively. For the remaining OMs, gray-zone results accounted for 0–1.6% of samples.

At the 100% carryover threshold, *Lactobacillus* spp. fell into the gray zone in 102 (55.1% of all patients), as did *L. crispatus* in 19 (10.3%), *L. iners* in 42 (22.7%), *L. jensenii* in 17 (9.2%), and *L. vaginalis* in 1 (0.5%). Among OMs, the highest proportions of gray-zone results were again observed for *G. vaginalis* and *Eubacterium* spp.—18 (9.7%) and 13 (7%), respectively. For the remaining OMs, gray-zone results accounted for 0–3.2% of samples.

After correction, the detection frequency of the most prevalent group, *Lactobacillus* spp., dropped from 126 (68.1%) pre-correction to 38 (20.5%) at the 30% threshold and 24 (13.0%) at the 100% threshold. Following correction, individual *Lactobacillus* species and OMs were detected in 0.5–16.2% of samples at the 30%

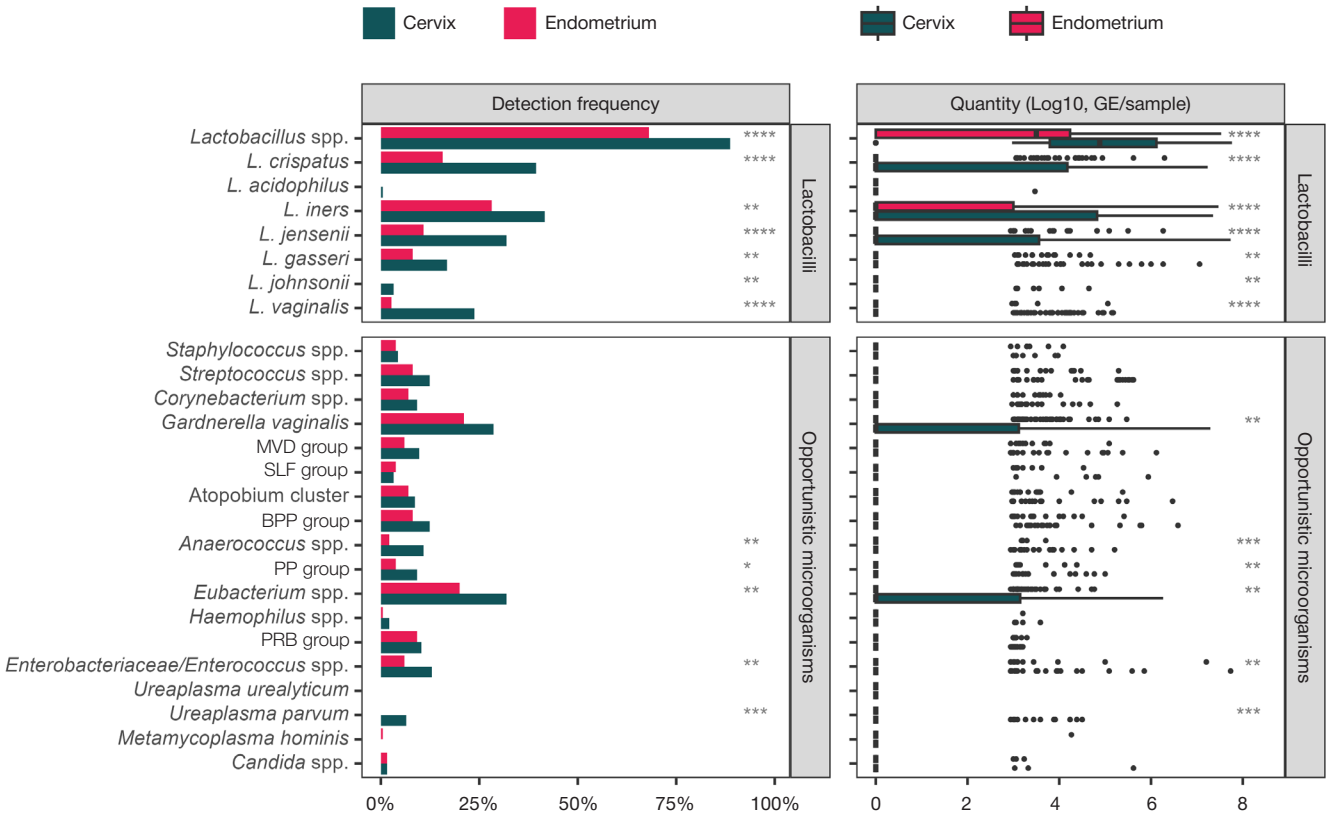

Fig. 1. Microbiota of cervical and endometrial samples. Detection frequency (*left panel*) and quantity (*right panel*) of target microbial groups. MVD — Megasphaera spp. / *Veillonella* spp. / *Dialister* spp.; SLF — *Sneathia* spp. / *Leptotrichia* spp. / *Fusobacterium* spp.; BPP — *Bacteroides* spp. / *Porphyromonas* spp. / *Prevotella* spp.; PP — *Peptostreptococcus* spp. / *Parvimonas* spp.; PRB — *Pseudomonas aeruginosa* / *Ralstonia* spp. / *Burkholderia* spp. Significance levels: * — $p < 0.05$, ** — $p < 0.01$, *** — $p < 0.001$, **** — $p < 0.0001$

threshold and 0.5–13% at the 100% threshold; signals for *L. acidophilus*, *L. johnsonii*, *U. urealyticum*, and *U. parvum* were completely absent from endometrial samples after correction, regardless of the threshold applied (Table 2).

DISCUSSION

Endometrial samples from the patient cohort yielded 22 of the 27 target microbial groups (Fig. 1). *Lactobacillus* spp. were detected in 68.1% of samples at a median quantity of $10^{3.5}$ GE/sample, whereas all other groups were identified in fewer than one-third of patients. This is consistent with the established understanding of the endometrial microbiota as a low-diversity, low-biomass community [1, 2, 21]. Notably, detection frequencies for all 22 groups were higher in cervical samples than in endometrial samples. *Lactobacillus* spp., for instance, were detected in 88.6% of cervical samples at a median quantity of $10^{4.9}$ GE/sample ($p < 0.0001$ for both frequency

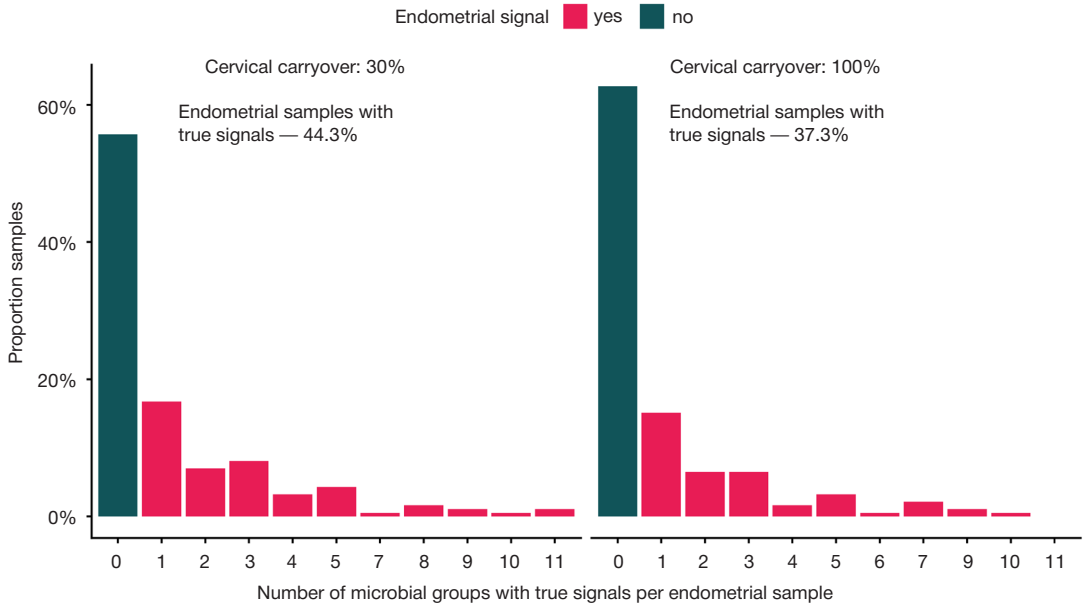

Fig. 2. Samples with endometrial microbiota after applying a 30% (*left panel*) and 100% (*right panel*) cervical DNA carryover threshold. A sample was considered to harbor endometrial microbiota if at least one target microbial group exceeded the established carryover threshold

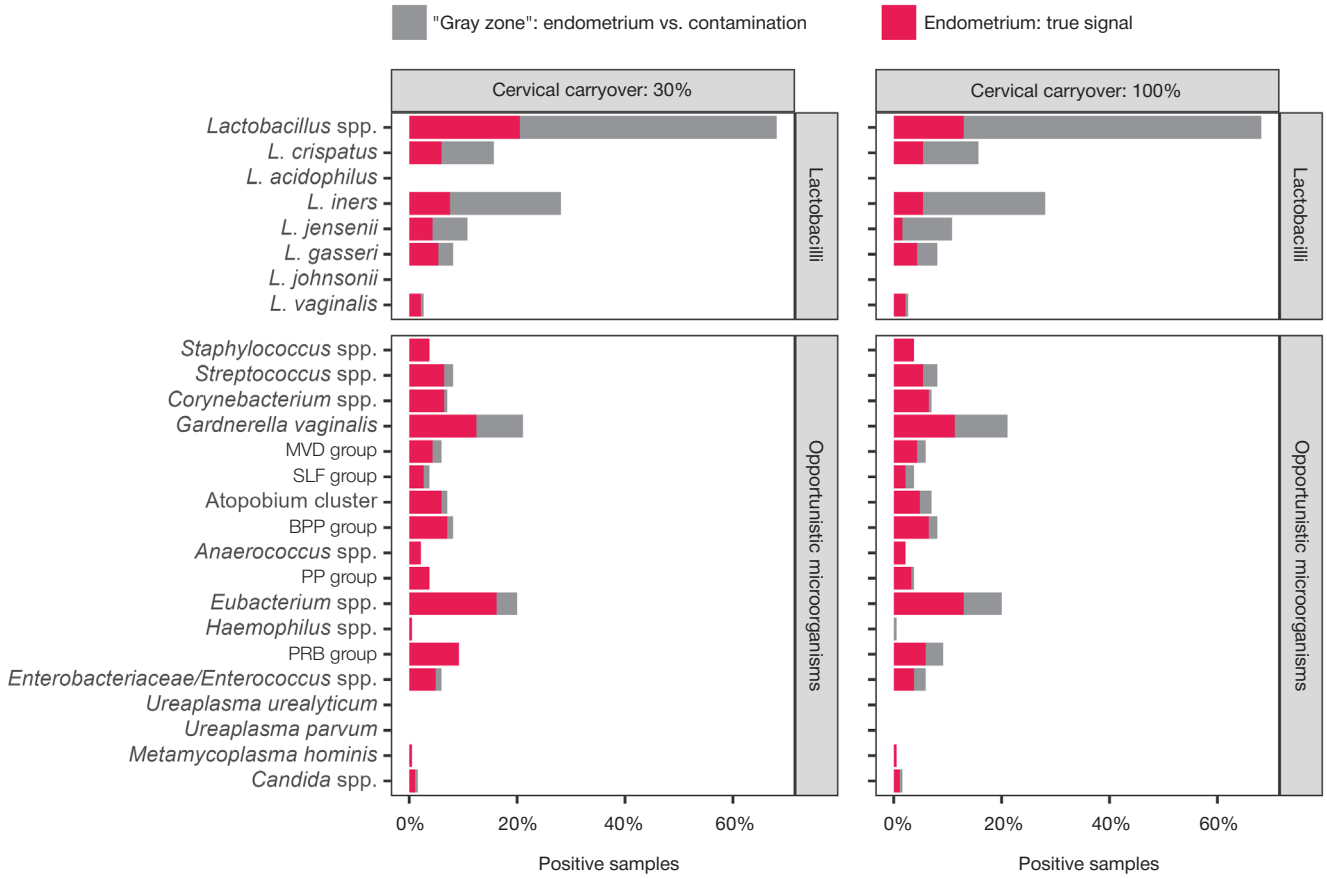

Fig. 3. Detection frequency of target microbial groups in endometrial samples after correction for 30% (*left panel*) and 100% (*right panel*) cervical DNA carryover. MVD — *Megasphaera* spp. / *Veillonella* spp. / *Dialister* spp.; SLF — *Sneathia* spp. / *Leptotrichia* spp. / *Fusobacterium* spp.; BPP — *Bacteroides* spp. / *Porphyromonas* spp. / *Prevotella* spp.; PP — *Peptostreptococcus* spp. / *Parvimonas* spp.; PRB — *Pseudomonas aeruginosa* / *Ralstonia* spp. / *Burkholderia* spp.

and quantity). This observation, combined with our earlier *in vitro* finding that the Endobrush device transfers approximately 30% of bacterial DNA from cervical mucus into the endometrial sample [22], strongly suggests that a substantial proportion of positive endometrial signals are attributable to cervical contamination.

To distinguish true endometrial signals from cervical carryover, we compared the quantity of DNA for each microorganism in the endometrial sample to that in the paired cervical sample from the same patient. We applied two carryover thresholds: 30% (the expected threshold based on our *in vitro* experiment [22]) and 100% (a conservative threshold requiring the quantity in the endometrium to exceed that in the cervix, thereby ruling out contamination entirely). At both thresholds, more than half of the endometrial samples lacked positive signals above the cutoff (Fig. 2). The presence of microorganisms in these samples could be fully explained by cervical carryover, meaning they could not be considered truly positive. Among the validated positive samples (44.3% at the 30% threshold and 37.3% at the 100% threshold), the majority contained no more than three microbial groups. Thus, after contamination correction, nearly half of the 144 (77.8%) initially positive endometrial samples were reclassified as non-interpretable, and the remaining positive samples harbored only a few taxa.

We next evaluated the results for each target microbial group after applying the contamination correction, assigning each sample to one of three categories: negative (no signal detected), gray zone (signal detected but not exceeding the established carryover threshold), or true endometrial signal (exceeding the threshold, thereby ruling out cervical contamination as the sole source). For *Lactobacillus* spp. and individual lactobacillus species, the majority of initially positive samples — ranging from two-thirds to three-quarters — fell into the gray zone (Fig. 3). Before correction, *Lactobacillus* spp. were detected in 126 (68.1%) of patients; after applying the 30% threshold, this dropped to 38 (20.5%), and after the 100% threshold, to 24 (13.0%). Similar patterns were observed for the three predominant lactobacillus species: *L. crispatus*, *L. iners,* and *L. jensenii*. For OMs, the proportion of samples falling into the gray zone was lower than for lactobacilli: 8.6% and 9.7% for *G. vaginalis*, and 3.8% and 7.0% for *Eubacterium* spp. at the 30% and 100% thresholds, respectively. For the remaining OMs, gray-zone results accounted for 0–1.6% and 0–3.2% of samples. Thus, among OMs-positive samples, the majority remained true positives after correction, although their overall detection frequency did not exceed 16.2% at the 30% threshold and 13% at the 100% threshold.

Our findings align with the cautious view advanced earlier [2] that the predominance of lactobacilli reported in transcervically collected endometrial samples [5, 18, 25–27] may reflect cervical or vaginal contamination. This interpretation is further supported by historical culture-based studies demonstrating higher rates of bacterial isolation from transcervically obtained endometrial samples compared with transabdominal sampling [28]. In the present study, we directly quantified the contribution of cervical contamination during transcervical sampling: using paired cervical samples and a threshold-based carryover model demonstrated that cervical contamination can account for most positive signals in endometrial samples. The observation that *Lactobacillus* spp. exhibited the highest proportion of gray-zone results supports the hypothesis that *Lactobacillus*-

Table 2. Detection frequency of microorganisms in endometrial samples after correction for potential contamination. Microorganisms are ranked by detection frequency at the 30% threshold

Microbial group	Frequency at the 30% threshold	Frequency at the 100% threshold
Lactobacillus spp.	38 (20,5%)	24 (13%)
Eubacterium spp.	30 (16,2%)	24 (13%)
Gardnerella vaginalis	23 (12,4%)	21 (11,4%)
PRB group	17 (9,2%)	11 (5,9%)
L. iners	14 (7,6%)	10 (5,4%)
BPP group	13 (7%)	12 (6,5%)
Streptococcus spp.	12 (6,5%)	12 (6,5%)
Corynebacterium spp.	12 (6,5%)	10 (5,4%)
L. crispatus	11 (5,9%)	10 (5,4%)
L. gasseri	11 (5,9%)	9 (4,9%)
Atopobium cluster	10 (5,4%)	8 (4,3%)
Enterobacteriaceae/Enterococcus spp.	9 (4,9%)	7 (3,8%)
L. jensenii	8 (4,3%)	3 (1,6%)
MVD group	8 (4,3%)	8 (4,3%)
PP group	7 (3,8%)	6 (3,2%)
Staphylococcus spp.	7 (3,8%)	7 (3,8%)
SLF group	5 (2,7%)	4 (2,2%)
L. vaginalis	4 (2,2%)	4 (2,2%)
Anaerococcus spp.	4 (2,2%)	4 (2,2%)
Candida spp.	2 (1,1%)	2 (1,1%)
Haemophilus spp.	1 (0,5%)	0 (0%)
Metamycoplasma hominis	1 (0,5%)	1 (0,5%)
L. acidophilus	0 (0%)	0 (0%)
L. johnsonii	0 (0%)	0 (0%)
Ureaplasma parvum	0 (0%)	0 (0%)
Ureaplasma urealyticum	0 (0%)	0 (0%)

Note: PRB — *Pseudomonas aeruginosa* / *Ralstonia* spp./ *Burkholderia* spp. BPP — *Bacteroides* spp. / *Porphyromonas* spp. / *Prevotella* spp.; MVD — *Megasphaera* spp. / *Veillonella* spp. / *Dialister* spp.; PP — *Peptostreptococcus* spp. / *Parvimonas* spp.; SLF — *Sneathia* spp. / *Leptotrichia* spp. / *Fusobacterium* spp.

dominance in endometrial samples may be an artifact of the sampling procedure [2]. Moreover, after applying the contamination correction, *G. vaginalis* and *Eubacterium* spp. emerged as the most frequently detected microorganisms in endometrial samples alongside *Lactobacillus* spp., surpassing all individual lactobacillus species (Table 2).

Detection of a target microorganism in the endometrium at quantities exceeding the established cervical carryover threshold does not constitute absolute proof of its endometrial origin. However, it likely reflects a genuine presence in the uterine cavity, as such a signal cannot be explained by cervical contamination within our model framework. In this study, 37.3% of patients retained positive microbial signals in endometrial samples even at the conservative 100% threshold. This finding cannot be fully explained by cervical contamination, pointing to the presence of an autochthonous endometrial microbiota. In most cases, however, this microbiota was represented by only one to three non-lactobacillus taxa, and the detection frequency of even the most prevalent group did not exceed 13%.

The fact that lactobacilli predominantly fell into the gray zone does not necessarily imply their absence from the endometrium. It is plausible that lactobacilli were present in some samples but at quantities too low to be reliably distinguished from cervical carryover. The anatomical proximity of the cervix and uterine cavity may lead to genuine overlap in the microbial communities of these two sites. Notably, even when post-hysterectomy specimens and 16S rRNA gene sequencing were used, no significant differences were found between the cervical and endometrial microbiota [2].

Crucially, the majority of OMs detected in endometrial samples remained true positives even after applying the conservative 100% contamination threshold (Fig. 3). While the biological mechanisms underlying this pattern require further investigation, the finding has immediate clinical relevance. Unlike lactobacilli, which largely fell into the gray zone, the detection of OMs in an endometrial sample likely reflects genuine presence in the uterine cavity rather than a sampling artifact. This is highly meaningful in a clinical context, as OMs are traditionally associated with endometrial pathology and represent the primary targets of microbiological investigation in intrauterine samples.

A key strength of this study is its paired-sample design, in which cervical and endometrial specimens were collected from the same patient during a single procedure. This approach allowed each patient's individual cervical microbial load to serve as the reference for contamination assessment rather than relying on averaged cohort values, thereby eliminating the confounding effect of inter-individual clinical variability. The use of two distinct carryover thresholds — 30% (expected, based on our *in vitro* model [22]) and 100% (conservative, completely ruling out contamination) — enabled an assessment of the robustness of our findings across threshold choice. The use

of quantitative PCR targeting 27 microbial groups provided high analytical sensitivity and allowed assessment of both the frequency and absolute quantity of each target group, offering a distinct advantage over studies relying solely on 16S rRNA gene sequencing.

A practical implication of our findings is the need to reconsider current approaches to investigating the endometrial microbiota. The use of sheathed sampling devices such as the Endobrush, even when combined with antiseptic preparation, does not reliably distinguish endometrial from cervical microorganisms. In the short term, it may be more appropriate to study the combined cervico-endometrial microbiota by pooling the cervical and endometrial samples into a single specimen obtained during transcervical sampling. This approach, at a minimum, does not create the illusion of selective endometrial sampling. In the longer term, methods that effectively minimize cervical contamination must be developed.

Limitations of the study

This study has several limitations. First, our contamination model assumed that a single cervical sample adequately reflects the microbial load along the entire length of the cervical canal; however, regional variability in microbial concentrations may exist, potentially leading to under- or overestimation of the carryover level. Second, the DNA extraction protocol differed between cervical and endometrial samples: endometrial samples underwent a preliminary deproteinization step, which could have influenced DNA extraction efficiency and the ratio of microbial quantities between the two biotopes. Third, the PCR panels were limited to 27 target microbial groups; unlike 16S rRNA gene sequencing, this approach does not capture the full taxonomic composition of the microbiota and cannot detect microorganisms not included in the panels. Fourth, quantitative PCR cannot distinguish viable microorganisms from extracellular DNA; therefore, some of the detected signals may have originated from non-viable bacteria or free DNA that reached the uterine cavity from the lower reproductive tract, a consideration that should be taken into account when interpreting results clinically. Fifth, vaginal samples were collected but not analyzed in the present study. Although the risk of endometrial contamination by vaginal microbiota is considered low when the device is introduced under visual guidance, the absence of these data limits our ability to assess the full continuum of microbial communities along the lower reproductive tract. Finally, this was a single-center study, and its findings require independent replication.

CONCLUSIONS

This study demonstrates that transcervical endometrial sampling using the Endobrush device does not reliably distinguish endometrial from cervical microbiota in the majority of patients. True endometrial signals were detected by quantitative PCR in approximately 40% of women and were typically limited to one to three taxa. The majority of endometrial samples positive for lactobacilli (approximately two-thirds of those initially positive for *Lactobacillus* spp.) fell into the gray zone and could reflect either genuine endometrial presence or cervical contamination. In contrast, detection of OMs in endometrial samples can be interpreted as a marker of their genuine presence, as their quantities exceeded the established cervical carryover thresholds in most cases. These findings underscore the need for either the development of novel endometrial sampling methods that effectively eliminate cervical contamination or the interpretation of results from such specimens as representing a combined cervico-endometrial microbiota.

References

1. Mitchell CM, Haick A, Nkwopara E, Garcia R, Rendi M, Agnew K, et al. Colonization of the upper genital tract by vaginal bacterial species in nonpregnant women. American journal of obstetrics and gynecology. 2015; 212 (5): 611–e1. Available from: https://doi.org/10.1016/j.ajog.2014.11.043.
2. Winters AD, Romero R, Gervasi M, Gomez-Lopez N, Tran MR, Garcia-Flores V, et al. Does the endometrial cavity have a molecular microbial signature? Scientific Reports. 2019; 9: 9905. Available from: https://doi.org/10.1038/s41598-019-46173-0.
3. Polifke A, Schwedler A von, Gulba R, Bensmann R, Dilthey A, Nassar NN, et al. Differential characteristics of vaginal versus endometrial microbiota in IVF patients. Scientific Reports. 2024; 14 (1): 1–16. Available from: https://doi.org/10.1038/s41598-024-82466-9.
4. Franasiak JM, Scott RT. Endometrial microbiome. Current Opinion in Obstetrics and Gynecology. 2017; 29 (3): 146–52. Available from: https://doi.org/10.1097/GCO.0000000000000357.
5. Fang RL, Chen LX, Shu WS, Yao SZ, Wang SW, Chen YQ. Barcoded sequencing reveals diverse intrauterine microbiomes in patients suffering with endometrial polyps. American journal of translational research. 2016; 8 (3): 1581.
6. Verstraelen H, Vilchez-Vargas R, Desimpel F, Jauregui R, Vankeirsbilck N, Weyers S, et al. Characterisation of the human uterine microbiome in non-pregnant women through deep sequencing of the V1-2 region of the 16S rRNA gene. PeerJ. 2016; 4: e1602. Available from: https://doi.org/10.7717/peerj.1602.
7. Kurcer MA, Egikyan NM, Saveleva NA, Sinicyna OV, Vatagina MA, Kutakova YuYu. Sravnitel'naya harakteristika vaginal'nogo i endometrial'nogo mikrobioma u pacientok so vtorichnym besplodiem, associirovannym s nishej rubca na matke posle kesareva secheniya. Ginekologiya. 2021; 23 (6): 499–503. Dostupno po ssylke: https://doi.org/10.26442/20795696.2021.6.201300. Russian.
8. Karahalis LYu, Kononenko TS. Taksonomicheskij profil' mikrobioma endometriya pri hronicheskom endometrite. Akusherstvo i ginekologiya: Novosti Mneniya Obucheniya. 2022; 10 (4): 23–30. Dostupno po ssylke: https://doi.org/10.33029/2303-9698-2022-10-4-23-30. Russian.
9. Bui BN, Hoogenhuijze N van, Viveen M, Mol F, Teklenburg G, Bruin JP de, et al. The endometrial microbiota of women with or without a live birth within 12 months after a first failed IVF/ICSI cycle. Scientific reports. 2023; 13 (1): 3444. Available from: https://doi.org/10.1038/s41598-023-30591-2.
10. Jain M, Mladova E, Dobychina A, Kirillova K, Shichanina A, Anokhin D, et al. Comparison of microbial profiles and viral status along the vagina-cervix-endometrium continuum of infertile patients. Systems Biology in Reproductive Medicine. 2023; 69 (4): 310–9. Available from: https://doi.org/10.1080/19396368.2023.2195040.
11. Masucci L, D'Ippolito S, De Maio F, Quaranta G, Mazzarella R, Bianco DM, et al. Celiac disease predisposition and genital tract microbiota in women affected by recurrent pregnancy loss. Nutrients. 2023; 15 (1): 221.
12. Ying X, Xu G, Wang H, Wang Y. An altered uterine microbiota with endometrial hyperplasia. BMC microbiology. 2024; 24 (1): 258. Available from: https://doi.org/10.1186/s12866-024-03379-1.
13. Krysanova AA, Storozheva KV, Budilovskaya OV, Husnutdinova TA, Shalepo KV, Tapilskaya NI, i dr. Arhitektonika mikrobioty endometriya u zhenshchin s besplodiem razlichnogo geneza. Klinicheskaya laboratornaya diagnostika. 2024; 69 (9): 478–86. Dostupno po ssylke: https://doi.org/10.51620/0869-2084-2024-

69-9-478-486. Russian.
14. Moreno I, Garcia-Grau I, Bau D, Perez-Villaroya D, Gonzalez-Monfort M, Vilella F, et al. The first glimpse of the endometrial microbiota in early pregnancy. American journal of obstetrics and gynecology. 2020; 222 (4): 296–305. Available from: https://doi.org/10.1016/j.ajog.2020.01.031.
15. Zhang H, Zou H, Zhang C, Li X, Wang Z, Liu C, et al. Chronic endometritis and the endometrial microbiota: implications for reproductive success in patients with recurrent implantation failure. Annals of Clinical Microbiology and Antimicrobials. 2024; 23: 49. Available from: https://doi.org/10.1186/s12941-024-00710-6.
16. Zhao Y, Liao Y, Xu G, Wang Y. Endometrial microbiota alteration in female patients with endometrial polyps based on 16S rRNA gene sequencing analysis. Frontiers in Cellular and Infection Microbiology. 2024; 14: 1351329. Available from: https://doi.org/10.3389/fcimb.2024.1351329.
17. Vanakova AI, Dolgushina NV, Denisov PA, Goncharuk OD, Muraveva VV, Priputnevich TV. Osobennosti mikrobioty polosti matki u pacientok s polipami endometriya. Vestnik Rossijskogo gosudarstvennogo medicinskogo universiteta. 2025; 1 (6): 6. Dostupno po ssylke: https://doi.org/10.24075/vrgmu.2025.007. Russian.
18. Khan KN, Fujishita A, Masumoto H, Muto H, Kitajima M, Masuzaki H, et al. Molecular detection of intrauterine microbial colonization in women with endometriosis. European Journal of Obstetrics & Gynecology and Reproductive Biology. 2016; 199: 69–75. Available from: https://doi.org/10.1016/j.ejogrb.2016.01.040.
19. Chen C, Song X, Wei W, Zhong H, Dai J, Lan Z, et al. The microbiota continuum along the female reproductive tract and its relation to uterine-related diseases. Nature Communications. 2017; 8: 875. Available from: https://doi.org/10.1038/s41467-017-00901-0.
20. Riganelli L, Iebba V, Piccioni M, Illuminati I, Bonfiglio G, Neroni B, et al. Structural Variations of Vaginal and Endometrial Microbiota: Hints on Female Infertility. Frontiers in Cellular and Infection Microbiology. 2020; 10: 350. Available from: https://doi.org/10.3389/fcimb.2020.00350.
21. Voroshilina ES, Zornikov DL, Koposova OV, Islamidi DK, Ignatova KY, Abakumova EI, et al. The use of real-time PCR for evaluation of endometrial microbiota. Bulletin of RSMU. 2020; 1: 14–20. DOI: 10.24075/brsmu.2020.012.
22. Zornikov DL, Bekhter AA, Kornilov DO, Simarzina VM, Nechaeva DM, Karyakina AE, et al. Pipelle and endobrush catheters do not prevent contamination of endometrial samples by cervical microbiota. Bulletin of RSMU. 2025; (6): 89–95. DOI: 10.24075/brsmu.2025.073
23. Oboskalova T, Gluhov E, Lavrenteva I, Bogdanova A, Kozyreva E, Neff E, i dr. Profilaktika i lechenie vospalitel'nyh zabolevanij v akusherstve i ginekologii s ispol'zovaniem metoda ul'trazvukovoj kavitacii lekarstvennyh rastvorov. Prakticheskoe rukovodstvo dlya vrachej. Ekaterinburg: Vip-Ural, 2014. Russian.
24. Plotko EE. Prognozirovanie, profilaktika, diagnostika i lechenie oslozhnenij iskusstvennogo preryvaniya beremennosti. Moskva, 2013. Russian.
25. Moreno I, Codoñer FM, Vilella F, Valbuena D, Martinez-Blanch JF, Jimenez-Almazán J, et al. Evidence that the endometrial microbiota has an effect on implantation success or failure. American journal of obstetrics and gynecology. 2016; 215 (6): 684–703. Available from: https://doi.org/10.1016/j.ajog.2016.09.075.
26. Wee BA, Thomas M, Sweeney EL, Frentiu FD, Samios M, Ravel J, et al. A retrospective pilot study to determine whether the reproductive tract microbiota differs between women with a history of infertility and fertile women. Australian and New Zealand Journal of Obstetrics and Gynaecology. 2018; 58 (3): 341–8. Available from: https://doi.org/10.1111/ajo.12754.
27. Pelzer ES, Willner D, Buttini M, Huygens F. A role for the endometrial microbiome in dysfunctional menstrual bleeding. Antonie Van Leeuwenhoek. 2018; 111 (6): 933–43. Available from: https://doi.org/10.1007/s10482-017-0992-6.
28. Duff P, Gibbs RS, Blanco JD, Clair PJS. Endometrial culture techniques in puerperal patients. Obstetrics & Gynecology. 1983; 61 (2): 217–22.

Литература

1. Mitchell CM, Haick A, Nkwopara E, Garcia R, Rendi M, Agnew K, et al. Colonization of the upper genital tract by vaginal bacterial species in nonpregnant women. American journal of obstetrics and gynecology. 2015; 212 (5): 611–e1. Available from: https://doi.org/10.1016/j.ajog.2014.11.043.
2. Winters AD, Romero R, Gervasi M, Gomez-Lopez N, Tran MR, Garcia-Flores V, et al. Does the endometrial cavity have a molecular microbial signature? Scientific Reports. 2019; 9: 9905. Available from: https://doi.org/10.1038/s41598-019-46173-0.
3. Polifke A, Schwedler A von, Gulba R, Bensmann R, Dilthey A, Nassar NN, et al. Differential characteristics of vaginal versus endometrial microbiota in IVF patients. Scientific Reports. 2024; 14 (1): 1–16. Available from: https://doi.org/10.1038/s41598-024-82466-9.
4. Franasiak JM, Scott RT. Endometrial microbiome. Current Opinion in Obstetrics and Gynecology. 2017; 29 (3): 146–52. Available from: https://doi.org/10.1097/GCO.0000000000000357.
5. Fang RL, Chen LX, Shu WS, Yao SZ, Wang SW, Chen YQ. Barcoded sequencing reveals diverse intrauterine microbiomes in patients suffering with endometrial polyps. American journal of translational research. 2016; 8 (3): 1581.
6. Verstraelen H, Vilchez-Vargas R, Desimpel F, Jauregui R, Vankeirsbilck N, Weyers S, et al. Characterisation of the human uterine microbiome in non-pregnant women through deep sequencing of the V1-2 region of the 16S rRNA gene. PeerJ. 2016; 4: e1602. Available from: https://doi.org/10.7717/peerj.1602.
7. Курцер М. А., Егикян Н. М., Савельева Н. А., Синицына О. В., Ватагина М. А., Кутакова Ю. Ю. Сравнительная характеристика вагинального и эндометриального микробиома у пациенток со вторичным бесплодием, ассоциированным с нишей рубца на матке после кесарева сечения. Гинекология. 2021; 23 (6): 499–503. Доступно по ссылке: https://doi.org/10.26442/20795696.2021.6.201300.
8. Карахалис Л. Ю., Кононенко Т. С. Таксономический профиль микробиома эндометрия при хроническом эндометрите. Акушерство и гинекология: Новости Мнения Обучения. 2022; 10 (4): 23–30. Доступно по ссылке: https://doi.org/10.33029/2303-9698-2022-10-4-23-30.
9. Bui BN, Hoogenhuijze N van, Viveen M, Mol F, Teklenburg G, Bruin JP de, et al. The endometrial microbiota of women with or without a live birth within 12 months after a first failed IVF/ICSI cycle. Scientific reports. 2023; 13 (1): 3444. Available from: https://doi.org/10.1038/s41598-023-30591-2.
10. Jain M, Mladova E, Dobychina A, Kirillova K, Shichanina A, Anokhin D, et al. Comparison of microbial profiles and viral status along the vagina-cervix-endometrium continuum of infertile patients. Systems Biology in Reproductive Medicine. 2023; 69 (4): 310–9. Available from: https://doi.org/10.1080/19396368.2023.2195040.
11. Masucci L, D'Ippolito S, De Maio F, Quaranta G, Mazzarella R, Bianco DM, et al. Celiac disease predisposition and genital tract microbiota in women affected by recurrent pregnancy loss. Nutrients. 2023; 15 (1): 221.
12. Ying X, Xu G, Wang H, Wang Y. An altered uterine microbiota with endometrial hyperplasia. BMC microbiology. 2024; 24 (1): 258. Available from: https://doi.org/10.1186/s12866-024-03379-1.
13. Крысанова А. А., Сторожева К. В., Будиловская О. В., Хуснутдинова Т. А., Шалепо К. В., Тапильская Н. И., и др. Архитектоника микробиоты эндометрия у женщин с бесплодием различного генеза. Клиническая лабораторная диагностика. 2024; 69 (9): 478–86. Доступно по ссылке: https://doi.org/10.51620/0869-2084-2024-69-9-478-486.
14. Moreno I, Garcia-Grau I, Bau D, Perez-Villaroya D, Gonzalez-Monfort M, Vilella F, et al. The first glimpse of the endometrial microbiota in early pregnancy. American journal of obstetrics and gynecology. 2020; 222 (4): 296–305. Available from: https://doi.org/10.1016/j.ajog.2020.01.031.
15. Zhang H, Zou H, Zhang C, Li X, Wang Z, Liu C, et al. Chronic endometritis and the endometrial microbiota: implications for reproductive success in patients with recurrent implantation failure.

Annals of Clinical Microbiology and Antimicrobials. 2024; 23: 49. Available from: https://doi.org/10.1186/s12941-024-00710-6.
16. Zhao Y, Liao Y, Xu G, Wang Y. Endometrial microbiota alteration in female patients with endometrial polyps based on 16S rRNA gene sequencing analysis. Frontiers in Cellular and Infection Microbiology. 2024; 14: 1351329. Available from: https://doi.org/10.3389/fcimb.2024.1351329.
17. Ванакова А. И., Долгушина Н. В., Денисов П. А., Гончарук О. Д., Муравьева В. В., Припутневич Т. В. Особенности микробиоты полости матки у пациенток с полипами эндометрия. Вестник Российского государственного медицинского университета. 2025; 1 (6): 6. Доступно по ссылке: https://doi.org/10.24075/vrgmu.2025.007.
18. Khan KN, Fujishita A, Masumoto H, Muto H, Kitajima M, Masuzaki H, et al. Molecular detection of intrauterine microbial colonization in women with endometriosis. European Journal of Obstetrics & Gynecology and Reproductive Biology. 2016; 199: 69–75. Available from: https://doi.org/10.1016/j.ejogrb.2016.01.040.
19. Chen C, Song X, Wei W, Zhong H, Dai J, Lan Z, et al. The microbiota continuum along the female reproductive tract and its relation to uterine-related diseases. Nature Communications. 2017; 8: 875. Available from: https://doi.org/10.1038/s41467-017-00901-0.
20. Riganelli L, Iebba V, Piccioni M, Illuminati I, Bonfiglio G, Neroni B, et al. Structural Variations of Vaginal and Endometrial Microbiota: Hints on Female Infertility. Frontiers in Cellular and Infection Microbiology. 2020; 10: 350. Available from: https://doi.org/10.3389/fcimb.2020.00350.
21. Ворошилина Е. С., Зорников Д. Л., Копосова О. В., Исламиди Д. К., Игнатова К. Ю., Абакумова Е. И., и др. Возможности оценки микробиоты полости матки с использованием ПЦР в реальном времени. Вестник РГМУ. 2020; (1): 14–21. Доступно по ссылке: https://doi.org/10.24075/brsmu.2020.012.
22. Зорников Д. Л., Бехтер А. А., Корнилов Д. О., Симарзина В. М., Нечаева Д. М., Карякина А. Е., и др. Урогенитальные зонды типа Пайпель-С не предотвращают контаминацию эндометриальных образцов цервикальной микробиотой. Вестник РГМУ. 2025; 6: 95–102. Доступно по ссылке: https://doi.org/10.24075/vrgmu.2025.073.
23. Обоскалова Т., Глухов Е., Лаврентьева И., Богданова А., Козырева Е., Нефф Е., и др. Профилактика и лечение воспалительных заболеваний в акушерстве и гинекологии с использованием метода ультразвуковой кавитации лекарственных растворов. Практическое руководство для врачей. Екатеринбург: Vip-Ural, 2014.
24. Плотко Е. Э. Прогнозирование, профилактика, диагностика и лечение осложнений искусственного прерывания беременности. Москва, 2013.
25. Moreno I, Codoñer FM, Vilella F, Valbuena D, Martinez-Blanch JF, Jimenez-Almazán J, et al. Evidence that the endometrial microbiota has an effect on implantation success or failure. American journal of obstetrics and gynecology. 2016; 215 (6): 684–703. Available from: https://doi.org/10.1016/j.ajog.2016.09.075.
26. Wee BA, Thomas M, Sweeney EL, Frentiu FD, Samios M, Ravel J, et al. A retrospective pilot study to determine whether the reproductive tract microbiota differs between women with a history of infertility and fertile women. Australian and New Zealand Journal of Obstetrics and Gynaecology. 2018; 58 (3): 341–8. Available from: https://doi.org/10.1111/ajo.12754.
27. Pelzer ES, Willner D, Buttini M, Huygens F. A role for the endometrial microbiome in dysfunctional menstrual bleeding. Antonie Van Leeuwenhoek. 2018; 111 (6): 933–43. Available from: https://doi.org/10.1007/s10482-017-0992-6.
28. Duff P, Gibbs RS, Blanco JD, Clair PJS. Endometrial culture techniques in puerperal patients. Obstetrics & Gynecology. 1983; 61 (2): 217–22.

CONSTRUCTION AND CHARACTERIZATION OF THE ATTENUATED RECOMBINANT INFLUENZA VIRUS STRAINS EXPRESSING HUMAN INTERLEUKIN 1β

Romanovskaya-Romanko EA ✉, Ozhereleva OO, Plotnikova MA, Altuhov AS, Stukova MA

Smorodintsev Research Institute of Influenza, St. Petersburg, Russia

The use of live attenuated influenza vectors requires a balance between decreasing virulence and preserving immunogenicity. One possible approach to enhancing immunogenicity and protective efficacy of such attenuated strains is the integration of transgenes capable of activating the innate and adaptive immunity in the viral genome. The experimental study aimed to construct recombinant attenuated influenza viruses capable of expressing human IL1β and conduct comparative analysis of their replication properties, immunostimulatory activity, and safety profile *in vivo*. Recombinant strains with different transgene localization were generated by the reverse genetics method; their growth characteristics and transgene expression levels were assessed. Activation of the innate immunity genes in response to infection with recombinant strains was assessed in the A549 cell culture. The attenuated phenotype was confirmed in the mouse model. In the reported study, recombinant attenuated influenza viruses having the NS1 protein truncated to 124 amino acids and expressing human IL1β were constructed and produced. It was confirmed that recombinant strains could express the functionally active IL1β; the increase in relative expression of the innate immunity genes (RIG-I, MDA5, OAS1) and pro-inflammatory cytokines (IL6 and TNFα) in response to the infection of cells with recombinant strains compared to the empty vector NS124 was shown. Thus, the IL6 gene expression increased more than 10-fold ($p < 0.0001$) and that of the TNFα gene increased 3–4-fold ($p < 0.0001$). The attenuated phenotype of the recombinant strains produced was confirmed in *in vivo* experiments, which suggests preservation of the safety profile along with the enhanced immunostimulatory activity.

Keywords: influenza A virus, recombinant influenza vector, interleukin-1 beta, NS1 protein

Funding: the study was supported by the Russian Science Foundation (project No. 25-25-00939).

Author contribution: Romanovskaya-Romanko EA — concept, testing, material processing, manuscript writing; Ozhereleva OO — literature review, constructing plasmids, testing, statistical data processing; Plotnikova MA — testing, statistical data processing; Altuhov AS — testing; Stukova MA — approval of the final version of the article.

Compliance with ethical standards: the study was approved by the Ethics Committee of the Smorodintsev Research Institute of Influenza of the Ministry of Health of the Russian Federation (protocol No. 07 dated April 23, 2026). Animals were kept under standard conditions in accordance with the Directive 2010/63/EC, federal guidelines, and the institutional policy of the Smorodintsev Research Institute of Influenza of the Ministry of Health of the Russian Federation.

✉ **Correspondence should be addressed:** Ekaterina A. Romanovskaya-Romanko
Professora Popova, 15/17, St. Petersburg, 197022, Russia; romromka@yandex.ru

Received: 02.07.2026 **Accepted:** 28.07.2026 **Published online:** 17.08.2026

DOI: 10.24075/brsmu.2026.044

КОНСТРУИРОВАНИЕ И ХАРАКТЕРИСТИКА АТТЕНУИРОВАННЫХ РЕКОМБИНАНТНЫХ ШТАММОВ ВИРУСА ГРИППА, ЭКСПРЕССИРУЮЩИХ ИНТЕРЛЕЙКИН-1β ЧЕЛОВЕКА

Е. А. Романовская-Романько ✉, О. О. Ожерельева, М. А. Плотникова, А. С. Алтухов, М. А. Стукова

Научно-исследовательский институт гриппа имени А. А. Смородинцева, Санкт-Петербург, Россия

Применение живых аттенуированных гриппозных векторов требует баланса между снижением вирулентности и сохранением иммуногенности. Один из возможных подходов для усиления иммуногенности и защитной эффективности таких аттенуированных штаммов — встраивание в геном вируса трансгенов, способных активировать врожденный и адаптивный иммунитет. Цель экспериментального исследования — сконструировать рекомбинантные аттенуированные вирусы гриппа, способные экспрессировать IL1β человека, и провести сравнительный анализ их репликативных свойств, иммуностимулирующей активности и профиля безопасности *in vivo*. Рекомбинантные штаммы с различным положением трансгена получили методом обратной генетики, провели оценку их ростовых характеристик и уровня экспрессии трансгена. Активацию генов врожденного иммунитета изучали в культуре клеток A549 в ответ на заражение рекомбинантными штаммами. Аттенуированный фенотип подтверждали в модели мышей. В представленном исследовании были сконструированы и получены рекомбинантные аттенуированные вирусы гриппа, имеющие укороченный до 124 аминокислот белок NS1 и экспрессирующие IL1β человека. Подтверждена способность рекомбинантных штаммов экспрессировать функционально активный IL1β, показано усиление относительной экспрессии генов врожденного иммунитета (RIG-I, MDA5, OAS1), а также провоспалительных цитокинов (IL6 и TNFα) в ответ на инфицирование клеток рекомбинантными штаммами по сравнению с пустым вектором NS124. Так, экспрессия гена IL6 увеличивалась более чем в 10 раз ($p < 0,0001$), а гена TNFα — в 3–4 раза ($p < 0,0001$). В экспериментах *in vivo* был подтвержден аттенуированный фенотип полученных рекомбинантных штаммов, что свидетельствует о сохранении профиля безопасности наряду с усиленной иммуностимулирующей активностью.

Ключевые слова: вирус гриппа А, рекомбинантный гриппозный вектор, интерлейкин-1 бета, белок NS1

Финансирование: работа выполнена при поддержке Российского научного фонда (проект № 25-25-00939).

Вклад авторов: Е. А. Романовская-Романько — концепция, выполнение исследований, обработка материала, написание статьи; О. О. Ожерельева — обзор литературы, конструирование плазмид, выполнение исследований, статистическая обработка данных; М. А. Плотникова — выполнение исследований, статистическая обработка данных; А. С. Алтухов — выполнение исследований; М. А. Стукова — утверждение окончательного варианта статьи.

Соблюдение этических стандартов: исследование одобрено этическим комитетом ФГБУ НИИ гриппа им. А. А. Смородинцева (протокол № 07 от 23 апреля 2026 г.). Животных содержали в стандартных условиях в соответствии с Директивой 2010/63/ЕС, федеральными руководящими принципами и институциональной политикой ФГБУ НИИ гриппа им. А. А. Смородинцева.

✉ **Для корреспонденции:** Екатерина Андреевна Романовская-Романько
ул. Профессора Попова, д. 15/17, г. Санкт-Петербург, 197022, Россия; romromka@yandex.ru

Статья получена: 02.07.2026 **Статья принята к печати:** 28.07.2026 **Опубликована онлайн:** 17.08.2026

DOI: 10.24075/vrgmu.2026.044

The use of live attenuated influenza vectors requires a subtle balance between decreasing the strain virulence and preserving its immunogenicity. One possible way to achieve such balance is a targeted immune response modulation through expression of immunomodulatory molecules being part of the influenza vector genome aimed to enhance the protective response without desreasing the strain virulence.

The attenuated influenza virus strains with the modified NS1 protein represent a promising platform for the development of a live influenza vaccine with a broad protective efficacy range, as well as to create vectors for delivery of target antigens [1]. Viruses with truncated NS1 proteins are capable of effective replication in production substrates; these also have an attenuated phenotype in immunocompetent systems [2]. Attenuation of such strains results from the fact that viruses with the truncated non-structural NS1 protein cannot inhibit the host's innate immune response due to loss of the C-terminal effector domain mediating the interplay with the cellular immune regulation factors and mRNA processing [3]. However, preservation of the RNA-binding domain in the N-terminal fragment of the NS1 protein can result in preservation of immunosuppressive activity of such viruses through limitation of processing and maturation of the key inflammasome-dependent signaling mediators: interleukin 1β (IL1β) and interleukin 18 (IL18) [4]. Since these cytokines play the most important role in developing an effective immune response, limitation of the strain immunostimulatory potential can be observed in the case of the influenza strain having the NS1 protein truncated to 124 amino acid bases. In this regard, further optimization of safety and immunogenicity of such influenza vectors is a relevant task.

One promising approach to enhancing the attenuated strains' immunogenicity is integration of additional trangenes encoding the immunomodulatory factors capable of ensuring the targeted innate and adaptive immune response activation in the viral genome.

In the context of enhancing the anti-influenza immune response, cytokines of the interleukin 1 family, capable of enhancing both humoral and cell-mediated immune response when administered intranasally together with the antigen, are of special interest [5]. Previously it was shown that intranasal administration of IL1β in combination with the influenza antigen induces the formation of tissue-resident memory T cells playing a key role in developing the cross-protection against heterologous influenza virus strains [6]. Expression of the IL1β bioactive molecule with the recombinant attenuated influenza virus strain can contribute to enhancing the specific immune response to influenza antigens, ensuring the effective broad protection.

The study aimed to construct and produce recombinant attenuated influenza virus strains having the NS1 truncated to 124 amino acid bases and expressing human IL1β, as well as to perform comparative analysis of their replication properties, immunostimulatory activity, and safety profile *in vivo*.

METHODS

Plasmid constructs

To assemble recombinant strains, two plasmids with different design encoding sequences of the NS chimeric genome segment with the inserted IL1β sequence active form were obtained [7]. The plasmid for the recombinant strain IL1b_2A_NS124 was produced based on the earlier constructed plasmid pHW-PR8-sF-NS [8]: the IL1β sequence with the signal peptide IgGκ synthesized *de novo* (Evrogen, Russia) was integrated into the N-terminal part of a chimeric polyprotein comprising the transgene followed by the sequences of NS1 truncated to 124 amino acid bases and NS2/NEP, separated by 2A sites; the NEP expression was ensured by the 2A site without splicing. As for the recombinant strain NS124_SS_IL1b, the transgene sequence with the IgGκ signal peptide was inserted in the plasmid after the sequence of the NS1 truncated to 124 amino acid bases through the cassette of the overlapping stop-start codons ensuring the translation re-initiation. The plasmids encoding the sequences of other internal and surface proteins of the influenza virus A/Puerto Rico/8/1934 (A/PR/8/34) were obtained from the collection of the Smorodintsev Research Institute of Influenza.

Cell cultures

The MDCK cells (#FR-58; IRR, USA) were cultured in the AlphaMEM medium (Biolot, Russia) supplemented with the SC-biol 10% embryonic serum (Biolot, Russia). The A549 (CCL-185; ATCC, USA) and HEK293 (Smorodintsev Research Institute of Influenza) cells were cultured in the DMEM/F12 medium (Biolot, Russia) supplemented with the SC-biol 10% serum (Biolot, Russia).

Production of recombinant viruses

Recombinant virus strains were produced by transfection of the MDCK/HEK293 co-culture with the set of eight plasmids encoding the influenza virus genome segments. The GenJect39 reagent (Molecta, Russia) was used as a transfection agent. Further steps of passaging recombinant viral strains were accomplished in the 10-day developing chicken embryos (DCE) (Poultry Farm Sinyavskaya, Priladozhsky village, Russia) at a temperature of 34 °C. The influenza vector (NS124) having the NS1 protein truncated to 124 amino acid bases without any inserted transgene was obtained from the collection of the Smorodintsev Research Institute of Influenza of the Ministry of Health of the Russian Federation (laboratory of vector vaccines).

Determination of infectious activity

Infectious activity of the recombinant virus strains was determined by the limiting dilution method in the DCE system and the MDCK cell culture [8]. The Reed and Muench method was used to determine the 50% infectious dose; the titer was expressed in $\log_{10}$ EID_{50} ($TCID_{50}$)/mL.

Determination of the chimeric NS segment length by RT-PCR

Viral RNA was isolated using the RNeasy Mini Kit (Qiagen, Netherlands). The genetic material was amplified using the MioMaster RT-PCR–Extra kit (BioLabMix, Russia) and primers specific for the NS segment [9]. Amplification was performed in the sensor GenTier 96E PCR Cycler (TianLong, China). The PCR product length was assessed by the 1% agarose gel electrophoresis using the ×1 TAE buffer.

IL1β quantification

To obtain the samples, the 10-day DCEs (24-h MDCK cell monolayer) were infected with recombinant virus strains or the empty NS124 vector in a dose of 2×10^5 EID_{50} (1.0 $TCID_{50}$/cell). Samples were collected after 48 h (24 h) of incubation at a temperature of 34 °C (37 °C, 5% CO_2). IL1β in the samples was quantified by enzyme immunoassay (ELISA) using the Interleukin-1 beta-ELISA-BEST kit (Vector-Best, Russia).

IL1β biological activity measurement

The IL1β biological activity was determined by the cell proliferation test based on the stimulation of the D10.G4.1 IL1-dependent cell line proliferation in the presence of the suboptimal concanavalin A concentration. Cells were cultured in the RPMI-1640 medium and introduced into the 96-well plates together with serial dilutions of the reference sample (WHO IL1β) and test samples. After the 72-h incubation at 37 °C, 5% CO_2 proliferation was assessed based on the optical density using the XTT assay. The samples' activity was calculated based on the calibration curve relative to the international standard and expressed in IU/mL.

Quantification of infected cells

The percentage of infected cells was determined by flow cytometry. The 24-h A549 cell monolayer was infected with recombinant strains or the empty vector in a dose of 1.0 $TCID_{50}$/cell in three independent replicates for each virus and incubated for 20 h in the medium containg 2% of the serum. Uninfected cells (CC) were used as a negative control. The percentage of infected cells was calculated using the flow cytometer, staining the cells with the Zombie Aqua Fixable Viability Kit and FITC-labeled antibodies against the influenza virus NP. Data acquisition was performed using the CytoFLEX Flow Cytometer (Beckman Coulter, USA); the analysis was conducted using the Kaluza Analysis v2 software (Beckman Coulter, USA).

Immunofluorescence

The MDCK cells were infected with recombinant strains or the empty vector in a dose of 1.0 $TCID_{50}$/cell and incubated for 20 h in the medium containg 2% of the serum. A polyclonal mouse serum and the goat-anti mouse Alexa488 conjugate (Abcam, UK) were used to detect the influenza A virus NS1 protein in the cells permeabilized with Triton X-100. Imaging of cells by fluorescence microscopy was performed using the Cytell Imaging System (Image Solutions, UK).

Expression assessment by RT-PCR

To assess the expression of the innate immune response genes, the 24-h monolayer of the A549 cells was infected with recombinant strains or the empty vector in a dose of 1.0 $TCID_{50}$/cell (in four replicates). After 24 h, total RNA was extracted from the cells using the ExtractRNA kit (Evrogen, Russia). RNA was treated with the DNAase containing no RNAse RQ1 (Promega, USA). The RT reaction was conducted using 1 μg of RNA, 0.5 μg of oligo-dT16 primers (DNA synthesis, Russia) and the RNAscribe RT kit (BioLabMix, Russia). The BioMaster HS-PCR kit (BioLabMix, Russia) and the previously developed sequences of primers and probes were used to conduct PCR [10]. The Ct values were normalized relative to the GAPDH gene (housekeeping gene). Relative expression was calculated by the ΔΔCt method, the expression of target genes in uninfected cells was taken as a unit.

Laboratory animals

CD1 female outbred mice aged 6–8 weeks were purchased from the Rappolovo laboratory animal nursery (Rappolovo laboratory animal nursery, National Research Centre "Kurchatov Institute", Leningrad Region, Russia).

Safety of the recombinant vectors intranasally administered to mice

Viral strains were intranasally administered to mice under the light ether anesthesia in the amount of 30 μL using a mechanical dispenser. Recombinant strains and the empty vector were administered to animals in a dose of 5.5 $\log_{10}$ EID_{50}, and the virus A/Puerto Rico/8/34 with the full-sized NS genome (PR8 wt) was administered in a dose of 3.5 $\log_{10}$ EID_{50}.

Statistical processing

Statistical analysis and graphic visualization were performed using the GraphPad Prism 9.0 software (GraphPad Software, Inc., USA). The data are presented as the mean ± standard deviation (SD). The analysis of variance with the Tukey's post-hoc test or nonparametric Kruskal–Wallis test was used for the intergroup comparison, as specified in captions to the figures. The value $p < 0.05$ was considered significant.

RESULTS

Construction and characterization of the attenuated influenza viruses expressing human IL1β

The recombinant influenza virus strains expressing IL1β were generated based on the strain A/Puerto Rico/8/34 (H1N1) containing the NS1 protein truncated to 124 amino acid bases [11]. Two plasmid variants encoding the modified NS gene were used to assembly the viruses. In the first case, the transgene sequence was inserted after the sequence encoding the first 124 amino acids of the influenza virus NS1 protein (NS124_SS_IL1b). In the second variant, the transgene sequence with the IgGκ signal peptide was inserted before the sequence encoding the NS124 viral protein, it was separated from the latter by the 2A site ensuring the co-translational separation of proteins (IL1b_2A_NS124) (Fig. 1A).

To assess the genetic stability of the heterologous insertion preserved in the NS genome segment, the recombinant viral strains were cultured throughout five consecutive passages in the DCE system, and the transgene insertion preservation stability was assessed by RT-PCR. Both viral vectors were genetically stable; the RT-PCR results showed that the length of the NS genome segment of the recombinant strains corresponded to that of control plasmids in all passages (Fig. 1B).

The recombinant strains' reproductive activity in the DCE system and the MDCK cell culture was similar. The NS124_SS_IL1b strain growth characteristics did not differ from the characteristic of the original influenza strain with the truncated NS1 protein carrying no transgene; the infectious titer reaching 8.0 (9.0) $\log_{10}$ $TCID_{50}$ (EID_{50})/mL was significantly higher (by 1-1.5 $\log_{10}$) compared to that of the recombinant strain IL1b_2A_NS124 expressing IL1β before the NS1 protein (Fig. 1C). Meanwhile the capability of infecting the permissive culture was comparable in both strains and did not differ from that of the original strain without the insertion. When infecting the cell monolayer with the NS124_SS_IL1b, IL1b_2A_NS124, and NS124 strains in a dose of 1.0 unfectious unit per cell, the share of infected cells was 83 ± 3.5%, 75 ± 8.0%, and 81 ± 4.0%, respectively (Fig. 1D).

The cytokine expression was quantified by ELISA in the allantoic fluid and supernatant of the infected MDCK cells. The IL1β expression in the cell culture and in the embryos was many times higher for the IL1b_2A_NS124 strain (38,000 ± 2000 pg/mL; 28.0 ± 2.0 pg/mL), than the NS124_SS_IL1b strain (6400 ± 51

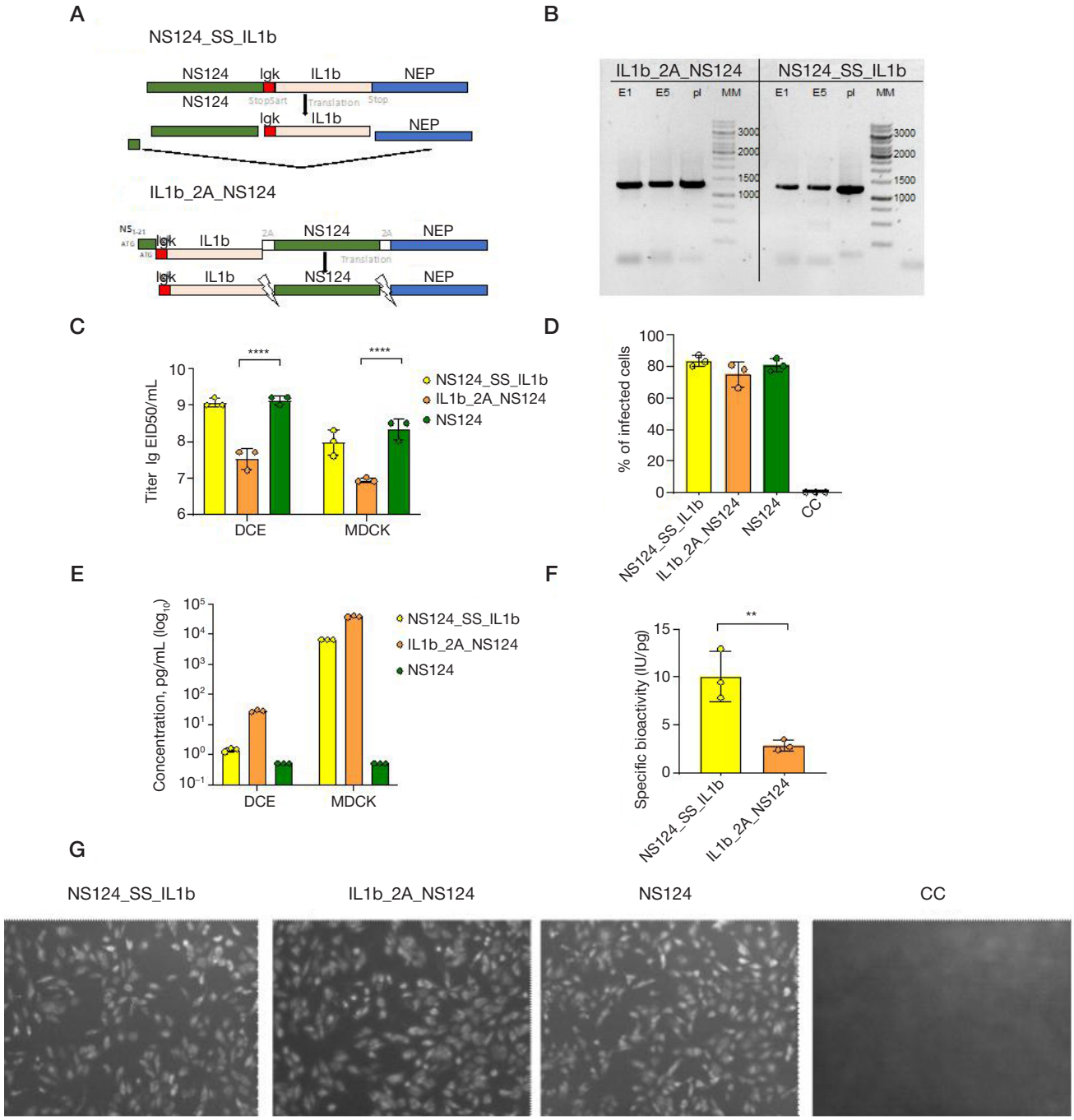

Fig. 1. Construction and characterization of the recombinant influenza A viruses expressing IL1β. **A**. Schemes of genomic constructs of the chimeric genome segment NS of recombinant viruses IL1b_2A_NS124 and NS124_SS_IL1b. **B**. Electropherogram of the recombinant strains' genome segment NS amplification products. MM — molecular weight marker; E1 — first embryo passage; E5 — fifth embryo passage; pl — control plasmid. **C**. Reproductive properties of recombinant viral strains in the 10-day DCE system and the MDCK cell culture. Here we present the results of infectious activity assessment for the fifth embryo passage, the mean titer $\log_{10}$ EID50 ($TCID_{50}$) ± SD. **D**. Effectiveness of the A549 cell infection with recombinant viral strains. Here we present the mean percentage of infected cells for three replicates ± SD. **E**. IL1β quantification in the allantoic fluid and the cellular supernatant of the MDCK cells infected with recombinant strains by ELISA. **F**. IL1β specific bioactivity. Estimated quantity of the IL1β bioactive form dtemined in the proliferation test using the HEK-Blue IL1β reporter system recalculated for 1 pg of IL1β detected by ELISA. **G**. Representative images of the A549 obtained by fluorescence microscopy. The results of staining the NS1 protein detected using Alexa Fluor 488(488/509 nm) are highlighted in gray. 40× magnification

pg/mL; 1.4 ± 0.21 pg/mL) (Fig. 1E). Specific cytokine bioactivity was determined for the interleukin-containing allantois samples using the HEK-Blue IL1β reporter system. The bioactive form share reported for the NS124_SS_IL1b strain was higher (10.0 ± 2.61 IU/pg), than that reported for IL1b_2A_NS124, which was 2.8 ± 0.56 IU/pg (Fig.1F). However, the total quantity of the IL1β biactive form was higher in the IL1b_2A_NS124 strain compared to NS124_SS_IL1b.

Using the immunofluorescence method it was demonstrated that the transgene insertion before the NS1 protein sequence in the IL1b_2A_NS124 strain did not prevent the NS1 viral protein expression in the infected cells (Fig. 1G).

Activation of the innate immune response genes by recombinant strains

For recombinant strains expressing human IL1β, activation of the expression of the RIG I and MDA5 intracellular sensors, MxA and OAS1 antiviral proteins, and human IL1β, IL6, IL18, TNFa, IL4, and IL10 cytokines in response to infection compared to

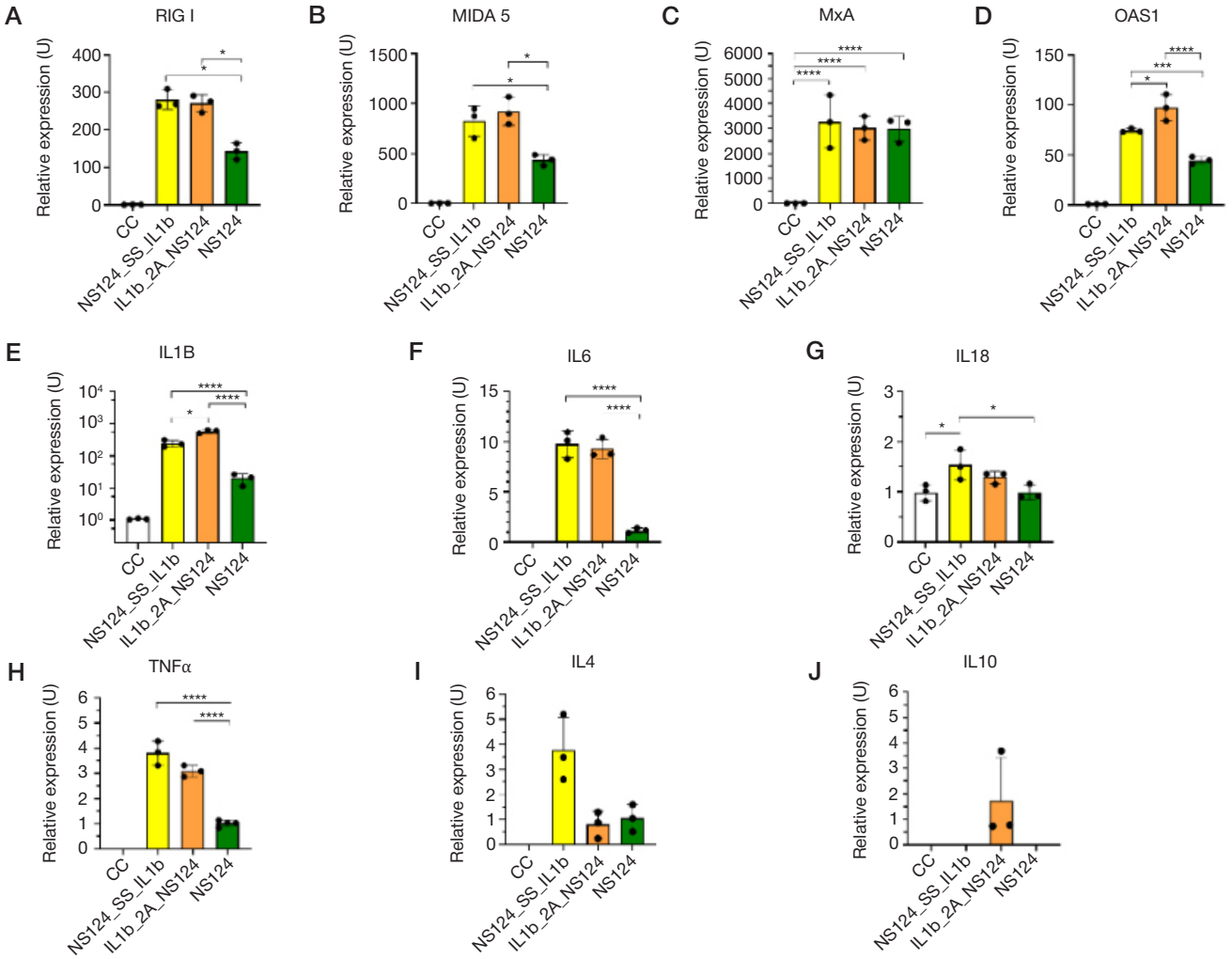

Fig. 2. Activation of the expression of intracellular sensors **(A, B)**, antiviral proteins **(C, D)**, and cytokines **(E–J)** in the A549 cells in response to infection with the recombinant influenza virus strains expressing IL1β. The relative expression of messenger RNA (mRNA) is presented as mean values for three biological replicates (bars) and individual values for each measurement (point). One-way analysis of variance (ANOVA) was used to assess significance of differences in the normalized ΔCt values, and Tukey's test was used for multiple comparisons (* — $p < 0.05$; ** — $p < 0.01$; *** — $p < 0.001$; **** — $p < 0.0001$)

the original influenza vector having no transgene insertion was assessed in the A549 cells.

In general, recombinant influenza strains IL1b_2A_NS124 and NS124_SS_IL1b showed similar transcription profiles for almost all studied genes. Furthermore, these profiles were significantly different from that induced by the empty NS124 vector.

Infection with recombinant constructs was associated with the upregulation of IL1β, the levels of which exceeded the control values more than 100 times. The pronounced induction of the IL6 (more than 10-fold increase) and TNFa (3-4-fold increase) gene expression was shown that was significantly higher, than when the cells were infected with the empty vector NS124 (Fig. 2).

Infection of cells with both recombinant strains, as well as the empty vector resulted in the IL4 expression induction. In case of the NS124_SS_IL1b strain, the IL4 mRNA levels were higher, but no significant differences from two other strains were reported. The IL10 transcript was found only when the cells were infected with the recombinant strain IL1b_2A_NS124.

The analysis of the components of the system of pathogen recognition in response to the infection of cells with both recombinant strains revealed a significant increase in the levels of mRNA of the RIG-I and MDA5 intracellular sensors relative to the empty vector, which can indicate the enhancement of the signaling pathways that initiate the innate antiviral response.

As for interferon-stimulated genes (ISG), it was shown that all influenza strains activated the MxA and OAS1 gene expression, regardless of the presence of the transgene, which was consistent with the well-known ability of influenza viruses having the truncated NS1 protein to induce an interferon response. As for the strain carrying the IL1β insertion, the significantly higher expression of the gene OAS1 was shown, while the MxA gene activation level did not depend on the presence of the insertion encoding IL1β in the viral genome and was comparable for all viral srains.

Safety of recombinant influenza strains intranasally administered to mice

Since the constructed recombinant vectors expressing IL1β can be potentially used to develop vaccines, one of the main parameters are their safety and preservation of the attenuated phenotype resulting from the NS1 truncation to 124 amino acid bases. In this regard, the recombinant strain safety was assessed based on such indicators, as weight loss, lethality, and the infectious virus shedding from the animal's respiratory tract (Fig. 3A).

The animals that received both recombinant strains showed the negligible weight loss compared to that in the group of animals that received the empty vector (Fig. 3B). Lethality was

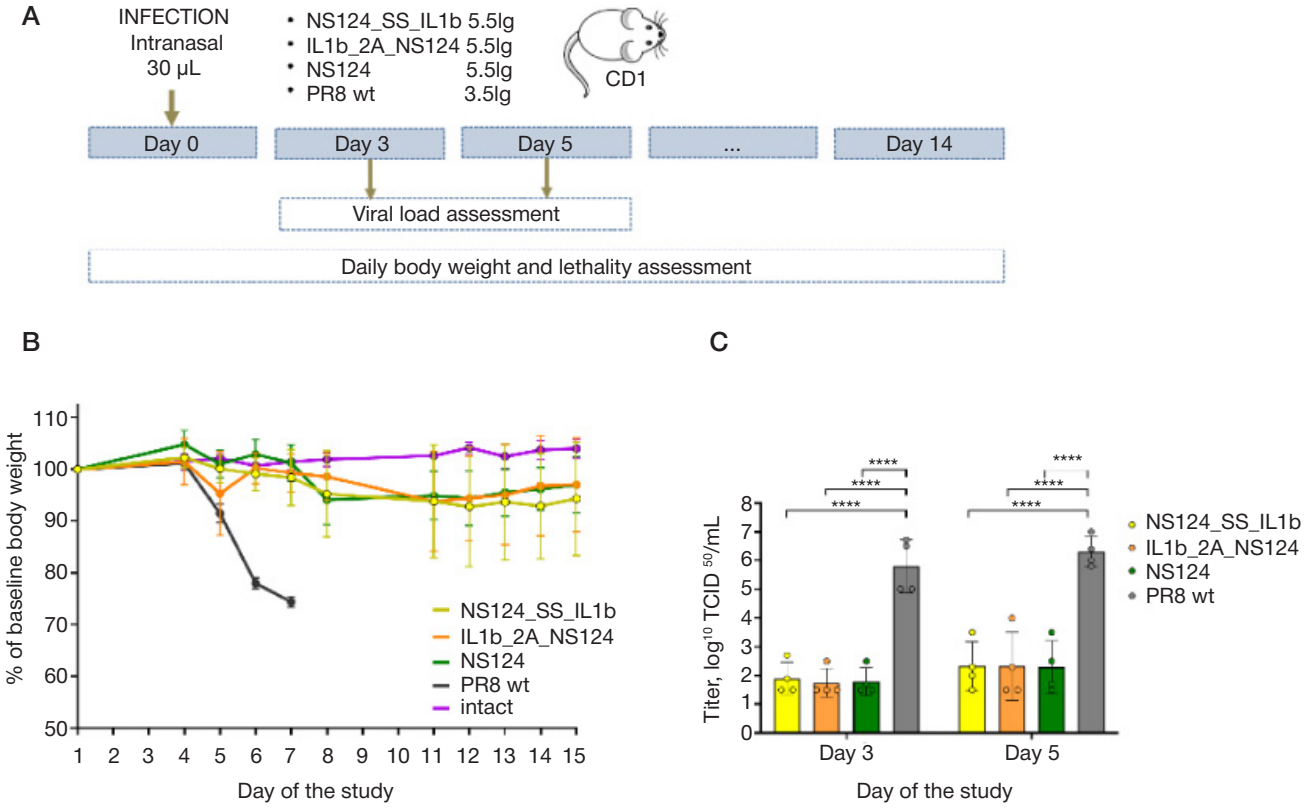

Fig. 3. Assessment of safety of the recombinant influenza strains expressing IL1β that were intranasally administered to mice. **A**. Experimental design. **B**. Dynamic changes in the animals' body weight (n = 5 per group) after the intranasal administration of recombinant viruses. **C**. Evaluation of viral load in the lung tissues of mice on days 3 and 5 after the intranasal administration of recombinant viral strains expressing IL1β. Bars represent the mean indicator value for the group (n = 4) ± SD, points represent individual indicator values for each animal. Two-way analysis of variance was used to assess significance of differences in the average group values, and the Dunnett's test was used for multiple comparisons with the control group PR8 wt (**** — $p < 0.0001$)

reported in none of the groups of animals that received strains with the truncated NS1 protein, while lethality in the group of the wild type virus was 100% by day 7 of the study. The recombinant strains' replication levels in the lung tissues were low, comparable with the values reported for the empty vector. The virus infectious titer of both strains was significantly lower (10^4 times) compared to the wild type influenza virus (Fig. 3C).

DISCUSSION

In the reported study, recombinant influenza viruses expressing human IL1β were constructed based on the attenuated virus with the truncated NS1 protein, which were distinguished by the transgene localization. It was shown that the transgene incorporation into the viral genome resulted in further activation of the innate immune response genes, and the insertion position relative to the open reading frame of the NS1 protein affected the strain reproductive properties and the target protein expression levels. Furthermore, both strains retained the attenuated phenotype because the IL1β expression did not compensate for the NS1 protein's defect in suppressing the host immune response.

Both recombinant strains generated were genetically stable, which was an important parameter for production strains, but had different growth characteristics. The NS124_SS_IL1b strain retained the growth characteristics comparable with that of the empty vector, while the IL1b_2A_NS124 strain replication properties were lower by 1.0–1.5 $\log_{10}$. The decrease in the IL1b_2A_NS124 growth properties can result from the co-translational transgene expression, since in this construct IL1β and the NS1 protein are synthesized as one polyprotein with subsequent splitting at the 2A site, which may create steric hindrance or affect the virion assembly kinetics. Furthermore, it was shown that the transgene incorporation did not prevent the infection of permissive cells and did not decrease the expression levels of the NS1 protein itself.

It has been shown that the order of transgene insertion into the influenza vector genome is important for the expression level of the latter [12]. Higher IL1β production has been reported for the IL1b_2A_NS124 strain. The findings can be explained by the fact that in the IL1b_2A_NS124 strain construct the transgene is located before the NS1 protein sequence. As a result, the more efficient translation can be ensured due to early access to the ribosome and the absence of secondary structures associated with viral RNA. Despite the fact that the IL1β specific bioactivity (IU/pg) was higher in the case of the strain NS124_SS_IL1b, the higher total quantity of the functionally active cytokines was reported for the strain IL1b_2A_NS124. This suggests that the trasgene insertion position can affect not only the quantity of the protein produced, but also posttranslational modifications and processing of the mature IL1β form [8].

The analysis of the expression of the innate immunity genes in the A549 cells in response to infection with recombinant strains showed the qualitatively similar activation profiles for both constructs, which were significantly different from the indicators, in response to infection with the empty vector NS124. Infection of cells with the recombinant strains NS124_SS_IL1b and IL1b_2A_NS124 led to the increase in the RIG-I and MDA5 intracellular sensor mRNA levels, which was consistent with the concept of the cross-talk between inflammatory signaling pathways and the pathogen recognition system. The RIG-I/MDA5 pathway activation can strenghthen a positive feedback enhancing the cells' ability to detect the viral genetic material and initiate the interferon response cascade [13]. The interferon-

stimulated gene expression activation in response to infection with the recombinant strains expressing IL1β and the empty vector NS124 was different. Thus, all strains, including the empty vector, activated the MxA expression to the comparable extent, which reflects the well-known ability of viruses with the truncated NS1 protein to induce the interferon response. The significantly higher OAS1 expression levels were reported for the constructs expressing IL1β. This difference demonstrates that IL1β can selectively modulate certain ISG response branches, possibly through the signaling pathways associated with NF-kB or MAPK, which are targets for the IL1 receptor signaling [14]. Further OAS1 expression enhancement can be physiologically significant, since the OAS1 protein is directly involved in the viral RNA degradation through activation of the L ribonuclease, which can more effectively limit the virus at early stages of infection, ensuring the attenuated virus phenotype [15].

Since IL1β is not only an immunostimulator, but also a pyrogenic factor, it was necessary to evaluate the preservation of the attenuated phenotype of recombinant strains in order to determine the possibility of their use as live vaccine strains. During the study it was shown that the IL1β incorporation into the influenza vector NS124 as a transgene did not disrupt the attenuated phenotype resulting from the NS1 protein deletion. In the mouse respiratory tract, both recombinant strains, NS124_SS_IL1b and IL1b_2A_NS124, showed low replication similar to that reported for the empty vector and significantly lower compared to the wild type virus. Despite limited replication resulting from the NS1 deletion, adding IL1β, as shown in *in vivo* experiments, potentiates the innate immunity activation, which suggests that the transgene expression can ensure the adaptive immune response enhancement without increasing the reactogenicity associated with high replication of live viruses, even with low viral load. *In vivo* studies of the recombinant strain immunogenicity and protective activity will be conducted to confirm this hypothesis. In general, our data are in line with the earlier studies showing the effectiveness of cytokine (IL15, IL2 or CXCL10) incorporation into the influenza virus genome aimed at increasing immunogenicity [16–18].

CONCLUSIONS

The data obtained suggest that the IL1β immunomodulatory molecule incorporation into the attenuated influenza virus genome can modulate the innate immune response and represent a possible strategy for the creation of candidate live vaccines with the increased immunogenicity without any harm to their safety profiles. However, due to limitations of the *in vitro* model, this approach should be further tested in animal models, and the effect reproducibility should be assessed to determine its clinical significance and safety.

References

1. Zhang H, Wang L, An Y, Chen Z. The applications of live attenuated influenza a virus with modified NS1 gene. Mol Ther Nucleic Acids. 2025; 36 (1): 102471.
2. García-Sastre A, Egorov A, Matassov D, Brandt S, Levy DE, Durbin JE, et al. Influenza A virus lacking the NS1 gene replicates in interferon-deficient systems. Virology. 1998; 252 (2): 324–30.
3. Zhang H, Floyd K, Fang Z, Hoffmann FA, Lee A, Froggatt HM, et al. Mucosal vaccination in mice provides protection from diverse respiratory threats. Science. 2026; eaea1260.
4. Stasakova J, Ferko B, Kittel C, Sereinig S, Romanova J, Katinger H, et al. Influenza A mutant viruses with altered NS1 protein function provoke caspase-1 activation in primary human macrophages, resulting in fast apoptosis and release of high levels of interleukins 1beta and 18. J Gen Virol. 2005; 86 (Pt 1): 185–95.
5. Gwinn WM, Kirwan SM, Wang SH, Ashcraft KA, Sparks NL, Doil CR, et al. Effective induction of protective systemic immunity with nasally administered vaccines adjuvanted with IL-1. Vaccine. 2010; 28 (42): 6901–14.
6. Lapuente D, Ruzsics Z, Thirion C, Tenbusch M. Evaluation of adenovirus 19a as a novel vector for mucosal vaccination against influenza A viruses. Vaccine. 2018; 36 (19): 2712–20.
7. Hailey KL, Li S, Andersen MD, Roy M, Woods VLJ, Jennings PA. Pro-interleukin (IL)-1beta shares a core region of stability as compared with mature IL-1beta while maintaining a distinctly different configurational landscape: a comparative hydrogen/deuterium exchange mass spectrometry study. J Biol Chem. 2009; 284 (38): 26137–48.
8. Pulkina A, Vasilyev K, Muzhikyan A, Sergeeva M, Romanovskaya-Romanko E, Shurygina AP, et al. IgGκ Signal Peptide Enhances the Efficacy of an Influenza Vector Vaccine against Respiratory Syncytial Virus Infection in Mice. Int J Mol Sci. 2023; 24 (14).
9. Dittmann M, Hoffmann HH, Scull MA, Gilmore RH, Bell KL, Ciancanelli M, et al. A serpin shapes the extracellular environment to prevent influenza a virus maturation. Cell [Internet]. 2015; 160 (4): 631–43. Available from: http://dx.doi.org/10.1016/j.cell.2015.01.040.
10. Oleinik V, Plotnikova M, Yolshin N, Romanovskaya-Romanko E. Development and approbation of a quantitative PCR system for studying the expression of endosomal receptors and cytosolic nucleic acid sensors in mice. Med Acad journal. 2025; 1 (1): 90–100.
11. Hoffmann E, Neumann G, Kawaoka Y, Hobom G, Webster RG. A DNA transfection system for generation of influenza A virus from eight plasmids. Proc Natl Acad Sci USA. 2000; 97 (11): 6108–13.
12. Yildiz S, El Zahed SS, Villalón-Letelier F, Wang Q, Yelleswarapu S, Dawodu G, et al. Re-engineering segment 8 facilitates generation of a versatile live-attenuated influenza A virus vector platform for secretory protein delivery. J Virol. 2026; 100 (5): e0034726.
13. Gaudino M, Lion A, Sagné E, Nagamine B, Oliva J, Terrier O, et al. The Activation of the RIG-I/MDA5 Signaling Pathway upon Influenza D Virus Infection Impairs the Pulmonary Proinflammatory Response Triggered by Mycoplasma bovis Superinfection. J Virol. 2023; 97 (2): e0142322.
14. Lin CC, Kuo CT, Cheng CY, Wu CY, Lee CW, Hsieh HL, et al. IL-1 beta promotes A549 cell migration via MAPKs/AP-1- and NF-kappaB-dependent matrix metalloproteinase-9 expression. Cell Signal. 2009; 21 (11): 1652–62.
15. Harioudh MK, Perez J, Chong Z, Nair S, So L, McCormick KD, et al. Oligoadenylate synthetase 1 displays dual antiviral mechanisms in driving translational shutdown and protecting interferon production. Immunity. 2024; 57 (3): 446–461.e7.
16. van Rikxoort M, Michaelis M, Wolschek M, Muster T, Egorov A, Seipelt J, et al. Oncolytic effects of a novel influenza A virus expressing interleukin-15 from the NS reading frame. PLoS One. 2012; 7 (5): e36506.
17. Ozhereleva O, Mustafaeva A, Pulkina A, Plotnikova M, Shuklina M, Shurygina AP, et al. A CXCL10-Expressing Influenza Vector Induces Robust Adaptive Immunity Despite Strong Attenuation. Pharmaceutics. 2026; 18 (6).
18. Kittel C, Ferko B, Kurz M, Voglauer R, Sereinig S, Romanova J, et al. Generation of an influenza A virus vector expressing biologically active human interleukin-2 from the NS gene segment. J Virol. 2005; 79 (16): 10672–7.

Литература

1. Zhang H, Wang L, An Y, Chen Z. The applications of live attenuated influenza a virus with modified NS1 gene. Mol Ther Nucleic Acids. 2025; 36 (1): 102471.
2. García-Sastre A, Egorov A, Matassov D, Brandt S, Levy DE, Durbin JE, et al. Influenza A virus lacking the NS1 gene replicates in interferon-deficient systems. Virology. 1998; 252 (2): 324–30.
3. Zhang H, Floyd K, Fang Z, Hoffmann FA, Lee A, Froggatt HM, et al. Mucosal vaccination in mice provides protection from diverse respiratory threats. Science. 2026; eaea1260.
4. Stasakova J, Ferko B, Kittel C, Sereinig S, Romanova J, Katinger H, et al. Influenza A mutant viruses with altered NS1 protein function provoke caspase-1 activation in primary human macrophages, resulting in fast apoptosis and release of high levels of interleukins 1beta and 18. J Gen Virol. 2005; 86 (Pt 1): 185–95.
5. Gwinn WM, Kirwan SM, Wang SH, Ashcraft KA, Sparks NL, Doil CR, et al. Effective induction of protective systemic immunity with nasally administered vaccines adjuvanted with IL-1. Vaccine. 2010; 28 (42): 6901–14.
6. Lapuente D, Ruzsics Z, Thirion C, Tenbusch M. Evaluation of adenovirus 19a as a novel vector for mucosal vaccination against influenza A viruses. Vaccine. 2018; 36 (19): 2712–20.
7. Hailey KL, Li S, Andersen MD, Roy M, Woods VLJ, Jennings PA. Pro-interleukin (IL)-1beta shares a core region of stability as compared with mature IL-1beta while maintaining a distinctly different configurational landscape: a comparative hydrogen/deuterium exchange mass spectrometry study. J Biol Chem. 2009; 284 (38): 26137–48.
8. Pulkina A, Vasilyev K, Muzhikyan A, Sergeeva M, Romanovskaya-Romanko E, Shurygina AP, et al. IgGκ Signal Peptide Enhances the Efficacy of an Influenza Vector Vaccine against Respiratory Syncytial Virus Infection in Mice. Int J Mol Sci. 2023; 24 (14).
9. Dittmann M, Hoffmann HH, Scull MA, Gilmore RH, Bell KL, Ciancanelli M, et al. A serpin shapes the extracellular environment to prevent influenza a virus maturation. Cell [Internet]. 2015; 160 (4): 631–43. Available from: http://dx.doi.org/10.1016/j.cell.2015.01.040.
10. Oleinik V, Plotnikova M, Yolshin N, Romanovskaya-Romanko E. Development and approbation of a quantitative PCR system for studying the expression of endosomal receptors and cytosolic nucleic acid sensors in mice. Med Acad journal. 2025; 1 (1): 90–100.
11. Hoffmann E, Neumann G, Kawaoka Y, Hobom G, Webster RG. A DNA transfection system for generation of influenza A virus from eight plasmids. Proc Natl Acad Sci USA. 2000; 97 (11): 6108–13.
12. Yildiz S, El Zahed SS, Villalón-Letelier F, Wang Q, Yelleswarapu S, Dawodu G, et al. Re-engineering segment 8 facilitates generation of a versatile live-attenuated influenza A virus vector platform for secretory protein delivery. J Virol. 2026; 100 (5): e0034726.
13. Gaudino M, Lion A, Sagné E, Nagamine B, Oliva J, Terrier O, et al. The Activation of the RIG-I/MDA5 Signaling Pathway upon Influenza D Virus Infection Impairs the Pulmonary Proinflammatory Response Triggered by Mycoplasma bovis Superinfection. J Virol. 2023; 97 (2): e0142322.
14. Lin CC, Kuo CT, Cheng CY, Wu CY, Lee CW, Hsieh HL, et al. IL-1 beta promotes A549 cell migration via MAPKs/AP-1- and NF-kappaB-dependent matrix metalloproteinase-9 expression. Cell Signal. 2009; 21 (11): 1652–62.
15. Harioudh MK, Perez J, Chong Z, Nair S, So L, McCormick KD, et al. Oligoadenylate synthetase 1 displays dual antiviral mechanisms in driving translational shutdown and protecting interferon production. Immunity. 2024; 57 (3): 446–461.e7.
16. van Rikxoort M, Michaelis M, Wolschek M, Muster T, Egorov A, Seipelt J, et al. Oncolytic effects of a novel influenza A virus expressing interleukin-15 from the NS reading frame. PLoS One. 2012; 7 (5): e36506.
17. Ozhereleva O, Mustafaeva A, Pulkina A, Plotnikova M, Shuklina M, Shurygina AP, et al. A CXCL10-Expressing Influenza Vector Induces Robust Adaptive Immunity Despite Strong Attenuation. Pharmaceutics. 2026; 18 (6).
18. Kittel C, Ferko B, Kurz M, Voglauer R, Sereinig S, Romanova J, et al. Generation of an influenza A virus vector expressing biologically active human interleukin-2 from the NS gene segment. J Virol. 2005; 79 (16): 10672–7.

FTIR SIGNATURES OF PROTEIN CONFORMATIONAL CHANGES IN GINGIVAL CREVICULAR FLUID IN CHILDREN WITH CARIES AND GINGIVITIS

Seredin PV[1]✉, Ippolitov YuA[1,2], Ippolitov IYu[1,2], Goloshchapov DL[1], Litvinova TA[1]

[1] Voronezh State University, Voronezh, Russia
[2] Burdenko Voronezh State Medical University, Voronezh, Russia
[3] Belgorod State National Research University, Belgorod, Russia

The relevance of the study is associated with the search for minimally invasive molecular signatures of the dentogingival complex tissue condition in children. A pilot study aimed to identify spectral signatures of protein conformational changes in gingival crevicular fluid from children aged 8–14 years with dental caries and gingival inflammation (gingivitis) based on analysis of the IR spectral Amide III band in a pilot cohort. Gingival crevicular fluid samples collected from 20 children aged 8–14 years with different dental status were analyzed. FTIR spectra were acquired using synchrotron-based Fourier transform infrared spectroscopy in a Bruker Vertex 80/v spectrometer in the range of 3800–700 cm^{-1} with a focus on the Amide III region. Spectral deconvolution combined with multivariate analysis was used to estimate the contribution of protein secondary-structure elements. In the pilot cohort, dental caries was associated with a directed increase in the total contribution of components related to β-sheet structures. Based on the summed contributions of the main secondary structure elements, the β-sheet contribution exceeded 50% across the four analytical groups, the disordered component ranged approximately from 21 to 31%, and the contributions of β-turns and α-helical components remained below 10–11%. Inflammatory gingival changes showed a tendency toward a decreased contribution of β-turns and a relative increase in disordered conformations. Thus, the Amide III profile may reflect integral physicochemical changes in proteins of gingival crevicular fluid in individuals with caries and gingivitis. The reported features should be regarded as candidate spectral signatures of a hypothesis-generating nature that require further clinical validation.

Keywords: gingival crevicular fluid, Fourier transform infrared spectroscopy, Amide III band, protein secondary structure, spectral deconvolution, multivariate analysis, dental caries, gingivitis

Funding: the study was supported by the Russian Science Foundation, project No. 26-15-00389, https://rscf.ru/project/26-15-00389.

Acknowledgments: the authors express their gratitude to the staff of the Pohang Accelerator Laboratory synchrotron radiation-based infrared beamline (Pohang, Republic of Korea), where some experiments were conducted within the framework of the proposal 2023-1st-12D-001 IRS.

Author contribution: Seredin PV — study concept, methods, spectral data interpretation, manuscript writing; Ippolitov YuA — clinical design of the study, participant recruitment, dental patient examination; Ippolitov IYu — participant recruitment, dental patient examination; Goloshchapov DL — spectrum acquisition and processing, deconvolution and multivariate analysis; Litvinova TA — literature review, statistical processing, manuscript writing and editing.

Compliance with ethical standards: the study approved by the Ethics Committee of the Burdenko Voronezh State Medical University (protocol No. 3 dated March 24, 2026) was conducted in accordance with ethical standards and the World Medical Association Declaration of Helsinki (2013 update). The informed consent for participation in the study was obtained from legal representatives of all subjects.

✉ **Correspondence should be addressed:** Pavel V. Seredin
Universitetskaya pl. 1, Voronezh, 394018, Russia; paul@phys.vsu.ru

Received: 15.06.2026 **Accepted:** 21.07.2026 **Published online:** 31.07.2026

DOI: 10.24075/brsmu.2026.042

FTIR-ПРИЗНАКИ ПЕРЕСТРОЙКИ БЕЛКОВ ДЕСНЕВОЙ ЖИДКОСТИ У ДЕТЕЙ ПРИ КАРИЕСЕ И ГИНГИВИТЕ

П. В. Середин[1]✉, Ю. А. Ипполитов[1,2], И. Ю. Ипполитов[1,2], Д. Л. Голощапов[1], Т. А. Литвинова[1]

[1] Воронежский государственный университет, Воронеж, Россия
[2] Воронежский государственный медицинский университет имени Н. Н. Бурденко, Воронеж, Россия
[3] Белгородский государственный национальный исследовательский университет, Белгород, Россия

Актуальность исследования связана с поиском малоинвазивных молекулярных признаков состояния тканей зубодесневого комплекса у детей. Цель пилотного исследования — выявить в пилотной выборке спектральные признаки перестройки белков десневой жидкости у детей 8–14 лет при кариесе и воспалительных изменениях десны (гингивите) на основе анализа ИК-спектральной полосы Амид III. Проанализированы образцы десневой жидкости, полученные у 20 детей 8–14 лет с различным стоматологическим статусом. ИК-спектры регистрировали методом синхротронной ИК-Фурье-спектроскопии на спектрометре Bruker Vertex 80/v в диапазоне 3800–700 $см^{-1}$ с акцентом на область Амид III. Вклад элементов вторичной структуры белков оценивали с помощью деконволюции спектрального профиля и методов многомерного анализа. В пилотной выборке кариес ассоциировался с направленным увеличением суммарного вклада компонент, соответствующих β-складчатым структурам. По данным суммарной оценки основных элементов вторичной структуры, вклад β-складчатых компонентов во всех четырех аналитических группах превышал 50%, вклад неупорядоченных конформаций составлял примерно 21–31%, а вклад β-поворотов и α-спиральных компонент оставался менее 10–11%. При воспалительных изменениях десны отмечена тенденция к уменьшению вклада β-поворотов и относительному увеличению неупорядоченных конформаций. Таким образом, профиль полосы Амид III может отражать интегральные физико-химические изменения белков десневой жидкости при кариесе и гингивите. Выявленные особенности следует рассматривать как кандидатные спектральные признаки, имеющие гипотезо-генерирующий характер и требующие дальнейшей клинической проверки.

Ключевые слова: десневая жидкость, ИК-Фурье-спектроскопия, полоса Амид III, вторичная структура белков, деконволюция спектров, многомерный анализ, кариес, гингивит

Финансирование: исследование выполнено при финансовой поддержке Российского научного фонда, проект № 26-15-00389, https://rscf.ru/project/26-15-00389.

Благодарности: авторы благодарят сотрудников инфракрасной линии синхротронного излучения Pohang Accelerator Laboratory (Pohang, Republic of Korea), где часть экспериментов была выполнена в рамках proposal 2023-1st-12D-001 IRS.

Вклад авторов: П. В. Середин — концепция, методология, интерпретация спектральных данных, написание текста; Ю. А. Ипполитов — клинический дизайн, формирование выборки, стоматологическое обследование; И. Ю. Ипполитов — формирование выборки, стоматологическое обследование; Д. Л. Голощапов — регистрация и обработка спектров, деконволюция и многомерный анализ; Т. А. Литвинова — анализ литературы, статистическая обработка, подготовка и редактирование рукописи.

Соблюдение этических стандартов: исследование одобрено этическим комитетом ФГБОУ ВО ВГМУ имени Н. Н. Бурденко Минздрава России (протокол № 3 от 24 марта 2026 г.), выполнено в соответствии с этическими стандартами и Хельсинкской декларацией ВМА (2013 г.). От законных представителей участников получено добровольное информированное согласие на участие в исследовании.

✉ **Для корреспонденции:** Павел Владимирович Середин
Университетская площадь, д. 1, г. Воронеж, 394018, Россия; paul@phys.vsu.ru

Статья получена: 15.06.2026 **Статья принята к печати:** 21.07.2026 **Опубликована онлайн:** 31.07.2026

DOI: 10.24075/vrgmu.2026.042

Gingival crevicular fluid represents a local biological medium of the gingival sulcus reflecting the dentogingival complex tissue physicochemical state. The fluid composition is determined by proteins, peptides, components of inflammatory exudate, and tissue remodeling products, therefore it is suitable for spectroscopic analysis. In contrast to targeted biochemical methods, the Fourier transform infrared (FTIR) spectroscopy allows one to obtain integral molecular characteristics of low-volume samples and assess re-distribution of the contributions of various sample protein component conformations [1–4].

The issue is especially relevant for pediatric dentistry. However, the data on local molecular markers of gingival crevicular fluid in children is still limited. Current reviews show that inflammatory gingival changes are often found in children and adolescents, and the tissue state is further affected by age, dentition stage, pubertal changes, plaque levels, and orthodontic load [5–7]. In this regard, gingival crevicular fluid is of interest as a minimally invasive test substrate that can be re-collected and correlated with a certain dentogingival complex region [1, 5–6]. In theory, microbial factors, local proteolysis, oxidative stress, and inflammatory remodeling processes that change the composition and conformational state of proteins in gingival crevicular fluid can have an effect on such spectral shifts.

The region of the Amide III band that is sensitive to the contribution of α-helical, β-sheet, β-turn, and disordered structures is of special interest for analysis of the protein component. Compared with the Amide I and Amide II regions, its interpretation is less complicated by the influence of water and hydrogen-bonded background, which is especially important when assessing low volumes of hydrogen-containing biological media, including gingival crevicular fluid [4, 8–10]. At the same time, to correctly interpret the protein system spectra in this region it is necessary to consider the IR band overlap, select the pre-processing scheme and deconvolution parameters [4, 8–10]. That is why, in complex biological media, it is reasonable to consider not single peaks as direct markers, but the integrated spectral profile as a reflection of the directed protein component changes [4, 8].

Such studies are further limited by small sample size, so it is required to use multivariate analysis methods adjusted to spectral data and the limited number of observations. Previously it was shown that multivariate analysis of the gingival crevicular fluid IR spectra allowed one to identify the underlying patterns associated with the patient's clinical status and individual characteristics [11]. This makes the combination of the Amide III band deconvolution with multivariate statistical analysis a promising approach to assessment of the directional changes in the secondary structure of proteins in gingival crevicular fluid [11].

We proceeded from the working hypothesis that in children with caries and gingival inflammation the gingival crevicular fluid Amide III band profile would change directionally through redistribution of the spectral-associated components related to various secondary protein structure elements. The study aimed to identify such directional changes in the Amide III band spectral profile and assess the possibility of considering those as candidate spectral signatures of changes in the gingival crevicular fluid protein component.

METHODS

Research design and characteristics of the sample

A total of 20 children aged 8–14 years, from whom gingival crevicular fluid was collected after the dental examination, were included in the study. Inclusion criteria: age 8–14 years; availability of the legal representative's informed consent; possibility of standard dental examination and gingival crevicular fluid collection; no antimicrobial or other therapy capable of significantly affecting the test biological medium composition at the time of examination. Exclusion criteria: other age and non-compliance with the inclusion criteria. It was a pilot single-center study. Since some patients had a combination of clinical factors, the study was focused primarily on identifying the spectral shift directional nature, not on the rigorous assessment of the independent contribution of each factor.

The dental caries status was assessed clinically; groups with no clinical signs of caries, early caries lesions, and multiple caries lesions were allocated. The gingival state was characterized based on the presence and severity of inflammatory changes as no clinically significant changes, mild or moderate inflammation. Comorbid medical conditions were taken into account based on the medical history and medical records. Four analytical groups were allocated for in-depth comparison of spectral profiles and their deconvolution (Table).

Gingival crevicular fluid sampling

The protein component of gingival crevicular fluid, the complex multicomponent biological medium locally associated with the dentogingival interface tissues, was a research object. Sampling was performed at the Department of Pediatric Dentistry and Orthodontics of the Burdenko Voronezh State Medical University (Voronezh, Russia). Gingival crevicular fluid was collected in the morning without prior stimulation using microcapillaries. Such a sampling regime minimized the effects of circadian oscillation and ensured comparability of spectrum acquisition conditions [12]. After collection samples were placed in sterile containers and stored at a temperature of 1–2 °C prior to spectroscopic analysis within the same pre-analytical regime.

Fourier transform infrared spectroscopy

IR spectra were acquired by synchrotron-based Fourier transform infrared spectroscopy using the Bruker Vertex 80/v vacuum spectrometer (Bruker Optik GmbH, Ettlingen, Germany) in the range of 3800–700 cm^{-1}. The Amide III band was considered as the main range, since it allowed one to analyze conformational features of the protein component with the less methodological dependence on the water

Table. Description of four analytical groups of gingival crevicular fluid samples included in deconvolution of Amide III spectral profiles

Internal code of the analytical group	Sex	Age subgroup	Dental caries stage	Gingival inflammation	Comorbid condition
FYNNN	F	Younger (Y)	No caries (N)	No gingival inflammation (N)	No comorbidity (N)
FAENN	F	Adolescent (A)	Early caries (E)	No gingival inflammation (N)	No comorbidity (N)
FAEMO	F	Adolescent (A)	Early caries (E)	Moderate inflammation (M)	Oncological disease (O)
MAMLG	M	Adolescent (A)	Multiple caries (M)	Mild gingival inflammation (L)	Gastrointestinal disease (F)

Note: The analytical group internal code consists of five symbols: 1st — sex, 2nd — age subgroup, 3rd — caries status, 4th — gingival state, 5th — comorbid condition.

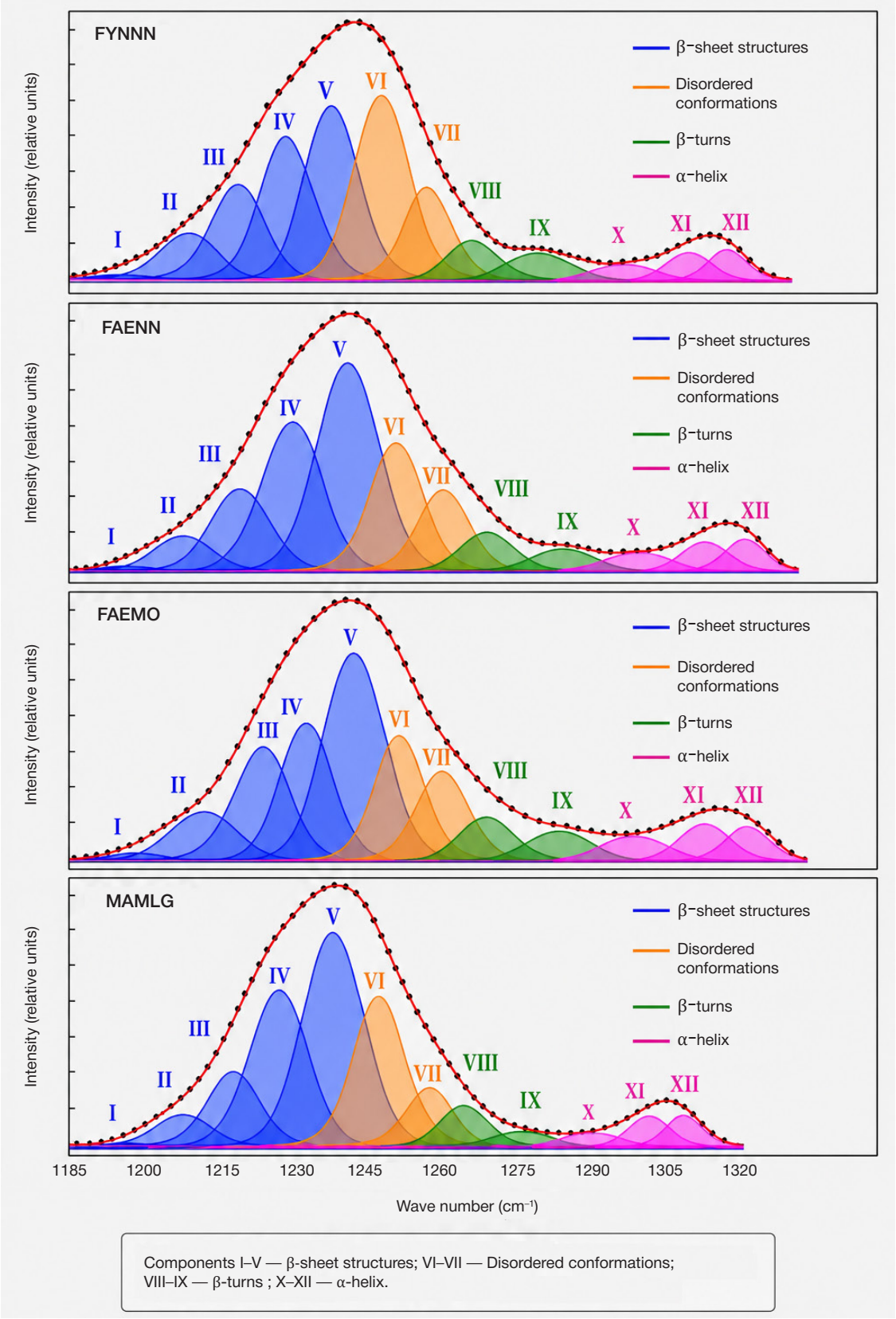

Fig. 1. Deconvolution of the gingival crevicular fluid Amide III band spectral profile in children aged 8–14 years with various clinical statuses. Internal codes of the samples are provided in Table 1. Components I–V in the spectral profile are correlated to β-sheet structures, VI–VII — to disordered conformations, VIII–IX — to β-turns, X–XII — to α-helical components

background compared to the Amide I and Amide II regions [4, 8–10]. Standard acquisition parameters were used in the initial experimental cycle: spectral resolution 4 cm^{-1}, 3-term Blackman–Harris apodization, Mertz phase correction, and the zero filling coefficient of 2. The contents of each sample were divided into ten portions, for each of which a distinct IR spectrum was acquired; the spectral profile was further characterized based on the average data.

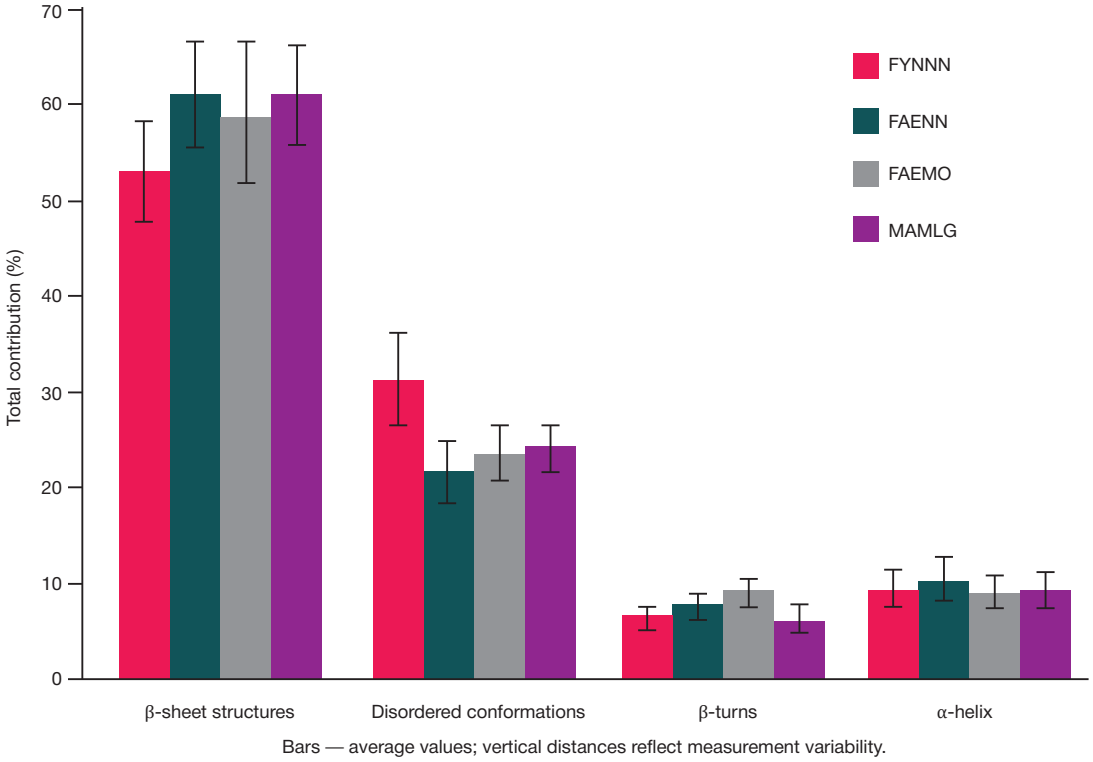

Fig. 2. Relative contribution of the main secondary structure elements of gingival crevicular fluid proteins in the integral profile of the Amide III band

Spectrum pre-processing and deconvolution

Primary processing of IR spectra included smoothing of the curves using a Savitzky–Golay filter with a polynomial order of 2 and window length of 25 points. Baseline correction was performed by the asymmetric least squares method in the range of 4000–500 cm^{-1} with the threshold value of 0.01 and asymmetry factor of about 0.001. The pre-processing parameters were selected in such a way as to reduce smoothing and baseline correction artifacts preserving sensitivity to the Amide III band shape alteration.

To quantitatively describe the Amide III band profile, deconvolution with isolation of the components correlated to α-helical, β-sheet, β-turn, and disordered conformations was performed. Gaussian functions were used for approximation. Preliminary search for balance centers and bandwidth at half-height was carried out using the 2nd and 4th derivatives of the smoothed spectra. Further modeling was accomplished in Fityk v.1.3.1 (developed by M. Wojdyr, Poland) using the Levenberg–Marquardt algorithm. To ensure comparability of results, the same number of components was maintained in all samples. Box constraints were used in the modeling: ± 2 cm^{-1} for maxima positions, 7–10 cm^{-1} for FWHM values. The best fit between theoretical and experimental curves based on the χ^2 test was used as an approximation termination criterion. The resulting components were considered as spectral-associated contributions, not direct absolute measures of the content of appropriate secondary structures [4, 8–10]. Components I–XII were correlated with the protein secondary structure elements based on the earlier published data on interpretation of the Amide III band and ranges of maxima of the corresponding IR bands [4, 8–10]. The selected box constraints were set within the ranges ensuring stability of approximation and consistence with the ranges of maxima positions and bandwidths for the Amide III band reported in the literature [4, 8–10]. The same number of components, the same box constraints, and the same approximation scheme for all samples were used to improve reproducibility and comparability of deconvolution results.

Multivariate and statistical analysis

After pre-processing the spectral data set was analyzed by the principal components method to assess relative positions of samples in the multidimensional space and interpret the correlations between spectral variability and clinical factors. Spectral intensities in the Amide III band region were used as quantitative variables, and characteristics of patients were considered as categorical traits used in the phase of interpretation. The FactoMineR software package for R was used for analysis, and the factoextra package was used for visualization. At this stage it was determined, which clinical factors were most strongly associated with the main directions of spectral variability, and the proximity of samples in the principal component space was assessed. In the phase of interpretation we also assessed how the levels of categorical clinical traits correlated with the sample positions and the main directions of spectral variability identified by the method of principal components. Categorical clinical traits were not included in the model as covariates; these were used for clinical interpretation of sample distribution in the principal component space, which was consistent with the pilot design of the study.

In the next phase, after identifying the key factors of variability, samples were selected for further deconvolution of spectral profiles, and the exploratory pairwise comparison was performed. For that the BSDA package and the tsum.test with Bonferroni correction for multiple comparisons were used. The analysis was conducted with the significance level of 0.05.

RESULTS

Amide III band spectral profile

In the Amide III band region, the gingival crevicular fluid samples were characterized by the complex multi-component contour formed by the overlapping bands belonging to different conformations (Fig. 1). That is why the integral

intensity was only partially informative, while re-distribution of the contributions of distinct spectral components within the common profile turned out to be a more meaningful parameter. The components correlated to β-sheet structures and disordered conformations were the main contributors to the integral intensity; the contribution of α-helical components was less pronounced [8–10]. Based on the summed contributions of the main secondary structure elements (Fig. 2), the β-sheet component contribution exceeded 50% across the four analytical groups, the contribution of disordered conformations was approximately 21–31%, while the contributions of β-turns and α-helical components remained below 10–11%. The key clinical characteristics of the test groups are provided in Table, and a typical deconvolution profile is presented in Fig. 1. In Fig. 2, bars represent the average values of total contributions and vertical distances represent the measurement variability. The multivariate analysis data were used to select four analytical groups; the revealed spectral heterogeneity of samples was generally consistent with the directional nature of shifts determined during further deconvolution of the Amide III band. Partial delineation of analytical groups was observed in the first principal component space, which was generally consistent with the subsequent differences in total contributions of β-sheet components and β-turns.

Internal codes of the samples are provided in Table. Components I–V in the spectral profile are correlated to β-sheet structures, VI–VII to disordered conformations, VIII–IX to β-turns, X–XII to α-helical components. Such distribution was also given in the explanatory block of Fig. 1 to make the graphic material interpretation easier.

Spectral shifts associated with caries

In the pilot cohort, the directed increase in the relative contribution of the components associated with β-sheet structures in samples from children with caries was the most stable feature. The total contribution of β-sheet components reached approximately 59–61% in the groups with caries vs. approximately 53% in the group without any clinically significant dental alterations (Fig. 2). This shift had the same direction across different combinations of associated clinical features, although its magnitude varied from comparison to comparison. In this study, it is correct to consider such a result not as a diagnostic criterion, but a candidate spectral signature of changes in the gingival crevicular fluid protein component [11, 13–14].

As for its direction, this observation is consistent with the literature data on the Fourier transform infrared spectroscopy of the Amide III band region in adults, where β-sheet components were also described as the most stable shift associated with dental caries [11, 13–14]. However, the same direction does not mean equivalent conclusions: the adult and pediatric cohorts are different in age, clinical context, and the set of confounding factors. Therefore, it is about the preliminary cross-study consistency, not the full-fledged external replication.

Spectral shifts associated with the periodontal tissue inflammatory changes

Individuals with inflammatory gingival changes showed a tendency toward a decreased contribution of β-turns and a relative increase in disordered conformations. In the research set, the share of β-turns remained low and did not exceed approximately 10%, while the contribution of disordered conformations was within the range of about 21–24% for groups with inflammatory gingival changes. From the physicochemical point of view, such a shift can reflect changes in the protein component composition, enhanced proteolytic activity, and the increased share of the structurally less organized protein states in the local inflammatory remodeling medium [2–3, 15].

International data on the gingival crevicular fluid composition analysis by molecular identification methods support this common logic: when there is periodontal disease, samples may have different molecular profiles, and changes in cytokines, metalloproteinases, and matrix proteins turn out to be significant [2–3, 15–16]. In this study, the spectral shifts identified should be interpreted as an integral signal of the inflammatory remodeling medium, not as the characteristics of distinct target proteins or protein panels.

Comorbid medical conditions

The decrease in the contribution of α-helical components was reported in some children with comorbid medical conditions. Biologically, such a shift is possible, since the "α-helix/β-sheet structure" type ratio in protein samples was described for various diseases and stress conditions [4, 17–18]. However, considering small sample size and the combination of clinical factors, such a result should be interpreted as an observational trend, not a proven independent effect of the comorbid condition. In the context of children's gingival crevicular fluid, the Fourier transform infrared analysis should be considered as an integral molecular profiling method, not a substitute for target protein panels [4, 17–18]. The distribution of contributions of the main secondary protein structure elements is presented in Fig. 2.

DISCUSSION

The data obtained suggest that the Amide III band profile in gingival crevicular fluid should be considered primarily as integral spectral characteristics of a complex protein mixture, not a direct quantitative measure of the contents of distinct secondary structures. That is why interpretation of the results should take into account the limitations associated with the band overlap, pre-processing scheme, and the deconvolution model used [4, 8–10].

The directional increase in the contribution of β-sheet components in individuals with caries is consistent with the ones earlier reported in papers about IR spectroscopy of oral biological media, it expands these results to the pediatric cohort [11, 13–14]. Such a trend can reflect changes in the ratio of more organized to less organized protein states in the context of the local caries process. In turn, the trend towards lower contribution of β-turns and relative increase in disordered conformations associated with inflammatory gingival changes is biologically credible and consistent with modern views of the gingival crevicular fluid molecular profile rearrangement in the inflammatory remodeling medium [1–3, 15–16].

Thus, in this study, multivariate analysis and deconvolution of the spectral Amide III band had mutually reinforcing functions: PCA was used to detect the general spectral heterogeneity and select analytical groups, while deconvolution made it possible to interpret such variability through rearrangement of the Amide III band component contributions. Such alignment of two approaches increases evidentiality of the identified directional shifts, but due to pilot design does not replace their further clinical testing.

Limitations of the study

Interpretation of the detected shifts is limited by the clinical heterogeneity of observations and the fact that deconvolution results depend on the spectrum pre-processing algorithms [4, 8]. Furthermore, in the cohort of children, the gingival crevicular fluid composition is potentially affected by age, dentition stage, orthodontic load, and pubertal changes [5–7]. Features of the pre-analytical phase, including material volume and time between sampling and spectrum acquisition, could be other sources of variability. Finally, in this pilot study, comorbid medical conditions were not analyzed as an independent factor. That is why the features identified should be considered as hypothesis-generating and requiring further validation using the expanded clinically stratified material. One more limitation is that in this pilot study the dental caries status and the gingival inflammation severity were described by the exploratory clinical stratification, not the expanded index assessment, which should be taken into account when interpreting the results.

CONCLUSIONS

The analysis of the gingival crevicular fluid Amide III band in children aged 8–14 years made it possible to identify differences in the protein component IR spectral profile depending on the dental status. In the pilot cohort, caries was associated with the larger contribution of β-sheet structures, and inflammatory gingival changes were associated with the trend towards growing disordered conformations and lower contribution of β-turns. Thus, the analysis of the Amide III IR spectral band can be useful as a research approach to assessment of molecular changes in gingival crevicular fluid, but its clinical significance needs to be further confirmed.

References

1. Cuevas-González MV, Cuevas-González JC, Espinosa-Cristóbal LF, Tovar-Carrillo KL, Saucedo-Acuña RA, García-Calderón AG, et al. The potential of gingival crevicular fluid as a tool for molecular diagnosis: a systematic review. Biomed Res Int. 2024; 2024: 5560866. DOI: 10.1155/2024/5560866.
2. Buduneli N, Bıyıkoğlu B, Kinane DF. Utility of gingival crevicular fluid components for periodontal diagnosis. Periodontol 2000. 2024; 95 (1): 156–75. DOI: 10.1111/prd.12595.
3. Torres A, Michea MA, Végvári Á, Arce M, Pérez V, Alcota M, et al. A multi-platform analysis of human gingival crevicular fluid reveals ferroptosis as a relevant regulated cell death mechanism during the clinical progression of periodontitis. Int J Oral Sci. 2024; 16 (1): 43. DOI: 10.1038/s41368-024-00306-y.
4. Tintor Đ, Ninković K, Milošević J, Polović NĐ. Gaining insight into protein structure via ATR-FTIR spectroscopy. Vib Spectrosc. 2024; 134: 103726. DOI: 10.1016/j.vibspec.2024.103726.
5. American Academy of Pediatric Dentistry. Periodontal conditions in pediatric dental patients. In: The Reference Manual of Pediatric Dentistry. Chicago (IL): American Academy of Pediatric Dentistry, 2025; p. 527–44.
6. Deng Q, Wong HM, Peng S. Salivary and gingival crevicular fluid biomarkers of periodontal health and/or obesity among children and adolescents: a systematic review and meta-analysis. Heliyon. 2024; 10 (1): e23782. DOI: 10.1016/j.heliyon.2023.e23782.
7. Iwamoto Y, Mitsuhata C, Ikeda S, Ito Y, Hamaguchi S, Tabata E, et al. Development of a novel method to evaluate gingivitis in children by combining rapid saliva test systems. Sci Rep. 2025; 15: 41033. DOI: 10.1038/s41598-025-24982-w.
8. De Meutter J, Goormaghtigh E. Searching for a better match between protein secondary structure definitions and protein FTIR spectra. Anal Chem. 2021; 93 (3): 1561–8. DOI: 10.1021/acs.analchem.0c03943.
9. Cai S, Singh BR. Identification of beta-turn and random coil amide III infrared bands for secondary structure estimation of proteins. Biophys Chem. 1999; 80 (1): 7–20. DOI: 10.1016/S0301-4622(99)00060-5.
10. Stani C, Vaccari L, Mitri E, Birarda G. FTIR investigation of the secondary structure of type I collagen: new insight into the amide III band. Spectrochim Acta A Mol Biomol Spectrosc. 2020; 229: 118006. DOI: 10.1016/j.saa.2019.118006.
11. Seredin P, Litvinova T, Ippolitov Y, Goloshchapov D, Peshkov Y, Kashkarov V, et al. A study of the association between primary oral pathologies (dental caries and periodontal diseases) using synchrotron molecular FTIR spectroscopy in view of the patient's personalized clinical picture (demographics and anamnesis). Int J Mol Sci. 2024; 25 (12): 6395. DOI: 10.3390/ijms25126395.
12. Papagerakis P, Zheng L, Kim D, Said R, Ehlert AA, Chung KKM, et al. Saliva and gingival crevicular fluid collection for biomarker screening. In: Papagerakis P, editor. Odontogenesis: Methods and Protocols. New York: Springer, 2019; p. 549–62. DOI: 10.1007/978-1-4939-9012-2_41.
13. Seredin P, Goloshchapov D, Ippolitov Y, Vongsvivut J. Comparative analysis of dentine and gingival fluid molecular composition and protein conformations during development of dentine caries: a pilot study. Vib Spectrosc. 2020; 108: 103058. DOI: 10.1016/j.vibspec.2020.103058.
14. Seredin P, Goloshchapov D, Ippolitov Y, Vongsvivut J. Spectroscopic signature of the pathological processes of carious dentine based on FTIR investigations of the oral biological fluids. Biomed Opt Express. 2019; 10 (8): 4050–8. DOI: 10.1364/BOE.10.004050.
15. Teles F, Martin L, Patel M, Hu W, Bittinger K, Kallan MJ, et al. Gingival crevicular fluid biomarkers during periodontitis progression and after periodontal treatment. J Clin Periodontol. 2025; 52 (1): 40–55. DOI: 10.1111/jcpe.14061.
16. Esberg A, Kindstedt E, Isehed C, Lindquist S, Holmlund A, Lundberg P. LIGHT protein: a novel gingival crevicular fluid biomarker associated with increased probing depth after periodontal surgery. J Clin Periodontol. 2024; 51 (7): 852–62. DOI: 10.1111/jcpe.13964.
17. Portaccio M, d'Apuzzo F, Perillo L, Grassia V, Errico S, Lepore M. Infrared microspectroscopy characterization of gingival crevicular fluid during orthodontic treatment. J Mol Struct. 2019; 1176: 847–54. DOI: 10.1016/j.molstruc.2018.09.013.
18. Lepore M, Portaccio M, d'Apuzzo F, Nucci L, Grassia V, Annunziata M, et al. Rapid acquisition of gingival crevicular fluid FT-IR spectra for monitoring orthodontic treatments. In: 2024 IEEE Sensors Applications Symposium (SAS), 2024; p. 1–5. DOI: 10.1109/SAS60918.2024.10636387.

Литература

1. Cuevas-González MV, Cuevas-González JC, Espinosa-Cristóbal LF, Tovar-Carrillo KL, Saucedo-Acuña RA, García-Calderón AG, et al. The potential of gingival crevicular fluid as a tool for molecular diagnosis: a systematic review. Biomed Res Int. 2024; 2024: 5560866. DOI: 10.1155/2024/5560866.
2. Buduneli N, Bıyıkoğlu B, Kinane DF. Utility of gingival crevicular fluid components for periodontal diagnosis. Periodontol 2000. 2024; 95 (1): 156–75. DOI: 10.1111/prd.12595.
3. Torres A, Michea MA, Végvári Á, Arce M, Pérez V, Alcota M, et al. A multi-platform analysis of human gingival crevicular fluid reveals

ferroptosis as a relevant regulated cell death mechanism during the clinical progression of periodontitis. Int J Oral Sci. 2024; 16 (1): 43. DOI: 10.1038/s41368-024-00306-y.
4. Tintor Đ, Ninković K, Milošević J, Polović NĐ. Gaining insight into protein structure via ATR-FTIR spectroscopy. Vib Spectrosc. 2024; 134: 103726. DOI: 10.1016/j.vibspec.2024.103726.
5. American Academy of Pediatric Dentistry. Periodontal conditions in pediatric dental patients. In: The Reference Manual of Pediatric Dentistry. Chicago (IL): American Academy of Pediatric Dentistry, 2025; p. 527–44.
6. Deng Q, Wong HM, Peng S. Salivary and gingival crevicular fluid biomarkers of periodontal health and/or obesity among children and adolescents: a systematic review and meta-analysis. Heliyon. 2024; 10 (1): e23782. DOI: 10.1016/j.heliyon.2023.e23782.
7. Iwamoto Y, Mitsuhata C, Ikeda S, Ito Y, Hamaguchi S, Tabata E, et al. Development of a novel method to evaluate gingivitis in children by combining rapid saliva test systems. Sci Rep. 2025; 15: 41033. DOI: 10.1038/s41598-025-24982-w.
8. De Meutter J, Goormaghtigh E. Searching for a better match between protein secondary structure definitions and protein FTIR spectra. Anal Chem. 2021; 93 (3): 1561–8. DOI: 10.1021/acs.analchem.0c03943.
9. Cai S, Singh BR. Identification of beta-turn and random coil amide III infrared bands for secondary structure estimation of proteins. Biophys Chem. 1999; 80 (1): 7–20. DOI: 10.1016/S0301-4622(99)00060-5.
10. Stani C, Vaccari L, Mitri E, Birarda G. FTIR investigation of the secondary structure of type I collagen: new insight into the amide III band. Spectrochim Acta A Mol Biomol Spectrosc. 2020; 229: 118006. DOI: 10.1016/j.saa.2019.118006.
11. Seredin P, Litvinova T, Ippolitov Y, Goloshchapov D, Peshkov Y, Kashkarov V, et al. A study of the association between primary oral pathologies (dental caries and periodontal diseases) using synchrotron molecular FTIR spectroscopy in view of the patient's personalized clinical picture (demographics and anamnesis). Int J Mol Sci. 2024; 25 (12): 6395. DOI: 10.3390/ijms25126395.
12. Papagerakis P, Zheng L, Kim D, Said R, Ehlert AA, Chung KKM, et al. Saliva and gingival crevicular fluid collection for biomarker screening. In: Papagerakis P, editor. Odontogenesis: Methods and Protocols. New York: Springer, 2019; p. 549–62. DOI: 10.1007/978-1-4939-9012-2_41.
13. Seredin P, Goloshchapov D, Ippolitov Y, Vongsvivut J. Comparative analysis of dentine and gingival fluid molecular composition and protein conformations during development of dentine caries: a pilot study. Vib Spectrosc. 2020; 108: 103058. DOI: 10.1016/j.vibspec.2020.103058.
14. Seredin P, Goloshchapov D, Ippolitov Y, Vongsvivut J. Spectroscopic signature of the pathological processes of carious dentine based on FTIR investigations of the oral biological fluids. Biomed Opt Express. 2019; 10 (8): 4050–8. DOI: 10.1364/BOE.10.004050.
15. Teles F, Martin L, Patel M, Hu W, Bittinger K, Kallan MJ, et al. Gingival crevicular fluid biomarkers during periodontitis progression and after periodontal treatment. J Clin Periodontol. 2025; 52 (1): 40–55. DOI: 10.1111/jcpe.14061.
16. Esberg A, Kindstedt E, Isehed C, Lindquist S, Holmlund A, Lundberg P. LIGHT protein: a novel gingival crevicular fluid biomarker associated with increased probing depth after periodontal surgery. J Clin Periodontol. 2024; 51 (7): 852–62. DOI: 10.1111/jcpe.13964.
17. Portaccio M, d'Apuzzo F, Perillo L, Grassia V, Errico S, Lepore M. Infrared microspectroscopy characterization of gingival crevicular fluid during orthodontic treatment. J Mol Struct. 2019; 1176: 847–54. DOI: 10.1016/j.molstruc.2018.09.013.
18. Lepore M, Portaccio M, d'Apuzzo F, Nucci L, Grassia V, Annunziata M, et al. Rapid acquisition of gingival crevicular fluid FT-IR spectra for monitoring orthodontic treatments. In: 2024 IEEE Sensors Applications Symposium (SAS), 2024; p. 1–5. DOI: 10.1109/SAS60918.2024.10636387.

CHRONIC FATIGUE IN SIBLINGS OF PEDIATRIC CANCER SURVIVORS: CHILDREN'S SELF-REPORTS AND PARENTS' PROXY-REPORTS

Likhomanova EN[1,2] ✉, Shevaldova OV[1], Kovaleva AV[1]

[1] Federal Research Center for Innovator and Emerging Biomedical and Pharmaceutical Technologies, Moscow, Russia

[2] Dmitry Rogachev National Medical Research Center of Pediatric Hematology, Oncology and Immunology, Moscow, Russia

The psychological effects of childhood cancer and its treatment extend to all family members, particularly healthy siblings, of the affected child. Previous studies have reported reduced quality of life and self-esteem, as well as increased death anxiety and loneliness, among these children. This study aimed to compare the severity of chronic fatigue in siblings of children with cancer and in children from families without a seriously ill family member, with consideration of the informant: the child's self-report or the parent's proxy report. A total of 113 parent–child dyads participated in this controlled cross-sectional study. The sibling group comprised 65 healthy children whose brother or sister had cancer, and the control group comprised 48 children from families without a seriously ill family member. The groups were matched for the children's sex and age (7–11 years). Chronic fatigue was assessed using the Chronic Fatigue Severity Questionnaire. Linear mixed-effects models revealed a significant group × informant interaction ($p < 0.001$). In the control group, parents rated fatigue severity lower ($\Delta = -10$ points) than did the children themselves. In the sibling group, parental ratings were comparable to or higher than the children's self-ratings ($\Delta = 2$ points, $p < 0.001$). Parent–child agreement was stronger in the sibling group ($r = 0.73$, $p < 0.001$) than in the control group ($r = 0.34$, $p = 0.019$). No between-group differences were found in the total fatigue scores based on the children's self-reports. Siblings reported greater physiological discomfort ($p = 0.037$), but less decline in general well-being, cognitive comfort, and social functioning than controls (all $p < 0.001$). The results suggest that in families of children with cancer, parental assessments of a healthy child's fatigue differ from the child's own perception of their condition. Parents tend to rate fatigue as more severe than do the children themselves, whereas the opposite pattern is observed in control families. This informant discrepancy should be considered when assessing the well-being of healthy siblings and when providing psychological support to families affected by childhood cancer.

Keywords: chronic fatigue, siblings, parents, family stress, pediatric cancer, rehabilitation

Funding: RSF grant No. 25-25-00898 "Psycho-Physiological Indicators of Healthy Siblings' (Brothers' and Sisters') Adaptation in Families of Children With Cancer".

Acknowledgments: the authors express their gratitude to A.F. Karelin for the opportunity to conduct the study at the Russkoye Pole Treatment and Rehabilitation Research Center (Dmitry Rogachev National Medical Research Center of Pediatric Hematology, Oncology and Immunology) and A.A. Devyaterikova for the expert opinion about the manuscript.

Author contribution: Likhomanova EN — conceptualization, methodology, research procedure, data processing, manuscript editing; Shevaldova OV — statistical analysis, preparation of illustrations for the article, manuscript writing; Kovaleva AV — project management, administration, manuscript editing.

Compliance with ethical standards: the study was approved by the Ethics Committee of the Anokhin Research Institute of Normal Physiology (protocol No. 18/1 dated February 15, 2023), as well as the Ethics Committee of the Dmitry Rogachev National Medical Research Center of Pediatric Hematology, Oncology and Immunology (protocol No. 8э/16-17 dated October 27, 2017). The children's parents submitted the informed consent to take part in the study.

✉ **Correspondence should be addressed:** Elena N. Likhomanova
Baltijskaya, 8, Moscow, 125315; likhomanova_en@academpharm.ru

Received: 03.06.2026 **Accepted:** 29.06.2026 **Published online:** 18.07.2026

DOI: 10.24075/brsmu.2026.040

ХРОНИЧЕСКОЕ УТОМЛЕНИЕ У СИБЛИНГОВ ДЕТЕЙ С ОНКОЛОГИЧЕСКИМИ ЗАБОЛЕВАНИЯМИ: САМООТЧЕТЫ ДЕТЕЙ И НАБЛЮДЕНИЯ РОДИТЕЛЕЙ

Е. Н. Лихоманова[1,2] ✉, О. В. Шевалдова[1], А. В. Ковалева[1]

[1] Федеральный исследовательский центр оригинальных и перспективных биомедицинских и фармацевтических технологий, Москва, Россия

[2] Национальный медицинский исследовательский центр детской гематологии, онкологии и иммунологии имени Д. Рогачева, Москва, Россия

Психологические последствия лечения онкологического заболевания ребенка затрагивают всех членов семьи, в частности здоровых братьев и сестер (сиблингов). Известно о снижении качества их жизни, самооценки, страхе смерти и одиночества. Цель исследования — сравнить уровень хронического утомления у сиблингов детей с онкологическими заболеваниями и у детей из семей без тяжелобольных близких в зависимости от информанта: по данным самооценки ребенка и наблюдения родителя. В поперечном контролируемом исследовании заполняли опросник «Степень хронического утомления» 113 диад «родитель–ребенок»: 65 пар, где есть второй больной ребенок (группа сиблингов), и 48 контрольных пар. Группы были сопоставимы по полу и возрасту детей (7–11 лет). Линейными смешанными моделями выявлено значимое взаимодействие «группа × информант» ($p < 0{,}001$). В контроле родители занижали уровень утомления в сравнении с самооценкой детей (–10 балла), а у сиблингов родительские оценки были сопоставимы с детскими или превышали их по большинству шкал, кроме социальной сферы ($\Delta = 2$ балла, $p < 0{,}001$). Внутренняя корреляция в группе сиблингов оказалась сильнее ($r = 0{,}73$, $p < 0{,}001$), чем в контрольной ($r = 0{,}34$, $p = 0{,}019$). Межгрупповые самооценки детей по общему баллу не различались, но у сиблингов выраженность физиологического дискомфорта была выше ($p = 0{,}037$), а снижение общего самочувствия, когнитивного дискомфорта и нарушения в социальной сфере — ниже ($p < 0{,}001$). Вывод: в семьях с тяжелобольным ребенком родители систематически завышают уровень утомления здорового ребенка, а сами дети оценивают свое состояние иначе. Это расхождение необходимо учитывать при медико-психологическом сопровождении семей.

Ключевые слова: хроническое утомление, сиблинги, родители, семейный стресс, детская онкология, реабилитация

Финансирование: грант РНФ № 25-25-00898 «Психофизиологические индикаторы адаптации здоровых сиблингов (братьев и сестер) в семьях детей с онкологическими заболеваниями».

Благодарности: А. Ф. Карелину за возможность проведения исследования на базе ЛРНЦ «Русское поле» НМИЦ ДГОИ имени Д. Рогачева и А. А. Девятериковой за экспертную оценку рукописи.

Вклад авторов: Е. Н. Лихоманова — концептуализация, методология, проведение исследования, обработка данных, редактирование; О. В. Шевалдова — статистический анализ, подготовка иллюстраций, написание рукописи; А. В. Ковалева — руководство проектом, администрирование, редактирование.

Соблюдение этических стандартов: исследование было одобрено этическим комитетом ФГБНУ «НИИ нормальной физиологии имени П. К. Анохина» (протокол № 18/1 от 15 февраля 2023 г.), а также этическим комитетом ФГБУ «НМИЦ ДГОИ им. Д. Рогачева» (протокол № 8э/16-17 от 27 октября 2017 г.). Родители детей подписали добровольное информированное согласие на участие в исследовании.

✉ **Для корреспонденции:** Елена Николаевна Лихоманова
ул. Балтийская, д. 8, г. Москва, 125315; likhomanova_en@academpharm.ru

Статья получена: 03.06.2026 **Статья принята к печати:** 29.06.2026 **Опубликована онлайн:** 18.07.2026

DOI: 10.24075/vrgmu.2026.040

Malignant neoplasms (MNs) are among the leading causes of mortality in children. In Russia, in 2024, MNs were reported in 0.013% of the population aged 0–17 years (12.7 cases per 100,000 population); of these cases, 32.4% were stage I–II MNs, and the incidence peaked in children under 4 years of age [1]. In 2022, the global incidence exceeded 211,000 cases per year [2]. Russian population-based studies have reported a steady increase in the survival rate of children with cancer, from 82.4% in 2000 to 89.0% in 2021 [3], reaching 95% for certain types of cancer [4]. In this context, the focus of researchers and clinicians has shifted to the future quality of life of both patients and their families [5].

The consequences of childhood cancer affect every family member. The family's usual way of life and distribution of responsibilities change, and family income often decreases [6–9]. In this situation, healthy brothers and sisters of the affected child (siblings) require particular attention. Their difficulties often go unnoticed: parents who are focused on the affected child may be unable to adequately monitor the well-being of their other children, while clinicians usually do not work directly with them [10, 11]. Although the mean anxiety and depression scores of most siblings remain within age-appropriate ranges, many experience symptoms of post-traumatic stress, reduced quality of life, and problems at school [10]. According to studies conducted by Russian-speaking authors, low self-esteem, fear of death, loneliness, auto-aggression, and anxiety are common among siblings [12, 13]. With regard to somatic problems, siblings have been reported to have higher rates of pain complaints, sleep and eating problems [14], and emergency department visits [15], which may reflect allostatic load, that is, persistent physiological alterations caused by chronic stress [16]. A study involving a large cohort of families with seriously ill children showed that healthy members of such families sought medical care significantly more often, regardless of sex [5].

The feeling of persistently increased fatigue is one of the common manifestations of accumulated stress [5, 15]. In this paper, fatigue is considered not as a clinical diagnosis, but as a subjective feeling of reduced energy — a persistent feeling that children are able to describe themselves. Fatigue can affect physical well-being, emotional state, cognitive functioning, and social motivation. The reliability of such self-assessment in school-age children (from approximately 7–8 years of age) has been confirmed in numerous studies [17, 18].

Parents' proxy reports (parents' perceptions of their children's condition) are widely used in clinical practice and scientific research alongside children's self-reports. Comparing these two sources of information represents a separate scientific issue. Studies involving children undergoing cancer treatment have shown that parents tend to systematically rate their children's fatigue as more severe than the children do themselves. In particular, a multicenter study conducted in 2020 found that parents rated fatigue, on average, 13.7 points higher than the children themselves, and the parents' own fatigue severity further increased this discrepancy [17]. A questionnaire for assessing fatigue in children with cancer aged 7–17 years has been translated into Russian and validated [19]. The questionnaire includes two versions: a child self-report and a parent proxy report based on the parent's observations. The question of how parent and child assessments compare in families in which a child with cancer has healthy siblings has received little attention in the scientific literature. However, parents experiencing chronic stress and primarily focused on caring for a child with cancer and monitoring his or her physical condition may also be particularly sensitive to physical symptoms in their healthy children.

This study focused on assessing chronic fatigue in siblings of children with cancer compared with healthy children who did not have a seriously ill brother or sister. The analysis was based on two sources of information (the child's self-report and the parent's proxy report) and examined the nature and direction of discrepancies between these sources in the two groups. The research hypothesis was that the severity of chronic fatigue in siblings of children with cancer differs significantly from that in children from families without a seriously ill family member, and that the nature of these differences depends on the source of information (child self-report vs. parent proxy report). The study aimed to compare the severity of chronic fatigue in siblings of children with cancer and in children from families without a seriously ill family member, taking into account the informant (child self-report vs. parent proxy report).

METHODS

The study included 113 parent–child dyads divided into two groups. Only mothers played the role of "parents". The group of siblings of children with cancer (hereinafter "siblings") consisted of 65 dyads, in whose families the followed-up children with cancer were raised. Among siblings, relative to the cancer survivors, there were four fraternal twins, 29 younger and 31 elder siblings. The sex was concordant in 32 sibling pairs and discordant in 33 pairs. The median age difference with the survivors was 3.11 years [IQR: 3.10; 4.48]. The maximum number of children per family in this group was 8. In the group of siblings, 24 families (37%) were multi-child (three or more children). Inclusion criteria for siblings: living in the same household as the affected child before the cancer diagnosis and for at least one year thereafter; no history of acute ot chronic disorder, no acute ot chronic disorder at the time of assessment (including the period of 14 days before the beginning of the study); taking no medications; fluency in Russian.

The control group consisted of 48 dyads in which the assessed child: was healthy; used no drugs; was fluent in Russian; had no close relatives with life-threatening disorders. Among them there were 18 elder, three middle, 10 younger, and 17 only children (there were no twins). Parents of the control group had a maximum of three children; there were only five multi-child families (12.5%), and in three of those (60%) the eldest children were full-aged and lived apart from the family.

Groups were matched by age (Me = 9.65 [IQR: 8.36; 11.0] years in the control group and Me = 9.56 [IQR: 8.59; 10.9] years in the group of siblings; $p = 0.454$), gender (50.0 and 52.3% of girls, respectively; $p = 0.788$). Groups were not matched by the fact of having/not having many children (Fischer's exact test; $p = 0.005$).

The standardized Chronic Fatique Severity questionnaire was used to assess the chronic fatigue severity subjective perception [20]. The method consists of 36 items, each of which is graded on a three-point scale (unambiguous agreement, ambiguous agreement or disagreement). The total score represents the Chronic Fatigue Index (CFI) allowing one to estimate the condition severity: no signs of fatigue, early stage, advanced stage, severe chronic fatigue and asthenic syndrome (transformation into disease).

In addition to CFI, the questionnaire includes another four subscales characterizing manifestations of chronic fatigue in various spheres of life. Since the number of points per subscale is unequal, the authors recommend convert these into percentages to ensure the correct interscale comparison. The original version of the questionnaire was designed for assessment of adults, so it was adapted for children: lexemes with the root "work" were replaced by lexical equivalents of

Table 1. Chronic Fatique Severity questionnaire subscale and authorized abbreviations

Subscale full title	Short title used in the text	Reliability indicators
Physiological Discomfort Symptoms	Physiological Discomfort	α = 0.756 ω = 0.786
General Well-Being Decline and Cognitive Discomfort	General Well-Being Decline	α = 0.710 ω = 0.726
Emotional and Affective Disturbances	Emotional Disturbances	α = 0.813 ω = 0.817
Decreased Motivation and Social Communication Changes	Social Functioning Impairment	α = 0.738 ω = 0.742
Total score (chronic fatigue index, CFI)	Total score / CFI	α = 0.847 ω = 0.848

educational activities: "learning" (No. 12, 28), "learn" (No. 21, 25), and "school" (No. 33). The internal consistency evaluation (Cronbach's alpha (α) and McDonald's omega (ω)) confirmed the modified method validity (according to the generally accepted threshold α, ω ≥ 0.7 [21]). Short titles of the subscales used below and appropriate reliability values are provided in Table 1.

Testing was performed in Russian and implemented on an online platform. Data from mothers were acquired remotely: they filled the questionnaire at a place and time convenient for them. Children completed the questionnaire in person in the presence of a clinical psychologist on a provided computer. The child completed the questionnaire either independently or in the form of a semi-structured interview, in which a specialist read the questions aloud, helped to interprete instructions, and recorded the child's answer options. Thus, two independent estimates of the condition of each child were obtained for each dyad: self-assessment and parent's assessment. Furthermore, subjects answered the survey questions about the frequency of getting ill (ARVI) throughout the year, as well as about regular sports, music, and dancing.

Statistical data processing was performed in Jamovi version 2.3.28 (The jamovi project, Australia). Quantitative variables were described using the median (Me) and interquartile range [Q_1; Q_3]; categorical variables were described using absolute and relative frequencies (*n*, %). The Mann–Whitney U-test was used to compare two independent groups based on quantitative indicators; the Kruskal–Wallis test was used for three or more independent groups; Pearson's chi-squared test (χ^2) or Fishers'exact test (with the expected frequencies less than 5) was used for categorical variables.

Linear Mixed Models (LMM) with the parameter estimation by the Restricted Maximum Likelihood (REML) method were used as the main analysis method. The nested data structure was considered by including a random participant effect (random intercept based on the dyad ID), which allowed us to correctly model the relationship between the child's and parent's assessment within the same dyad. The following were included in the model as fixed effects: group (control/siblings), informant (child/parent), and their interaction (group × informant). Covariates included the child's sex, frequency of acute respiratory disorders, and regular exercise (sports and dancing).

The parents' and children's assessment coherence was determined using two additional methods: we calculated the Spearman's rank correlation coefficient for paired scores within each group; the difference Δ = (parent's assessment) — (child's assessment) was also calculated for each dyad; groups were compared based on the Δ values using the Mann–Whitney U-test. The Wilcoxon test for related samples was used to assess intergroup differences between the parents' and children's estimates. The critical significance level for all analyses was as follows: $p < 0.05$.

RESULTS

There were no age and sex differences between the control group and the group of siblings. ARVI was significantly more often reported in the group of siblings (more than five episodes per year): 41.5% vs. 20.8% in the control group ($p = 0.001$). Siblings were less often engaged in sports (35.4% vs. 56.3%; $p = 0.002$) and dancing (16.9% vs. 31.3%; $p = 0.016$) (Table 2). None of the fatigue indicators turned out to be associated with the birth order — neither in the group of siblings ($p > 0.4$), nor in the control group (Kruskal–Wallis test; $p > 0.2$). The age difference (fraction of a year) between the healthy and affected siblings turned out to have no significant association with any of fatigue indicators (Spearman's rank correlation coefficient; $p > 0.05$). In the group of siblings, when the healthy sibling's sex did not match the affected one's sex, the CFI was higher according to both chilren's self-reports ($U = 270$, $p = 0.003$; $Me_{same\ sex} = 13.0$, $Me_{different\ sex} = 25.0$) and mothers' proxy-reports ($U = 307$, $p = 0.015$; $Me_{same\ sex} = 17.0$, $Me_{different\ sex} = 24.0$). Furthermore, the children's self-assessment was higher in siblings of different gender based on two subcales: Physiological Discomfort ($U = 201$, $p = 0.019$; $Me_{same\ sex}$ =

Table 2. Socio-demographic and clinical and anamnestic characteristics of the sample

Indicator	Control (*n* = 48)	Siblings (*n* = 65)	*p*
Age, Me [Q_1–Q_3], years	9.65 [8.36–11.0]	9.56 [8.59–10.9]	0.454
Girls, *n* (%)	24 (50.0%)	34 (52.3%)	0.788
Frequent ARVI (>5 episodes/year), *n* (%)	10 (20.8%)	27 (41.5%)	0.001
Regular sports, *n* (%)	27 (56.3%)	23 (35.4%)	0.002
Regular music, *n* (%)	9 (18.8%)	14 (21.5%)	0.738
Regular dancing, *n* (%)	15 (31.3%)	11 (16.9%)	0.016

Note: The data are presented as Me [Q_1–Q_3] or *n* (%). Quantitative variables were compared using the Mann–Whitney U-test; categorical ones were compared using Pearson's chi-squared test (χ^2) or Fischer's exact test.

Table 3. Chronic fatigue indicators by subscales and linear mixed model results

Subscale	Group	Parents, Me [Q_1–Q_3]	Children, Me [Q_1–Q_3]	*p* (group)	*p* (informant)	*p* (group × informant)
Total score (CFI)	Control	12.0 [6.0–16.0]	20.0 [16.0–25.0]	0.002	< 0.001	< 0.001
	Siblings	22.0 [15.0–29.0]	20.0 [12.0–28.0]			
Physiological Discomfort	Control	7.0 [0.0–10.0]%	13.0 [7.0–20.8]%	< 0.001	0.002	0.005
	Siblings	23.0 [10.0–30.0]%	20.0 [13.0–30.0]%			
General Well-Being Decline	Control	14.1 [0.0–26.3]%	30.0 [20.0–40.0]%	0.513	0.009	< 0.001
	Siblings	30.0 [15.0–40.0]%	20.0 [10.0–30.0]%			
Emotional Disturbances	Control	17.0 [0.0–33.0]%	25.0 [17.0–42.0]%	0.01	0.508	< 0.001
	Siblings	49.4 [25.0–66.7]%	25.0 [10.0–58.3]%			
Social Functioning Impairment	Control	40.0 [10.0–60.0]%	60.0 [50.0–70.0]%	0.58	< 0.001	< 0.001
	Siblings	40.0 [30.0–60.0]%	50.0 [30.0–60.0]%			

Note: The data are presented as the median and interquartile range [Q_1–Q_3]; for subscales — as the percentage of the maximum score. LMM with fixed effects of the group, informant, and their interaction; random effect — dyad ID. Covariates: frequency of ARVI, engagement in sports and dancing.

13.0, $Me_{different\ sex}$ = 28.5) and Social Functioning Impairment (U = 205, p = 0.023; $Me_{same\ sex}$ = 40.0, $Me_{different\ sex}$ = 60.0). The number of children in families with affected children was correlated to none of the fatigue parameters (p > 0.17 in all cases).

Comparison of groups based on the chronic fatigue severity: linear mixed model results

LMMs were used to assess intergroup differences considering the "dyad" data structure. The CFI analysis revealed significant effects of the group (p = 0.002), informant (p < 0.001), and their interaction (p < 0.001). This suggests that the nature of differences between the parents' and children's estimates is significantly different in two groups (Table 3).

In the control group, parents regularly underestimated the child's fatigue severity compared to the children's self-assessment (Me_{CFI}: 12.0 [6.0–16.0] in parents vs. 20.0 [16.0–25.0] in children). In the group of siblings, the pattern was inverted: the parents' estimates were comparable with the children's or higher (22.0 [15.0–29.0] in parents vs. 20.0 [12.0–28.0] in children).

The analysis of subscales using the LMM showed that the "group × informant" interaction was significant for all the studied indicators (all p < 0.01), which suggests the systemic nature of the differences revealed (Table 3).

The effect of the group was most pronounced for the subscales Physiological Discomfort (p < 0.001) and Emotional Disturbances (p = 0.010): the siblings' parents assessed the children's condition as more severe, than parents of the control group, based on both indicators. As for the General Well-Being Decline (p = 0.513) and Social Functioning Impairment (p = 0.580) subscales, the effect of the group was non-significant, but the significant interaction was preserved, which suggests different patterns of estimates in the groups. In most cases, the covariates included had no significant effect on the model results.

Coherence of parents' and children's estimates

To thoroughly assess the nature of the "group × informant" interaction, we conducted a number of additional analyses involving assessment of correlations within groups, analysis of the difference Δ, and pairwise comparison of estimates within the dyads.

The correlation analysis (Table 4, Fig. 1) revealed significant differences in coherence of estimates between groups. In the control group, the correlation between the parents' and children's CFI assessment was weak (r = 0.34, p = 0.019). A strong positive correlation was observed in the group of siblings (r = 0.73, p < 0.001), which suggests much higher coherence of the child's condition perception in the dyads of siblings.

The analysis of the difference Δ confirmed a fundamental difference in the nature of the ratio of estimates. In the control group, parents underestimated the children's fatigue: MeΔ = −10.0 [−14.0; −3.0] points. In the group of siblings, the estimates were comparable or slightly exceeded the chidlren's self-assessment (MeΔ = 2.0 [−4.0; 4.0]). The intergroup differences in Δ values were significant (Mann–Whitney U-test: U = 625, p < 0.001, r = 0.6).

Intragroup and intergroup differences in parents' and children's estimates

We conducted a pairwise comparative analysis of parents' and children's estimates both within each group and between groups. The results are provided in Fig. 2.

In the control group, the parents' estimates were significantly lower, than the children's, based on all subscales and CFI (p ≤ 0.045), which suggests a persistent tendency among parents of healthy children to underestimate the fatigue severity in their children. In the group of siblings, the pattern was inverted: there were no differences between the parents' and children's estimates based on the Physiological Discomfort

Table 4. Correlation between the parents' and children's assessment of chronic fatigue severity (CFI) by groups

Group	Spearman's *r*	*p*
Control (n = 48)	0.34	0.019
Siblings (n = 65)	0.73	< 0.001

Note: Spearman's rank correlation coefficients between the parent's and child's estimates within the same dyad are provided.

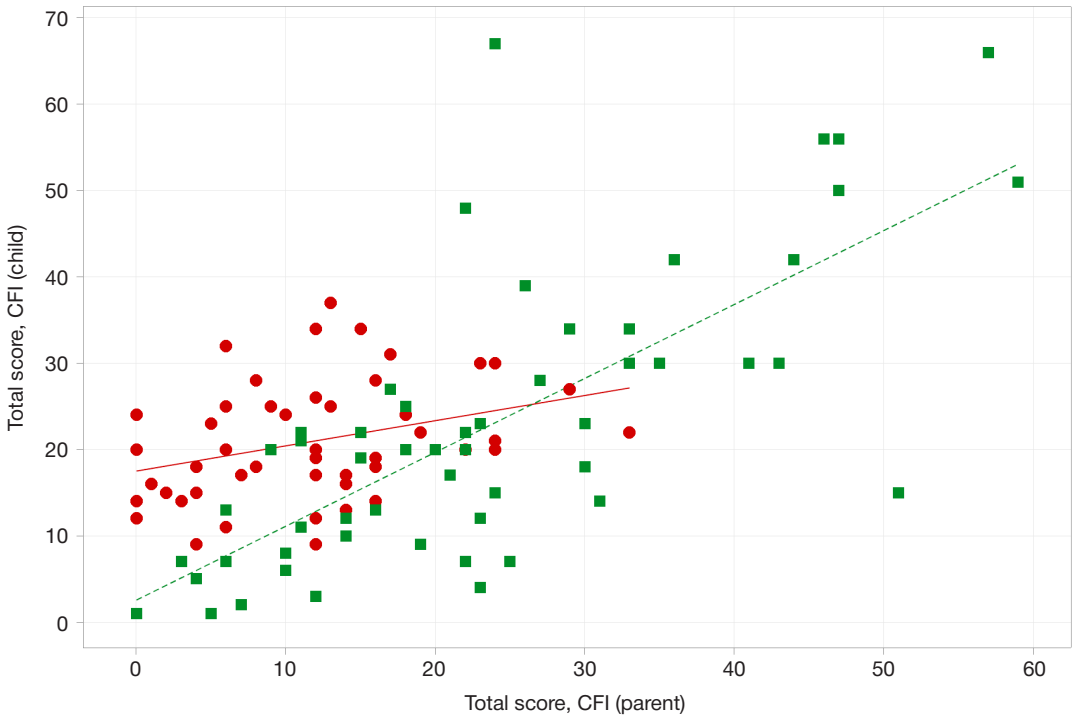

Fig. 1. Scatter charts with the linear regression lines for CFI assessment by parents and children in the control group (*red*) and siblings (*green*). X axis — parent's estimate; Y axis — child's estimate.

and Social Functioning Impairment subscales, as well as total CFI ($p = 0.997$; $p = 0.474$; $p = 0.241$, respectively). Significant differences directed towards overestimation by parents were reported for the General Well-Being Decline ($p = 0.005$) and Emotional Disturbances ($p = 0{,}002$) subscales.

When performing an intergroup comparison separately by informants, the pattern also turned out to be asymmetric. According to the parents, significant intergroup differences were revealed based on four indicators out of five: Physiological Discomfort, General Well-Being Decline, Emotional Disturbances, and total CFI (all $p < 0.001$). According to the children's self-reports, significant differences were reported only based on distinct subscales: Physiological Discomfort ($p = 0.037$), General Well-Being Decline ($p < 0.001$), and Social Functioning Impairment ($p = 0.016$). There were no significant differences in children's self-assessment based on the total CFI and the Emotional Disturbances subscale ($p = 0.729$ and $p = 0.631$, respectively). Thus, the parents', not children's, estimates were the main contributors to intergroup differences, which is consistent with the linear mixed model results.

DISCUSSION

There were significantly more multi-child ones among the families, where children with cancer were raised, which is in line with the large sociological study of 1298 Russian parents having children with cancer [12]. It was demonstrated, how the existential stress faced by such families was associated with changes in their life purpose orientations and the system of needs, which, taken together, resulted in the multi-child lifestyle.

The sex difference rate in both groups turned out to be associated with the chronic fatigue severity: it was higher in cases where the siblings were of different sexes. This effect was revealed when performing further analysis, so we can only put forward a number of hypotheses discussed in the literature and requiring further research. Parents may behave differently with children of different sexes, making different demands and expectations on them, building emotional relationships with them in different ways, devoting time to them in different proportions [22]. It should be noted that the literature data are controversial [23–25]. According to large family-based studies of behavioral and psychological traits, the same genes contribute to interindividual differences in both males and females, which makes the genetic explanation of the sex differences identified less likely compared to socio-psychological ones [26].

Intergroup differences in the children's lifestyle and health revealed that siblings in our sample were less likely to engaged in sports and dancing, twice more often got ARVI (Table 2). These findings are consistent with the results of different studies showing that brothers and sisters of childhood cancer survivors more often seek medical care compared to healthy peers [5, 14, 27]. The siblings' lower engagement in the organized physical activities is natural: the family schedule restructuring, deterioration of the family's financial resources, parents' focus on the sick child's needs, and the sibling's own anxiety reduce the time and resources for leisure activities [10, 28]. Considering the fact that regular physical activity represents one of the reliably determined factors protecting children against fatigue [29], the physical activity decrease can be an intermediate between chronic family stress and subjective feeling of fatigue. At the same time, motor activity was included in the linear mixed models as a covariate, but it did not explain the main effects, which suggests that there were additional mechanisms.

As for CFI, there were no significant differences in children's self-assessment in two groups, but the analysis of subscales revealed a more differentiated pattern. The siblings' Physiological Discomfort subscale scores were higher, than that of the control group, while differences on the General Well-Being Decline subscale were oppositely directed: the scores of control children turned out to be significantly higher. There were no significant differences in self-assessment of two groups on the Emotional Disturbances subscale, while the Social Functioning Impairment subscale scores of control children were also significantly higher. Thus, according to the children's self-assessment, the fatigue indicators in siblings are significantly higher compared to that in the control group based

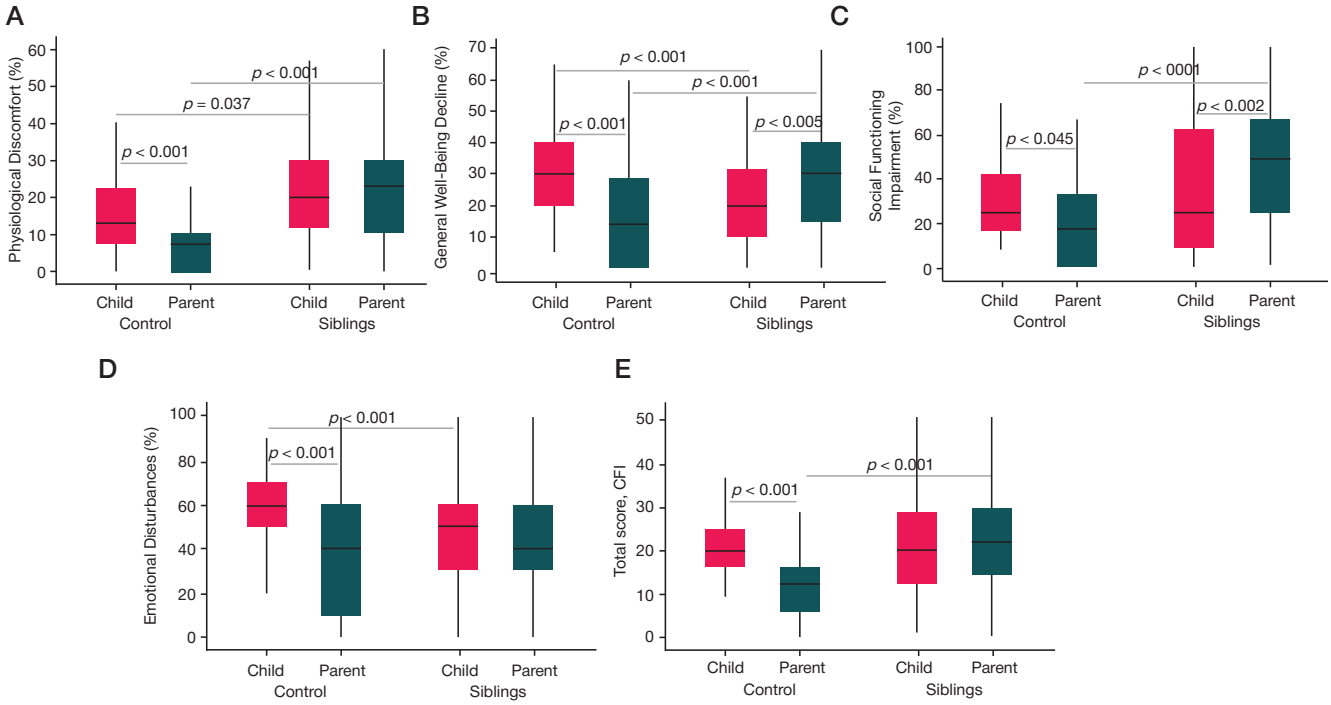

Fig. 2. Box plots of the distribution of chronic fatigue indicators by subscales in the control group and group of siblings. *Red box plots* — children's estimates; *green* — parents' estimates. Intragroup differences between the child's and parent's estimates (Wilcoxon test for related samples) and intergroup differences between the control group and group of siblings (Mann–Whitney U-test) are designated by red brackets with *p*-values. Only statistically significant comparisons are shown ($p < 0.05$). **A**. Physiological Discomfort Symptoms subscale. **B**. General Well-Being Decline and Cognitive Discomfort subscale. **C**. Emotional and Affective Disturbances subscale. **D**. Decreased Motivation and Social Communication Changes subscale. **E**. chronic fatigue index (CFI, total score)

on the physiological component only; there are no differences or indicators of the control group are significantly higher in the emotional, cognitive-affective, and social spheres. The latter can reflect the acceleration effect of the chronic family stress load: siblings of childhood cancer survivors often show higher levels of pro-social behavior and empathy, as well as a tendency not to transmit their own difficulties, feeling an unspoken prohibition against demonstrating weakness in a situation of family stress [10]. Parents more often ask healthy siblings for instrumental help (for example, more often ask for help with their chores), despite the fact that parents themselves less often provide similar support to their children (for example, less often allow them to skip school) [11]. Furthermore, acceleration processes were illustrated by the siblings' anthropometric measurements: their body height and body mass index were higher compared to that of their peers (according to the WHO), and the higher body height was reported in siblings, who were older, than survivors [30].

When comparing the parents' and children's estimates within each group, it was found that in the control group parents rated the child's fatigue lower, than children, on all five scales. This is consistent with the data showing that the parents' assessment based on their insights is often lower compared to the children's self-assessment regarding subjective, especially emotional and social, aspects of the condition, since the age of 7 [31]. The pattern was inverted in the group of siblings. The parents' General Well-Being Decline and Emotional Disturbances subscale scores were significantly higher compared to children's. As for Physiological Discomfort, Social Functioning Impairment, and total CFI, there were no differences between the parents' and children's estimates in the group of siblings.

At the age of 7–11 years children actively shape their internal pictures of illness (IPI) and health (IPH). At this age, subjective well-being is already accessible to reflection, but the assessment of one's condition as health or illness still depends heavily on the interpretations and reactions of significant adults [32]. The developmental trajectory of the IPI/IPH involves a gradual shift toward greater autonomy in self-assessment. This pattern was observed in our control group, where children's self-assessments on several subscales exceeded those of their parents. Such a discrepancy suggests that the child has his/her own well-being assessment criteria, that are different from the parents', which reflects the developing ability to rely on the internal sensations and ideas, not only on the ones transmitted by external sources. In the context of chronic family stress experienced by the family having a child with the life-threatening disease, the typical development can be modified. The constant presence of a child with the objectified suffering in the family and the transmitted parents' anxiety can "shift" the criteria of normal [33]. Thus, the lack of significant differences between the parents' and children's estimates in the group of siblings can reflect not so much the objective differences in the children condition, but rather the features of the sibling's IPI/H ontogenesis, during which his/her own IPI/H remains "fused" with parental assessments and subject to the anxiety of the family environment for longer.

The linear mixed model analysis revealed a significant interaction of the "group × informant" factors for all the studied indicators. Intergroup differences are ensured mainly by the parents', not children's, estimates. According to the parents, fatigue indicators on all subscales, except the social one, are higher in the group of siblings. The pattern based on the children's self-assessment is different: based on the General Well-Being Decline and Social Functioning Impairment siblings described their condition as better compared to control children, while based on Physiological Discomfort the condition was described as slightly worse. Such an asymmetric pattern, with which intergroup differences are determined primarily by the parents' estimates, is consistent with the hypothesis about the indirect influence of parents' assessment on the IPI shaping in siblings of children with cancer.

In 2020, it was shown that the parents' awareness about the sibling's conditions and accuracy of their assessment are determined primarily by the quality of communication in the family. Chronic stress associated with the other child's illness, being overwhelmed with care and focused on the cancer patient's needs limit the parents' capability of monitoring the healthy child's condition and discuss his/her experiences with him/her [34]. In the context of family crisis, parents often develop the increased anxiety about the children's health in general — the phenomenon described within the framework of the concept of the "child's health anxiety by proxy": excessive, difficult to control fears about the child's possible ill-being, which are not necessarily consistent with the child's actual condition [33]. Parents of children with cancer often experience significant fatigue and emotional distress themselves [35]. The caregiver's own health status and well-being are associated with the discrepancy between his/her and child's estimates. In particular, such discrepancy increased as the caregiver's own condition worsened based on the fatigue domain [14]. A combination of these factors (low awareness resulting from the lack of communication, background anxiety for a healthy child, the parent's own distress) creates conditions for inflated estimates of the sibling's condition.

Coherence of parents' and children's estimates in the group of siblings was significantly higher, than in the control group. Similar results were obtained by the researchers, who showed that coherence of parental and child reports was higher in families affected with cancer. Apparently, under these conditions parents are more sensitive to any changes in children's condition [36]. It must be emphasized that the high correlation reflects the coherence of the direction of changes only, not the accuracy of absolute estimates. In our study, the high correlation was combined with the parents' overestimation on a number of subscales, which underscores the need to differentiate these two aspects when analyzing the inter-informant consensus.

Limitations of the study

The cross-sectional study design made it impossible to examine changes within parent–child dyads over time.

Only subjective measures were collected and analyzed (children's self-reports and mothers' proxy reports); therefore, the influence of social desirability bias cannot be ruled out.

The analysis of the family context was limited. We had no information on the mothers' age at the birth of their first child, their mental health status, or the availability and quality of parenting support. We also lacked information on the degree of fathers' involvement in child-rearing and did not consider the family's socioeconomic characteristics (place of residence, housing conditions, household income, parental education, and employment).

We did not stratify the sibling group according to the clinical characteristics of the child with cancer (cancer diagnosis, treatment duration and intensity, disease recurrence, follow-up period, comorbidities, or symptom severity).

CONCLUSIONS

The study has shown that subjective chronic fatigue in siblings of children with cancer is not a homogeneous phenomenon and is perceived differently by different informants (the child and the parent). According to the children's self-reports, between-group differences are limited to the physiological domain. In contrast, parent proxy reports indicate differences across most of the studied domains and consistently yield higher fatigue ratings than the children's self-reports.

The key finding is the reversal of the discrepancy between parent and child ratings depending on the family context: whereas parents in the control group tend to underestimate their children's fatigue, parents of children with cancer tend to overestimate the fatigue of their healthy children. This discrepancy itself represents an important indicator that should be taken into account when conducting psychosocial screening of siblings.

These findings support the inclusion of healthy siblings in psychological follow-up programs for families in pediatric oncology and rehabilitation. Further longitudinal studies incorporating parental stress and anxiety as predictors of parent–child agreement will help clarify the mechanisms underlying the observed phenomenon and facilitate the development of more accurate recommendations for supporting families affected by childhood cancer. In the present study, we did not consider several potentially important factors, including family composition, socioeconomic status, the availability and nature of social support, and attachment style; these factors should be addressed in future research.

References

1. Kaprin AD, Starinskij VV, Shahzadova AO, redaktory. Sostoyanie onkologicheskoj pomoshchi naseleniyu Rossii v 2024 godu. M.: MNIOI im. P.A. Gercena — filial FGBU «NMIC radiologii» Minzdrava Rossii, 2025; s. 10. Russian.
2. Wang M, Bi Y, Fan Y, Fu X, Jin Y. Global incidence of childhood cancer by subtype in 2022: a population-based registry study. EClinicalMedicine. 2025; 89: 103571. DOI: 10.1016/j.eclinm.2025.103571.
3. Merabishvili VM. Sostoyanie onkologicheskoj pomoshchi v Rossii: vyzhivaemost' detej (0–14 let). Populyacionnoe issledovanie na urovne federal'nogo okruga. Chast' II. Rossijskij zhurnal detskoj gematologii i onkologii. 2025; 12 (1): 14–19. DOI: 10.21682/2311-1267-2025-12-1-14-19. Russian.
4. Tihonova OA, Krutikova NYu, Karelin AF, Zhukovskaya EV, Rumyancev AG. Vliyanie zlokachestvennyh novoobrazovanij na costoyanie kostno-myshechnoj sistemy u detej (obzor literatury). Onkogematologiya. 2018; 13 (4): 60–66. DOI: 10.17650/1818-8346-2018-13-4-60-66. Russian.
5. Feudtner C, Nye RT, Boyden JY, Schwartz CE, Korn E, Wolfe J, et al. Association between children with life-threatening conditions and their parents' and siblings' mental and physical health. JAMA Netw Open. 2021; 4 (12): e2137250. DOI: 10.1001/jamanetworkopen.2021.37250.
6. Dussel V, Bona K, Heath JA, Hilden JM, Weeks JC, Wolfe J. Unmeasured costs of a child's death: perceived financial burden, work disruptions, and economic coping strategies used by American and Australian families who lost children to cancer. J Clin Oncol. 2011; 29 (8): 1007–13. DOI: 10.1200/JCO.2009.27.8960.
7. Mazurova NV. Osobennosti adaptacii roditelej k bolezni rebenka. Rossijskij pediatricheskij zhurnal. 2013; 5: 50–56. Russian.
8. Erker C, Yan K, Zhang L, Bingen K, Flynn KE, Panepinto JA, et al. Impact of pediatric cancer on family relationships. Cancer Med. 2018; 7 (5): 1680–8. DOI: 10.1002/cam4.1393.
9. Mazurova NV, Podolskaya TA. Psihologo-pedagogicheskaya pomoshch' roditelyam dlitel'no i tyazhelo boleyushchih detej. M.: Pero, 2021; 383 s. ISBN 978-5-00171-525-2. Russian.
10. Long KA, Lehmann V, Gerhardt CA, Carpenter AL, Marsland AL, Alderfer MA. Psychosocial functioning and risk factors among siblings of children with cancer: an updated systematic

review. Psychooncology. 2018; 27 (6): 1467–79. DOI: 10.1002/pon.4669.
11. Wawrzynski SE, Schaefer MR, Schvaneveldt N, Alderfer MA. Social support and siblings of children with cancer: a scoping review. Psychooncology. 2021; 30 (8): 1232–45. DOI: 10.1002/pon.5689.
12. Antonov AI, Guseva MA. Dispozicionnaya regulyaciya reproduktivnogo i samosohranitel'nogo povedeniya v netipichnyh sem'yah s bol'nym rebenkom. Social'nye aspekty zdorov'ya naseleniya. 2019; 1 (65): 2. DOI: 10.21045/2071-5021-2019-65-1-2. Russian.
13. Kokoreva ME. Rol' social'noj sluzhby v organizacii medicinskoj reabilitacii semej, imeyushchih rebenka s onkologicheskim zabolevaniem. Pediatricheskij vestnik YUzhnogo Urala. 2020; (1): 72–79. Russian.
14. Sheikh IN, Roth M, Stavinoha PL. Prevalence of sleep disturbances in pediatric cancer patients and their diagnosis and management. Children. 2021; 8 (12): 1100. DOI: 10.3390/children8121100.
15. Sirveaux V, Puterman-Salzman L, Zhang YQ, Hercun J, Olivier C, Sultan S, et al. Adverse physical health outcomes and healthcare service utilization in siblings of children with cancer: a systematic review. Cancer Med. 2025; 14 (15): e71035. DOI: 10.1002/cam4.71035.
16. Guidi J, Lucente M, Sonino N, Fava GA. Allostatic load and its impact on health: a systematic review. Psychother Psychosom. 2021; 90 (1): 11–27. DOI: 10.1159/000510696.
17. Mack JW, McFatrich M, Withycombe JS, Maurer SH, Jacobs SS, Lin L, et al. Agreement between child self-report and caregiver-proxy report for symptoms and functioning of children undergoing cancer treatment. JAMA Pediatr. 2020; 174 (11): e202861. DOI: 10.1001/jamapediatrics.2020.2861.
18. Leahy AB, Steineck A. Patient-reported outcomes in pediatric oncology: the patient voice as a gold standard. JAMA Pediatr. 2020; 174 (11): e202868. DOI: 10.1001/jamapediatrics.2020.2868.
19. Deviaterikova AA, Kasatkin VV, Velichovsky BB. The validity and reliability of the Turkish scale for the assessment of fatigue in pediatric oncology patients aged 7–18 in Russia. Psychology in Russia: State of the Art. 2021; 14 (1): 39–48. DOI: 10.11621/pir.2021.0104.
20. Leonova AB, Kuznecova AS. Psihologicheskie tekhnologii upravleniya sostoyaniem cheloveka. M.: Smysl; 2015. 311 s. Russian.
21. Nunnally JC, Bernstein IH. Psychometric Theory. 3rd ed. McGraw-Hill, 1994.
22. Her Y-C, Batur ZZ, Vergauwen J, Mortelmans D. Siblings' similarities and dissimilarities: A review of theoretical perspectives and empirical insights. Journal of Family Theory & Review. 2021; 13 (4): 447–62. DOI: 10.1111/jftr.12436.
23. Deary IJ, Irwing P, Der G, Bates TB. Brother–sister differences in the g factor in intelligence: Analysis of full, opposite-sex siblings from the NLSY1979. Intelligence. 2007; 35 (5): 451–6. DOI: 10.1016/j.intell.2006.09.003.
24. Boomsma DI, van Beijsterveld T Beem AL, Hoekstra RA, Polderman TJC, Bartels M. Intelligence and birth order in boys and girls. Intelligence. 2008; 36 (6): 630–4. DOI: 10.1016/j.intell.2008.01.005.
25. Alekseeva O, Rzhanova I. Polovye razlichiya po kognitivnym i lichnostnym harakteristikam u siblingov v dvuhdetnyh sem'yah. Psihologicheskie issledovaniya. 2016; 9 (45). DOI: 10.54359/ps.v9i45.487. Russian.
26. Vink JM, Bartels M, Van Beijsterveldt TC, Van Dongen J, Van Beek JH, Distel MA, Boomsma DI. Sex differences in genetic architecture of complex phenotypes? PloS one. 2012; 7 (12): e47371. DOI: 10.1371/journal.pone.0047371.
27. Martinez B, Pechlivanoglou P, Meng D, Traubici B, Mahood Q, Korczak D, et al. Clinical health outcomes of siblings of children with chronic conditions: a systematic review and meta-analysis. J Pediatr. 2022; 250: 83–92.e8. DOI: 10.1016/j.jpeds.2022.07.002.
28. Ohlsen TJD, Buchbinder DK, Dupuis LL, Sung L, Tomlinson D, Hinds PS, et al. Financial toxicity among pediatric oncology families during therapy and early survivorship: a qualitative analysis. Support Care Cancer. 2025; 33 (1): 36. DOI: 10.1007/s00520-024-09093-y.
29. Braam KI, van der Torre P, Takken T, Veening MA, van Dulmen-den Broeder E, Kaspers GJ. Physical exercise training interventions for children and young adults during and after treatment for childhood cancer. Cochrane Database Syst Rev. 2016; 3 (3): CD008796. DOI: 10.1002/14651858.CD008796.pub3.
30. Lihomanova EN, Gorbacheva AK, Kovaleva AV, Chechelnickaya SM. Osobennosti fizicheskogo razvitiya detej, perenesshih lechenie po povodu opuholi golovnogo mozga, i zdorovyh siblingov onkologicheskih pacientov (pilotnoe issledovanie). Vestnik Moskovskogo universiteta. Seriya 23. Antropologiya. 2024; (2): 62–72. DOI: 10.55959/MSU2074-8132-24-2-5. Russian.
31. Eiser C, Varni JW. Health-related quality of life and symptom reporting: similarities and differences between children and their parents. Eur J Pediatr. 2013; 172 (10): 1299–304. DOI: 10.1007/s00431-013-2049-9.
32. Nikolaeva VV, Arina GA. Tyazhelo bol'noj rebenok, shtrihi k psihologicheskomu portretu. Shkola zdorov'ya. 1994; 2 (2), 86. Russian.
33. Ingeman K, Frostholm L, Frydendal DH, Rask CU, Mikkelsen HT, Høgh M, et al. A new measure of excessive parental worries about children's health: development of the Health Anxiety by Proxy Scale (HAPYS). Nord J Psychiatry. 2021; 75 (7): 523–31. DOI: 10.1080/08039488.2021.1900389.
34. Pariseau EM, Chevalier L, Muriel AC, Long KA. Parental awareness of sibling adjustment: perspectives of parents and siblings of children with cancer. J Fam Psychol. 2020; 34 (6): 698–708. DOI: 10.1037/fam0000615.
35. Kearney JA, Salley CG, Muriel AC. Standards of psychosocial care for parents of children with cancer. Pediatr Blood Cancer. 2015; 62 (S5): S632–S683. DOI: 10.1002/pbc.25761.
36. Paul V, Inhestern L, Winzig J, Escher C, Rutkowski S, Bergelt C, et al. Emotional and behavioral problems of pediatric cancer survivors and their siblings: concordance of child self-report and parent proxy-report. Psychooncology. 2023; 32 (8): 1248–56. DOI: 10.1002/pon.6175.

Литература

1. Каприн А. Д., Старинский В. В., Шахзадова А. О., редакторы. Состояние онкологической помощи населению России в 2024 году. М.: МНИОИ им. П.А. Герцена — филиал ФГБУ «НМИЦ радиологии» Минздрава России, 2025; с. 10.
2. Wang M, Bi Y, Fan Y, Fu X, Jin Y. Global incidence of childhood cancer by subtype in 2022: a population-based registry study. EClinicalMedicine. 2025; 89: 103571. DOI: 10.1016/j.eclinm.2025.103571.
3. Мерабишвили В. М. Состояние онкологической помощи в России: выживаемость детей (0–14 лет). Популяционное исследование на уровне федерального округа. Часть II. Российский журнал детской гематологии и онкологии. 2025; 12 (1): 14–19. DOI: 10.21682/2311-1267-2025-12-1-14-19.
4. Тихонова О. А., Крутикова Н. Ю., Карелин А. Ф., Жуковская Е. В., Румянцев А.Г. Влияние злокачественных новообразований на состояние костно-мышечной системы у детей (обзор литературы). Онкогематология. 2018; 13 (4): 60–66. DOI: 10.17650/1818-8346-2018-13-4-60-66.
5. Feudtner C, Nye RT, Boyden JY, Schwartz CE, Korn E, Wolfe J, et al. Association between children with life-threatening conditions and their parents' and siblings' mental and physical health. JAMA Netw Open. 2021; 4 (12): e2137250. DOI: 10.1001/jamanetworkopen.2021.37250.
6. Dussel V, Bona K, Heath JA, Hilden JM, Weeks JC, Wolfe J. Unmeasured costs of a child's death: perceived financial burden, work disruptions, and economic coping strategies used by American and Australian families who lost children to cancer. J Clin Oncol. 2011; 29 (8): 1007–13. DOI: 10.1200/JCO.2009.27.8960.
7. Мазурова Н. В. Особенности адаптации родителей к болезни ребенка. Российский педиатрический журнал. 2013; 5: 50–56.
8. Erker C, Yan K, Zhang L, Bingen K, Flynn KE, Panepinto JA, et al. Impact of pediatric cancer on family relationships. Cancer Med. 2018; 7 (5): 1680–8. DOI: 10.1002/cam4.1393.
9. Мазурова Н. В., Подольская Т. А. Психолого-педагогическая помощь родителям длительно и тяжело болеющих детей. М.:

Перо, 2021; 383 с. ISBN 978-5-00171-525-2.
10. Long KA, Lehmann V, Gerhardt CA, Carpenter AL, Marsland AL, Alderfer MA. Psychosocial functioning and risk factors among siblings of children with cancer: an updated systematic review. Psychooncology. 2018; 27 (6): 1467–79. DOI: 10.1002/pon.4669.
11. Wawrzynski SE, Schaefer MR, Schvaneveldt N, Alderfer MA. Social support and siblings of children with cancer: a scoping review. Psychooncology. 2021; 30 (8): 1232–45. DOI: 10.1002/pon.5689.
12. Антонов А. И., Гусева М. А. Диспозиционная регуляция репродуктивного и самосохранительного поведения в нетипичных семьях с больным ребенком. Социальные аспекты здоровья населения. 2019; 1 (65): 2. DOI: 10.21045/2071-5021-2019-65-1-2.
13. Кокорева М. Е. Роль социальной службы в организации медицинской реабилитации семей, имеющих ребенка с онкологическим заболеванием. Педиатрический вестник Южного Урала. 2020; (1): 72–79.
14. Sheikh IN, Roth M, Stavinoha PL. Prevalence of sleep disturbances in pediatric cancer patients and their diagnosis and management. Children. 2021; 8 (12): 1100. DOI: 10.3390/children8121100.
15. Sirveaux V, Puterman-Salzman L, Zhang YQ, Hercun J, Olivier C, Sultan S, et al. Adverse physical health outcomes and healthcare service utilization in siblings of children with cancer: a systematic review. Cancer Med. 2025; 14 (15): e71035. DOI: 10.1002/cam4.71035.
16. Guidi J, Lucente M, Sonino N, Fava GA. Allostatic load and its impact on health: a systematic review. Psychother Psychosom. 2021; 90 (1): 11–27. DOI: 10.1159/000510696.
17. Mack JW, McFatrich M, Withycombe JS, Maurer SH, Jacobs SS, Lin L, et al. Agreement between child self-report and caregiver-proxy report for symptoms and functioning of children undergoing cancer treatment. JAMA Pediatr. 2020; 174 (11): e202861. DOI: 10.1001/jamapediatrics.2020.2861.
18. Leahy AB, Steineck A. Patient-reported outcomes in pediatric oncology: the patient voice as a gold standard. JAMA Pediatr. 2020; 174 (11): e202868. DOI: 10.1001/jamapediatrics.2020.2868.
19. Deviaterikova AA, Kasatkin VV, Velichovsky BB. The validity and reliability of the Turkish scale for the assessment of fatigue in pediatric oncology patients aged 7–18 in Russia. Psychology in Russia: State of the Art. 2021; 14 (1): 39–48. DOI: 10.11621/pir.2021.0104.
20. Леонова А. Б., Кузнецова А. С. Психологические технологии управления состоянием человека. М.: Смысл; 2015. 311 с.
21. Nunnally JC, Bernstein IH. Psychometric Theory. 3rd ed. McGraw-Hill, 1994.
22. Her Y-C, Batur ZZ, Vergauwen J, Mortelmans D. Siblings' similarities and dissimilarities: A review of theoretical perspectives and empirical insights. Journal of Family Theory & Review. 2021; 13 (4): 447–62. DOI: 10.1111/jftr.12436.
23. Deary IJ, Irwing P, Der G, Bates TB. Brother–sister differences in the g factor in intelligence: Analysis of full, opposite-sex siblings from the NLSY1979. Intelligence. 2007; 35 (5): 451–6. DOI: 10.1016/j.intell.2006.09.003.
24. Boomsma DI, van Beijsterveld T Beem AL, Hoekstra RA, Polderman TJC, Bartels M. Intelligence and birth order in boys and girls. Intelligence. 2008; 36 (6): 630–4. DOI: 10.1016/j.intell.2008.01.005.
25. Алексеева О, Ржанова И. Половые различия по когнитивным и личностным характеристикам у сиблингов в двухдетных семьях. Психологические исследования. 2016; 9 (45). DOI: 10.54359/ps.v9i45.487.
26. Vink JM, Bartels M, Van Beijsterveldt TC, Van Dongen J, Van Beek JH, Distel MA, Boomsma DI. Sex differences in genetic architecture of complex phenotypes? PloS one. 2012; 7 (12): e47371. DOI: 10.1371/journal.pone.0047371.
27. Martinez B, Pechlivanoglou P, Meng D, Traubici B, Mahood Q, Korczak D, et al. Clinical health outcomes of siblings of children with chronic conditions: a systematic review and meta-analysis. J Pediatr. 2022; 250: 83–92.e8. DOI: 10.1016/j.jpeds.2022.07.002.
28. Ohlsen TJD, Buchbinder DK, Dupuis LL, Sung L, Tomlinson D, Hinds PS, et al. Financial toxicity among pediatric oncology families during therapy and early survivorship: a qualitative analysis. Support Care Cancer. 2025; 33 (1): 36. DOI: 10.1007/s00520-024-09093-y.
29. Braam KI, van der Torre P, Takken T, Veening MA, van Dulmen-den Broeder E, Kaspers GJ. Physical exercise training interventions for children and young adults during and after treatment for childhood cancer. Cochrane Database Syst Rev. 2016; 3 (3): CD008796. DOI: 10.1002/14651858.CD008796.pub3.
30. Лихоманова Е. Н., Горбачева А. К., Ковалева А. В., Чечельницкая С. М. Особенности физического развития детей, перенесших лечение по поводу опухоли головного мозга, и здоровых сиблингов онкологических пациентов (пилотное исследование). Вестник Московского университета. Серия 23. Антропология. 2024; (2): 62–72. DOI: 10.55959/MSU2074-8132-24-2-5.
31. Eiser C, Varni JW. Health-related quality of life and symptom reporting: similarities and differences between children and their parents. Eur J Pediatr. 2013; 172 (10): 1299–304. DOI: 10.1007/s00431-013-2049-9.
32. Николаева В. В., Арина Г. А. Тяжело больной ребенок, штрихи к психологическому портрету. Школа здоровья. 1994; 2 (2), 86.
33. Ingeman K, Frostholm L, Frydendal DH, Rask CU, Mikkelsen HT, Høgh M, et al. A new measure of excessive parental worries about children's health: development of the Health Anxiety by Proxy Scale (HAPYS). Nord J Psychiatry. 2021; 75 (7): 523–31. DOI: 10.1080/08039488.2021.1900389.
34. Pariseau EM, Chevalier L, Muriel AC, Long KA. Parental awareness of sibling adjustment: perspectives of parents and siblings of children with cancer. J Fam Psychol. 2020; 34 (6): 698–708. DOI: 10.1037/fam0000615.
35. Kearney JA, Salley CG, Muriel AC. Standards of psychosocial care for parents of children with cancer. Pediatr Blood Cancer. 2015; 62 (S5): S632–S683. DOI: 10.1002/pbc.25761.
36. Paul V, Inhestern L, Winzig J, Escher C, Rutkowski S, Bergelt C, et al. Emotional and behavioral problems of pediatric cancer survivors and their siblings: concordance of child self-report and parent proxy-report. Psychooncology. 2023; 32 (8): 1248–56. DOI: 10.1002/pon.6175.

INTEGRATIVE PHARMACOGNOSTICAL PROFILING & *IN VITRO* ANTIBACTERIAL ACTIVITY ASSESSMENT OF *MURRAYA KOENIGII* (L.) SPRENG

Ashwaq T. Kareem ✉

Department of Pharmacognosy, College of Pharmacy, Thi-Qar University, Thi-Qar, Iraq

The evolution of multi drug-resistant bacterial diseases enforces the need for new botanical anti-microbiological drugs. Curry leaf (M*urraya koenigii L. Spreng*) is often used in traditional medicine; however the pharmacognosic effects and extraction efficiency need to be affirmed meticulously. The study aimed at qualitative phytochemical profiling and physicochemical standardization of *M. koenigii* leaf powder by aqueous, ethanolic and methanolic solvent systems, conducted for the first time. MICs were measured by microdilution to determine antibacterial activities against a panel of clinically relevant pathogens; the disc diffusion method was used for microbiological analysis. Tukey's post-hoc test was used after one-way ANOVA to examine statistical differences. Physicochemical examination showed a total ash value of 15.4% ± 0.3% w/w and a low moisture content of 4.2% ± 0.3% w/w. We detected bioactive secondary metabolites, including as tannins, alkaloids, and, flavonoids were validated by phytochemical screening, with alcoholic solvents showing higher extraction yields than water. The ethanolic extract showed strong antibacterial activity against *Proteus mirabilis* (21.0 mm) and *Staphylococcus aureus* (21.0 mm) in disc diffusion experiments, but the aqueous extract was totally inactive (0.0, $p < 0.001$). *Bacillus* sp. and *Streptococcus mutans* showed the lowest MIC values for the ethanolic extract (0.156 mg/mL). These results validate *M. koenigii's* potential development as a natural therapeutic agent by establishing pharmacognostic quality markers for the plant and showing that its ethanolic extract contains extremely powerful antibacterial agents, especially effective against Gram-positive clinical isolates.

Keywords: *Murraya koenigii*, antibacterial activity, pharmacognosic standardization, phytochemical screening, minimal inhibition

✉ **Correspondence should be addressed:** Ashwaq T. Kareem
Thi-Qar University, Thi-Qar, Iraq; ashwaq.t.kareem@utq.edu.iq

Received: 18.07.2026 **Accepted:** 20.08.2026 **Published online:** 31.08.2026

DOI: 10.24075/brsmu.2026.047

КОМПЛЕКСНЫЙ ФАРМАКОГНОСТИЧЕСКИЙ АНАЛИЗ И ОЦЕНКА АНТИБАКТЕРИАЛЬНОЙ АКТИВНОСТИ *MURRAYA KOENIGII* (L.) SPRENG *IN VITRO*

Ашвак Т. Карим ✉

Фармацевтический колледж, Университет Ти-Кар, Ти-Кар, Ирак

Эволюция вызываемых бактериями с множественной лекарственной устойчивостью заболеваний обусловливает потребность в новых противомикробных препаратах на основе растительного сырья. Листья карри (*Murraya koenigii* L. Spreng.) часто используют в традиционной медицине, однако необходимо подтвердить их фармакологическое действие и эффективность экстракции. Цель исследования: провести качественное фитохимическое профилирование и физико-химическую стандартизацию порошка листьев карри с применением систем с водой, этанолом и метанолом в качестве растворителей. МПК измеряли методом микроразведений, чтобы определить наличие антибактериальной активности в отношении панели клинически значимых патогенов. Для микробиологического анализа использовали диско-диффузионный метод. Для оценки статистических различий после однофакторного дисперсионного анализа использовали апостериорный тест Тьюки. При проведении физико-химического анализа установлены содержание золы общей 15,4% ± 0,3% (по массе) и низкое содержание влаги, составившее 4,2% ± 0,3% (по массе). Выявлены биологически активные вторичные метаболиты, в том числе танины, алкалоиды и флавоноиды, наличие которых подтверждено при проведении фитохимического скрининга. Применение спиртовых растворителей продемонстрировало большую эффективность экстракции по сравнению с водой. Этанольный экстракт показал высокую антибактериальную активность в отношении *Proteus mirabilis* (21,0 мм) и *Staphylococcus aureus* (21,0 мм) в экспериментах с применением диско-диффузионного метода, а водный экстракт продемонстрировал полное отсутствие активности (0,0; $p < 0,001$). У *Bacillus* sp. и *Streptococcus mutans* были самые низкие значения МПК при применении этанольного экстракта (0,156 мг/мл). Полученные результаты подтверждают возможность разработки *M. koenigii* как природного лекарственного средства путем определения фармакогностических маркеров качества растения и демонстрации факта, что его этанольный экстракт содержит чрезвычайно мощные антибактериальные вещества, особенно эффективные против клинических изолятов грамположительных бактерий.

Ключевые слова: *Murraya koenigii*, антибактериальная активность, фармакогностическая стандартизация, фитохимический скрининг, минимальное ингибирование

✉ **Для корреспонденции:** Ашвак Т. Карим
Университет Ти-Кар, Ти-Кар, Ирак; ashwaq.t.kareem@utq.edu.iq

Статья получена: 18.07.2026 **Статья принята к печати:** 20.08.2026 **Опубликована онлайн:** 31.08.2026

DOI: 10.24075/vrgmu.2026.047

Multidrug-resistant (MDR) microorganisms are becoming more common, which is making the worldwide burden of bacterial illnesses worse. Growing bacterial resistance highlights the need for improved surveillance and novel therapies since it presents significant global health challenges [1].

Natural products made from plants have shown promise in resolving this issue. Compared to single-target synthetic medications, medicinal plants offer a rich supply of structurally diverse bioactive chemicals with numerous modes of action, which may lower the risk of resistance development Herbal

remedies are particularly popular in developing countries, where almost eighty percent of the people receives primary care from traditional natural plant medicines [2].

Murraya koenigii (L.) Spreng. is a tropical to subtropical tree that belongs to the Rutaceae family and is indigenous to Asia, particularly India and Sri Lanka [3]. Commonly referred to as curry leaf plant or kari patta, this evergreen tree is grown for its aromatic leaves that are a vital ingredient in South Asian cooking. Apart from its use in culinary practices, *M. koenigii* has been extensively reported as a traditional remedy for the management of many conditions in systems such as Ayurveda and Unani [4]. Historically the leaves were utilized internally as a tonic, stomachic, carminative, antihelminthic and for skin eruptions as well as vomiting [5].

The potential pharmacological properties of *M. koenigii* are attributed to its high phytochemical profile. Many secondary metabolites that produced by the plant include carbazole alkaloids, terpenoids, flavonoids, essential oils and polyphenols [6]. Koenigine, mahanimbine, and murrayanine belong to the class of alkaloids with carbazole skeletons, this composition being responsible for their diverse biological activities such as antioxidant, antibacterial, and anticancer abilities [7]. Recent scientific research has confirmed many conventional claims. Studies have demonstrated *M. koenigii's* significant anti-inflammatory, antibacterial, antioxidant, antidiabetic, and cytotoxic qualities. Scientific research has recently proved a great many old wives' tales. *M. koenigii* has been shown to possess considerable anti-inflammatory, antibacterial, antioxidant, antidiabetic and cytotoxic properties [8]. Additionally, the plant has shown potential for treating biofilm-associated infections [9]. Which is a crucial component of important antibiotic-resistant chronic bacterial disease. Pharmacognostic standardization is essential to guarantee the identity, quality and purity of herbal medicines [10].

The WHO states that defining pharmacognostic parameters — such as macroscopic and microscopic traits, physicochemical constants, and phytochemical profiles — is essential for assessing the quality of medicinal plants [11]. There are still few comprehensive investigations on the leaves of *M. koenigii*, however previous pharmacognostic research has focused on the stems and roots [12, 13].

The same is the case with the content of essential oil of *M. koenigii* which has been one subject for number of studies which indicates considerable variation based on the plant geographical origin. β-caryophyllene (16.6 to 26.6%) and α-humulene (15.2 to 26.7%) were the two primary volatile metabolites detected in Malaysian specimens [13]. Headspace analysis revealed that 27.4% of the constituents were β-caryophyllene and 37.5% were α-pinene which were the most common compounds in previous studies [14]. Linalool (32.83%), elemol (7.44%), geranyl acetate (6.18%), and myrcene (6.12%) were the primary components of the essential oil from southern India [15]. We aimed to analyze *Murraya koenigii* leaves comprehensively towards an integrated pharmacognostic approach for evaluation of antibacterial activity: MIC determination and in vitroantibacterial efficacy against clinically relevant pathogens.

METHODS

Authentication and Collection of the Plant Material

The leaves of *Murraya koenigii* were collected from the Sulaymaniyah Botanical Garden, Sulaymaniyah Iraq, in April 2025 and dried in the shade. The The plant material was identified and authenticated by a taxonomist by the earlier reported method [16]. The dried leaves were ground to a particle size of 250–500 μm. Extraction was performed using 70% ethanol at a raw material-to-solvent ratio of 1 : 10 (w/v) via maceration for 24 hours at room temperature. The evaporation process was then used to filter the extracts and concentrate [14].

Pharmacognostic Assessment

Parameters of Physicochemistry

Physicochemical analysis was performed on powdered leaf material in accordance with WHO recommendations for herbal medication quality control. Among the parameters established were: Examining foreign organic stuff visually and separating unnecessary materials. Determine the moisture content (loss on drying) by drying the powder at 105°C until its weight remains constant [11].

Acid-insoluble, water-soluble and total ash were measured by burning at 450°C in a muffle furnace [10].

Screening for Phytochemicals

To find saponins, tannins, steroids, terpenoids, flavonoids, cardiac glycosides, alkaloids, resins, amino acids, & other secondary metabolites, both the aqueous and solvent extracts underwent qualitative phytochemical screening using conventional techniques [17].

Antibacterial Action Assesment

Strains of Bacteria

A panel of Gram-positive and Gram-negative bacteria obtained from microbiology department, Thi Qar university, was used to evaluate the antibacterial actions against: *Staphylococcus aureus*, *Escherichia coli*, *Pseudomonas aeruginosa*, *Salmonella typhi*, *Bacillus subtilis*, *Klebsiella pneumonia*, *Proteus mirabilis*, and *Enterobacter aerogenes*.

Method of Disc Diffusion

The agar well diffusion method [18] was first used to screen the extracts for antibacterial actions. Mueller–Hinton agar plates were covered with bacterial cultures that had been cultivated overnight and adjusted to the 0.5 McFarland standard. The infected agar surface was covered with wells or discs that had been impregnated with different amounts of test samples. Positive controls were standard antibiotic discs. The zone of inhibition's diameter was determined in millimeters after that we incubated the plates for 24 hrs at 37 °C [19, 20]. Three replicates' means are used to calculate the values.

Determining the MIC

We performed the broth microdilution (two-fold) method to calculate the extracts' MIC. The test samples were serially diluted two times in microtiter 96-well plates. A bacterial suspension (about 1×10^2 CFU/mL) was added to each well. For a whole day, we incubated the plates at 37 °C. The minimum concentration exhibiting no discernible growth of bacteria was identified as the minimum inhibitory concentration (MIC) [21].

Table 1. The Physicochemical parameters of *M. koenigii* leaf

Parameter	Value (% w/w)
Foreign organic matter	< 1%
Moisture content	4.2 ± 0.3
The total ash	15.4 ± 0.3
The acid-insoluble ash	4.7 ± 0.2

Statistics Analysis

Every experiment was carried out in triplicate, and the mean ± standard deviation (SD) was used to express the results. One-way analysis of variance (ANOVA) and Tukey's post-hoc test for multiple comparisons were used in the statistical study. Statistical significance was defined as a *p*-value of less than 0.05. Each table lists the statistical tests that were applied [2, 19].

RESULTS

Physicochemical Parameters

Table 1 displays the determined physicochemical properties of the powdered leaf material.

The medicine was devoid of additional plant parts, molds, insects, and other animal contaminants because the foreign organic matter was less than 1% w/w. The dried leaf samples had a moisture level of roughly 4.2% w/w. The drug's dampness promotes the growth of common bacteria and mold, and inadequate drying results in the enzymatic breakdown of active ingredients. Therefore, the sample's low moisture level suggests that the leaves were properly dried to make storage easier.

The obtained total ash value was approximately 15.4% w/w. The low ash levels suggest that the plant medication has a low inorganic content. The crude medicine was less contaminated by inorganic elements like sand or soil, as indicated by the acid-insoluble ash value of roughly 4.7% w/w.

Screening for Phytochemicals

Several types of bioactive chemicals were found in the aqueous and solvent extracts using qualitative phytochemical screening (Table 2). Standard phytochemical tests were used for qualitative analysis. The mean of three separate experiments is shown in the results.

Tannins, saponins, steroids, terpenoids, and cardiac glycosides were found in the aqueous leaf extract according to phytochemical study. A more comprehensive profile with additional resin detection was displayed by the methanolic leaf extract.

Antibacterial Activity

Disc Diffusion Results

Table 3 and Figure show the antibacterial actions of *Murraya koenigii* ethanol and aqueous extracts of leaves against eight clinically relevant bacterial infections. Zones of inhibition are shown as mean ± standard deviation. While no activity (0.0 mm) was detected regarding the aqueous extract against any of the test organisms, the ethanol extract displyed strong antibacterial action against all the tested organisms, where inhibition zones ranged from 13 mm against Klebsiella pneumoniae to 21 mm against Staphylococcus aureus and Proteus mirabilis. The F-values ranged beyween 881.25 (*S. aureus*) and 433.50 (*K. pneumoniae*) which showed significant differences among the examined treatment groups for all the used bacterial strains.

We detected comparable activities between the positive control group regarding *B. subtilis* (20 mm/20 mm) and *S. aureus* (21 mm / 20 mm) In contrary, we detected significantly inferior action against Gram-negative organisms such as *K. pneumonia*, *E. coli*, *S. typhi*, *P. aeruginosa*, *P. mirabilis*, and *E. aerogenes* ($p < 0.05$).

The MIC values of the extracts against various test pathogens are presented in Table 4. *Bacillus sp*. and *S. mutans* showed the highest activity for the ethanolic extract, where MICs were 0.156 mg/mL, for both strains. MIC readings of higher concentration (0.625 mg/mL) were detected for *S. typhi*, E. coli, and *S. aureus*, without any efficacy of aqueous extract.

DISCUSSION

The physicochemical factors of our study provide reliable markers for recognizing adulteration & confirming batch-to-batch constancy in herbal medicinal mixes. According to our results, the foreign organic matter amount was < 1% w/w, which indicates that the medication didn't contain contamination from molds, insects, other animal elements or other plant parts [11]. This is a vital criterion of quality because using foreign ingredients may compromise the herbal and safety efficacy.

A content of moisture of 4% w/w in our results is crucial for the herbal remedy's stability. The high moisture levels may

Table 2. Phytochemical constituents detected in *M. koenigii* leaf extracts

Phytochemical Class	Aqueous Extract	Methanolic Extract	Ethanol Extract
Tannins	+	+	+
Saponins	+	+	+
Steroids	+	+	+
Terpenoids	+	+	+
Cardiac glycosides	+	+	+
Flavonoids	+	+	+
Alkaloids	+	+	+
Resins	–	+	+
Amino acids	+	+	+

Note: + — present, – — absent

Table 3. The antibacterial zones of inhibition of *Murraya koenigii* ethanol and aqueous extracts of leaves against tested bacterial

Test Organism	Ethanol Extract (mm)	Aqueous Extract (mm)	Positive Control Gentamicin 10 µg (mm)	*F*	*p*
Staphylococcus aureus	21	0	20	881.25	< 0.001
Escherichia coli	14	0	16	456	< 0.001
Pseudomonas aeruginosa	17	0	19	625.33	< 0.001
Salmonella typhi	16	0	18	522	< 0.001
Bacillus subtilis	20	0	20	600	< 0.001
Klebsiella pneumoniae	13	0	17	433.5	< 0.001
Proteus mirabilis	21	0	23	738	< 0.001
Enterobacter aerogenes	14	0	20	526	< 0.001

boost the appearance of common molds and bacteria, and active breakdown of substances. The low content of moisture in our sample shows that adequate drying were performed to enable storage and protect bioactive components [11].

The total ash value (15.4% w/w), offers an increase mineral content of the drug. The adequate ash levels exhibit that the inorganic material of the plant is not high, which is a good sign. The acid insoluble ash concentration (4.8% w/w) shows insignificant contamination of the crude product by sand or soil [10].

These pharmacognostic variables are consistent with studies conducted in different regions. Gujarati studies found that the moisture content was 1.12% ± 0.03% w/w and 1.31% ± 0.12% w/w, the acid-insoluble ash content was 0.59% ± 0.01% w/w and 0.20% ± 0.02% w/w, and the total ash content was 15.66% ± 0.32% w/w (Anand) and 12.29% ± 0.08% w/w [12]. The little differences that can be attributed to geographic factors, soil composition, and agricultural practices emphasize the need for regional pharmacognostic criteria.

According to earlier research, phytochemical screening was used to identify a variety of bioactive compounds [17]. These compounds are recognized for their antimicrobial properties and contribute to the plant's overall antibacterial activity.

Tannins have a remarkable bactericidal effect. Because they can bind to proteins and stop the formation of bacterial cell walls, tannins are polyphenolic compounds with bacteriostatic & bactericidal qualities. They can hinder the formation of biofilms by creating complexes with bacterial adhesins, according to numerous studies [22]. Saponins can cause cell lysis and compromise the integrity of bacterial cell membranes due to their amphiphilic properties [23]. Steroids and terpenoids are well known for their membrane-active properties and ability to inhibit bacterial enzymes [24].

Also in accordance with our results other studies showed that the antibacterial activity of *M. koenigii* extracts shown significant efficacy against a variety of therapeutically relevant pathogens, including both Gram-positive and Gram-negative bacteria [2, 25, 26]. The qualitative phytochemical screening of *Murraya koenigii* leaf extracts revealed that while resins were only present in the organic solvent extracts saponins, tannins, terpenoids, steroids, flavonoids, cardiac glycosides, amino acids, and alkaloids were present in all three extracts (aqueous, methanolic, and ethanolic). These different phytochemical groups are consistent with previous reports on *M. koenigii* that identified terpenoids, tannins, flavonoids and carbazole alkaloids, as unique components of this medicinal plant [27].

The complete absence of resins in the aqueous extract and their presence in both methanolic and ethanolic extracts show the superior extraction efficiency of organic solvents for non-polar bioactive compounds, supporting the notion that methanol and ethanol are better solvents for extracting a wider range of secondary metabolites than water [28]. In consistence with

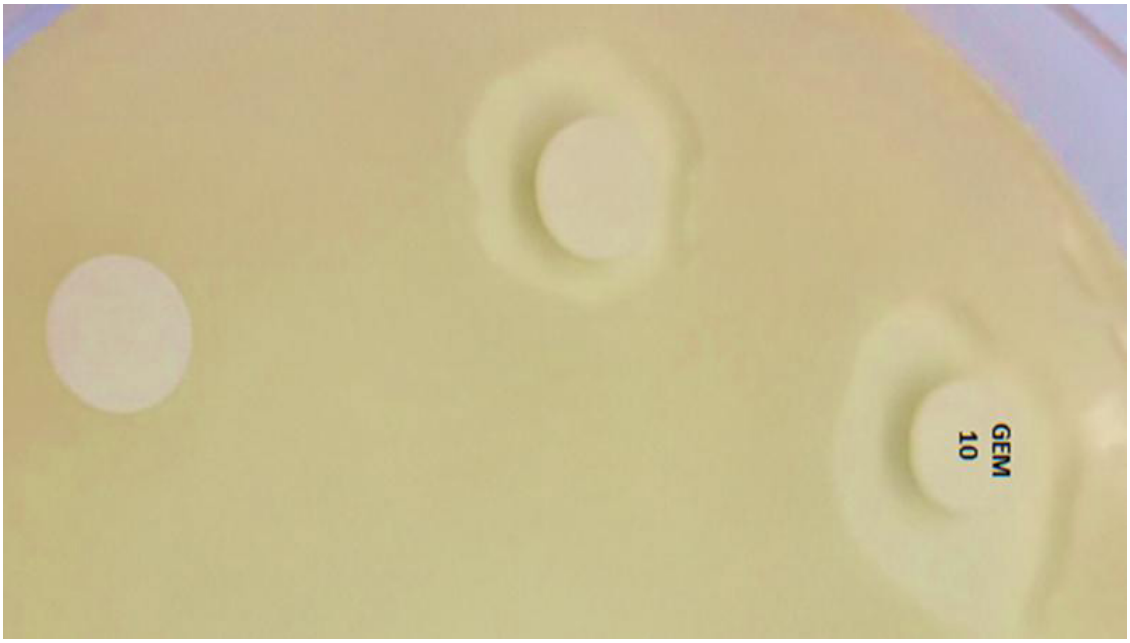

Fig. Showing different inhibition zones of aqueous, ethanolic, and positive control

Table 4. MIC values of *M. koenigii* extracts against test pathogens

Test Organism	Ethanol Extract	Aqueous Extract
S. mutans	0.156	–
S. aureus	0.625	–
E. coli	0.625	–
Salmonella typhi	0.625	–
Salmonella sp.	0.312	–
Bacillus sp.	0.156	–

previous studies, this study tested the phytochemical character and antibacterial action of *Murraya koenigii* (curry leaf) extracts. Flavonoids, alkaloids, phenols, steroids, terpenoids, glycosides, tannins, and saponins were the detected bioactive ingredients discovered in the ethanol extract, giving to phytochemical study. High alkaloid components were discovered a upon comparing to other therapeutic plants [27], which is consistent with our profile [27].

Disc diffusion and MIC techniques were used to evaluate the antibacterial effectiveness against 8 bacterial species. With inhibition zones ranged from 21.0 mm to 13.0 mm, the ethanol extract presented variable antibacterial activity. Stimulatingly, none of the tested bacteria were influenced by the aqueous extract. This may be due to water's weak ability to absorb non polar bioactive materials with antibacterial potentials, such as terpenoids, carbazole alkaloids, and flavonoids.

The ethanol extract's effecay against Gram-positive infections was established by the fact that its efficiency against *Bacillus subtilis* and *S. aureus* was equivalent to that of the positive control results. The earlier reported results [27] are consistent with our work. The thick peptidoglycan layer cell walls of Gram-positive bacteria, which endorses compound penetration in contrary to the outer membrane permeability barrier of Gram-negative bacteria, clarifies the detected difference in susceptibility, with Gram-positive bacteria being more susceptible.

The plant extract exhibited *Pseudomonas aeruginosa* (17.0 mm inhibition diameters), a common cause of hospital-acquired infections because of its resistance to antibiotic and biofilm production, was one of the clinically challenging bacteria against which the used extract had distinguished action. A detailed review (2024) was maintained by the presence of moderate activity against *S. typhi* and *E. coli*. Also, activity against *P. mirabilis* and *Enterobacter aerogenes* indicated the extract potential of broad-spectrum activity confirming the previous findings that the organic solvent extracts are better than aqueous ones [29].

Strong action was detected against *Bacillus* sp. and *Streptococcus mutans* (MIC = 0.156 mg/mL), with the influence against *S. mutans* being particularly notable owing to its contribution in dental caries. Higher MIC values were establish for Gram-negative and Gram-positive bacteria, such as *E. coli* and *S. typhi* and *S. aureus* (0.625 mg/mL), which is consistent with previous research. The traditional usage of curry leaves for gastrointestinal troubles is supported by the MIC against *Salmonella* sp. (0.312 mg/mL).

CONCLUSIONS

The combination of numerous phytochemicals, such as terpenoids, alkaloids, tannins, and flavonoids which disturb the bacterial cell membranes and enzymes, is accountable for the antibacterial action. The study supports *M. koenigii's* traditional usage by efficiently establishing pharmacognosic standards for the plant and viewing that its ethanol extract has strong, and broad-spectrum antibacterial action equivalent with other antibiotics. Although more *in vivo* and clinical studies is required, the results support the development of *M. koenigii*-based natural antibacterial products and emphasize the superiority of ethanol extraction solvent.

References

1. El-Shiekh RA, et al. Anticholinesterases activity of Murraya koenigii (L.) Spreng. and Murraya paniculata (L.) Jacq. essential oils with GC/MS analysis and molecular docking. Natural Product Research. 2024; 38 (12): 2155–9.
2. Aniqa A, Kaur S. Phytochemical screening of hydroethanolic Murraya koenigii Spreng leaves extract by spectroscopic methods. Journal of Drug Research in Ayurvedic Sciences. 2024; 9 (4): 273–85.
3. Maheswari KU, Sankar S. In silico molecular docking of phytochemicals of Murraya koenigii against Streptococcus mutans. Cureus. 2024; 16 (2).
4. Savitha G, Balamurugan S. Pharmacognostical and antibacterial evaluation of Murraya koenigii (L) Spreng. International Letters of Natural Sciences. 2014; 17.
5. Nagappan T, Ramasamy P, Vairappan CS. Chemotaxonomical markers in essential oil of Murraya koenigii. Natural Product Communications. 2012; 7 (10): 1934578X1200701034.
6. Verma RS, et al. Phytochemical diversity of Murraya koenigii (L.) Spreng. from western Himalaya. Chemistry & Biodiversity. 2013; 10 (4): 628–41.
7. Patil N, et al. Pharmacognostical, Preliminary phytochemical screening and Antibacterial activity of methanol Extract of Murraya koenigii. PharmaTutor. 2019; 7 (2): 18–20.
8. Rajendran MP, Pallaiyan BB, Selvaraj N. Chemical composition, antibacterial and antioxidant profile of essential oil from Murraya koenigii (L.) leaves. Avicenna journal of phytomedicine. 2014; 4 (3): 200.
9. Chibueze IJ, Emenike I. Murraya koenigi — a boon in different patological conditions. Universal Journal of Pharmaceutical Research. 2016.
10. Organization WH. Quality control methods for herbal materials. 2011: World Health Organization.
11. Sindhu RK, Arora S. Phytochemical and Pharmacognostical Studies on Murraya koenigii (L) spreng. Roots. Drug Invention Today. 2015; 7 (1).
12. Adebajo AC, et al. Evaluation of the Ethnomedical Claims of Murraya koenigii. Pharmaceutical Biology. 2005; 42 (8): 610–20.
13. Kumar KT, Sundar PD. Evaluation of antibacterial, antifungal and anthelmintic activity of Murraya Koenigii spreng. 2011.
14. Kaur S, et al. Chemopreventive activity of hydroethanolic Murraya koenigii leaves extract (HEMKLE) against chemically induced skin carcinogenesis in mice. International Journal for Vitamin and

Nutrition Research. 2020.
15. Handral HK, Pandith A, Shruthi S. A review on Murraya koenigii: multipotential medicinal plant. Asian J Pharm Clin Res. 2012; 5 (4): 5–14.
16. Handral HK, Jha PK. Pharmacognostic and phytochemical studies on the leaves of Murraya koenigii (L) Spreng. Pharmacophore. 2010; 1 (3): 231–8.
17. Meena S, et al. Transcriptomic insight into terpenoid and carbazole alkaloid biosynthesis, and functional characterization of two terpene synthases in curry tree (Murraya koenigii). Scientific Reports. 2017; 7 (1): 44126.
18. Kashyap S, Rathod Y, Biswas S. Murraya koenigii methanolic extract inhibits bacterial growth and biofilm of Staphylococcus aureus and Enterococcus faecalis. Scientific Reports. 2025; 15 (1): 34056.
19. Samanta SK, et al. Phytochemical portfolio and anticancer activity of Murraya koenigii and its primary active component, mahanine. Pharmacological research. 2018; 129: 227–36.
20. Saadoon SJ, et al. Surgical site infection: The Physiological Changes & the Effect of Using Preoperative Antibiotic Prophylaxis in Orthopedic Surgeries. Bulletin of Pharmaceutical Sciences Assiut University. 2026.
21. Patil R, Mandlik S, Mandlik D. Murraya koenigii (Curry Tree): A review of its phytochemistry, ethnomedicinal uses, and pharmacology with respect to molecular mechanisms. Current Traditional Medicine. 2024; 10 (5): 73–97.
22. Nandan S, et al. Quantitative analysis of bioactive carbazole alkaloids in Murraya koenigii (L.) from six different climatic zones of India using UPLC/MS/MS and their principal component analysis. Chemistry & Biodiversity. 2021; 18 (12): e2100557.
23. Mondal P, et al. Extract of Murraya koenigii selectively causes genomic instability by altering redox-status via targeting PI3K/AKT/Nrf2/caspase-3 signaling pathway in human non-small cell lung cancer. Phytomedicine. 2022; 104: 154272.
24. Nadaf S, et al. Antiproliferative and caspase-mediated apoptosis inducing effects of Murraya koenigii seeds against cancer cells. South African Journal of Botany. 2020; 132: 328–37.
25. Choudhury RP, Garg A. Variation in essential, trace and toxic elemental contents in Murraya koenigii–A spice and medicinal herb from different Indian states. Food Chemistry. 2007; 104 (4): 1454–63.
26. Gahlawat DK, Jakhar S, Dahiya P. Murraya koenigii (L.) Spreng: an ethnobotanical, phytochemical and pharmacological review. Journal of Pharmacognosy and Phytochemistry. 2014; 3 (3): 109–19.
27. Abdullah R, et al. Phytochemical and antimicrobial properties of different plants and in silico investigation of their bioactive compounds in wound healing and rheumatism. Saudi Journal of Biological Sciences. 2024; 31 (3): 103942.
28. Cowan MM. Plant products as antimicrobial agents. Clinical microbiology reviews. 1999; 12 (4): 564–82.
29. Franyoto, YD, A. Nurrochmad, and N. Fakhrudin, Murraya koenigii L. Spreng.: An updated review of chemical composition, pharmacological effects, and toxicity studies. Journal of Applied Pharmaceutical Science. 2024; 14 (6): 011–027.

Литература

1. El-Shiekh RA, et al. Anticholinesterases activity of Murraya koenigii (L.) Spreng. and Murraya paniculata (L.) Jacq. essential oils with GC/MS analysis and molecular docking. Natural Product Research. 2024; 38 (12): 2155–9.
2. Aniqa A, Kaur S. Phytochemical screening of hydroethanolic Murraya koenigii Spreng leaves extract by spectroscopic methods. Journal of Drug Research in Ayurvedic Sciences. 2024; 9 (4): 273–85.
3. Maheswari KU, Sankar S. In silico molecular docking of phytochemicals of Murraya koenigii against Streptococcus mutans. Cureus. 2024; 16 (2).
4. Savitha G, Balamurugan S. Pharmacognostical and antibacterial evaluation of Murraya koenigii (L) Spreng. International Letters of Natural Sciences. 2014; 17.
5. Nagappan T, Ramasamy P, Vairappan CS. Chemotaxonomical markers in essential oil of Murraya koenigii. Natural Product Communications. 2012; 7 (10): 1934578X1200701034.
6. Verma RS, et al. Phytochemical diversity of Murraya koenigii (L.) Spreng. from western Himalaya. Chemistry & Biodiversity. 2013; 10 (4): 628–41.
7. Patil N, et al. Pharmacognostical, Preliminary phytochemical screening and Antibacterial activity of methanol Extract of Murraya koenigii. PharmaTutor. 2019; 7 (2): 18–20.
8. Rajendran MP, Pallaiyan BB, Selvaraj N. Chemical composition, antibacterial and antioxidant profile of essential oil from Murraya koenigii (L.) leaves. Avicenna journal of phytomedicine. 2014; 4 (3): 200.
9. Chibueze IJ, Emenike I. Murraya koenigi — a boon in different patological conditions. Universal Journal of Pharmaceutical Research. 2016.
10. Organization WH. Quality control methods for herbal materials. 2011: World Health Organization.
11. Sindhu RK, Arora S. Phytochemical and Pharmacognostical Studies on Murraya koenigii (L) spreng. Roots. Drug Invention Today. 2015; 7 (1).
12. Adebajo AC, et al. Evaluation of the Ethnomedical Claims of Murraya koenigii. Pharmaceutical Biology. 2005; 42 (8): 610–20.
13. Kumar KT, Sundar PD. Evaluation of antibacterial, antifungal and anthelmintic activity of Murraya Koenigii spreng. 2011.
14. Kaur S, et al. Chemopreventive activity of hydroethanolic Murraya koenigii leaves extract (HEMKLE) against chemically induced skin carcinogenesis in mice. International Journal for Vitamin and Nutrition Research. 2020.
15. Handral HK, Pandith A, Shruthi S. A review on Murraya koenigii: multipotential medicinal plant. Asian J Pharm Clin Res. 2012; 5 (4): 5–14.
16. Handral HK, Jha PK. Pharmacognostic and phytochemical studies on the leaves of Murraya koenigii (L) Spreng. Pharmacophore. 2010; 1 (3): 231–8.
17. Meena S, et al. Transcriptomic insight into terpenoid and carbazole alkaloid biosynthesis, and functional characterization of two terpene synthases in curry tree (Murraya koenigii). Scientific Reports. 2017; 7 (1): 44126.
18. Kashyap S, Rathod Y, Biswas S. Murraya koenigii methanolic extract inhibits bacterial growth and biofilm of Staphylococcus aureus and Enterococcus faecalis. Scientific Reports. 2025; 15 (1): 34056.
19. Samanta SK, et al. Phytochemical portfolio and anticancer activity of Murraya koenigii and its primary active component, mahanine. Pharmacological research. 2018; 129: 227–36.
20. Saadoon SJ, et al. Surgical site infection: The Physiological Changes & the Effect of Using Preoperative Antibiotic Prophylaxis in Orthopedic Surgeries. Bulletin of Pharmaceutical Sciences Assiut University. 2026.
21. Patil R, Mandlik S, Mandlik D. Murraya koenigii (Curry Tree): A review of its phytochemistry, ethnomedicinal uses, and pharmacology with respect to molecular mechanisms. Current Traditional Medicine. 2024; 10 (5): 73–97.
22. Nandan S, et al. Quantitative analysis of bioactive carbazole alkaloids in Murraya koenigii (L.) from six different climatic zones of India using UPLC/MS/MS and their principal component analysis. Chemistry & Biodiversity. 2021; 18 (12): e2100557.
23. Mondal P, et al. Extract of Murraya koenigii selectively causes genomic instability by altering redox-status via targeting PI3K/AKT/Nrf2/caspase-3 signaling pathway in human non-small cell lung cancer. Phytomedicine. 2022; 104: 154272.
24. Nadaf S, et al. Antiproliferative and caspase-mediated apoptosis inducing effects of Murraya koenigii seeds against cancer cells. South African Journal of Botany. 2020; 132: 328–37.
25. Choudhury RP, Garg A. Variation in essential, trace and toxic elemental contents in Murraya koenigii–A spice and medicinal herb from different Indian states. Food Chemistry. 2007; 104 (4):

1454–63.
26. Gahlawat DK, Jakhar S, Dahiya P. Murraya koenigii (L.) Spreng: an ethnobotanical, phytochemical and pharmacological review. Journal of Pharmacognosy and Phytochemistry. 2014; 3 (3): 109–19.
27. Abdullah R, et al. Phytochemical and antimicrobial properties of different plants and in silico investigation of their bioactive compounds in wound healing and rheumatism. Saudi Journal of Biological Sciences. 2024; 31 (3): 103942.
28. Cowan MM. Plant products as antimicrobial agents. Clinical microbiology reviews. 1999; 12 (4): 564–82.
29. Franyoto, YD, A. Nurrochmad, and N. Fakhrudin, Murraya koenigii L. Spreng.: An updated review of chemical composition, pharmacological effects, and toxicity studies. Journal of Applied Pharmaceutical Science. 2024; 14 (6): 011–027.